EFFECT OF NEWLY CONSTRUCTED STRUCTURES SUPPORTED ON RAFT FOUNDATIONS ON EXISTING CONCRETE TUNNEL LININGS

by

Anna Maria Zakhem

Submitted in partial fulfilment of the requirements
for the degree of Doctor of Philosophy

at

Dalhousie University
Halifax, Nova Scotia
September 2019

This thesis is dedicated to the memory of my beloved

father Elias Zakhem and brother Toni Zakhem

TABLE OF CONTENTS

LIST OF TABLES

LIST OF FIGURES

ABSTRACT

In densely populated areas, there is increasing construction of high-rise buildings adjacent to existing tunnels. The interactions involved are complex and unavoidable. Based on experience and field monitoring, many tunnel owners impose exclusion zones for construction close to their tunnels. This research studies the effect of a newly constructed building supported by a shallow foundation on a pre-existing tunnel. With the aid of the PLAXIS software, a detailed three-dimensional finite element analysis is used to conduct a parametric study showing the interaction between the burial location of the pre-existing tunnel and the new shallow foundation. The concrete lining is modelled by using the newly developed concrete model included in the PLAXIS user-defined library. The model considers the non-linearity of the material behaviour and the distinction between strength in tension and compression. The constitutive soil where the tunnel system is constructed is simulated by using a hardening soil model with small-strain stiffness, which accounts for increased stiffness at small strains. The construction of the tunnel is divided into several phases, where each phase is simulated with the advancement of the shield boring machine. Accordingly, new design guidelines can be developed for shallow foundations in close proximity to pre-existing tunnels.

LIST OF ABBREVIATIONS AND SYMBOLS USED

c	Cohesion
Ψ	Dilatancy angle
ε_1	Axial strain
E_{28}	Young's modulus of concrete
E_{50}	Secant modulus at 50% strength
E_{oed}	Oedometer loading stiffness
E_{ur}	Triaxial unloading/reloading stiffness
φ_{max}	Maximum friction angle
$f_{c,28}$	Compressive strength of concrete
$f_{t,28}$	Tensile strength of concrete
$\gamma_{0.7}$	Strain level at which the shear modulus is reduced to about 70% of the small strain shear modulus
G_0^{ref}	Small-strain shear modulus
$G_{c,28}$	Compressive fracture energy of concrete
$G_{t,28}$	Tensile fracture energy of concrete
λ	Compression index
λ^*	Modified compression index
κ	Swelling index
κ^*	Modified swelling index
M	Tangent of the critical state line
ν	Poisson's ratio
p^{ref}	Reference overburden stress
σ_1	Major principal stress
σ_3	Minor principal stress

ACKNOWLEDGEMENTS

Firstly, I would like to express my genuine gratitude to my supervisor Dr. Hany El Naggar for the incessant support of my PhD study and related research, for his patience, motivation, and vast knowledge. His guidance helped me in all the time of research and writing of this thesis. I could not have imagined having a better supervisor and mentor for my PhD study.

In addition, I would like to thank the rest of my thesis committee: Dr. Craig Lake, Dr. Nouman Ali, and Dr. Zoheir Farhat, for their insightful comments and encouragement which incented me to widen my research from various perspectives. Also, I would like to extend my gratitude to all of the administrative staff in the Department of Civil and Resource Engineering at Dalhousie University. I will not forget the help and encouragement provided from Dr. El Naggar's team more specifically Ahmed Mahgoub.

My special thank goes to my mother Najah, my brother George and my sister Caroline with her family for their moral support.

As the last will be first, I express my enormous gratitude for my family: my son Nicodeme, my daughter Maria Danielle and my husband Dr. Dani Youssef for their multiple support in my life in general and specifically in this thesis.

CHAPTER 1 INTRODUCTION

1.1 STATEMENT OF THE PROBLEM

Traffic worldwide is increasing at the same rate or even higher as the population growth, especially in urban areas. Throughout the 20th century, urbanization has been occurring worldwide at an unprecedented rate [1]. According to a recent UN research in 1990, 43 percent (2.3 billion) of the world's population lived in urban areas. In 2010 over 50 percent of the global population was living in urban areas; by 2015, this had grown to 54 percent (4 billion). By 2030, it is expected to reach 60 percent and nearly 70 percent by 2050 [2]. This substantial urbanization shift over time has led to the emergence of the megacity. New York and Tokyo were the first known megacities; both reached a population of over 10 million by the 1950s. However, today, they are far from alone in their size [3]. In 2018 there were 33 megacities across the globe from Sao Paulo and Mexico City in the Americas, to Cairo and Lagos in Africa, and from Istanbul and Moscow in Europe to Beijing and Dhaka in Asia. Consequently, several adverse traffic and environmental conditions encounter this megacities evolution, for which underground infrastructure, such as tunnels, is the best practical solution.

The fact that land in megacities is scarce and very expensive has led to the construction of high-rise buildings close to pre-existing tunnels. The interaction between buried infrastructure and foundations is unavoidable, and the nature of this soil structure interaction (SSI) problem is complex. The associated SSI can reduce or increase the vertical or horizontal tunnel lining diameter, causing ovalization or squat phenomena. This can imply spalling at segment joints and cracking at various locations around the tunnel lining. It could also cause openings at the radial joints, resulting in the entry of saline water that could lead to significant concrete degradation in

the form of extensive concrete delamination and steel deterioration. Hence, several researchers have investigated this interaction problem considering several parameters such as the tunnelling process, construction sequence, proximity of the tunnel to the foundation, foundation type, burial depth of the tunnel, the associated ground movement and possible damage to adjacent buildings [4-6]. Many tunnel owners have developed restrictive guidelines including imposing an exclusion zone for the construction of foundations close to their tunnels. These guidelines are mostly based on experience, not on a fundamental understanding of this complex problem. The adverse effect of foundations on existing tunnels was monitored in a few field case studies where it was found to be considerable [7-9]. In addition, the long-term exposure of a reinforced concrete tunnel lining to sulphates or chlorides in groundwater can lead to concrete deterioration (as Shown in Figure 1-1) and consequently a reduction of its load carrying capacity.

Figure 1- 1: An example of concrete deterioration in tunnels [10].

1.2 THESIS OBJECTIVES AND ORIGINAL CONTRIBUTIONS

This complex interaction problem between the foundations of a new building built over a pre-existing tunnel was previously investigated using a combination of in situ observations and/or

numerical modelling. However, previous studies only simulated one aspect of the building, such as the basement excavation case of the building without consideration of the building itself as a whole [11 and 12]. Another group of studies did not simulate the actions of the tunnel boring machine (TBM) during excavation, including the face and grout pressures and consequently ignored a critical aspect of the problem. Also, the vast majority of previous research has modelled the tunnel lining as an elastic beam or plate and has considered it as a monotonic continuous structure. In fact, the shield tunnel lining is formed by assembling prefabricated concrete segments bolted together to form rings that are erected within the tunnel bore. Other researchers have studied the interaction between basement excavation and an existing tunnel by using a 2D plain strain scheme and have modelled the soil as elastic or elastic-perfectly plastic. However, models which assume that the soil is elastic, or elastic-perfectly plastic is not capable of modelling the different interactions in the soil during the tunnel excavation.

This project involves comprehensive numerical modelling using the finite element (FE) code PLAXIS 3D to investigate the considered problem by modelling all of its geometric and material aspects. In this study, the tunnel construction is divided into several phases to simulate in detail the construction sequence. Each phase simulates the advancement of the shield boring machine. The pressure at the face of the tunnel was assigned so as to maintain an equilibrium between the pressure inside the machine chamber due to the excavated soil, and the earth pressure outside the cutting surface. Other aspects being simulated include the shape of the machine, which is conical in most cases; injection of the grouting material in the gap left between the tail skin and the lining; the hydraulic jack forces driving the machine, which are exerted on the already installed lining; and installation of the new lining with an equivalent grout layer behind.

In addition, the effect of lining deterioration on the overall response of the system was investigated using 3D models considering various tunnel configurations and different levels of lining degradation. The degradation was simulated using a smeared approach in which reduced stiffness was localized at the degradation locations. The FE mesh was refined around and in close vicinity of the tunnel and near locations where non-linear behaviour is anticipated to assure high accuracy of the results. Interface elements allowing for both slippage and gapping to occur from the PLAXIS library were used to model the interface between the soil and the tunnel lining. Both intact and degraded concrete linings were modelled using the new concrete constitutive model, included in the PLAXIS user-defined library, modified to simulate the behaviour of reinforced concrete, in which, more realistic stress distributions can be obtained, as the non-linearity of the material behaviour and the distinct different strength performance in compression and tension is considered. Soil hardening and elasto-plastic constitutive models will be used to model the soil and the interface. This research will lead to the development of new design guidelines for shallow and deep foundations in close vicinity of existing tunnels.

1.3 SCOPE AND ORGANIZATION OF THE THESIS

This thesis comprises: (1) a detailed overview of previous studies considered the interaction between surface structures and tunnels; (2) investigating the effect of the constitutive material model employed on predictions of the behaviour of earth pressure balance shield-driven tunnels; (3) using the developed 3D model to investigate how newly constructed buildings supported on raft foundations affect pre-existing tunnels; (4) investigating how newly constructed buildings supported on raft foundations affect pre-existing deteriorated tunnels; and (5) developing a simplified procedure to incorporate the effect of pre-existing tunnels in the analysis of new buildings.

The layout and organization of the thesis are summarized in the following section:

Chapter 2 explores the interaction issue between surface structures and tunnels. In this chapter, a general overview of the previous research regarding soft ground tunnelling and the associated ground deformations is presented. In addition, the effect of tunnelling on existing structures was discussed utilizing two-dimensional finite element models.

Shield-driven tunnelling involves a complex SSI problem, where the stress history and its development during construction heavily influence the performance. Numerical modelling must, therefore, focus on selecting appropriate constitutive models for soils and structures as reliable numerical models to predict expected settlements, lining pressures, and other design parameters are essential for safe tunnel design. Hence, *Chapter 3* investigates the effect of the constitutive material model employed on predictions of the behaviour of earth pressure balance shield-driven tunnels.

Chapter 4 studies the effect of a newly constructed building supported by a shallow foundation on an intact pre-existing tunnel. A detailed three-dimensional finite element analysis was used to conduct a parametric study showing the interaction between the burial location of the pre-existing tunnel and the new shallow foundation. The intact concrete lining is modelled by using the newly developed concrete model included in the PLAXIS user-defined library. The model considers the non-linearity of the material behaviour and the distinction between strength in tension and compression. The soil, where the tunnel system is constructed, is simulated by using a hardening soil model with small-strain stiffness, which accounts for increased stiffness at small strains. The construction of the tunnel is divided into several phases, where each phase is simulated with the

advancement of the shield boring machine. Accordingly, new design guidelines were developed for shallow foundations in close proximity to pre-existing tunnels.

Chapter 5 presents the results of a comprehensive finite element analysis exercise conducted to investigate investigating how newly constructed buildings supported on raft foundations affect pre-existing deteriorated tunnels. Accordingly, a set of exclusion zones and design guidelines were developed for high-rise buildings supported on raft foundations in close proximity to pre-existing deteriorated tunnels.

In *Chapter 6*, the development of a simplified procedure to incorporate the effect of pre-existing tunnels in the analysis of new buildings is presented. Also, correction factors were obtained to accompany the proposed procedure.

Finally, *Chapter 7* summarizes the findings and conclusions deduced from the whole thesis and proposes areas for future research.

1.4 REFERENCES

[1] ITA Working Group (2012). Urban Problems – Underground Solutions. ITA Report Nº011/APR 2012. International Tunneling and Underground Space Association, Chatelaine, Switzerland.

[2] UN-HABITAT, Urbanization and Development: Emerging Futures, World Cities Report 2017.

[3] URBANIZATION AND THE MEGACITY https://worldpopulationhistory.org/urbanization-and-the-megacity.

[4] Namazi E. & Mohamad H. (2013) "Assessment of Building Damage Induced by Three-Dimensional Ground Movements". Journal of Geotechnical and Geoenvironmental Engineering, ASCE Vol. 139 (4): 608-618.

[5] Benton L. J. & Phillips A., (1991). "The behaviour of two tunnels beneath a building on piled foundations''. Proc. 10th European Conf. on Soil Mechanics and Foundation Engineering: 665-668.

[6] Higgins K. G., Chudleigh I., St John H. D. & Potts D. M. (1999). "An example of pile tunnel interaction problems". Proc. Int. Symp. Geotech. Aspects of Underground Construction in Soft Ground, IS-Tokyo, pp. 99–103.

[7] Schroeder F. C. (2002). "The influence of bored piles on existing tunnels: a case study". Ground Engng. Vol. 35 (7), pp. 32–34.

[8] Schroeder F.C., Potts D.M. & Addenbrooke T.I. (2004). "The influence of pile group loading on existing tunnels". Geotechnique. 54(6): 351-362.

[9] Dowding C. H. & Rozen A. (1978) “Damage to Rock Tunnels from Earthquake Shaking”. Journal of the Geotechnical Engineering Division, ASCE, Vol. 104, No. GT2.

[10] Robotic hydro demolition speeds repairs – TunnelTalk, February 2015.

[11] Sharma, J. S., Hefny, A. M., Zhao, J., & Chan, C. W. (2001). Effect of large excavation on deformation of adjacent MRT tunnels. *Tunnelling and Underground Space Technology Incorporating Trenchless Technology Research, 16*(2), 93-98. doi:10.1016/S0886-7798(01)00033-5.

[12] Devriendt, M., Doughty, L., Morrison, P., & Pillai, A. (2010). Displacement of tunnels from a basement excavation in London. *Proceedings of the Institution of Civil Engineers, 163*(3), 131-145. Retrieved from https://search.proquest.com/docview/906522924.

CHAPTER 2 LITERATURE REVIEW

2.1 INTRODUCTION

Tunnels are a crucial component of modern transportation infrastructure. They are often required for roads which cross mountain ranges or pass beneath rivers or canals. Several megacities in various parts of the world (e.g., New York, Washington DC, Toronto, London, and Mexico City) expanded their subway systems in the late 1960s to 1970s, and for the first time used precast segmental concrete tunnel linings. The concept of soil-structure interaction (SSI) evolved at that time and was widely implemented in tunnel lining design. Predicting the internal forces in tunnel linings is a major issue to be addressed in the design of new tunnels and, even more importantly, in the assessment and evaluation of older tunnels. These internal forces can result from geostatic in situ loads, or surface loads imposed by the foundations of new buildings. Vertical and/or horizontal tunnel lining deformations due to these loads can cause cracking or even crushing of the tunnel lining, especially near joint locations. Tunnelling in urban areas poses many challenges because of the potential to adversely affect existing subsurface and surface structures (Kolymbas, 2005). Conversely, new developments and surface structures can affect pre-existing tunnels.

Tunnelling in rural areas where there are no surface structures is referred to as greenfield tunnelling. In such cases, over-excavation of the soil during tunnelling is a primary concern, because it may lead to soil failure if sufficient support is not provided during construction (see Figure 2- 1).

In contrast, in urban areas the main focus is on controlling the effect on pre-existing structures of ground movements due to tunnelling and/or reducing the effect of surface structures on pre-existing tunnels. All of the analyses presented in this thesis consider the effect of foundations of

new buildings on pre-existing tunnels. However, a detailed explanation of the effect of tunnelling induced ground movements on existing structures is also presented to outline how problems involving soil-structure interactions between surface structures and tunnels are generally treated.

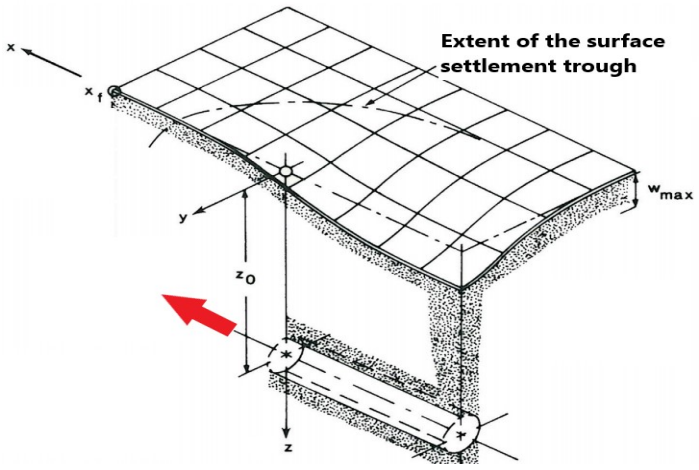

Figure 2- 1: Greenfield displacements caused by tunnelling (after Attewell et al., 1986)

Several researchers have explored how ground movements around tunnels translate into a distribution of settlements on the ground surface (i.e., settlement troughs). Early studies were confined to field observations. Later, various analytical procedures and closed form solutions were developed to predict tunnel lining internal forces and deformations. Each of these solutions can be applied to very specific conditions and geometry. Some of these solutions are concerned with the static analysis of linings and lining loads, while others focus on the prediction of settlement troughs. Generally, analytical procedures and closed form solutions possess several attractive features, including their relative simplicity and capability of partially accounting for soil-lining interactions.

This chapter presents a brief background on available tunnel excavation techniques. The chapter then provides a general overview of currently available methods for predicting ground surface

settlements in greenfield conditions, and the shortcomings of these methods. In addition, the chapter presents the results of a study conducted to assess the disturbance of nearby surface structures caused by tunnelling induced ground displacements, and describes the main features of this SSI problem, some aspects of which are also significant for the main topic of this thesis (i.e., the effect of surface structures on pre-existing tunnels). Furthermore, the effect of salts and freeze-thaw cycles on the performance of tunnel linings is discussed.

2.2 AVAILABLE TUNNEL EXCAVATION TECHNIQUES

2.2.1 Cut and cover tunnelling

The cut and cover construction technique has been used for many years as a means of building underground transportation facilities. This technique, which is used if excavation from the surface is possible, is economical if the tunnel is relatively short and at a shallow depth. The depth is considered to be shallow if the height of the cover above the tunnel is not much greater than the tunnel diameter (FHWA, 2009). Cut and cover tunnelling involves excavating an open cut by using traditional excavation methods, and then constructing the tunnel lining under normal construction conditions in the excavation. Once the lining is constructed and waterproofing and drainage measures have been undertaken, the tunnel is backfilled with suitable materials up to the initial ground level.

This construction technique may involve one or both of the two methods: bottom-up construction and top-down construction. In bottom-up construction, the final structure is independent of the support of the excavation walls; whereas, in top-down construction, the tunnel roof and ceiling are structural parts of the excavation walls. Bottom-up cut-and-cover construction involves the excavation of a trench in which the tunnel is built. Temporary structures, such as sheet pile walls and secant pile walls are typically required and installed. In this case, the side slopes of the

excavation may involve the removal of up to six times as much material as the volume of the tunnel itself, and may extend an additional three tunnel diameters on each side of the excavation, for a tunnel with a depth of cover equal to its diameter. The tunnel is constructed from the bottom slab, up to the tunnel walls and roof. The excavation is then covered, and the ground level is restored for use by above-ground operations. In contrast, the top-down cut-and-cover construction method is often employed if there is a limited width of right-of-way for excavation, or if use of the area above the tunnel (e.g., for above-ground transportation systems such as highways) is paramount and side wall deflections must be limited to minimize damage to adjacent structures (FHWA, 2009). In such cases, excavation support is installed first, consisting of structures such as slurry walls, secant pile walls, or sheet pile walls, which usually become the permanent walls of the tunnel. A shallow excavation is created, where the roof of the tunnel is constructed on grade. The excavation is then covered for continued use while the tunnel interior is excavated from below grade, with bracing provided to the support walls. The early covering of the excavation permits faster turnover from the beginning of construction to the restored availability of the ground surface. In both bottom-up and top-down construction sequences, dewatering of the work area may be necessary before the ground material is excavated.

Figure 2- 2: Cut and cover top-down tunnel (civildigital.com)

2.2.2 Rock tunneling methods

2.2.2.1 Drill and Blast

The drill and blast method is by far the most commonly used rock excavation technique. It is associated mainly with mining applications. The basic approach is to drill a pattern of small holes, load them with explosives, and then initiate an explosion to create an opening in the rock. The blasted rock is then removed, and the surface of the rock is supported.

Figure 2- 3: Drill and blast tunnel (civildigital.com)

2.2.2.2 Tunnel boring machine (TBM)

Tunnel boring machines excavate rock mass via rotating and crushing methods. Enormous pressure and large thrust forces are applied to the rock face while rotating and chipping actions are carried out by several disc cutters mounted on the machine cutterhead.

Figure 2- 4: Tunnel boring machine (civildigital.com)

2.2.2.3 Roadheaders

Rather than boring with the circular cross-section provided by TBMs, a road header machine has multiple heads that cut slots or other shapes that can be more efficient in terms of providing usable volume.

Figure 2- 5: Roadheaders machine (civildigital.com)

2.2.3 Soft ground tunneling

2.2.3.1 Shield tunneling

Earth pressure balance (EPB) and slurry face shield tunnel boring machines (SFM) are similar in that both types of machine have a revolving cutter wheel and an internal bulkhead, both rely on mechanization and computerization to control various functions, and both are associated with the use of precast concrete segments. However, in the case of EFB machines, pressure is transmitted to the face mechanically, via the soil. In contrast, SFM machines transmit pressure to the face hydraulically via a viscous fluid formed by the material cut and trapped at the face and mixed with slurry (essentially composed of bentonite and water).

Figure 2- 6: Earth pressure balance (EPB) tunnel boring machine (from Lovat)

Figure 2- 7: Slurry face boring machine (SFM) (from Herrenknecht)

2.2.4 Sequential Excavation Method (SEM) – NATM

The sequential excavation method (SEM), also commonly referred to as the new Austrian tunnelling method (NATM), is a concept that is based on understanding the behavior of the ground as it reacts to the creation of an underground opening. The strength of the ground is utilized and the ground itself becomes part of the tunnel support. A shotcrete lining redistributes loads in the ground by deflection. The NATM tunnelling procedure involves: classification of the ground; excavation and support based on ground investigations; definition of the excavation and support

by outlining the maximum unsupported excavation length; application and reinforcement of the shotcrete lining; ground reinforcement via bolts or dowels in the rock; subdivision of the tunnel into top heading, bench, invert, and side wall drifts; requirements for ring closure; and local additional initial support as required via dowels, bolts, spiles, face support wedges, and shotcrete.

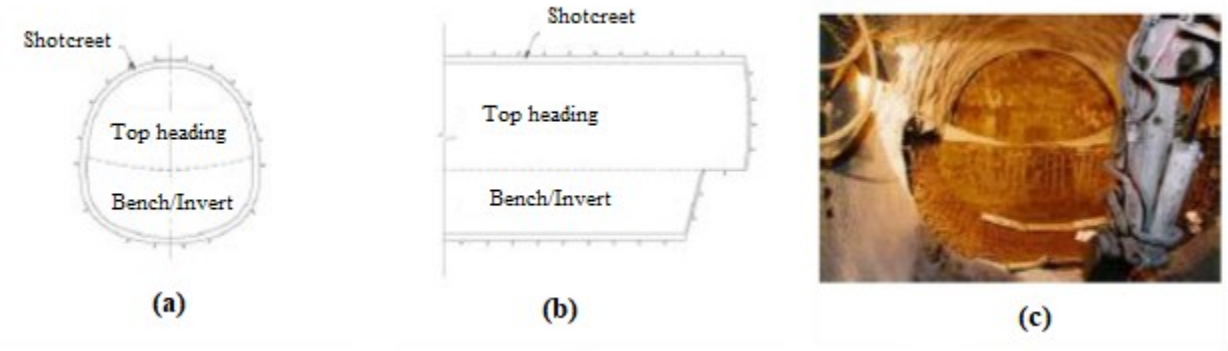

Figure 2- 8: London bridge station, London, UK, **(a)** cross section, **(b)** longitudinal section and **(c)** photo

2.3 GROUND DEFORMATION IN SOFT GROUND

1. In hard ground such as rock, usually ground movements during the tunnelling process are not a problem. However, in soft ground, displacements can arise for various reasons (after Mair and Taylor 1997, Figure 2- 9):
2. Deformation of the ground toward the face due to stress relief;
3. Radial ground movements due to the passage of the shield (necessitating correct alignment of the shield or tilting it up to prevent it from diving into the ground);

4. Presence of a tail void due to the difference in diameter of the tail of the shield and the installed lining, resulting in a tendency for the ground to move into this gap;
5. Distortion of the tunnel lining as it starts to take the ground loading;
6. Time-dependent consolidation in fine-grained soils (i.e., soft clays) as the construction process changes the stress regime locally around the tunnel. This causes changes in the water pressure within the pores between the soil particles. As these excess pore water pressures equilibrate over time the ground changes in volume and consolidates.

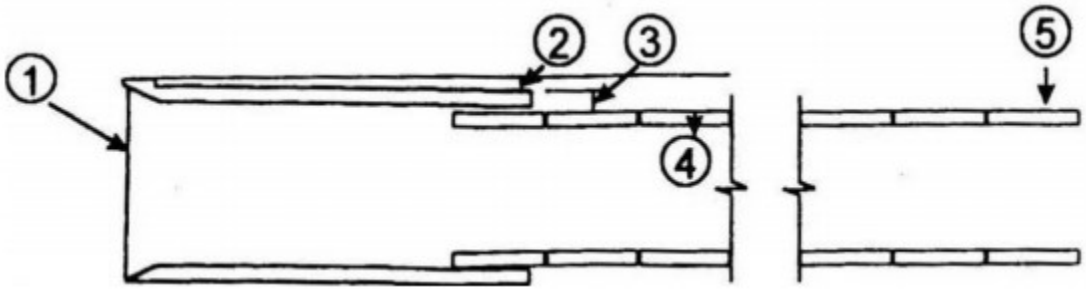

Figure 2- 9: Primary components of ground movements with shield tunnelling

These factors can result in displacements that reach the ground surface, where they can influence superimposed and adjacent structures.

2.4 EFFECT OF TUNNELING ON EXISTING STRUCTURES

During tunnelling operations, nearby structures and the tunnel interact. This interaction is affected by the size, shape and material of a structure and its position relative to the tunnel. Attewel et al.,

(1986) discuss some idealized modes of behavior of long and short buildings due to tunnel construction, as summarized below:

Short Building:

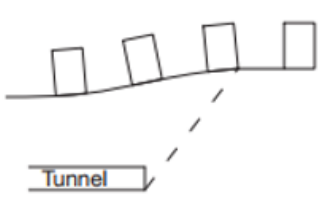

Short buildings ride the forward settlement wave with little significant sagging or hogging deformation.

Short buildings experience tilt as a rigid body, but with little significant sagging or hogging deformation across a transverse settlement.

Long Building:

Long buildings experience progressive deformation and differential settlements as the tunnel advances.

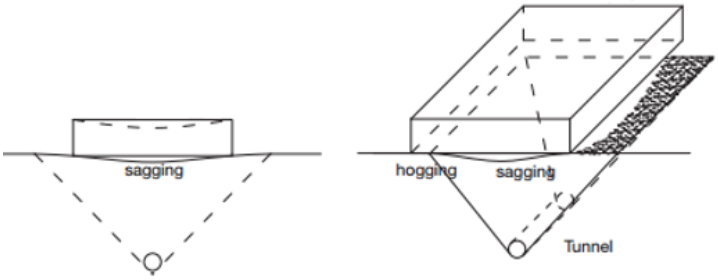

Potential sagging and hogging of a long building across a transverse settlement trough, when directly above the tunnel centerline, and offset from the centerline.

Several researchers have investigated cracks as an indication of distress in structures and have developed classification methods to assess structural damage.

2.4.1 Empirical Methods

Skempton and MacDonald (1956), Polshin and Tokar (1957), and Bjerrum (1963) proposed empirical methods focused on damage caused by settlement arising from the weight of a structure. Skempton and Macdonald (1956) defined their damage criterion, the angular distortion β, as the ratio of differential settlement, δ, to the distance, l, between two points. They found that structural damage occurred when $\beta > 1/150$, and that cracks in walls and partitions appeared when $\beta > 1/300$. They recommended $\beta = 1/500$ as the limit. Polshin and Tokar (1957) introduced the concept that tensile strains induced in a structure cause cracking and suggested a critical tensile strain of $\varepsilon_{crit} =$ 0.05%. They defined their damage criterion slope as the ratio of the differential settlement of two adjacent supports to the distance between them. For steel and concrete frame buildings, they recommended a slope $\leq 1/500$, and where there is no infill, they recommended a slope $\leq 1/200$. These recommendations agree well with those of Skempton and MacDonald.

2.4.2 Analytical Methods

Burland and Worth (1974) assumed that the beginning of cracking is associated with the average tensile strain in a building. Tensile strain can occur due to bending (vertical cracks/direct tensile strain) or shearing (diagonal cracks/diagonal tensile strain). The maximum tensile strain is then the greater of bending strain or shear strain. To obtain the maximum strain in buildings, they modelled building facades as a linear elastic deep beam undergoing sagging and hogging modes of deformation (see Figure 2- 10). They suggested that ε_{crit} ranged from 0.05% to 0.1% for masonry structures and from 0.03% to 0.05% for reinforced concrete beams. This approach was later updated by Burland (1997), who proposed the use of a deflection ratio rather than angular distortion. Furthermore, Burland et al. (1977) replaced the concept of critical tensile strain with

that of limiting tensile strain, ε_{lim}. These researchers defined six categories of damage, providing a framework for evaluating damage based on ease of repair and crack width (see Table 2.1).

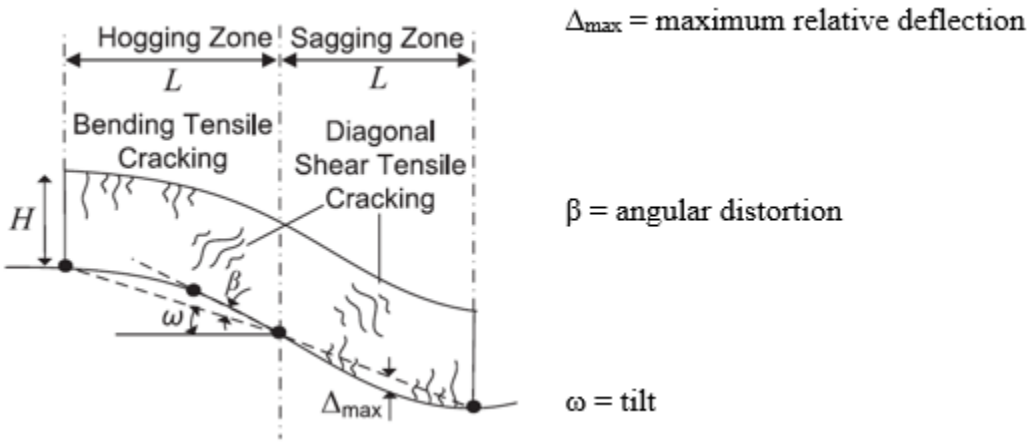

Figure 2- 10: Idealized representation of a building as an elastic beam

Table 2. 1: Classification of building damage after Burland et al., (1977)

Damage Category	Degree of severity	Description of typical damage
0	Negligible	Hairline cracks less than about 0.1mm wide.
1	Very slight	Fine cracks easily treated during normal decoration. Crack width up to 1mm.
2	Slight	Cracks are easily filled. Redecoration probably required. Crack width up to 5mm.
3	Moderate	Cracks can be patched by a mason. Repointing and possibly replacement of some brickwork. Crack width from 5-15mm.
4	Severe	Extensive repair work involving replacement. Crack widths from 15-25mm.
5	Very severe	Major repairs required including partial or complete re-building. Crack width typically greater than 25mm.

Boscardin and Cording (1989) included lateral strain by using simple superposition to consider the role of horizontal extension induced by adjacent excavation and tunnelling (see Figure 2- 11). Table 2.2 shows the relationship between limiting tensile strain, ε_{lim}, and category of damage,

which was first put forward by Boscardin and Cording (1989) and later updated by Son and Cording (2005).

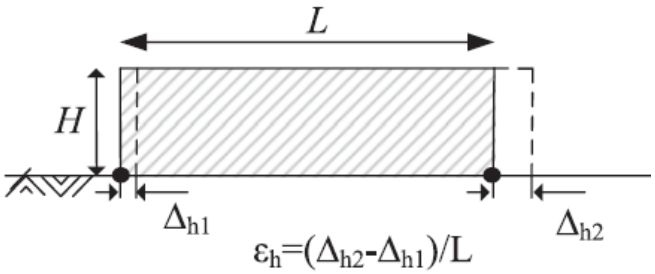

Figure 2- 11: Horizontal tensile strain

Table 2. 2: Damage Category Criteria after Boscardin and Cording, (1989) and Son and Cording, (2005)

	Method		
	Boscardin and Cording (1989)		Son and Cording (2005)
Category of damage	β ($\times 10^{-3}$)	ε_h (%)	ε_{crt} (%)
Negligible	0–1.1	0–0.05	0–0.05
Very slight	1.1–1.6	0.05–0.075	0.05–0.075
Slight	1.6–3.3	0.075–0.15	0.075–0.167
Moderate to severe	3.3–6.7	0.15–0.3	0.167–0.333
Severe to very severe	>6.7	>0.3	>0.333

Namazi and Mohamad (2012) extended Burland's beam model. They assumed that the horizontal and vertical forces of the building wall are dependent on tilt as one of the components that causes building damage. They concluded that, under a high degree of tilt, the tolerance of the building to deflection and horizontal displacement decreases.

2.4.3 Numerical Methods

2.4.3.1 Two-Dimensional Finite Element Models

A two-dimensional finite element analysis was undertaken by Fishermann et al., (1994) to predict settlement and damage of the Mansion House in London due to the construction of the Docklands Light Railway. Three separate tunnel sections were planned under the building (comprised of 5 storeys of masonry walls and suspended timber floors). The ground materials were gravel and London clay. The soil was modelled as linear elastic and the masonry façade as simple beam elements with a uniform elastic modulus of 1 GPa and a Poisson's ratio of 0.2. The predictions agreed well with the field data only when the vertical support of the orthogonal walls was modelled by using vertical springs at the ends of the investigated wall. This indicates that the 3D geometry of the building needed to be considered. By using 2D finite element methods, the researchers Potts and Addenbrooke (1997) studied the effect of building stiffness on settlement profiles due to tunnelling. The soil was modelled as a nonlinear elastic-plastic material and was given London clay properties. Plane strain conditions were assumed. The building was represented as a linear elastic beam. The analysis did not include the building weight or any three-dimensional effects.

Calabresi et al., (1999) predicted the damage to the Castel S. Angelo in Rome due to tunnelling. The soil was modelled as an elastic-plastic material and consisted of silty alluvial sands overlying stiff clay at a depth of 30 m. The structure was modelled as a massive masonry cylinder 64 m in diameter and 35 m high, with a slab foundation 6 m thick. The diameter of the tunnel was 11.8 m. Finite element results were compared to empirical predictions and gave good agreement in terms of damage prediction parameters. The evaluation of the damage to masonry buildings by modelling the masonry wall as nonlinear when the tunnel is driven symmetrically under a series of regularly spaced orthogonal masonry walls was performed by using 2D numerical analysis (Miliziano et al.,

2002). The soil was modelled by using an elasto-plastic Mohr-Coulomb model, with Young's modulus increasing linearly with depth. It was concluded that damage would be overestimated when neglecting the soil-structure interaction. Further analyses of masonry walls were carried out by Boonpichetvong and Rots, (2004). They presented a 2D tunnelling analysis including a full masonry façade modelled by using a fracture mechanics approach.

2.4.3.2 Three-Dimensional finite element method

Zakhem and El Naggar (2016) presented a detailed comprehensive 3D finite element model developed to study the induced structural distortions of adjacent structures due to tunnelling activities.

In this study, a comprehensive procedure is developed to assess settlement-induced damage to buildings, and the associated soil-structure interaction (SSI). This procedure is based on a finite element method where the building, the ground and the tunnelling processes are combined in a single numerical model. The lining of the tunnel is modelled by using a concrete constitutive model modified to simulate the behavior of reinforced concrete, so that more realistic stress distributions can be obtained, such as the nonlinearity of the material behavior, and the distinctly different strength performance in compression and tension can be taken into account.

2.4.3.2.1. Problem definition

This section presents the development of the FE models that were used to carry out the numerical analyses presented in this study. The problem considered involves a high-rise building (15 storeys with 1 basement) on a mat foundation resting on a thick sandy layer underlain by bedrock at a great depth (see Figure 2- 12). The 3D FE models were established by using the computer program PLAXIS 3D AE.01 (PLAXIS bv, 2015). A sensitivity analysis was conducted, and an appropriate

mesh size was utilized accordingly. The FE models were employed to perform a comprehensive parametric study to investigate the interaction between the building and the tunnel and to evaluate the forces within the different structural members. This study presents the results of the first stage of the research.

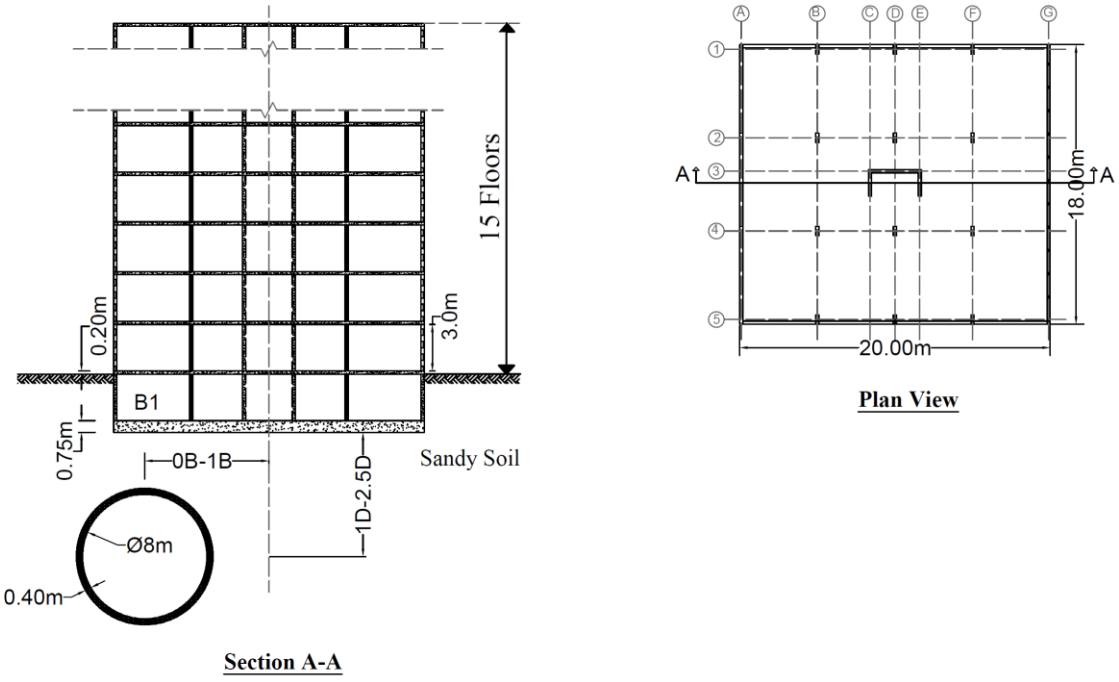

Figure 2- 12: Section and plan view

2.4.3.2.2. Geometry

The FE model considered is 180 m wide, extends 162 m in the *y*-direction, and is 60 m deep. These dimensions are sufficient to allow for any possible collapse mechanism to develop and to avoid any influence from the model boundaries. Figure 2.12 shows the geometry of the problem considered. The tunnels are assumed to be buried at depths ranging from 1D to 2.5D, where D is the tunnel diameter, and at horizontal locations ranging from 0B (directly beneath the centerline of the mat foundation) to 1B, where B is the width of the mat foundation.

2.4.3.2.3. Soil stratigraphy and used material model

The soil layer is assumed to be horizontal throughout the model. The ground water table is located well below the foundation level, so that there is no influence of the water table on the ultimate bearing capacity of the foundation. The analyses were conducted assuming drained conditions. The unit weight γ_{unsat} = 20 kN/m^3. The Mohr-Coulomb model was selected as the material model. The Mohr-Coulomb model involves only five basic parameters: (1) Young's modulus, E = 40,000 kPa, (2) Poisson's ratio, ν = 0.3, (3) cohesion, C = 0.2 kPa, (4) friction angle, φ = 38°, and (5) dilatancy angle, ψ = 0°.

2.4.3.2.4. Mat foundation

The 20 m x 18 m mat foundation considered in this analysis is located at the centre of the sand deposit. The foundation consists of concrete 0.75 m thick, with unit weight, γ = 24 kN/m^3. The foundation is modelled by using plate elements from the PLAXIS library with a linear isotropic behavior. Young's modulus, E_1 = 30,000,000 kPa, and Poisson's ratio, ν_{12} = 0.15.

2.4.3.2.5. Tunnel lining

The lining was modelled as volume elements by using the nonlinear elastoplastic concrete model developed by Schadlich and Schweiger (2014). According to the cases considered, the tunnel is modelled with lining thickness = 0.05D (i.e., 400 mm in this case). In all instances, the tunnel lining is modelled as concrete with unit weight, γ = 24 KN/m^3. The tunnel construction was simulated utilizing simplified approached by considering uniform surface contraction of 0.5% around the tunnel.

2.4.3.2.6. The used FE mesh and its boundary conditions

The model was built by using approximately 250,000 3D 10-node tetrahedral elements. Figure 2-13 shows the mesh generated for the model. The average size of the element was approximately 110 mm. The lateral boundaries were placed at least 4 times the width of the foundation in each direction to simulate the infinite medium. The bottom boundary was placed at 60 m below the ground surface.

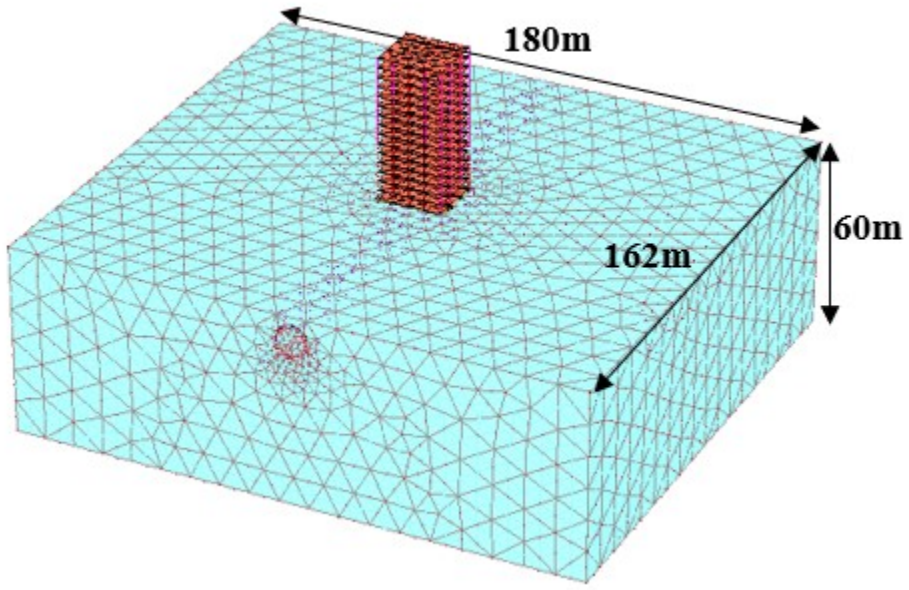

Figure 2- 13: Mesh generated for the model

2.4.3.2.7. Results

A parametric study was conducted to examine the effect of the tunnel burial depth on the performance of the mat foundation. The influence of the existing structure on moments and thrusts developed in the tunnel lining was also studied.

In the parametric study, the tunnel was assumed to be located directly beneath the centerline of the mat foundation. In addition, tunnel burial depths ranging from 1D to 2.5D, at horizontal locations ranging from 0B to 1B, were investigated.

A. Effect of the existing structure on moments and thrusts developed in the tunnel lining

Figure 2- 14 shows the percentage increases (in comparison to the case where there is no surface structure) of the thrust and moment in the tunnel lining at the springline and crown locations, when the tunnel is located directly beneath the centerline of the mat foundation at burial depths ranging from 1D to 2.5D. In comparison, Figure 2- 15 shows the percentage increases of the thrust and moment at the springline and crown locations, when the tunnel is located at a constant depth of 1D, at horizontal locations ranging from 0B (where the center of the tunnel is directly beneath the center of the mat foundation) to 1B.

It can be seen from Figure 2.14 that the thrust and moment increase considerably, in comparison to the case where there is no surface structure, especially when the tunnel is located directly beneath the centerline of the building close to the surface. Figure 2.14(a) shows that the thrust increases almost 120% at the springline and 30% at the crown. When the tunnel is located at a depth of 1D at a horizontal location 1B or more from the centerline of the foundation (see Figure 2.15), the percentage increase in the thrust and moment drops, since the tunnel is located further away from the strongest influence zone of the building.

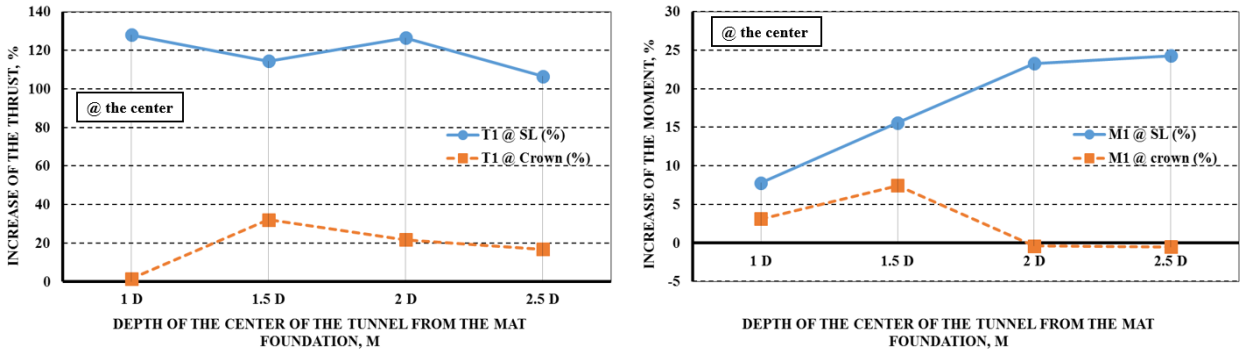

Figure 2- 14: Percentage increases in **(a)** thrust and **(b)** moment at the springline and crown of the tunnel lining, when the center of the tunnel is located directly beneath the centerline of the mat foundation at burial depths ranging from 1D to 2.5D

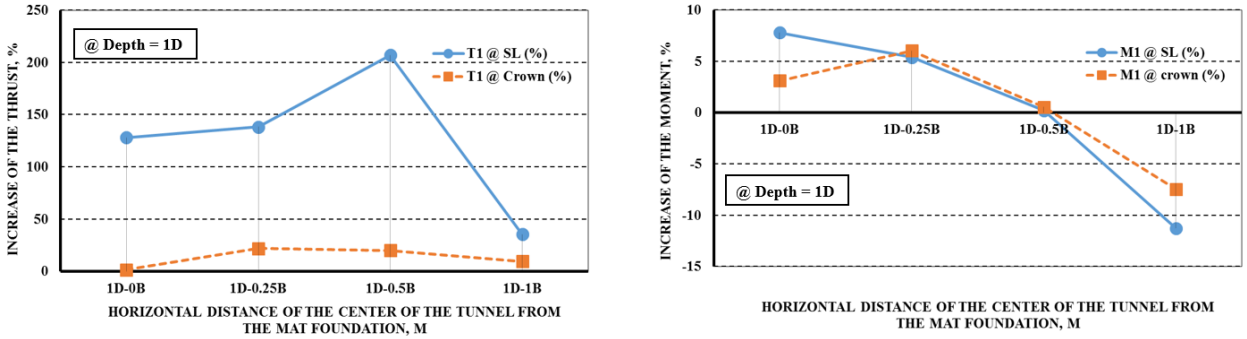

Figure 2- 15: (Percentage increases in **(a)** thrust and **(b)** moment at the springline and crown of the tunnel lining, when the center of the tunnel is located at horizontal distances ranging from 0B to 1B from the mat foundation centerline

B. Effect of an existing structure on displacement of the tunnel lining

Figures 2- 16(a) and 2- 16(b) show the vertical (crown) and horizontal (springline) deformation of the tunnel lining for a tunnel located directly beneath the centerline of the mat foundation at burial depths ranging from 1D to 2.5D, and for a tunnel with a burial depth of 1D at horizontal locations ranging from 0B to 1B from the mat foundation centerline, respectively. It can be seen from Figure 2- 16(a) that the vertical deformation increases as the burial depth of the tunnel increases. Similar

trends in behavior can be observed for horizontal deformation at the springline. It can be seen that the maximum deformation of the lining is less than the tolerable deformation (less than 1% of the diameter). This is within safety limits. The behavior illustrated in Figure 2- 16(b) is expected. As the tunnel is located further away from the foundation, stress due to the foundation interferes less with the tunnelling zone and consequently less deformation occurs. In Figure 2- 16(b) it can be seen that at location 0.5B (where part of the tunnel is under the mat foundation), the displacement values drop due to differential settlement.

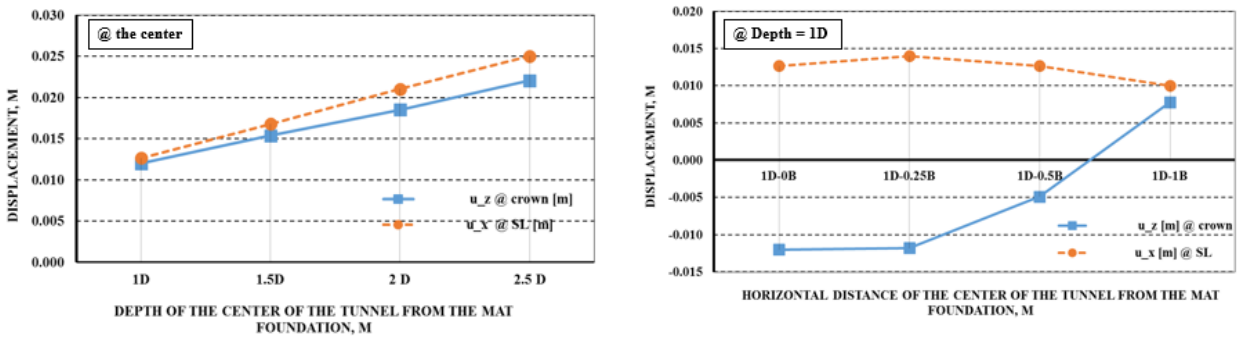

Figure 2- 16: Displacement of the springline and crown of the tunnel lining when the center of the tunnel is located **(a)** directly beneath the centerline of the mat foundation at burial depths ranging from 1D to 2.5D, and **(b)** at a burial depth of 1D, at horizontal locations ranging from 0B to 1B from the centerline of the mat foundation

C. Effect of the tunnel on the pressure below the existing mat foundation

From Figure 2- 17, which represents the distribution of vertical stress beneath the mat foundation, it can be seen that the pressures in general are not uniform. The maximum applied pressure in all cases is less than the calculated allowable bearing capacity of the soil.

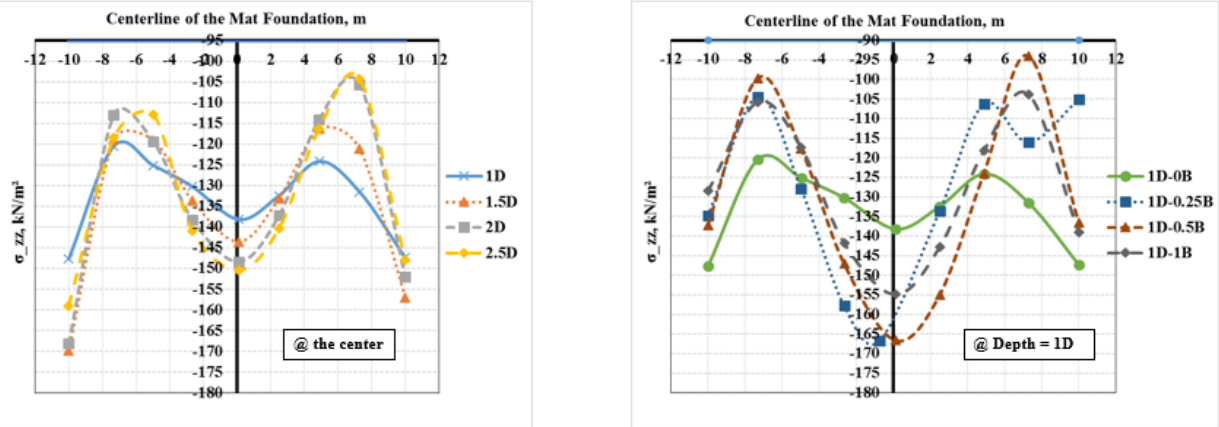

Figure 2- 17: Pressure beneath the centerline of the mat foundation when the center of the tunnel is located **(a)** directly beneath the centerline of the mat foundation at burial depths ranging from 1D to 2.5D, and **(b)** at a burial depth of 1D, at horizontal locations ranging from 0B to 1B from the mat foundation centerline

D. Effect of the tunnel on the settlement of the existing mat foundation

Figure 2- 18 shows the deformed shape of the centerline of the mat foundation. The maximum value at the center of the mat foundation is less than the tolerable settlement as can be seen from the figure. It can be seen from Figure 2.18(a) that there is less settlement of the mat foundation when the tunnel is located underneath the mat foundation, at a shallower burial depth close to the foundation. The deformed shape of the mat has increased by 23% when the tunnel's center burial depth varied from one tunnel diameter to 2.5 tunnel diameter. One of several factors influencing the settlement of shallow foundations is the supporting ground stiffness. Since the stiffness of the tunnel lining is greater than that of sand, the foundation soils become stiffer if a tunnel is present; thus, the settlement is reduced. In Figure 2.18(b), it can be seen that when the tunnel is located at 0.5B (where part of the tunnel is under the mat foundation), differential settlement occurs in the mat foundation.

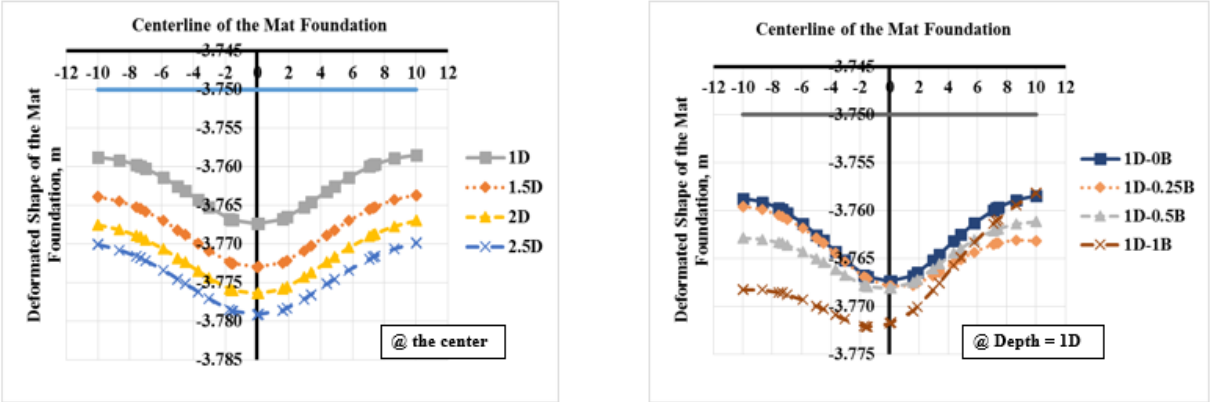

Figure 2- 18: Deformed shape of the centerline of the mat foundation when the center of the tunnel is located **(a)** directly beneath the centerline of the mat foundation at burial depths ranging from 1D to 2.5D, and **(b)** at a burial depth of 1D, at horizontal locations ranging from 0B to 1B from the centerline of the mat foundation

2.4.3.2.8. Summary of the main findings of the study

This study was conducted to examine the effect of pre-existing high-rise buildings on the forces and deformations developed in the tunnel lining and vice versa. The conclusions are summarized below:

1. When the tunnel is located within the overstressed zone (at a depth of up to 2D and at a horizontal distance from the foundation of up to 0.5B), the deformations, bending moment and thrusts increase substantially in comparison to the case where there is no surface structure, due to the interaction between the foundation and the tunnel.
2. The horizontal deformation of the lining at the springline and the vertical deformation at the crown decrease as the burial depth of the tunnel increases.
3. All of the above effects decrease substantially or disappear when the tunnel is located at a burial depth of 3D or more below the foundation.

4. The presence of the tunnel does not really affect the vertical pressure underneath the foundation and its deformed shape, due to the high stiffness of the tunnel lining, which acts as a support below the foundation.
5. The current engineering approach to modelling concrete linings in numerical simulations assumes a linear elastic material with a stepwise increase of Young's modulus in subsequent excavation stages. While realistic lining deformations may be obtained with this method, the lining stresses are usually too high, in particular if the lining is subjected to significant bending.
6. With the new constitutive model, more realistic stress distributions can be obtained, because the nonlinearity of the material behavior is taken into account. Furthermore, the stability of the tunnel can be checked at all intermediate stages without the need for additional capacity checks of the lining cross-section.

2.5 Effect Of Chloride Salts And The Freeze-Thaw Cycle On Tunnel Lining Performance

Corrosion of steel reinforcement is a common problem associated with reinforced concrete structures. Chlorides are one of the most common corrosion triggers. De-icing salts used in cold climate conditions are the most widespread source of chlorides that affect concrete structures.

Corrosion-induced cracks develop due to rust (iron oxide) accumulated on the reinforcement bars. Rust is the main product of corrosion. This accumulated layer of rust can occupy up to 6 times the volume of the original steel. As a result, the concrete is pushed apart and cracks develop. As the corrosion progresses, more and more rust accumulate and the cracks continue to grow.

When the cracks become wide enough, a portion of the concrete beneath the bars spalls off, leaving the bars completely exposed. Once the bars lose their bond with the concrete due to spalling, the section behaves more like a plain concrete section. As a result of corrosion, a structural member may lose a significant portion of its strength and might even collapse.

Corrosion cracks may widen if water gets into the cracks and freezes. The expanded ice within the cracks causes them to widen and leads to further deterioration.

In cold climates, freezing and thawing are the most common source of weather-related cracking in concrete structures. Concrete may be damaged by freezing of water in the paste, the aggregate, or both. Weather-related cracking can also be caused by volume changes in concrete as a result of alternate wetting and drying and heating and cooling of concrete structures.

Accordingly, water can damage tunnels in several ways during their working life. It can cause internal deterioration of the mortar, e.g., the strength of the concrete lining of the railway tunnel between Shimonoseki and Moji in Japan was reduced, with cracks developing in the concrete slabs and deterioration of the cement asphalt mortar (Howard, 1991). Water can also corrode the reinforcement, as occurred in the United Arab Emirates road tunnel between Dubai and Deira, where the reinforced concrete lining was damaged due to a high level of chloride in the concrete resulting from the seepage of salty water through the structure (Howard, 1991). Degradation and reduced strength of the concrete can likewise affect the tunnel lining, as in the case of the cement concrete tunnel lining of the Sabart hydroelectric gallery in France, where serious leakages were found due to dissolution of the binder and even the calcareous aggregate. Water can also affect the tunnel installation, with icicles appearing in the ceiling slab and the roads becoming icy on cold days, as happened in the road tunnel between Gollin and Werfen, Austria (Howard, 1991).

Gulikers (2003) used a simplified numerical model to investigate the electrochemical behavior of embedded passive steel reinforcement in tunnel linings with a restricted one-sided access to oxygen. Amleh and Ghosh (2006) then examined the influence of corrosion on bond strength at the steel-concrete interface, as well as the associated slip and cracking. They developed a nonlinear finite element model to account for the effect of corrosion on deterioration of the bond. Sun Fu (2007) concluded that the depth of the tunnel, the chloride diffusion coefficient and electrochemical corrosion are the main factors affecting the durability and expected service life of a tunnel lining, based on theoretical and laboratory experiments on the Xiang'an tunnel. Later Wang (2008) analyzed the effects of chloride ion diffusion, chloride concentration and thickness of the concrete cover on the carrying capacity of the tunnel lining structure of a harbor tunnel in China. In addition, Chen et al. (2010) measured the durability of a concrete lining under the combined action of a compressive load and carbon penetration, by studying the subsea tunnel between Qingdao and Jiaozhou. Tian et al. (2012) tested the durability of a concrete lining under the combined influence of a freeze-thaw cycle and carbonation.

2.6 SUMMARY AND RESEARCH NEEDS

The following section highlights the main research needs identified by the conducted literature review.

1. Previous studies simulated only one aspect of the building while considering the SSI between tunnels and surface structures. In most cases, these studies considered the basement excavation case of the building without consideration of the building itself as a whole. In this thesis the whole building is simulated in the numerical study including its basement excavation and construction sequence.

2. Most of the previous studies did does not simulate the actions of the tunnel boring machine (TBM) during excavation, including the face and grout pressures and consequently ignored a critical aspect of the problem. In this thesis, the developed numerical model accounts for the staged construction sequence, including the interaction between the TBM machine and the surrounding soil, the applied face pressure and jacking forces, the interaction between the segmental tunnel lining and the surrounding soil, and the injection pressure of the tail void grout and its hardening with time.
3. The vast majority of existing research modelled the tunnel lining as an elastic beam or plate and has considered it as a monotonic continuous structure. In fact, the shield tunnel lining is formed by assembling prefabricated concrete segments bolted together to form rings that are erected within the tunnel bore.
4. Several existing researches studied the interaction between basement excavation and an existing tunnel by using a 2D plain strain scheme. 2D models, however, cannot simulate complex 3D geometries, the 3D nature of the excavation process, or the effects of the passage of a tunnel in the longitudinal direction. Hence, 3D modelling is essential for fully capturing all the mechanisms of ground deformations and stress redistribution induced by tunnelling.
5. Many of research available in the literature modelled the soil using elastic or elastic-perfectly plastic soil models. Linear elastic-perfectly plastic models have been found to provide slightly better predictions than the elastic models but are still incapable of fully capturing the performance. Hence, to achieve better predictions, the conducted numerical analyses should utilize an advanced, non-linear constitutive soil model to model the soil behaviour.

6. Many tunnel owners have developed restrictive guidelines including imposing an exclusion zone for the construction of foundations close to their tunnels. These guidelines are mostly based on experience, not on a fundamental understanding of this complex problem. Hence, rigorous exclusion zones and design guidelines that can be used by tunnel owners, tunnel designers and other involved professionals is needed.

Accordingly, in an effort to answer some of the current research needs highlighted above, the present thesis presents the results of a comprehensive 3D finite element exercise to investigate how newly constructed buildings supported on raft foundations affect intact and degraded pre-existing tunnel linings. Thus, a new design guideline can be developed to impose an exclusion zone for the construction of structures close to pre-existing tunnels.

2.7 REFERENCES

Amleh L. & Ghosh A. (2006). "Modeling the effect of corrosion on bond strength at the steel concrete interface with finite element analysis". Can. J. Civ. Eng., 33, pp. 673–682.

Attewell, P. B. (1978). "Ground movements caused by tunnelling in soil." Proc., Int. Conf. on Large Movements and Structures, J. D. Geddes, ed., Pentech, London, 812–948.

Attewell, P. B., Yeates, J., and Selby, A. R. (1986). Soil movements induced by tunnelling and their effects on pipelines and structures, Blackie and Son Ltd., London.

Attewell P.B. (1988). "An overview of site investigation and long-term tunnelling induced settlement in soil". Engineering Geology of Underground Movements, Bell et al. (eds.), Geological Society Engineering Geology Special Publication No. 5, 55-61.

Bjerrum, L. (1963), "Allowable Settlement of Structures," Proc., European Conf. on Soil Mech. and Found. Engr., Weisbaden, Germany, Vol. 3, pp. 135-137.

Boonpichetvong M. & Rots J.G. (2004). "Settlement damage of masonry buildings in soft ground". The Structural Engineer, 4 January, 32-37.

Boscardin M. D. & Cording, E. J. (1989). "Building response to excavation-induced settlement." J. Geotech. Eng., 115(1), 1–21.

Burland J. B. (1995). "Assessment of risk of damage to buildings due to tunnelling and excavation." Proc., 1st Int. Conf. on Earthquake Geotechnical Engineering, K. Ishihara, ed., Vol. 3, Balkema, Rotterdam, Netherlands, 1189–1201.

Burland, J.B., Broms, B. and De Mello, V.F.B. (1977) Behaviour of foundations and structures. State of Art. Report. Session 2. Proc. 9th Int. Conf. on Soil Mech. and Found. Eng., 2, pp. 495.

Burland J. B. & Wroth C. P. (1974). "Settlement of buildings and associated damage." Proc., Conf. on Settlement of Structures, Pentech Press, London, 611–654.

Calabresi G., Rampello S. & Callisto L. (1999). "Prediction of tunnel-induced displacements in historic buildings: the case of Castel S. Angelo". Geotechnical Engineering for Transport Infrastructure, Barends et al. (eds.), Balkema Rotterdam.

Chen, Jingru, Song Xiaocui, Tiejun, Zhao, Li & Tian. (2010). "Service Life Prediction of Lining Concrete of Subsea Tunnel under Combined Compressive Load and Carbonation". Journal of Wuhan University of Technology-Mater. Sci. Ed.

Frischmann W.W., Hellings J.E., Gittoes G. & Snowden C. (1994). "Protection of the Mansion House against damage caused by ground movements due to the Docklands Light Railway extension". Proc. Instn. Civ. Engrs. Geotech. Engng., April 107, 65-67.

Gulikers J. (2003). "Problems encountered in the detection of reinforcement corrosion in concrete tunnel linings – theoretical considerations". Mater. Corros., 54, pp. 454–459.

Howard, A. J. (1991). ''Report on the damaging effects of water on tunnels during their working life.'' Tunnelling and underground space technology, 6(1), pp. 11-76.

Kolmybas D. (2005). Tunnelling and Tunnel Mechanics, Springer, Berlin.

Li, Tian, Jingru, Chen, Tiejun & Zhao. (2012). “Durability of Lining Concrete of Subsea Tunnel under Combined Action of Freeze-thaw Cycle and Carbonation”. Journal of Wuhan University of Technology-Mater. Sci. Ed.

Mair, R. J., and Taylor, R. N. (1997). “Theme lecture: Bored tunnelling in the urban environment.” Proc., 14th Int. Conf. on Soil Mechanics and Foundation Engineering, Hamburg, Balkema, Rotterdam, The Netherlands, 2353–2385.

Mair, R. J., Taylor, R. N., and Bracegirdle, A. (1993). “Subsurface settlement profiles above tunnels in clays.” Geotechnique, 43(2), 315–320.

Miliziano F.M., Soccodato F.M. & Burghignoli, A. (2002). “Evaluation of damage in masonry buildings due to tunnelling in clayey soils”. Geotechnical Aspects of Underground Construction in Soft Ground, Kastner, Emeriault, Dias, Guilloux (eds.), Balkema, Rotterdam, 335-340.

Namazi E. & Mohamad, H. (2012). “Potential damage assessment in buildings undergoing tilt.” Proc., Inst. Civil Eng. Geotech. Eng., in press.

Namazi E. & Mohamad H. (2013) “Assessment of Building Damage Induced by Three-Dimensional Ground Movements”. Journal of Geotechnical and Geoenvironmental Engineering, ASCE Vol. 139 (4): 608-618.

Polshin D. E. & Tokar, R. A. (1957). “Maximum allowable non-uniform settlement of structures.” Proc., 4th Int. Conf. on Soil Mechanics and Foundation Engineering, Vol. 1, Butterworths, London, 402–405.

Potts D.M. & Addenbrooke T.I. (1997). “A structure’s influence on tunnelling-induced ground movements”. Proc. Inst. Civ. Engrs., Geotech. Engng., 125, 2, 109-125.

Schadlich, B., & Schweiger , H. (2014). *Shotcrete model. Internal report: Implementation, validation and application of the shotcrete model.* Computational Geotechnics Group, Institute for Soil Mechanics and Foundation Engineering, Graz University of technology.

Skempton A. W. & MacDonald D. H. (1956). “The allowable settlement of buildings.” Proc. Inst. Civil Eng., 5(3), 727–768.

Son M. & Cording E. J. (2005). “Estimation of building damage due to excavation-induced ground movements.” J. Geotech. Geoenviron. Eng., 131(2), 162–177.

Sun Fu. (2007). “Life Prediction of Tunnel Lining Theoretical and Experimental Study”, PhD thesis, Tongji University. China.

Yongdong & Wang (2008). “Chloride Induced Corrosion of Steel Corrosion Durability of Underground Structures”. Master thesis, Tongji University, China.

Zakhem A.M., EL-Naggar H. (2016). “Damage to Nearby Surface Structures Caused by Tunneling Induced Ground Displacements”. Conference: CSCE 2016 Annual Conference, London, Canada.

CHAPTER 3 EFFECT OF THE CONSTITUTIVE MATERIAL MODEL EMPLOYED ON PREDICTIONS OF THE BEHAVIOUR OF EARTH PRESSURE BALANCE (EPB) SHIELD-DRIVEN TUNNELS

Anna Maria Zakhem and Hany El Naggar

Published in Transportation Geotechnics, 2019, Volume (21), Elsevier Ltd

3.1 ABSTRACT

Earth pressure balance (EPB) shield-driven tunnelling involves a complex soil-structure interaction problem, where performance is heavily influenced by stress history and its development during construction. Numerical modelling must therefore focus on selecting appropriate constitutive models for soils and structures, simulating construction procedures and sequences, and modelling the soil/structure interface. Reliable numerical models to predict expected settlements, lining pressures and other design parameters are essential for safe tunnel design.

This paper discusses these factors in detail by utilizing a well-documented case study of twin tunnels in Shanghai. A 3D finite element model of the behaviour of reinforced concrete tunnel linings is developed using the new PLAXIS concrete model. Predictions of four different advanced soil constitutive models are compared with measured field results to assess the model effectiveness and suitability. The undrained behaviour of the saturated soft silty clay soil at the tunnelling site is studied during and after advancement of the shield tunnelling machine. The comparison matrix includes surface settlement troughs along transverse sections, and changes developing in earth and

pore water pressures around the tunnel. The HSSmall soil model, which accounts for increased soil stiffness at small strains, was found to be the most suitable for addressing these problems.

Keywords: numerical modelling, soft clay, tunnelling, EPB, settlement, pore water pressure, case history, soil structure, hardening soil model, HSSmall soil model, modified cam-clay soil model, soft soil model

3.2 INTRODUCTION

Closed shield tunnel boring machines (TBMs), including earth pressure balance (EPB) TBMs, are frequently used to excavate and advance tunnels under any soil conditions, especially in soft soils below the groundwater table [8]. This tunnelling method permits more stable tunnel excavation, where the excavated soil mixes with the slurry and is pumped back under pressure to stabilize the working face, thus balancing the earth pressures in the ground. The use of EPB TBMs has grown rapidly in recent decades due to advantages such as safety, control of groundwater, minimal ground movements, and operating costs lower than those for other types of shield machinery. The modelling of tunnels constructed with this method must address not only the nonlinearity and anisotropy evident in tunnelling problems in general, but also the complexities arising from the excavation sequence, including the interaction between the TBM machine and the surrounding ground, applied face pressure, jacking forces, segmental lining, and tail void grouting and injection pressure.

Surface settlement induced by tunnel excavation with EPB TBM machines is commonly estimated by using approaches ranging from simplified empirical and analytical methods, to more rigorous finite element numerical simulations. Each of these methods varies in complexity and hence in the accuracy of its predictions. In practice, empirical and analytical methods are typically used in the

early stages of the preliminary design of TBM tunnels. They are useful for quickly studying the effect of excavation process parameters on settlements and their effects on surface structures. Peck [30] and Schmidt [39] estimated the vertical surface settlement trough by utilizing a Gaussian normal distribution function. This approach was later improved by Oteo & Moya [29] and Sagaseta et al. [34], who considered additional tunnel and ground parameters such as the tunnel radius, and the soil elastic modulus and Poisson's ratio. However, the Gaussian approach cannot estimate the subsurface movement or stress distribution. Hence, Sagaseta [35] and Uriel & Sagaseta [43] developed closed-form solutions for near surface tunnels in isotropic homogeneous incompressible soil, assuming an elastic half-space. These solutions account for volumetric compressibility, the effects of ground loss, and the ovalization of the tunnel. Verrujit & Booker [46] generalized Sagaseta's solution to calculate surface settlements for tunnels excavated in a semi-infinite medium, as well as displacements and stresses throughout the elastic half-space. Loganathan & Poulos [23] enhanced Verrujit and Booker's solution by the estimating ground loss and introducing a gap parameter that accounts for the void formed around the tunnel due to over-excavation. El Naggar et al. [14] and El Naggar & Hinchberger [13] developed two closed-form solutions for composite tunnel linings in elastic ground. The first solution considers the lining and the grout annulus as an inner thin-walled shell and an outer thick-walled cylinder, respectively, embedded in elastic ground. This solution accounts for the effect of ground convergence prior to the installation of the lining. In the second solution, the analysis is extended to account for the rotational stiffness of the tunnel joints. It should be emphasised that closed-form solutions can at best yield only a rough approximation of the ground behaviour. Nevertheless, they can provide a quick and useful method of settlement prediction.

The rapid advance of computers in the last few decades has allowed researchers to develop two-dimensional (2D), and three-dimensional (3D) numerical models which utilize the finite element (FE) method with different aspects of soil behaviour to estimate short- and long-term ground settlements due to tunnelling. However, most finite element tunnelling models available in the literature are two-dimensional and assume plane strain conditions [24,15,33,41,19,20,18,9,2,44, and13]. In most of these studies, the predictions of 2D plane strain FE models are compared with field data. Plane strain analyses are generally used because they require fewer computer resources and are less time-consuming than three-dimensional analyses [5]. 2D models, however, cannot simulate complex 3D geometries, the 3D nature of the excavation process, or the effects of the passage of a tunnel in the longitudinal direction. Hence, 3D modelling is essential for fully capturing all the mechanisms of ground deformations and stress redistribution induced by tunnelling [4,6,5,45,27]. There are some key aspects which control the prediction accuracy of 3D modelling of tunnelling problems, especially for soft ground. These include the constitutive soil model employed, modelling of the tunnel lining and its material performance, and modelling of the excavation process itself, including the construction process and sequence.

Several constitutive models for soft soils are reported in the literature. The linear elastic material model has been found to be inappropriate, because the calculated displacements involve heave due to unloading effects and stress relief [32,10]. Linear elastic-perfectly plastic models have been found to provide slightly better predictions than the elastic models but are still incapable of fully capturing the performance. For example, when a linear elastic-perfectly plastic soil model was used for 2D modelling of Shanghai Metro line 2, it predicted shallower and wider surface settlement troughs than those actually observed during construction [11]. This will be discussed further below. The modified cam-clay model (MCC) used by Mair et al. [25] was also found to

predict wider and flatter settlement troughs, because soil elasticity dominates the response. In particular, the FE model used was a 2D plane strain model and did not account for the excavation sequence. In the work of these researchers, the excavation was simulated simply by reducing the radial pressure along the inside boundary of the tunnel to zero. However, recently Xia et al. [48] developed a 2D model of Shanghai Metro line 2 by using a MCC model. The predicted results matched the measured data more closely than did the results of Mair et al. [24,25], however the predicted trough settlement differed by approximately 20% from the measured data. Hence, linear elastic-plastic models and other soil models based on them predict surface settlement troughs that are too wide and shallow. The reason for this is that they cannot correctly account for the nonlinear, inelastic soil behaviour which has been shown to occur at small strains and is an essential feature of the soil-structure interaction in tunnelling [7]. Furthermore, all structural elements including the tunnel lining are typically represented in available models in the literature by linear elastic models or at best elastic-perfectly plastic material models, despite the fact that concrete behaves differently in tension than in compression.

The primary objective of this paper is therefore to develop a comprehensive 3D finite element model capable of capturing, to a great extent, the complex soil-structure interaction associated with the tunnel excavation process. The model developed accounts for a staged construction sequence, including the interaction between the TBM machine and the surrounding soil, the applied face pressure and jacking forces, the interaction between the segmental tunnel lining and the surrounding soil, and the injection pressure of the tail void grout and its hardening with time. A concrete material model newly developed in PLAXIS is utilized to model the reinforced concrete elements of the tunnel lining. The effectiveness and suitability of four different advanced soil constitutive models are also assessed, by comparing their predictions with the measured results.

The four soil models considered are: i) the hardening soil model (HS); ii) the hardening soil model with small-strain stiffness (HSsmall); iii) the modified cam-clay model (MCC); and iv) the soft soil model (SS). The undrained behaviour of the saturated soft silty clay soil at the tunnelling site was studied during and after advancement of the shield tunnelling machine. The predictions of the models developed were verified against the measured field results of the well-documented twin tunnels of the Shanghai Metro line 2 case study [21]. The comparison matrix includes surface settlement troughs along transverse sections over the short and long term, and earth and pore water pressure changes around the monitored tunnel and their development with time.

3.3 THE CASE STUDY CONSIDERED

Shanghai, the largest and probably the most developed metropolis in mainland China, has the world's most extensive rapid transit system, comprised of 16 metro lines with a total length of 644 km. This paper examines the construction of the first phase of the second metro line in Shanghai. The construction of this phase started in December 1995 and was completed in February 1999. The line extends from the Pudong district in the east, under the Huangpu River, and connects with the Puxi district in the west. It consists of twin tunnels 16.4 km long, each with an outer diameter of 6.2 m and an inner diameter of 5.5 m, excavated by earth pressure balance closed shield tunnel boring machines (EPB-TBMs). The length and thickness of the lining rings are 1 m and 0.35 m, respectively. Each ring consists of 6 precast reinforced concrete segments joined together by 16 steel bolts in the circumferential and longitudinal directions. Because the twin tunnels pass underneath one of the busiest cities in China, an extensive system of field instrumentation was installed along the tunnel to monitor the construction process and to capture any effects on nearby infrastructure. The results of the 3D FE model developed in this paper are verified against the

measured field data of section S2, located at the intersection of Chengdu Road and Nanjing Road. Lee et al. [21] describe this case study in more detail.

3.3.1 Geology

Shanghai is located roughly 70 km from the seashore, on the Yangtse River Delta in the large coastal plain bounded by the East China sea and the Yangtse River. The subsoil of these coastal lowlands is composed of a thick sequence of normally consolidated soft soils. Metro line 2 is located in this area of alluvial and marine sediments. Several boreholes were drilled along the tunnel route to investigate the subsurface conditions in the project area. Figure 3-1 shows the locations of the boreholes along cross-section C-C [22]. Figure 3-2 illustrates the complex soil deposits comprising six clayey layers, which are sandwiched between five aquifers (aquifers I to V). Aquifers I and II are interconnected, which means that their ground water level and pore water pressure change simultaneously. This paper considers the top 50 m of soil, consisting of silty clays and sand as per Lee et al. [21]. The depth of the twin tunnels of line 2 is about 15 m. The tunnels are located in a soft silty clay deposit. Table 3.1 summarizes the soil properties obtained from the ground investigation program conducted at the site [21].

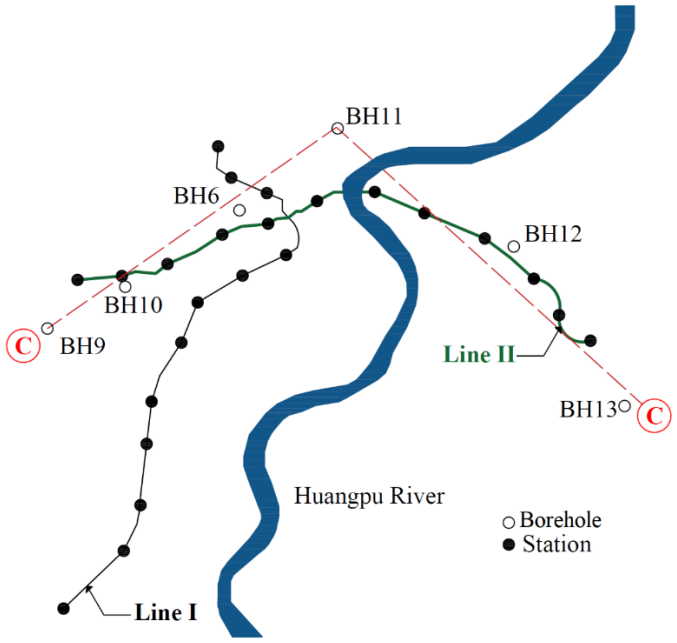

Figure 3- 1: Locations of boreholes along cross-section C-C (reproduced after [21])

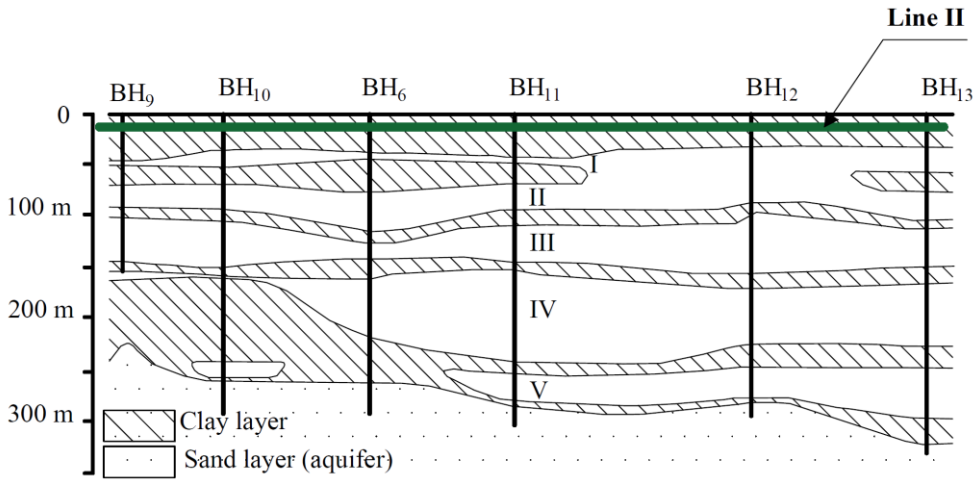

Figure 3- 2: Geological conditions along cross-section C-C (reproduced after [21])

Table 3. 1: Soil parameters obtained from the test site [21]

Layer no.	Name	Thickness (m)	Bulk density γ_{Bulk} (kN/m^3)	Specific density G_s	Water content w (%)	Void ratio e_o	Plastic index I_p (%)	Compression index C_c	Soil cohesion c' (kPa)	Coefficient of permeability k_v (m/s)	Coefficient of earth pressure at rest, K_0
1	Miscellaneous Fill	1.4 ~3.35	18.00			0.85		0.05	2	6.00E-06	0.43
2	Silty Clay	0.7~2.2	18.70	2.73	34.80	0.97	21.00	0.51	13	1.72E-09	0.46
3	Mucky-Silty Clay	3.3~4.9	18.00	2.72	40.50	1.13	17.80	0.65	7	2.18E-09	0.52
4	Mucky Clay	8.8~10.5	17.00	2.75	51.10	1.44	26.60	0.46	10	1.51E-09	0.57
5-1	Silty Clay	10.2~12.1	18.30	2.73	34.80	1.01	17.30	0.46	10	3.00E-09	0.50
5-2	Silty Clay with thin silty sand layers	10.2~12.2	18.30	2.72	33.00	0.98	22.10	0.37	20	1.42E-07	0.41
6	Silty Clay	1.8~3.8	19.90	2.72	23.80	0.70	15.10		30	3.00E-09	
7-1	Silty Sand with Silty Clay	3.7~7.0	20.10	2.70	22.50	0.64	11.20			1.57E-07	

3.3.2 Method of tunnel construction

The Shanghai Metro line 2 tunnel was constructed with earth pressure balance (EPB) tunnel boring machines (see Figure 3-3). The body of the TBM machine was 6.34 m in diameter and 6.24 m long. The most important principle of EPB is to control the removal of the soil volume into the soil chamber as the shield advances, while maintaining an equilibrium between the earth pressure inside the chamber and the earth and hydrostatic pressures outside the cutting surface. An imbalance can lead to run or flow soil conditions. The gap left between the tail skin and the lining is then injected with compensating grouting material composed of a mixture of fine round sand, fly ash, lime, and various admixtures.

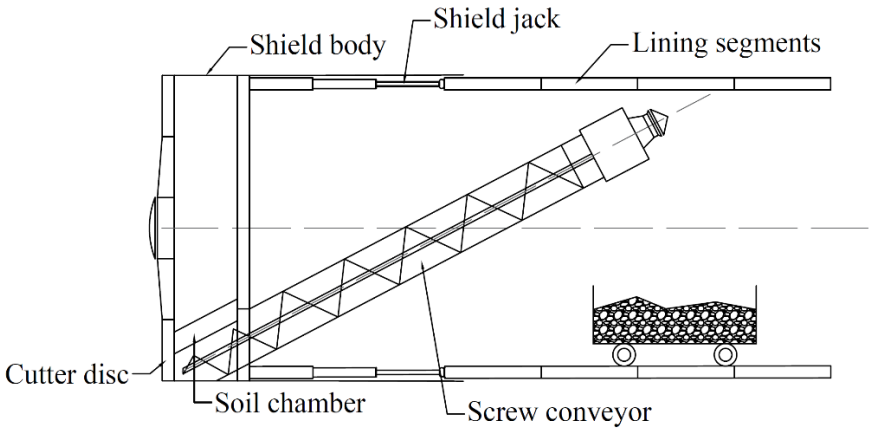

Figure 3- 3: Earth pressure balance shield tunnelling machine

3.4 SOIL/MATERIAL MODELS CONSIDERED

As mentioned above, a variety of soil constitutive models are available in the literature. These models vary in their complexity and thus in their modelling capabilities. The choice of a constitutive model depends on several aspects, of which the most important are generally the type of intended analysis, the expected precision of predictions, the expected soil behaviour, and available soil parameters.

The following section summarizes the features and capabilities of each of the four soil models considered, together with the concrete model used.

3.4.1 The hardening soil model (HS)

The hardening soil model is an advanced model capable of simulating the behaviour of different types of soft and stiff soils [38]. The HS model has superseded the hyperbolic model of Duncan and Chang [12], by using the theory of plasticity rather than the theory of elasticity (see Figure 3-4). The failure stress is determined by using the Mohr-Coulomb failure criterion. The yield surface of the hardening plasticity model is not fixed in the principal stress space and can expand due to plastic strains. In the hardening soil model, the stress dependency of soil stiffness is accurately described by using three different input stiffnesses. These are the triaxial loading stiffness, E_{50}, (see Figure 3-4(a)) which determines the magnitude of both the elastic and plastic strains; the oedometer loading stiffness, E_{oed}, (see Figure 3-4(b)) which accounts for the plastic strain due to primary compression; and the triaxial unloading/reloading stiffness, E_{ur}, (see Figure 3-4(a)) which, in conjunction with Poisson's ratio, υ_{ur}, determines the ground behaviour under unloading and reloading conditions. In Figure 3-4, σ_1 and σ_3 represent the major and minor principal stresses, c and φ are the soil strength parameters, ε_1 represents the axial strain, and p^{ref} represents the reference overburden stress. In the HS model, E_{50} is used instead of the initial modulus, E_o, for small strains. As a tangent modulus, this is more difficult to determine experimentally, and is given as:

$$E_{50} = E_{50}^{ref} \left(\frac{c \cos\varphi - \sigma_3 \sin\varphi}{c \cos\varphi + p^{ref} \sin\varphi} \right)^m \quad [1]$$

where E_{50}^{ref} is a reference stiffness modulus corresponding to the reference stress p^{ref}. The power m in the above equation reflects the amount of stress dependency. Likewise, the stress dependent stiffness modulus for unloading and reloading is given as:

$$E_{ur} = E_{ur}^{ref} \left(\frac{c \cos\varphi - \sigma_3 \sin\varphi}{c \cos\varphi + p^{ref} \sin\varphi} \right)^m \quad [2]$$

where E_{ur}^{ref} is a reference stiffness modulus for unloading and reloading corresponding to the reference stress p^{ref}.

The yield function (f_s) in the HS model is given as:

$$f_s = \overline{f_s} - \gamma^p \quad [3]$$

$$\overline{f}_s = \frac{q_a}{E_{50}} \left(\frac{(\sigma_1 - \sigma_3)}{q_a - (\sigma_1 - \sigma_3)} \right) - \frac{2(\sigma_1 - \sigma_3)}{E_{ur}} \quad [4]$$

where γ^p is the plastic shear strain and q_a is the asymptotic value of the shear strength, where $q_a = \frac{q_f}{R_f}$. R_f is the failure ratio, and q_f is the ultimate deviatoric stress given by:

$$q_f = \frac{6 \sin\varphi}{3 - \sin\varphi} (\sigma_3 + c \cot\varphi) \quad [5]$$

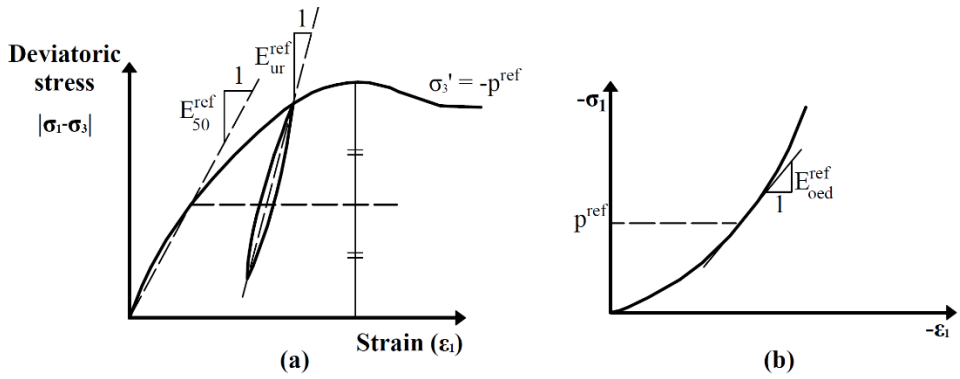

Figure 3- 4: Definitions of **(a)** E_{50}^{ref} and E_{ur}^{ref} for drained triaxial test results, and **(b)** E_{oed}^{ref} for oedometer test results

3.4.2 The hardening soil model with small-strain stiffness (HSSmall)

At low strain levels most soils exhibit a greater stiffness, which varies nonlinearly with strain and decreases to less than half of its initial value at higher strain levels. This relation is illustrated by the typical S-shaped stiffness-strain curve in Figure 3-5. This stiffness-strain relation is based on the Hardin and Drnevich [16] equation:

$$\frac{G}{G_o} = \frac{1}{1 + \left|\frac{\gamma}{\gamma_r}\right|} \qquad [6]$$

$$\gamma_r = \frac{\tau_{max}}{G_o} \qquad [7]$$

where $\frac{G}{G_o}$ is the ratio of shear modulus to the maximum shear modulus at a very small strain, and τ_{max} is the maximum shear stress at failure. The hardening soil model with small-strain stiffness (HSSmall) is an extension of the hardening soil model. The main difference is that HSSmall accounts for the increased stiffness at small strains by using two additional material parameters: (i) G_0^{ref}, the small-strain shear modulus, and (ii) $\gamma_{0.7}$, the strain level at which the shear modulus is reduced to about 70% of the small strain shear modulus [36]. In HSSmall it is also assumed that

the elastic modulus is dependent on the level of stress, as in the hardening soil model. Hence, G_o is a function of the strength parameters together with the state of stress and the reference shear modulus G_o^{ref}. Figure 3-6 shows an example of a stiffness reduction curve used in the HSSmall model.

$$G_o = G_o^{ref} \left(\frac{c \cos\varphi + \sigma_1 \sin\varphi}{c \cot\varphi + p^{ref} \sin\varphi} \right)^m \quad [8]$$

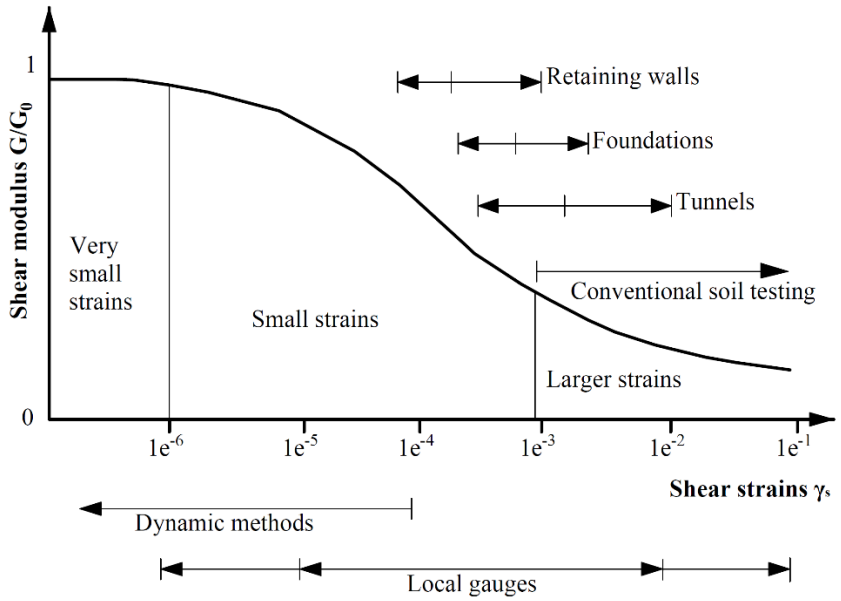

Figure 3- 5: Characteristic soil stiffness-strain behaviour, with strain ranges typical of laboratory tests and structures (after Atkinson & Sallfors [3])

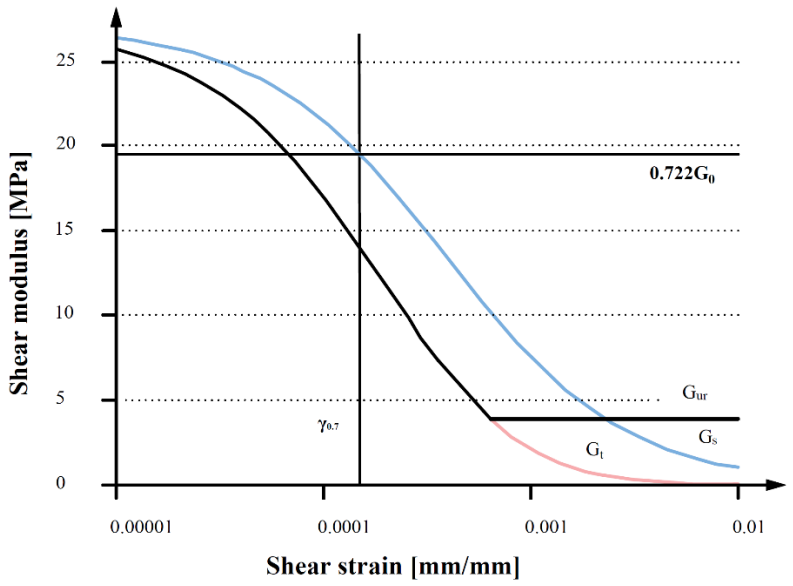

Figure 3- 6: Secant and tangent shear modulus reduction curve

3.4.3 The modified cam-clay model (MCC)

The modified cam-clay (MCC) model [31], one of the most commonly used soil models, is an elastic-plastic strain hardening model. The derivations of the MCC model utilize critical state theory, with a basic assumption that there is a logarithmic relationship between the mean stress, p', in virgin isotropic compression and the void ratio, e. In the MCC model the stiffness is assumed to increase linearly with the stress. The yield criterion of the MCC model is an ellipse. It is smooth in the p-q plane (see Figure 3-7), with a cross-section independent of the Lode angle, and is defined as a function of the pre-consolidated pressure (p_c) as described by:

$$f_y = q^2 + M^2(p' - p_c)p' = 0 \qquad [9]$$

where $p'$is the effective mean stress, and q is the effective deviatoric stress. M is the tangent of the critical state line, which determines the shape of the yield surface (height of the ellipse) and influences the coefficient of lateral pressure, K_o^{nc}, in a normally consolidated stress state under

one-dimensional compression. In this model the hardening is controlled by the pre-consolidated pressure, p_c , which depends on the volumetric strain as follows:

$$p_c = p_{co}\, e^{-B_p\, \varepsilon_{vol}} \quad [10]$$

$$B_p = \frac{1 + e_o}{\lambda - \kappa} \quad [11]$$

where p_{co} and e_o represent the initial consolidation pressure and the void ratio, respectively. ε_{vol} represents the volumetric strain, B_p is a parameter that depends on e_o, λ is the compression index which determines the compressibility of the material in primary loading, and κ is the swelling index which determines the compressibility of the material in unloading and reloading.

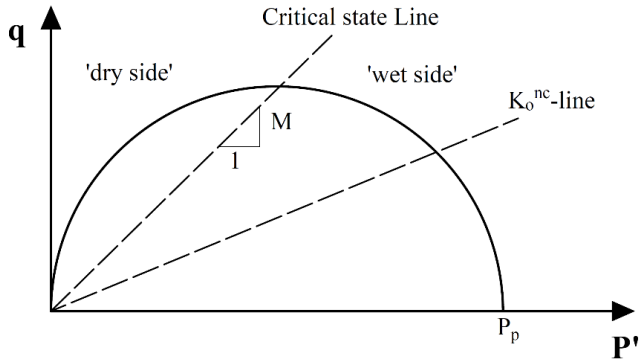

Figure 3- 7: Yield surface of the modified cam-clay model in the p'-q- plane

3.4.4 The soft soil model (SS)

The soft soil (SS) model, which is based on the MCC model, is intended mainly for primary compression of near normally consolidated clayey soils. The SS model utilizes the Mohr-Coulomb failure criterion, which is a function of the friction angle φ' and the cohesion c'. The yield function of the SS model in the p'-q' plane is an ellipse (see Figure 3-8(a)) that is dependent on the mean effective stress, p', and the effective deviatoric stress, q', together with the pre-consolidation stress, p_c , which it is determined from the plastic strain:

$$f = \overline{f} - p_c \quad [12]$$

$$\overline{f} = \frac{q'^2}{M^2(p' + c\ \cot\varphi)} + p' \quad [13]$$

$$p_c = p_{co} \exp\left(\frac{-\varepsilon_v^p}{\lambda^* - \kappa^*}\right) \quad [14]$$

where λ^* and κ^* are the modified compression and swelling indices, respectively (see Figure 3-8(b)). They distinguish between primary loading and unloading-reloading:

$$\lambda^* = \frac{C_c}{2.3(1+e)} = \frac{\lambda}{1+e} \quad [15]$$

$$\kappa^* \approx \frac{2C_s}{2.3(1+e)} = \frac{\kappa}{1+e} \quad [16]$$

where C_c is the compression index, C_s is the swelling index, e is the void ratio, and λ and κ are the cam-clay compression and swelling indices, respectively.

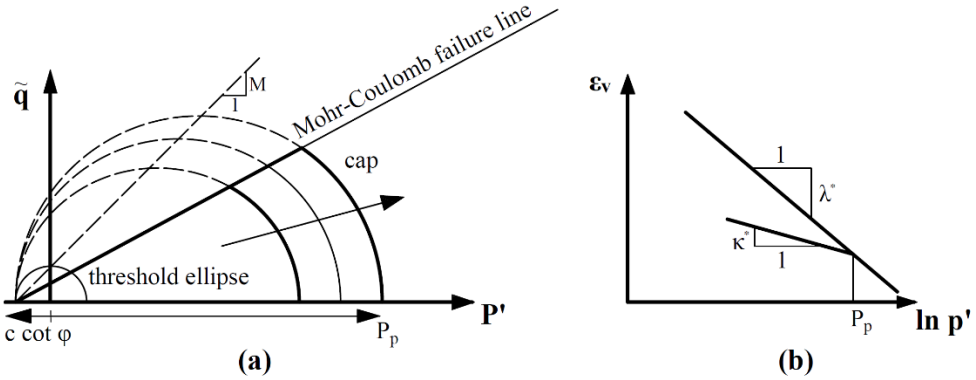

Figure 3- 8: (a) Yield surface of the soft soil model in the p'-$\tilde{q}$ plane, **(b)** Logarithmic relation between volumetric strain and mean stress

Table 3.2 summarizes the soil parameters of each four constitutive models defined previously and used in the finite element analysis.

Table 3. 2: Input parameters of the four constitutive soil models

	HS and HSSmall					MCC			SS	
Layer no.	E_{50}^{ref} (kPa)	E_{oed}^{ref} (kPa)	E_{ur}^{ref} (kPa)	G_0^{ref} (kPa)	$\gamma_{0.7}$	λ	κ	M	λ*	κ*
1	10,000	8,000	30,000	124,000	1.40E-04	0.0231	0.0111	1.418	0.0125	0.0060
2	1,111	888	7,184	29,000	3.00E-04	0.2217	0.0494	0.764	0.1126	0.0251
3	942	754	9,165	34,990	3.30E-04	0.2826	0.0418	0.760	0.1327	0.0196
4	1,525	1,220	7,026	29,270	3.30E-04	0.2000	0.0625	0.764	0.0820	0.0256
5-1	1,256	1,005	8,898	33,240	3.20E-04	0.2000	0.0407	0.814	0.0995	0.0202
5-2	1,539	1,231	6,862	28,590	3.20E-04	0.1609	0.0519	0.920	0.0812	0.0262
6	15,000	12,000	45,000	65,000	3.00E-04	0.0142	0.0068	0.764	0.0083	0.0040
7-1	20,000	16,000	60,000	75,000	3.10E-04	0.0102	0.0049	1.157	0.0062	0.0030

3.5 THE CONCRETE MODEL

Schadlich and Schweiger [37] introduced a new user-defined concrete model to PLAXIS 3D. Their concrete model is a nonlinear elastoplastic model which takes into consideration strain hardening/softening in both compression and tension, as well as the time-dependent strength and stiffness of concrete. The model is also capable of simulating the creep and shrinkage behaviour of concrete.

This concrete model utilizes the Mohr-Coulomb failure criterion for deviatoric loading and a Rankine yield surface when subjected to tensile loading conditions. In compression, the stress increases to the maximum compressive strength, $f_{c,28}$, and then softens to the residual strength; whereas in tension, the tensile stress increases linearly until reaching the ultimate tensile strength, $f_{t,28}$, and then softens to the residual tensile strength.

The behaviour is governed by two distinct yield functions in terms of the major and minor principal stresses (i.e., σ_1 and σ_3) as follows:

$$F_c = \frac{(\sigma_1 - \sigma_3)}{2} + \frac{(\sigma_1 + \sigma_3) - \sigma_{rot}}{2} \frac{f_{cy}}{2\,\sigma_{rot} + f_{cy}} \quad [17]$$

$$F_t = \sigma_1 - f_t \quad [18]$$

where f_{cy} and f_t represent the uniaxial compressive and tensile yield stresses, respectively. σ_{rot} represents the intersection of the Mohr-Coulomb failure envelope and the istropic axis, and is given by:

$$\sigma_{rot} = \frac{f_c}{2}\left(\frac{1}{\sin\varphi_{max}} - 1\right) \quad [19]$$

where φ_{max} represents the maximum inclination of the Mohr-Coulomb failure envelope, as shown in Figure 3-9.

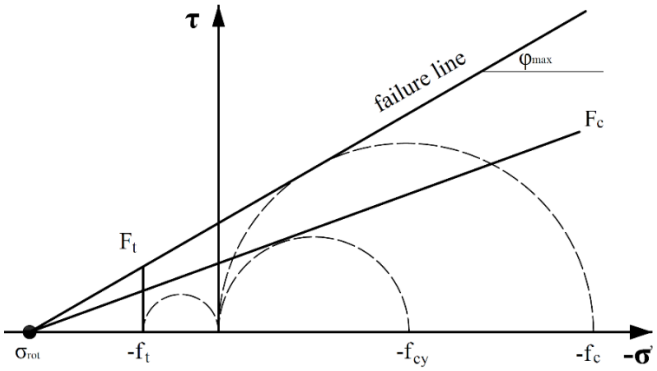

Figure 3- 9: Yield surfaces and failure envelope of the model

In compression, this model follows the approach proposed by Schutz et al. [40] where the stress-strain curve is divided into four zones, as shown in Figure 3-10(a). In tension, the behaviour is linear elastic until reaching the ultimate tensile strength, f_t, and then softens linearly to the residual tensile strength, as shown in Figure 3-10(b).

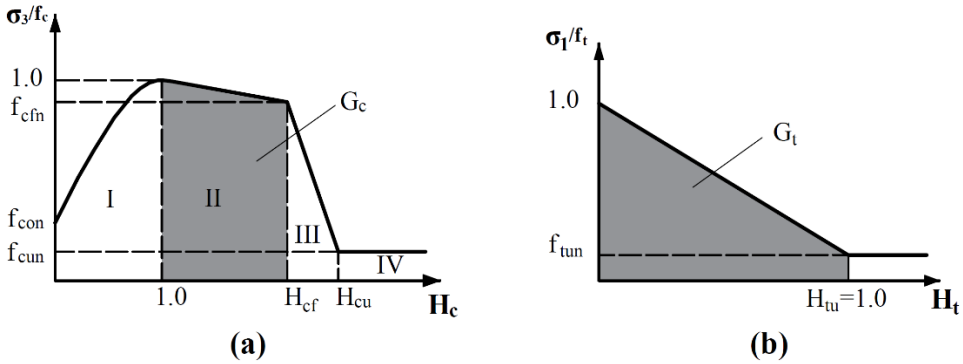

Figure 3- 10: Normalized stress-strain curve **(a)** in compression, and **(b)** in tension

The Schadlich and Schweiger [37] concrete model is a comprehensive constitutive model that involves 26 different parameters, as shown in Table 3.3. For more details, please refer to Schadlich and Schweiger [37].

Table 3. 3: Input parameters of the concrete model

Description	Value	Description	Value
Young's modulus of concrete, E_{28} (GPa)	31	Tensile fracture energy of concrete $G_{t,28}$ (kN/m)	6.9
Poisson's ratio, ν	0.15	Equivalent length (if no regularization is used), L_{eq} (m)	0
Compressive strength of concrete, $f_{c,28}$ (MPa)	45	Increase of ε_{cp} with increase of p', a (m)	18
Tensile strength of concrete, $f_{t,28}$ (MPa)	4.5	Maximum friction angle, φ_{max} (°)	37
Dilatancy angle, Ψ (°)	0	Ratio between creep and elastic strains, φ_{cr}	--
Time dependency of elastic stiffness, E_1/E_{28}	1	Time for 50% of creep strains, t_{50}^{cr}(days)	--
Time dependency of strength, $f_{c,1}/ f_{c,28}$	1	Final shrinkage strain, $\varepsilon_{\infty}^{shr}$	--
Normalized initially mobilized strength, f_{c0n}	0.15	Time for 50% of shrinkage strains, t_{50}^{shr}(days)	--
Normalized failure strength (compression), f_{cfn}	0	Safety factor for compressive strength, γ_{fc}	1
Normalized residual strength (compression), f_{cun}	0	Safety factor for tensile strength, γ_{ft}	1
Uniaxial plastic failure strain at 1h, 8h, 24h, ε_{cp}^{p}	-0.001	Time for full hydration (usually 28 days), t_{hydr}	28
Compressive fracture energy of concrete, $G_{c,28}$(kN/m)	100		
Ratio of residual vs. peak tensile strength, f_{tun}	0		

3.5.1 Verification of the concrete model used

This section summarizes the results of the study conducted to verify the newly proposed concrete model. Experimental data from the literature were used to evaluate its performance and predictability for plain concrete as well as for fiber-reinforced concrete in compression. For this

purpose, the time-dependant features of the model were muted because the behaviour compared was that of concrete at 28 days. Figure 3-11 (a) shows the mesh of the developed 3D numerical model that was used in the verification of the concrete model. The plain and fiber concrete were modelled by using higher order 10-node triangular volume elements. The verification models comprised around 980 nodes and 550 elements with an average element size of approximately 25 mm. The bottom boundary of the model was fixed in the z direction and free in the other two lateral directions. The input parameters of the plain and fiber concrete models are shown in Table 3.4.

Table 3. 4: Input parameters of the plain and fiber concrete models

	Young's modulus, E_{28} (kN/m^2)	**Compressive strength, $f_{c,28}$ (kN/m^2)**	**Tensile strength, $f_{t,28}$ (kN/m^2)**	**Compressive fracture energy, $G_{c,28}$ (kN/m)**	**Tensile fracture energy, $G_{t,28}$ (kN/m)**
Plain Concrete	$40x10^6$	$60x10^3$	3000	100	0.05
Fiber Concrete	$41x10^6$	$80x10^3$	4000	130	6.9

3.5.1.1 Stress–strain curve of plain concrete in compression

Wee et al. [47] carried out a comprehensive experimental investigation that involved testing 163 cylindrical specimens (100 x 200 mm) in a Denison closed-loop, servo-controlled hydraulic testing machine to generate stress-strain curves of concrete in compression, with a 28-day compressive strength ranging from 50 to 120 MPa. A 3D finite element model of a concrete cylinder with the same diameter and height was developed in PLAXIS for a $f_{c,28}$ of 60 MPa, by using the new concrete model. It can be seen from Figure 3-11(b) that the predictions of the proposed concrete model are in very good agreement with the experimental curve.

3.5.1.2 Stress–strain curve of fiber-reinforced concrete in compression

Mansur et al. [26] carried out an experimental investigation that involved testing 100 x 200 mm cylindrical specimens in a closed-loop, servo-controlled compression testing machine to generate stress-strain curves of high-strength fiber concrete in compression. The 28-day compressive strength of the specimens ranged from 70 to 120 MPa. The steel fibers used were Dramix hook-ended fibers of diameter Φ = 0.5 mm and length l = 30 mm, yielding an aspect ratio l/Φ of 60. Another 3D finite element model of a concrete cylinder with the same diameter and height, with $f_{c,28}$ of 80 MPa and fibre-reinforcement details, was developed in PLAXIS by using the new concrete model. It can be seen from Figure 3-11(c) that the predictions of the proposed concrete model are in excellent agreement with the experimental results.

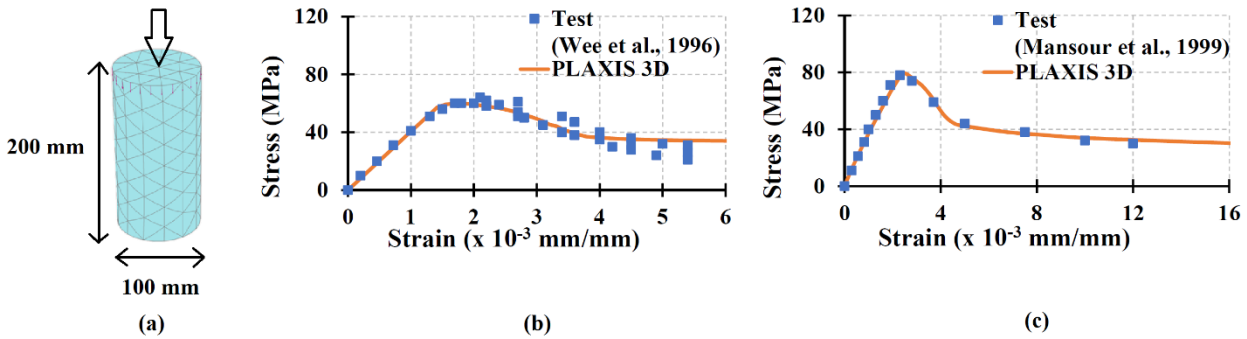

Figure 3- 11: (a) used mesh, **(b)** validation of plain concrete and **(c)** validation of fiber concrete

3.6 3D FINITE ELEMENT ANALYSIS

In order to investigate the influence of the soil model employed on predictions of the behaviour of shield-driven tunnels, four comprehensive finite element models were developed by using the commercial software package PLAXIS 3D-2017. The four models were designed to have the same geometry, layout, construction sequence and procedures as the case study under consideration, however, each of the models utilized a different constitutive soil model to simulate the soil behaviour. The predictions of the four models were then compared to the measured field results to assess the suitability of the different constitutive soil models. The comparison matrix included the surface settlement troughs along transverse sections measured at one month and three months after the construction. The ability of the finite element models to predict the pore water pressure development and the earth pressure changes around the monitored tunnel, and their development with time, was also assessed.

3.6.1 Geometry

Figure 3-12 shows the geometry of the problem under consideration. The centerline of the tunnels is located 15 m below the ground surface, in layers 4 and 5-1. Figure 3-13 shows one of the developed 3D numerical models that was used in the verification. The natural ground and the tunnel lining were modelled by using higher order 10-node triangular volume elements. The verification models comprised around 100,000 elements with an average element size of approximately 120 mm in the zone between the tunnel and the grouted annulus. The large number of small elements ensured high accuracy, especially at locations where nonlinear behaviour was anticipated.

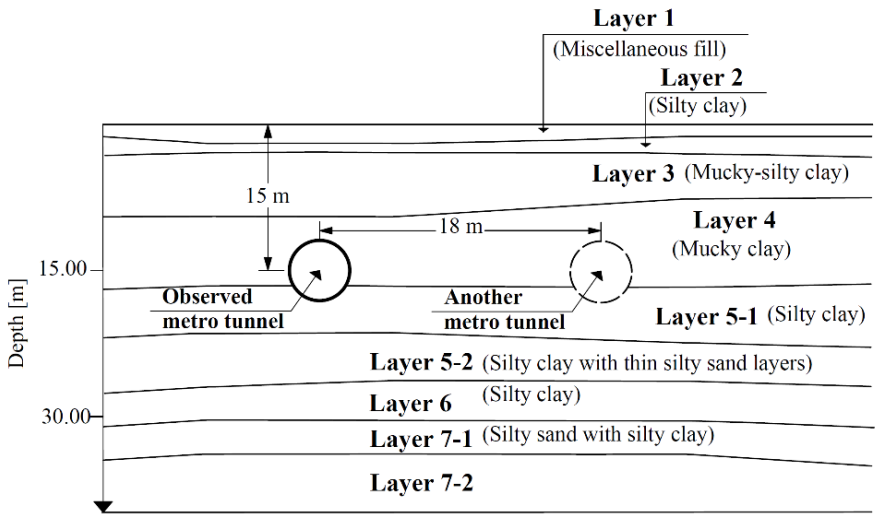

Figure 3- 12: Geological profile of the observed site (S2) (after Lee et al. [21])

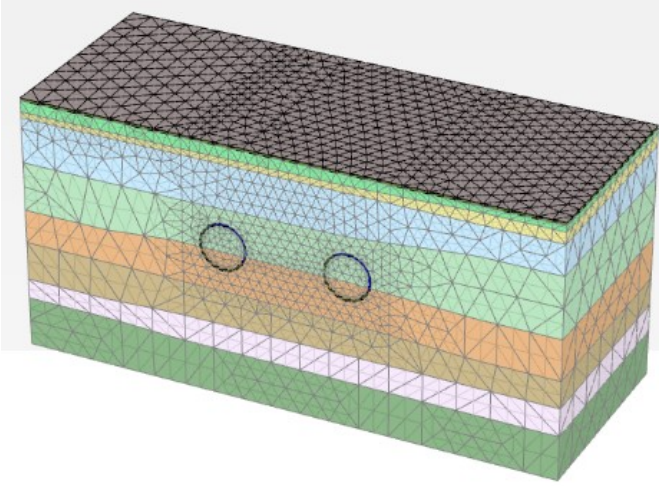

(a) The 3D mesh used

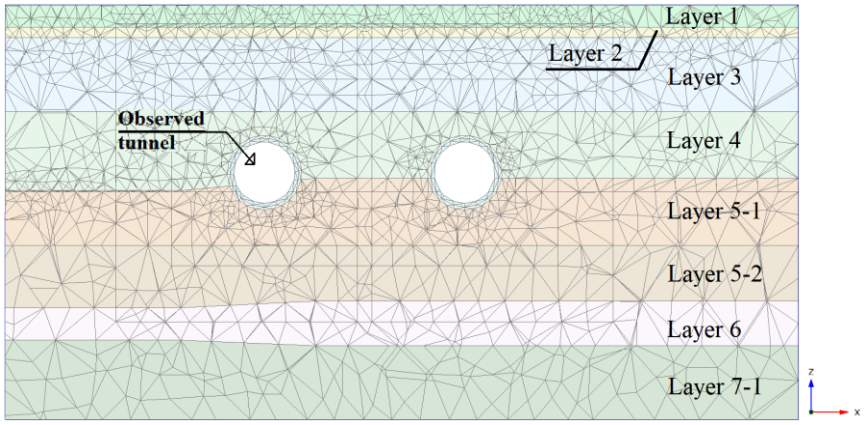

(b) Cross-section through the model

Figure 3- 13: Details of the 3D finite element model utilized for the Shanghai Metro line 2 tunnel

3.6.2 Soil stratigraphy and material model used

At the observed site, boreholes near the instrumentation section revealed that the subsurface stratification is relatively consistent, as shown in Figures 3-12 and 3-13(b). The various soil strata and their soil properties are summarized in Table 3.1. The ground water table was assumed to be 1.5 m below the ground surface, and the pore pressure was assumed to be hydrostatic with depth. The analyses were conducted assuming undrained conditions. Four different 3D models were used, each with a different type of material model: The hardening soil model (HS), the hardening soil

model with small-strain stiffness (HSsmall), the modified cam-clay model (MCC), and the soft soil model (SS). The soil parameters utilized for the four constitutive models in short- and long-term conditions were obtained from the laboratory experimental results presented by Lee et al. [21] for the Shanghai soft clay encountered.

3.6.3 Tunnel lining

Shanghai Metro line 2 consists of twin tunnels. The outer diameter of each tunnel is 6.2 m and the inner diameter is 5.5 m. A cross-section of the tunnel lining is shown in Figure 3-14. The linings were modelled as volume elements by using the nonlinear elastoplastic concrete model newly developed by Schadlich and Schweiger [37]. This concrete model accounts for strain hardening/softening in both compression and tension, as well as the time-dependent strength and stiffness of the concrete. In compression, the stress is allowed to increase to the maximum compressive strength, $f_{c,28}$, and then soften to its residual strength; while in tension, the tensile stress increases linearly until reaching the ultimate tensile strength, $f_{t,28}$, and then softens to its residual strength. Table 3.2 summarizes the concrete parameters used.

Moreover, the friction behaviours at the tunnel-grout interface and the grout-soil interface were modelled by using five-noded interface elements from the PLAXIS library, and the roughness of the interaction was modelled by utilizing a strength-reduction factor at the interface, $R_{inter} = 0.67$.

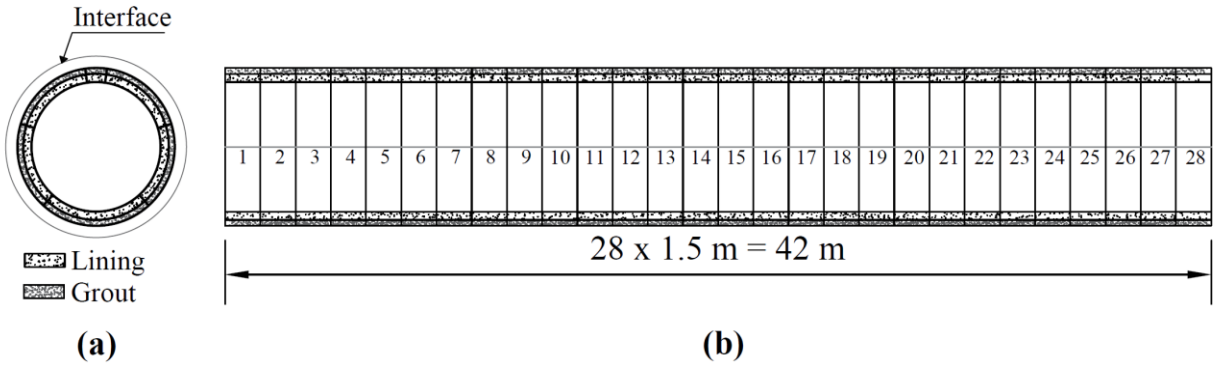

Figure 3- 14: (a) Cross-section, and **(b)** trajectory of the tunnel lining

3.6.4 Boundary conditions

A fully fixed boundary condition was assumed at the base of the models, at 21 m below the tunnel invert. In the models, the width considered was 78 m, and the lateral boundary conditions were assigned to be free in the vertical direction and fixed in the horizontal direction. These dimensions are sufficient to allow any possible collapse mechanism to develop and to avoid any influence from the model boundaries. In addition, a sensitivity analysis was performed to check the effects of the model size, the lateral boundaries, and the mesh quality (i.e., the number of elements). The analysis confirmed the suitability of the model dimensions used.

3.6.5 Numerical simulation for the tunnel construction process

The construction process of a typical EPB shield tunnel involves repetitive excavation procedures (i.e., steps) with the installation of each ring. Each step consists of several consecutive sub-steps, which must be properly modelled in the numerical simulation. The 3D finite element model developed in this study employed the following sub-steps for each excavation step: First, the soil in front of the EPB shield was excavated, and support pressure was applied at the tunnel face. The tunnel face pressure was a bentonite pressure increasing linearly with depth, with $\sigma_{n,ref}$ set to 210 kPa and $\sigma_{n,inc}$ set to 20 kPa/m. The EPB shield was then activated and the conicity of the shield was modelled. The joints were simulated in the model where the lining segments were installed

successively in the circumferential direction one after another to form a ring (each ring comprised 6 segments). Then, as the EPB machine advances in the longitudinal direction, the next ring, forms the same way with its 6 segments activated successively. This process continues for the whole construction process. In a typical EPB shield construction, cement grout is injected at the back of the shield to fill the annular gap between the extrados of the lining and the surrounding ground. In this model, the grout pressure at the back of the EPB shield resulting from the backfill grouting was set to 220 kPa at the crown, and increased with depth at a rate of 20 kPa/m. As fresh grout hardens with time and stiffens, its elastic modulus and strength increase. Thus, the applied grout pressure decreases with distance. The model accounted for this process by changing the material properties of the elements in the grouting annulus to the properties of fresh grout in the current step, half-hardened grout at the previous ring, and fully hardened grout at the ring preceding the previous ring. This process was repeated with each tunnel advancement. The grout behaviour was modeled by using the concrete model discussed above. Also, the model applied the force exerted on the already installed lining by the hydraulic jacks driving the EPB shield and modelled the installation of a new lining ring. It should be noted that the first excavation step differs from the following excavation steps, as in this step the tunnel is activated for the first time. Hence, in the first excavation step of the model the tunnel has already advanced 6 m into the soil, whereas in each of the subsequent steps, each advancement of the tunnel is only 1.5 m. Figures 3-14(b) and 3-15 illustrate the steps and sub-steps followed in the developed model.

In this study, the calculation consists of several plastic phases, following the procedure described above, to excavate the first and then the second tunnel of line 2. For the long-term study, consolidation phases were utilized.

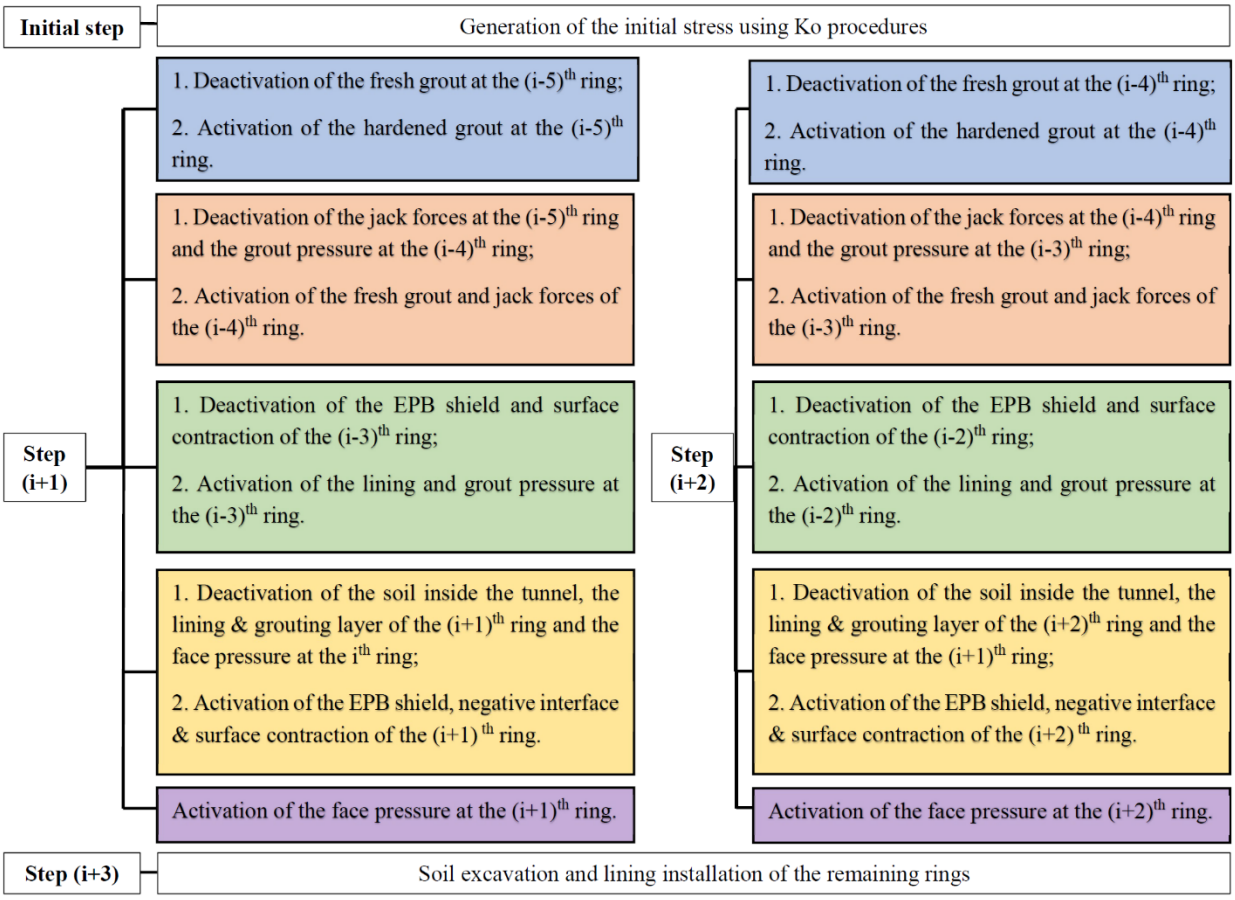

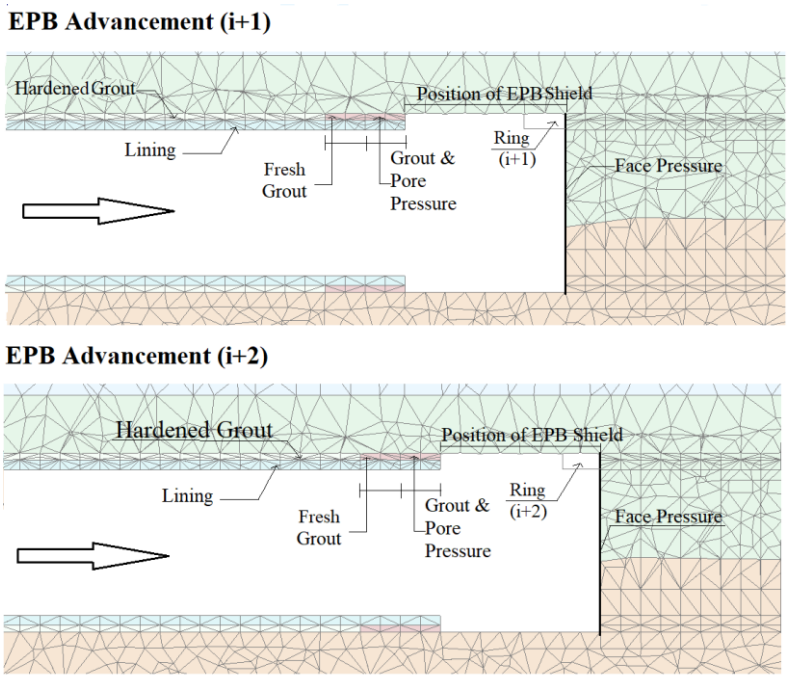

Figure 3- 15: Numerical simulation steps for the tunnel excavation

3.7 RESULTS AND DISCUSSION

3.7.1 Surface settlement troughs along transverse sections

During the approach of the tunnel shield to the instrumentation section, S2, a slight heaving of the ground was observed. This was because the soil pressure in the EPB bulkhead was equal to 210 kPa, which is larger than the in-situ total horizontal earth pressure at the tunnel axis depth, which was around 205 kPa. During the passage of the shield body, a small increase in surface settlement was detected, due to the excavation of the soil ahead. Surface settlement tended to increase while the gap that was left between the tail skin and the concrete lining ring was filled with grout material. A remarkable increase in surface settlement was observed until the dissipation of most of the excess pore water pressure.

In Figure 3-16, the predicted surface settlement obtained by utilizing the four constitutive soil material models (HSSmall, HS, MCC, and SS) is compared to the field measurements reported by Lee et al. [21]. Figure 3-16 shows the numerical predictions for surface settlement above the center line of the observed tunnel at cross-section S2 after 1 month (Figure 3-16(a)) and after 3 months (Figure 3-16(b)). The maximum vertical surface settlement above the crown after one month predicted by the HSSmall model is only 0.54% less than the measured value. On the other hand, the values predicted by the HS, SS and MCC models are 4%, 27% and 32% greater than the measured value, respectively. Hence, it can be seen that the hardening soil models (HSSmall and HS) generate realistic predictions because they account for most of features of soil behaviour, such as densification, stress-dependent stiffness, pre-consolidation effects, dilatancy, and the development of irreversible strains at yielding. In addition, the most important criterion is the incorporation of the three input stiffness parameters, E_{50}, E_{oed} and E_{ur}. Thus, the magnitude of soil deformation development and progress is accurately modelled by these models. The HSSmall

model predicted the same maximum settlement after three months as that obtained from the field measurements. The other material models failed to perform satisfactorily for long-term settlement, as their predicted settlement values were around 2.5 times or more larger than those obtained by field measurements. The enhanced features of the HSSmall model, such as the variation of stiffness with increased shear strain, and the nonlinear hysteretic stress-strain relationship in the small strain domain allowed the HSSmall model to predict the displacement trough accurately for long-term settlement (after 3 months in consolidation). In addition, as can be seen from Figure 3-16, at the right side of the observed tunnel, the HSSmall model predicted a settlement trough similar to that shown by field measurements, whereas the HS, MCC and SS models predicted a heave which did not occur in reality. It can be seen that the shape of the settlement trough is predicted very well by the HSSmall model. The advanced non-linear HSSmall constitutive model is characterized by its ability to account for high soil stiffness at very small strains. This feature played a major role in this study, because the tunnels penetrate through highly nonlinear soft soils. These observations are similar to those reported by other researchers such as Addenbrooke et al. [1], Moller & Vermeer [28] and Hejazi et al. [17] when using 2D finite element analyses. Hence, it can be concluded that precise modelling of the variation of the stiffness modulus with a change in strain level is of key importance in the modelling of EPB tunnelling problems.

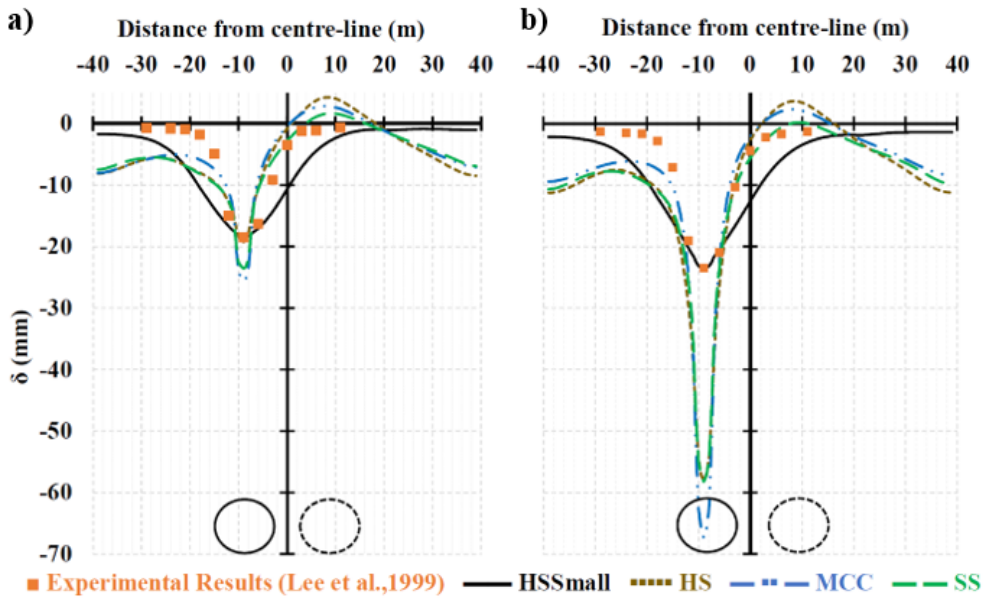

Figure 3- 16: Settlement trough at cross-section S2 **(a)** after1 month, and **(b)** after 3 months

3.7.2 Pore water pressure changes around the tunnel

Figure 3-17 shows the locations of five vibrating wire piezometers installed around the monitored tunnel. During the approach of the tunnel shield to the instrumentation section, S2, pore water pressures started to increase due to the pressure generated at the cutting face. During the passage of the shield body, the excess pore water pressures began to decrease. Throughout the grouting process, an increase of the pore pressure was observed, because the grouting pressure was greater than the total earth stress. This excess started to dissipate slowly with time after the grouting procedure commenced.

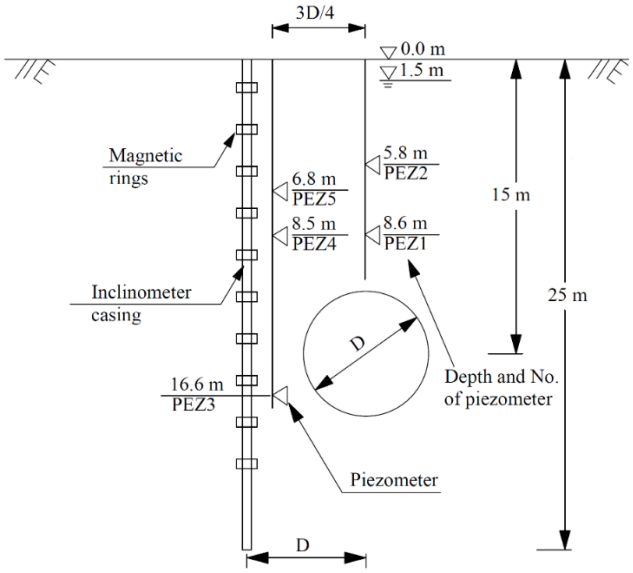

Figure 3- 17: Layout of instrumentation with respect to the cross-section of the tunnel

Figure 3-18 illustrates changes of pore water pressure with time at five piezometers over a period of 180 days. Piezometers 1 and 2 were located above the center line of the tunnel crown at depths of 8.6 m and 5.8 m respectively, and piezometers 3, 4 and 5 were located at 3D/4 away from the center line of the tunnel (where D is the diameter of the tunnel), at depths of 16.6 m, 8.5 m and 6.8 m, respectively. In Figure 3-18, the pore water pressure dissipation with time predicted by using the soil constitutive models under consideration is compared to field measurements reported by Lee et al. [21]. At the first piezometer, the pore water pressure after 180 days predicted by using the HSsmall model is within 8% of the field measurement, and the predictions of the HS, MCC and SS models are even closer to the field measurement. At the second piezometer, the pore water pressure after 180 days predicted by using the HSsmall model is within 2% of the field measurement, however, the predictions of the HS, MCC and SS models are 16%, 12% and 16% greater than the field measurement, respectively. At the third piezometer, the pore water pressure

after 180 days predicted by using the HSsmall, HS, MCC and SS models is within 2% of the field measurement. A similar trend was found for the fourth and fifth piezometers.

It can be seen from Figure 3-18 that there is a reduction of pore water pressures around the tunnel, because of the slow dissipation with time of the excess pore water pressure developed in the soil during the subsequent excavation and lining installation sequences. During the same period, as shown in Figure 3-16, additional consolidation settlement is detected on the ground surface. Changes of the pore water pressure with time change the structure of the soil body, due to shearing. The HSSmall model is again in good agreement with the field measurements. The shear hardening mechanism tends to degrade the soil stiffness in the soil model, and then a non-linear stress-strain relationship can be reproduced.

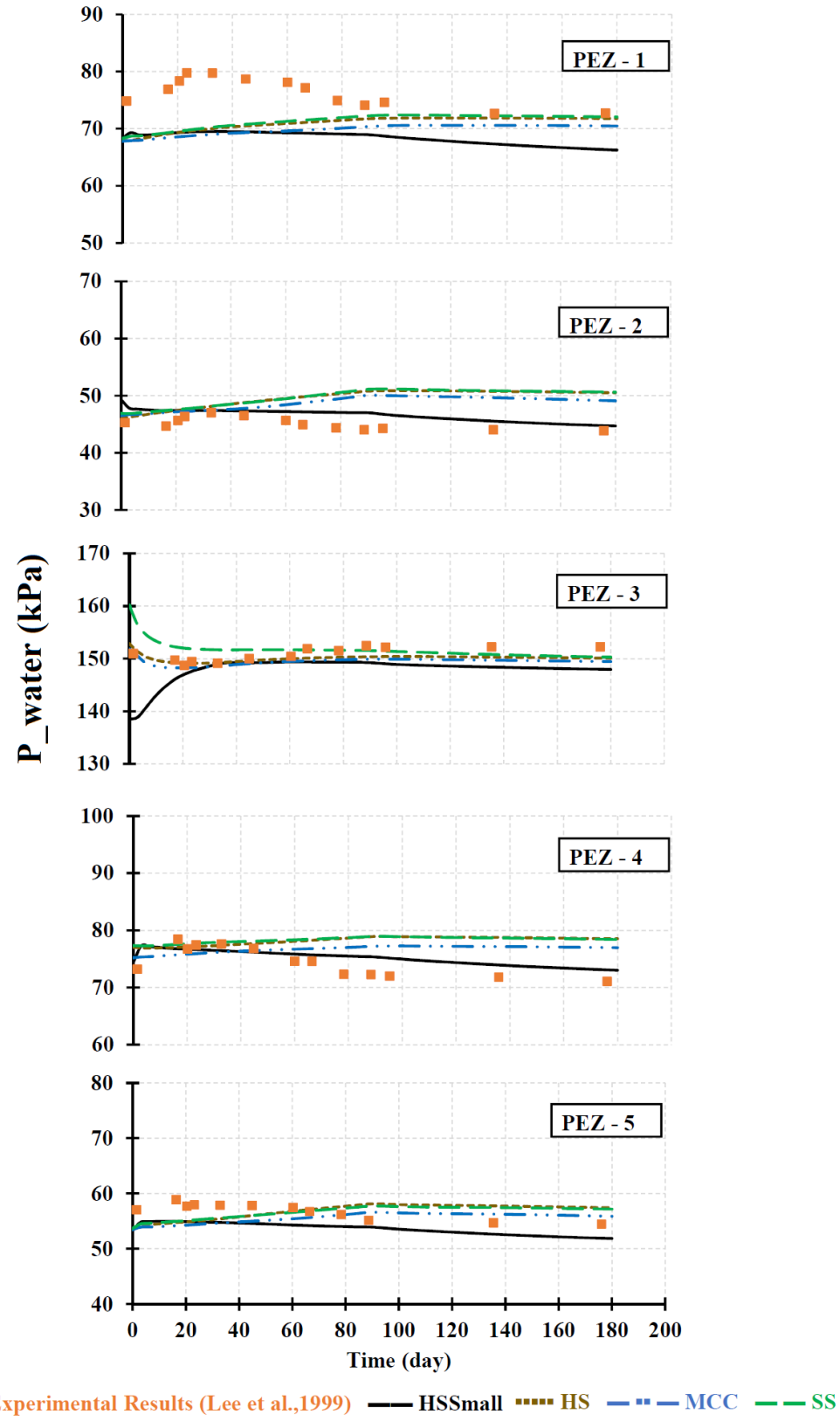

Figure 3- 18: Changes of pore water pressure with time at piezometers 1, 2, 3, 4 and 5

3.7.3 Lateral movements in directions transverse to the tunnelling direction

Figure 3-19 shows variation of the lateral displacement in directions transverse to the tunnelling direction, at 3 m away from the side of the tunnel, where an inclinometer casing was installed (see Figure 3-17). Figure 3-19(a) shows the lateral displacement at 1 month, and Figure 3-19(b) shows the lateral displacement at 3 months after excavation of the Shanghai Metro line 2 tunnel. In Figure 3-19, the lateral displacements predicted by using the four constitutive soil models are compared with the field measurements reported by Lee et al. [21]. It can be seen from Figure 3-19 that the lateral ground deflection is outward except near the ground surface, where it is inward. The maximum deflection is developed at the upper quarter of the tunnel opening. The lateral displacements found three months after the tunnel excavation differ only slightly from those found after one month, indicating that most of the lateral movement occurred in the first month following the passage of the shield machine. It can be seen that only the HSSmall model is able to mimic the shape and distribution of the lateral ground movements around the tunnel and in the vertical direction. The maximum lateral displacement after one month is overestimated by only 1 mm by the HSSmall model. All of the other models failed to produce a good prediction of either the shape or the magnitude of the measured curves. As can be seen from Figure 3-19(b), a similar trend was found for the lateral displacement after three months. It can be also seen from Figure 3-19 that the central bulge at the upper quarter of the tunnel opening predicted by the HSSmall model closely matches that of the field measurements at 1 and 3 months, and below the tunnel opening (i.e., below 20 m) the soil deflection is very slight. The improvement in the prediction of the lateral displacement profile is a result of the small strain stiffness component of the model.

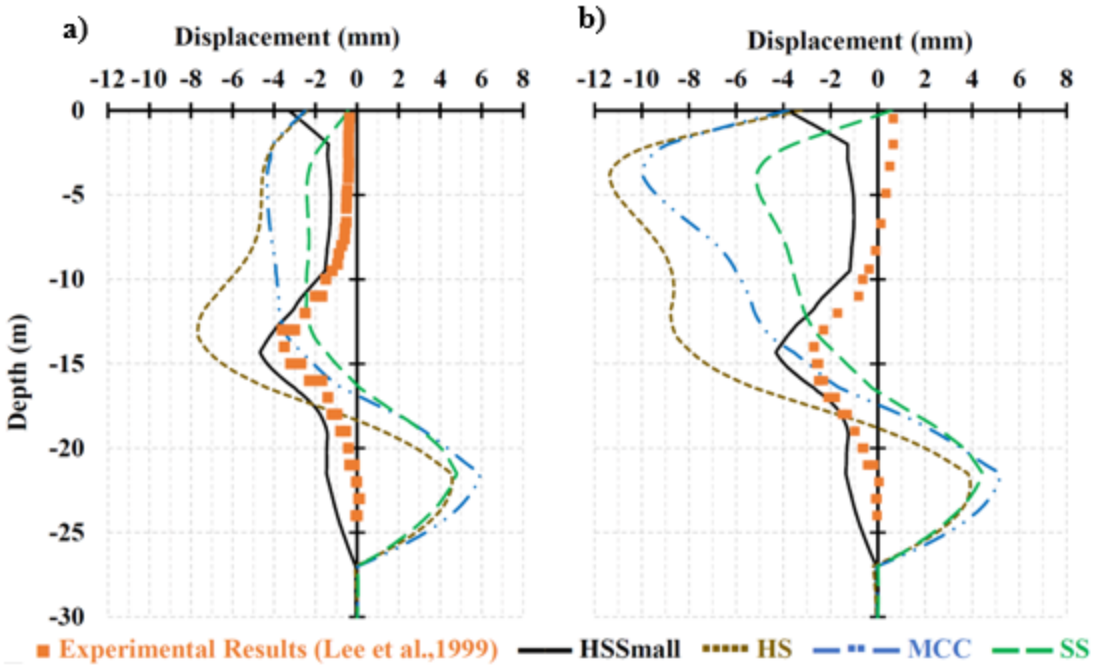

Figure 3- 19: Lateral displacement in the directions transverse to the tunnelling direction at 3 m away from the side of the tunnel **(a)** after 1 month, and **(b)** after 3 months

3.7.4 Distribution of Earth Pressure

Figure 3-21 shows the variation of total earth pressure with time at five pressure cells (see Figure 3-20) installed on the outer side of the lining segments. Figure 3-21 compares the total earth pressure distribution with time predicted by the proposed soil material constitutive models with the field measurements reported by Lee et al. [21]. It can be seen from Figure 3-21 that the decrease in earth pressure occurs gradually with time, due to the consolidation effect of the grouting material. For the first cell, the predictions of both the HSSmall and the MCC models closely match the field measurements. Weaker agreement was exhibited by the predictions of the other two models, where the difference between the predicted and measured values were in the range of 15% to 20%. For the second pressure cell, the predictions of the HSSmall model provided the closest match with the measured results. The HS, MCC and SS models overestimated the earth pressure by 17%, 14% and 22%, respectively. Similarly, for the third pressure cell, the earth pressures

predicted by the HSSmall model were within 2% of the field results, but the HS, MCC and SS models overestimated the pressures by 8%, 14% and 11%, respectively. Similar trends were found for pressure cells 4 and 5, where the HSSmall model was able to produce predictions in better agreement with the field measurements [11].

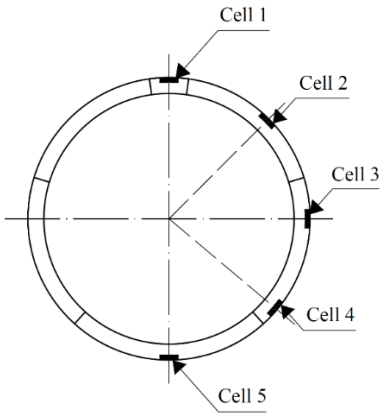

Figure 3- 20: Layout of the earth pressure cells

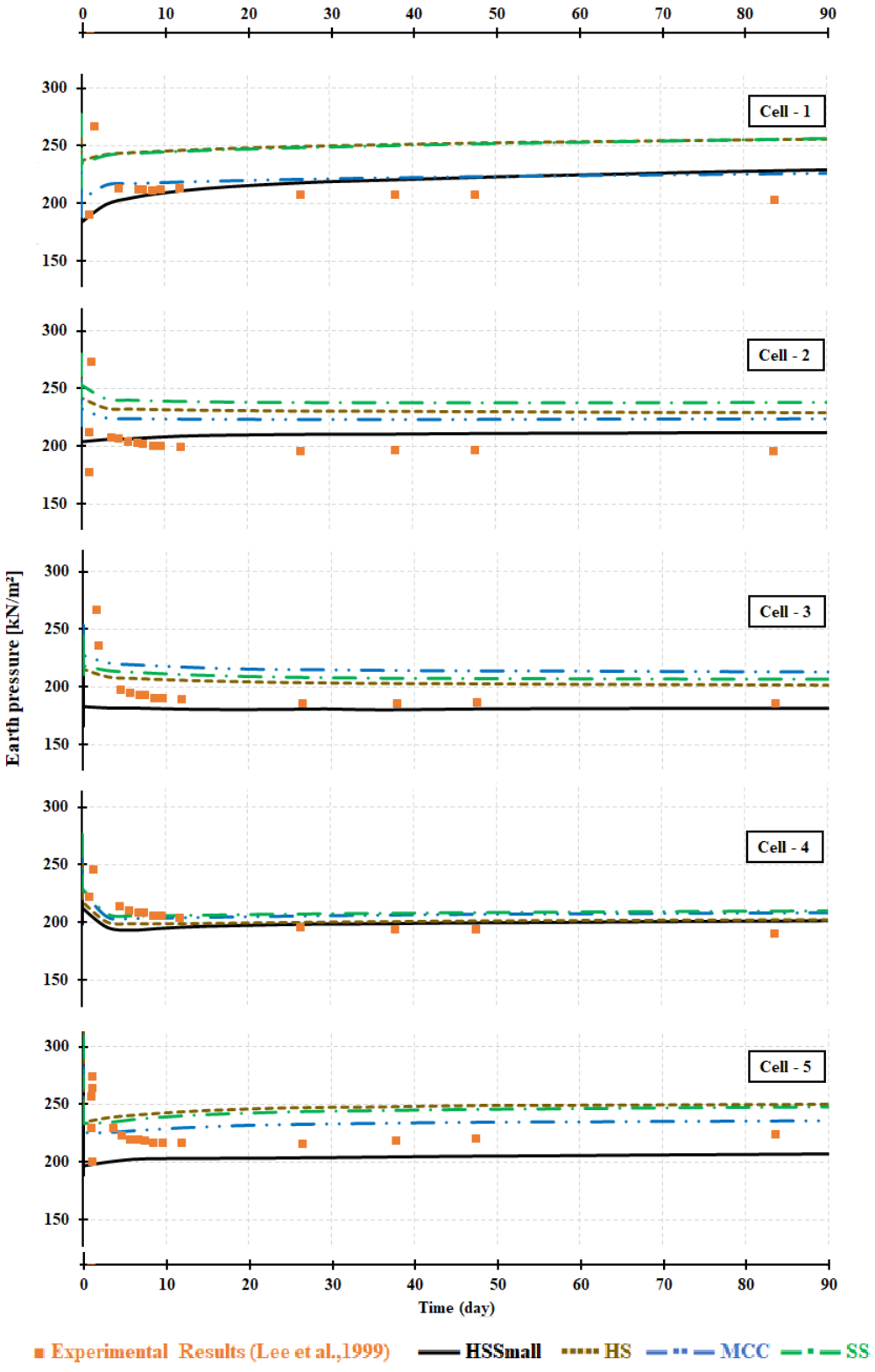

Figure 3- 21: Development of the total earth pressure around the tunnel lining

3.8 CONCLUSIONS

Reliable numerical models for the prediction of expected settlements, lining pressures and other relevant design parameters are essential for safe tunnel design. The selection of appropriate constitutive material models for soils and structures is of great importance for the precise modelling of EPB tunnelling problems. Furthermore, detailed simulation of the construction procedures and sequence is also very important. These factors are essential for the development of numerical models which can achieve reliable predictions and are effective in mimicking the actual performance of the structures.

3D finite element models were developed by using a new concrete model, to model the behaviour of concrete tunnel linings. In the FE models developed, four different advanced soil constitutive models were utilized to model the soil behaviour. The predictions of each of the models developed were compared with measured field results to assess the model effectiveness and suitability. The hardening soil model with small-strain stiffness (HSSmall) was superior to the other models under consideration in the modelling of soil behaviour. This superiority is attributable mainly to the ability of the model to mimic the variations in stiffness that accompany changes in strain level, especially at small strains. This is a key feature that governs the behaviour particularly of soft soils.

3.9 REFERENCES

[1] Addenbrooke , T., Potts , D., & Puzrin , A. (1997). The influence of prefailure soil stiffness on the numerical analysis of tunnel construction. *Geotechnique 47 (3), 693–712, 47*(3), 693-712.

[2] Addenbrooke, T., & Potts D.M. , D. (1996). Twin tunnels construction-ground movements and lining behaviour. *Proceedings of geotechnical aspects of underground construction in soft ground*, (pp. 15-7). City University, London.

[3] Atkinson, J., & Sallfors, G. (1991). Experimental determination of soil properties. *Proceedings of the 10th ECSMFE*, *3*, pp. 915-956. Florence.

[4] Attewell, P., Yeates, J., & Selby, A. (1986). *Soil movements induced by tunnelling and their effects on pipelines and structures.* Glasgow, U.K.: Blackie and Son Ltd.

[5] Augarde, C. (1997). *Numerical modelling of tunnelling processes for assessment of damage to buildings.* Oxford University Research Archive.

[6] Burd, H., Houlsby, G., Augarde, C., & Liu, G. (1994). *Prediction of tunnel-induced settlement damage to masonry structures.* Parks Road, Oxford: University of Oxford, Departement of Engineering Science.

[7] Calabresi, G., Rampello, S., & Callisto, L. (1999). Prediction of tunnel-induced displacements in historic buildings: the case of Castel S. Angelo. *Twelfth European Conference on Soil Mechanics and Geotechnical Engineering* . Amsterdam, Netherlands.

[8] Chapman, D., Metje, N., & Stärk, A. (2010). *Introduction to tunnel construction (Applied geotechnics).* Milton Park, Abingdon, Oxon; New York, NY: Spon Press.

[9] Chen, W., & Baldauf, S. (1994). Prediction of ground deformation due to excavation-Application to tunnel lining design in weak rock. *Computer Methods and advane in Geomechanics*, 2565-2570.

[10] Chow, L. (1994). *Prediction of surface settlement due to tunneling in soft ground.* M.Sc. thesis, University of Oxford.

[11] De Melo, G. P., & Pereira, S. C. (2002). Three-dimensional numerical modelling of the construction of an EPBS tunnel for Shanghai Metro - Line 2. *Geotechnical Aspects of Underground Construction in Soft Ground*, 323-328.

[12] Duncan, J. M. (1970). Non-linear analysis of stress and strain in soils. *Journal of the Soil Mechanics and Foundations Division, 96*(5), 1629-1653.

[13] El Naggar, H., & Hinchberger, S. (2008). An analytical solution for jointed tunnel linings in elastic soil or rock. *Canadian Geotechnical Journal, 45*(11), 1572-1593.

[14] El Naggar, H., Hinchberger, S., & Lo, K. (2008). A closed-form solution for composite tunnel linings in a homogeneous infinite isotropic elastic medium. *Canadian Geotechnical Journal, 45*(2), 266-287.

[15] Finno, R., & Clough, G. (1985). Evaluation of soil response to EPB shield tunneling. *Journal of Geotechnical Engineering, 111*(2), 155-173.

[16] Hardin, B. O., & Drnevich, V. (1972). Shear Modulus and Damping in Soils: Design Equations and Curves. *Geotechnical Special Publication, 98*(118).

[17] Hejazi , Y., Dias, D., & Kastner, R. (2008). Impact of constitutive models on the numerical analysis of underground constructions. *Acta Geotech. , 3*(4), 251-258.

[18] Leca, E., & Clough, W. (1992). Preliminary design for NATM tunnel support in soil. *Journal of Geotechnical Engineering, 118*(4), 558-575.

[19] Lee, K., & Rowe, R. (1990a). Finite element modelling of the three-dimensional ground deformations due to tunnelling in soft cohesive soils. Part I. Methods of analysis. *Computers and Geotechnics, 10*(2), 87-110.

[20] Lee, K., & Rowe, R. (1990b). Finite element modelling of the three-dimensional ground deformations due to tunnelling in soft cohesive soils. Part II. Results. *Computers and Geotechnics, 10*(2), 111-138.

[21] Lee, K., Ji , H., Shen , C., Liu , J., & Bai , T. (1999). Ground response to the construction of Shanghai metro tunnel-line 2. *Soils and foundations, 39*(3), 113-134.

[22] Li, Q. (2013). *Long-term settlement mechanisms of shield tunnels in Shanghai soft clay.* Hong kong: Hong Kong University of Science and Technology.

[23] Loganathan , N., & Poulos, H. (1998). Analytical prediction for tunneling-induced ground movements in clays. *J. Geotech. Geoenviron. Eng. ASCE, 124*(9), 846-586.

[24] Mair, R., Gunn, M., & O'Reilly, M. (1981). Ground movements around shallow tunnels in soft clay. *Proc. Xth Int. Conf. SMFE*, *2.* Stockholm.

[25] Mair, R., Gunn, M., & O'Reilly, M. (1982, June). Ground movements around shallow tunnels in soft clay. *Tunnels &Tunnelling*.

[26] Mansur , M., Chin, M., & Wee , T. (1999). Stress-strain relationship of high-strength fiber concrete in compression. *ASCE Journal of Materials in Civil Engineering, 11*(1), 21-29.

[27] Moeinossadat, S. R., & Ahangari, K. (2019). Estimating maximum surface settlement due to EPBM tunneling by Numerical-Intelligent approach – A case study: Tehran subway line 7. *Transportation Geotechnics, 18*, 92-102.

[28] Moller , S., & Vermeer , P. (2008). On numerical simulation of tunnel installation. *Tunn. Undergr. Sp. Technol. , 23*(4), 461-475.

[29] Oteo, C., & Moya, J. (1979). Estimation of the soil parameters of Madrid in relation to the tunnel construction. *Proc 7th Euro conf. on soil mechanics and foundation engineering*, *3*, pp. 239-47. Brighton.

[30] Peck, R. (1969). Deep excavation and tunneling in soft ground. State-of-the-art report. *Proc 7th int. conf. soil mechanics and found engineering*, (pp. 225-90). Mexico.

[31] Roscoe, K., & Burland, J. (1968). On the Generalized Stress-Strain Behavior of Wet Clays. *J. Heyman, F. Leckie (Eds.), Engineering plasticity, Cambridge University Press*, (pp. 535-609). Cambridge.

[32] Rowe, R., & Kack, G. (1983). A theoretical examination of the settlements induced by tunnelling: four case histories. *Canadian Geotechnical Journal, 20*, 299-314.

[33] Rowe, R., & Lee, K. (1989). Parameters for predicting deformations due to tunnelling. *Proceedings, 12th International Conference on Soil Mechanics and Foundation Engineering*, (pp. 793-796). Rio de Janeiro.

[34] Sagaseta , C., Moya, J., & Oteo, C. (1980). Estimation of ground subsidence over urban tunnels. *Proc 2nd conference on ground movement and structure*, (pp. 331-44). Cardiff.

[35] Sagaseta, C. (1988). Discussion on: Sagaseta C.: "Analysis of undrained soil deformation due to ground loss". Author's replay to B. Smhmidt. *Géotechnique, 38*(4), 647-649.

[36] Santos, J., & Correia, A. (2001). Reference threshold shear strain of soil, its application to obtain a unique strain-dependent shear modulus curve for soil. *Proceedings of the 15th International Conference on Soil Mechanics and Geotechnical Engineering*, *1*, pp. 267-270. Balkema, Istanbul.

[37] Schadlich, B., & Schweiger , H. (2014). *Shotcrete model. Internal report: Implementation, validation and application of the shotcrete model.* Computational Geotechnics Group, Institute for Soil Mechanics and Foundation Engineering, Graz University of technology.

[38] Schanz, T. (1999). Formulation and verification of the Hardening-Soil Model. *RBJ Brinkgreve, Beyond 2000 in Computational Geotechnics*, 281-290.

[39] Schmidt, B. (1969). Prediction of settlements due to tunneling in soil: three case histories. *Proc 2nd rapid excavation tunneling conference*, (pp. 801-12). San Francisco, CA.

[40] Schütz, R., Potts, D., & Zdravkovic, L. (2011). Advanced constitutive modelling of shotcrete: Model formulation and calibration. *Computers and Geotechnics, 38*(6), 834-845.

[41] Swoboda, G., Mertz, W., & Schmid, A. (1989). Three dimensional numerical models to simulate tunnel excavation.

[42] The hardening soil model (isotropic hardening). (2018). In *Material models manual* (pp. 69-83). PLAXIS.

[43] Uriel , A., & Sagaseta, C. (1989). Selection on design parameters for underground construction. *Proc. of the 12th international congress on soil mechanics, Rio de Janeiro*, *9*, pp. 2521-2551. Balkema, Rotterdam.

[44] Van Jaarsveld, E., Plekkenpol, J., & Messemaeckers van ed Graa, C. (1999). Ground deformations due to the boring of the second Heinenoord tunnel. *Twelfth European Conference on Soil Mechanics and Geotechnical Engineering* . Amsterdam, Netherlands.

[45] Vermeer , P. (2001). On a smart use of 3D-FEM in tunnelling Plaxis Bulletin (11), 2-7. *11*, 2-7. Plaxis Bulletin .

[46] Verrujit, A., & Booker, J. (1996). Surface settlements due to deformation of a tunnel in an elastic half plane. *Géotechnique, 46*(4), 753-756.

[47] Wee , T., Chin , M., & Mansur , M. (1996). Stress-strain relationship of high-strength concrete in compression. *ASCE Journal of Materials in Civil Engineering, 8*(2), 70-6.

[48] Xia, B., Hong, Z.-S., & Ding, J.-W. (2016). Evaluating the effect of soil structure on the ground response during shield tunnelling in Shanghai soft clay. *Tunnelling and Underground Space Technology, 58*, 120-132.

CHAPTER 4 THREE-DIMENSIONAL INVESTIGATION OF HOW NEWLY CONSTRUCTED BUILDINGS SUPPORTED ON RAFT FOUNDATIONS AFFECT PRE-EXISTING TUNNELS

4.1 ABSTRACT

In densely populated areas, there is increasing construction of high-rise buildings adjacent to existing tunnels. The interactions involved are complex. Based on experience and field monitoring, many tunnel owners impose exclusion zones for construction close to their tunnels. This paper studies the effect of a newly constructed building supported by a shallow foundation on an intact pre-existing tunnel. With the aid of PLAXIS software, a detailed three-dimensional finite element analysis is used to conduct a parametric study showing the interaction between the burial location of the pre-existing tunnel and the new shallow foundation. The intact concrete lining is modelled by using the newly developed concrete model included in the PLAXIS user-defined library. The model considers the non-linearity of the material behaviour and the distinction between strength in tension and compression. The constitutive soil where the tunnel system is constructed is simulated by using a hardening soil model with small-strain stiffness, which accounts for increased stiffness at small strains. The construction of the tunnel is divided into several phases, where each phase is simulated with the advancement of the shield boring machine. Accordingly, new design guidelines can be developed for shallow foundations in close proximity to pre-existing tunnels.

Keywords: three-dimensional analyses, shallow foundation, existing tunnel, small-strain stiffness, new user-defined concrete model, stage construction, exclusion zone.

4.2 INTRODUCTION

According to a 2018 United Nations report, the number of people living in urban areas will grow to 2.5 billion by 2050 (United Nations, 2018). This will result in an increased demand for housing, transportation and other public services. The fact that land in megacities is scarce and expensive has led to the construction of high-rise buildings with basements very close to pre-existing tunnels. Influence of newly constructed adjacent buildings is of major interest for tunnel operators in urban areas, due to the high level of interaction between the substructure of the buildings and existing tunnels (Doležalová 2001; Sharma et al. 2001; and Devriendt et al. 2010). New developments adjacent to pre-existing tunnels disturb the stress path in the ground, which can affect the durability and safety of the tunnels. The associated soil-structure interaction (SSI) can reduce or increase the vertical or horizontal tunnel lining diameter, causing ovalization or squat phenomena. This can imply spalling at segment joints and cracking at various locations around the tunnel lining. It could also cause openings at the radial joints, resulting in the entry of saline water that could lead to significant concrete degradation in the form of extensive concrete delamination and steel deterioration. As well, additional water could lead to the flooding of the tunnel (Doran et al. 2000). For example, excavation for a high-rise building with a basement five levels deep to the east of the Taipei Rapid Transit System (TRTS) tunnels in Taiwan damaged a section of the tunnel. This is an example of a damage case history resulted from the construction of a new building over a pre-existing tunnel (Chang et al. 2001).

This interaction problem was previously investigated using a combination of in situ observations and/or numerical modelling. However, previous studies only considered the basement excavation case without consideration of the building itself as a whole. For instance, a series of field tests were conducted to study the effect of basement excavation on adjacent existing tunnels. Burford

(1988) found that excavation of the Shell Centre basement over Bakerloo line tunnels has led to long-term heave of the London clay. Lo and Ramsay (1991) investigated the influence of the construction of phase III of the York Mills Centre above the Toronto Transit Commission (TTC) subway tunnels. By using a finite layer analysis program (FLANS), they highlighted the importance of the soil deformation modulus parameter in unloading and emphasized that construction procedures and monitoring programs must be carefully executed in the case of construction over existing tunnels. In 2002, Abdel-Meguid et al. (2002) studied the same Lo and Ramsay project. By using a 3D elasto-plastic finite element program and a 2D plain strain analysis, they showed the importance of performing 3D analyses in such cases. Good agreement was found when comparing the results with the field measurements. Doležalová (2001) used the 2D CRISP-90 FEM code to evaluate the influence of a deep excavation on Prague underground railway tunnels. Three tunnels were at a depth of 20 m, and two were at a depth of 35 m. The results were compared with field measurements and interpreted by performing a stress path analysis. Sharma et al. (2001) evaluated the effect of excavating a large hospital basement near Singapore's Mass Rapid Transit (MRT) system. By performing a 2D plain strain model analysis with the aid of the CRISP FE program, they compared the finite element analysis results with field measurements. They found that the FE results were overestimated and highlighted the role of lining stiffness in the lining displacement and distortion. Zheng and Wei (2008) performed a 2D plain strain model analysis by using the FE program ABAQUS to study the effect of an overlying pit excavation on existing tunnels. They concluded that the most complex case occurred when the center of the tunnel was located under the center of the diaphragm wall. Devriendt et al. (2010) performed a 3D finite element analysis by using the program LS-DYNA to assess the effect of demolition, excavation of a new basement, and construction of a new development on the nearby London Underground

Central line. They found good agreement between the results of the FEA and field measurements. By using the 3D FE program ABAQUS, Wang et al. (2013) evaluated the effect of excavating an underpass above an existing tunnel in Shanghai and compared the FE results with the field data. Shi et al. (2015) performed a 3D numerical analysis to examine the effect of excavating a basement in dry sand over an existing tunnel.

Most previous research has modelled the tunnel lining as an elastic beam or plate and has considered it as a continuous structure. In fact, the shield tunnel lining is formed by assembling prefabricated concrete rings bolted together and erected within the tunnel bore. Usually, a tunnel ring has a length of approximately 1 to 2 m. During the construction of a lining segment, the boring machine remains stationary. Once the placement of the segment is complete, the machine resumes excavation for the placement of the next ring. For this reason, in this study, tunnel construction is divided into several phases. Each phase simulates the advancement of the shield boring machine. The pressure at the face of the tunnel should be assigned so as to maintain an equilibrium between the pressure inside the machine chamber due to the excavated soil, and the earth pressure outside the cutting surface. Other aspects simulated include the shape of the machine, which is conical in most cases; injection of the grouting material in the gap left between the tail skin and the lining; the hydraulic jack forces driving the machine, which are exerted on the already installed lining; and installation of the new lining with an equivalent grout layer behind. Other researchers have studied the interaction between basement excavation and an existing tunnel by using a 2D plain strain scheme and have modelled the soil as elastic or elastic-perfectly plastic. However, models which assume that the soil is elastic or elastic-perfectly plastic may not be capable of modelling the different interactions in the soil during the tunnel excavation.

The present research conducts a 3D finite element parametric analysis to investigate how newly constructed buildings supported on raft foundations affect intact pre-existing tunnel linings. Various tunnel configurations are considered, with the aid of the finite element program PLAXIS 3D (2018). The behaviour of tunnel concrete lining elements is assumed to obey the newly developed concrete model in PLAXIS 3D, which takes into consideration the non-linearity of the material behaviour, and the strain hardening or softening in both compression and tension that is particularly relevant for modelling concrete. In addition, the conducted numerical analyses utilized an advanced, non-linear constitutive soil model to model the soil behaviour. The used hardening soil model with small-strain stiffness (HSSmall) accounts for increased stiffness at small strains. Ng et al. (2015) used a centrifuge model test and concluded that a constitutive model which can capture variations in soil stiffness with the strain and stress path could offer a better prediction of soil heave during the excavation of a basement adjacent to an existing tunnel. Thus, a new design guideline can be developed to impose an exclusion zone for the construction of structures close to pre-existing tunnels.

4.3 THREE-DIMENSIONAL FINITE ELEMENT PARAMETRIC ANALYSIS

With the aid of the software PLAXIS 3D, three-dimensional finite element analyses were performed to study the interaction between a newly constructed building on a mat foundation and a pre-existing tunnel in a sandy layer. In this study, the thrust force, bending moment, and vertical and horizontal displacements of the tunnel lining were investigated. In addition, the maximum and differential settlements underneath the building foundation were examined.

4.3.1 Numerical analysis program

The relationship between a newly constructed building supported on a raft foundation and the burial location of an intact existing tunnel was examined by conducting a parametric study. The problem considered involves a high-rise building (20 stories with one basement) on a raft foundation that rests on a thick sandy layer. The main structural system of the high-rise building consists of flat slabs of uniform thickness connected to columns (without the use of beams). The gravity and lateral loads are withstood by the lift shear walls shown in Figure 4-1. A large number of three-dimensional finite element runs was performed. In each run, the burial location of the existing tunnel was changed. Thus, burial depths ranging from 1D to 6D (where D is the tunnel diameter) in the vertical direction, and locations from 0D (with the tunnel center directly beneath the centerline of the shallow foundation) to 10D in the horizontal direction were examined. The FE model considered has a depth of 60 m and extends 160 m in the x-direction and 100 m in the y-direction. These dimensions are sufficient to allow the development of any possible collapse mechanism and to avoid influence from the model boundaries (see Figures 4-1 and 4-2).

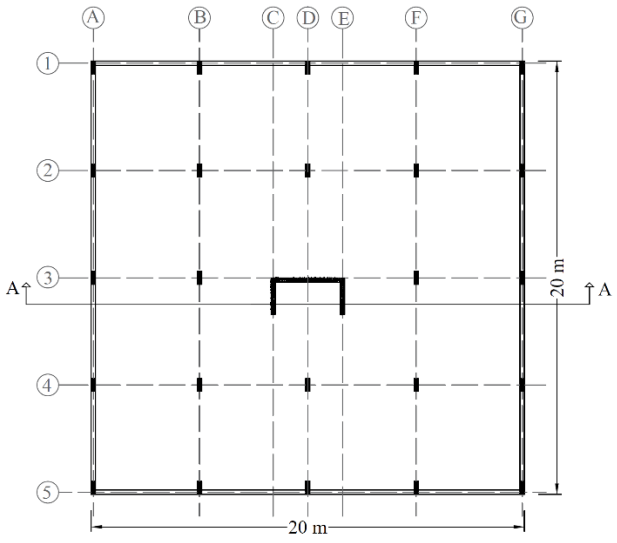

Figure 4- 1: Plan view of high-rise building

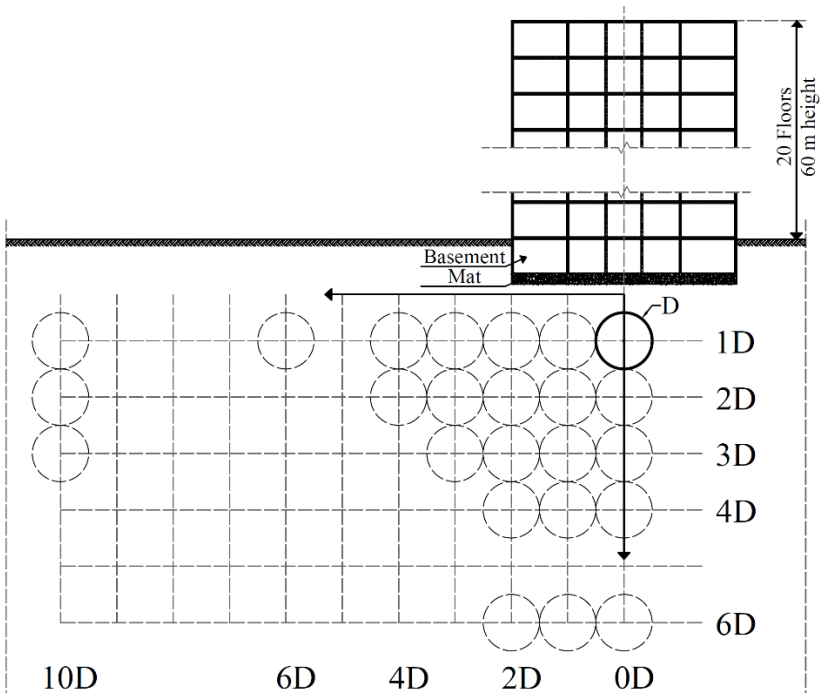

Figure 4- 2: Design of the parametric study

4.3.2 Typical finite element mesh

Figure 4-3 shows a typical mesh generated for the model. To ensure high-quality results, the FE mesh was refined in close proximity to the tunnel, and near locations where non-linear behaviour was expected. The model was built by using approximately 350,000 elements. The sand stratum and existing tunnel volumes were modelled by means of 10-node tetrahedral elements. The newly constructed building was simulated utilizing plate elements, except for the columns, which were simulated using beam elements. The bottom boundary of the model was fixed in all directions. Vertical model boundaries parallel to the yz-plane were fixed in the x-direction, and those parallel to the xz-plane were fixed in the y-direction.

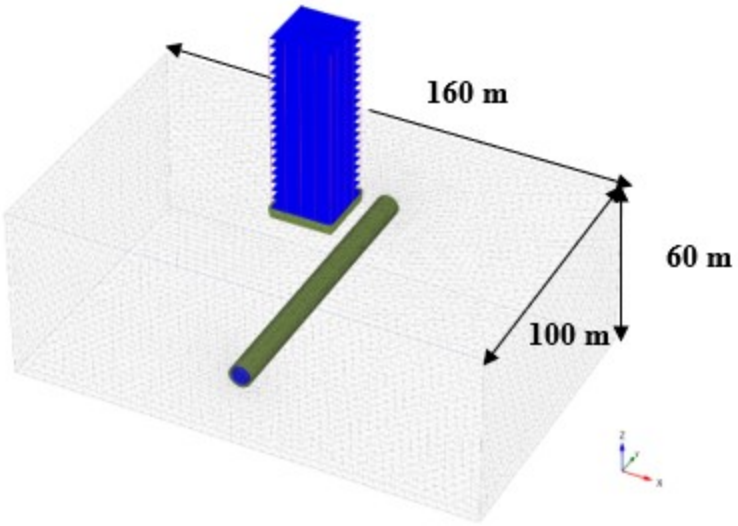

Figure 4- 3: Typical three-dimensional finite element mesh

4.3.3 Simulation of the tunnel construction process

A cross-section of the tunnel lining is shown in Figure 4-4. The outer diameter is 5.5 m, and the inner diameter is 5 m. The tunnel lining is assumed to obey the concrete model, a new constitutive model in the PLAXIS software, where the non-linearity of the material behaviour is considered, and more realistic stress distributions can be obtained. Table 4.1 summarizes the used tunnel lining material parameters. Interface elements permitting the occurrence of either slippage or gapping were used to model the interface between the soil and the tunnel lining.

The tunnel is assumed to have been driven by using a tunnel boring machine (TBM). A schematic diagram of the TBM shield is presented in Figure 4-5. An imbalance between the earth pressure inside the TBM soil chamber and the earth and hydrostatic pressures beyond the cutter disc leads to a flow of the soil conditions. Thus, controlling excavation of the soil is an important TBM concept. Grouting material is used to infuse the gap left between the tunnel lining and the tail skin. The behaviour of fresh and hardened grouting materials was simulated by a linear elastic model

with moduli of elasticity of 2 GPa and 10 GPa, respectively, a Poisson's ratio (ν) of 0.2, and unit weight of 18 kN/m^3.

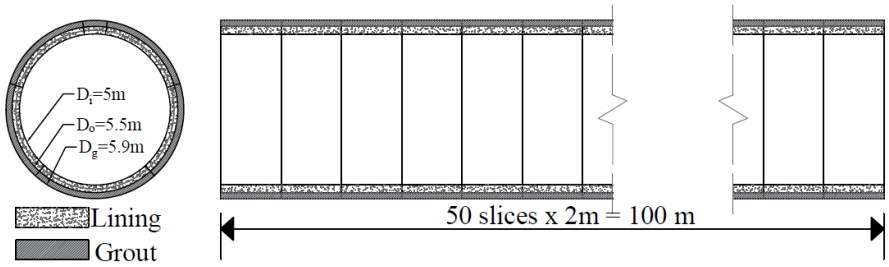

Figure 4- 4: Transverse and longitudinal cross-sections of the tunnel

Table 4. 1: Summary of the tunnel lining material parameters adopted for the finite element analysis

Unit weight, γ (kN/m^3)	25
Young's modulus of cured shotcrete at t_{hydr}, E_{28} (kN/m^2)	31 x 10^6
Poisson's ratio, ν	0.15
Uniaxial compressive strength of cured shotcrete at t_{hydr}, $f_{c,28}$ (kN/m^2)	45 x 103
Uniaxial tensile strength of cured shotcrete at t_{hydr}, $f_{t,28}$ (kN/m^2)	4,500
Time dependency of elastic stiffness, E_1/E_{28}	1
Time dependency of strength, $f_{c,1}/ f_{c,28}$	1
Normalized initially mobilized strength, f_{c0n}	0.15
Uniaxial plastic failure strain at 1h, 8h, 24h, ϵ_{cp}^{p}	-1 x 10^{-3}
Compressive fracture energy of cured shotcrete at t_{hydr}, $G_{c,28}$ (kN/m)	100
Tensile fracture energy of cured shotcrete at t_{hydr}, $G_{t,28}$ (kN/m)	6.9
Increase of εcp with increase of p', a (m)	18
Maximum friction angle, φ_{max} (°)	37
Safety factor for compressive strength, γ_{fc}	1
Safety factor for tensile strength, γ_{ft}	1
Time for full hydration, t_{hydr} (days)	28

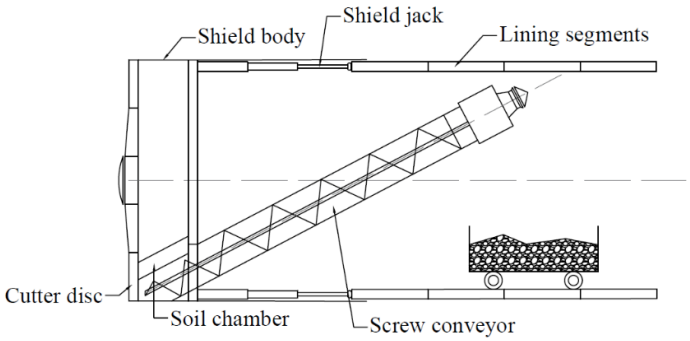

Figure 4- 5: Tunnel boring machine (TBM) schematic cross-section

Figure 4-6 defines the sequencing of the tunnel construction. The sequencing simulation procedures can be summarized in detail as follows.

Step_1, face excavation: The volume inside the tunnel is excavated, and the water conditions are set to dry. At the outer surface, the TBM shield, negative interface, and surface construction are activated. All the surface loads in the front plane are activated to simulate the face pressure.

Step_2, TBM shield with conicity: The remaining conical part of the TBM shield is defined. The face pressure in the front plane is deactivated.

Step_3 and Step_4, TBM shield with constant shield diameter and tail: The last two parts of the shield have a constant diameter. Hence, the surface contraction at the outer surface is set to uniform.

Step_5, grouting and jack thrusting: At the outer surface, the TBM shield and surface contraction are deactivated. For the outer volumes, the lining is activated, and the fresh grout with defined pore water conditions is activated, simulating the pressure due to the back-fill grouting. At the rear plane, the surface load simulating jack thrusting is activated.

Step_6, pre-final lining: Water conditions of the fresh grout material are set to dry, and the jack forces are deactivated.

Step_7, final lining: The fresh grout material is reset to hardened grout.

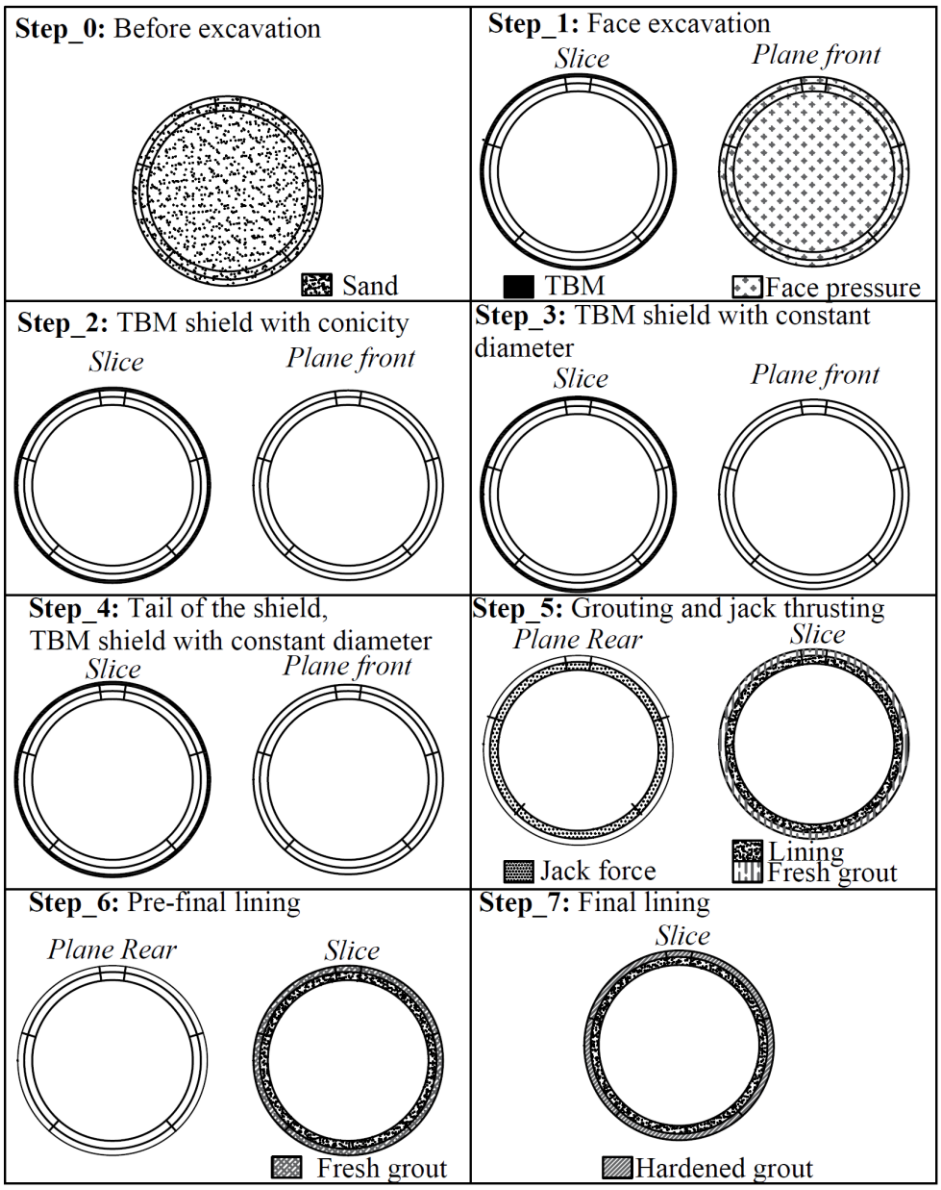

Figure 4- 6: Numerical simulation steps for tunnel excavation sequencing

4.3.4 Constitutive models and parameters

Sand behaviours are described by using the hardening soil model with small-strain stiffness (HSSmall) included in the PLAXIS software package. This material model accounts for increased stiffness at small strains by using two parameters: G_0^{ref}, the small-strain shear modulus; and $\gamma_{0.7}$, the strain level at which the shear modulus is reduced to approximately 70% of the small strain

shear modulus. More details on the HSSmall can be found in Benz (2006). Table 4.2 summarizes the material parameters of the sand that are adopted in the finite element analysis.

Table 4. 2: Summary of the material parameters adopted for the sand.

Secant stiffness in standard drained triaxial test, E_{50}^{ref} (KN/m^2)	38,000
Tangent stiffness for primary oedometer loading, E_{oed}^{ref} (kN/m^2)	38,000
Unloading/reloading stiffness, E_{ur}^{ref} (kN/m^2)	114,000
Power for stress-level dependency of stiffness, m	0.5
Small-strain shear modulus, G_0^{ref} (kN/m^2)	103,000
Strain level at which the shear modulus is reduced to approximately 70% of the small strain shear modulus, $\gamma_{0.7}$	1.36×10^{-4}
Unit weight, γ (kN/m^3)	17.6
Cohesion, c (kN/m^2)	1
Angle of internal friction, φ (°)	36

The 20 m x 20 m mat foundation considered in this analysis is positioned in the middle of the sand deposit. It consists of concrete 1 m thick, with unit weight γ = 25 kN/m^3. The foundation was modelled by using PLAXIS library plate elements with a linear isotropic behaviour, with Young's modulus E = 30 GPa, and Poisson's ratio ν = 0.15. The high-rise building elements such as floor slabs, shear walls, and retaining walls were simulated as plate elements, and the columns were treated as beam elements in the finite element analyses. Surface loads were assigned to each floor slab to simulate live loads as per the National Building Code of Canada (NBC, 2015). Interface elements were used to model the interface between the soil and the mat foundation and basement walls.

4.3.5 Numerical modelling calculations

The simulation procedures can be summarized in detail as follows.

Step 1: Initial *in-situ* stresses for the model are generated.

Step 2: Tunnel construction is simulated in several stages by using the numerical method described previously in Section 2.3. In addition, a number of subsequent phases were executed to model the advancement of the tunnel boring machine by 2 m each time.

Step 3: Construction of the building is simulated in terms of excavating the basement, laying the mat foundation, and building the basement enclosure and then the different floors sequentially.

4.4 JUSTIFICATION OF THE PROPOSED NUMERICAL SIMULATION OF THE TUNNEL CONSTRUCTION

4.4.1 Greenfield settlement trough due to the tunnel excavation

In this section three-different methods of tunnel simulation techniques were utlized. In the first method, the tunnel was excavated according the detailed method described in the previous section. In the second method, the tunnel was modelled also in the three-dimensions, however, it was assumed as a continuous monotone structure (i.e., the true construction sequencing was not considered). In the third method, the study was conducted utilizing two-dimensional finite element analysis (for more details see section 6.3.4.1.3, simulation of the tunnel construction process). All considered modeling methods, are compared with the empirical method of Peck-Fujita (Fujita, 1982). The tunnel burial location for the considered case for comparison is at 2D in the vertical direction, and beneath the centerline of the raft foundation.

4.4.1.1 Peck-Fujita method

Ground settlement over tunnels may be presented by Gaussian distribution curve as:

$$S_{(x)} = S_{max} exp\left(\frac{-x^2}{2i^2}\right) \quad [1]$$

Where,

S is the settlement, S_{max} is the maximum trough settlement

x is the distance from the tunnel centerline in the transverse direction.

i is the distance to the inflection point of the curve.

It can be seen from the Figure 4-7 a dimensionless relationship between i/R ratio versus depth of tunnel Z/2R for tunnel driven through different materials, where R is the radius of the tunnel and Z is the centerline depth of the tunnel. To evaluate S_{max}, maximum settlement, in the Peck empirical method, Fujita (1982), based on the analyses of 94 cases in Japan, predicted the maximum surface settlement for different type of shield machine driven through different soils. His major findings are summarized in Table 4.3.

Table 4. 3: Predicted maximum surface settlement (Fujita, 1982, The origin table is abridged)

		Predicted settlements and errors (mm)			
Additional Measures	**Soil Type**	Open shield	Blind shield	Slurry shield	EPB shield
Not adopted	**Clay**	100 ± 30	40 ± 20	40 ± 20	60 ± 25
	Sand	-	-	40 ± 25	20 ± 10

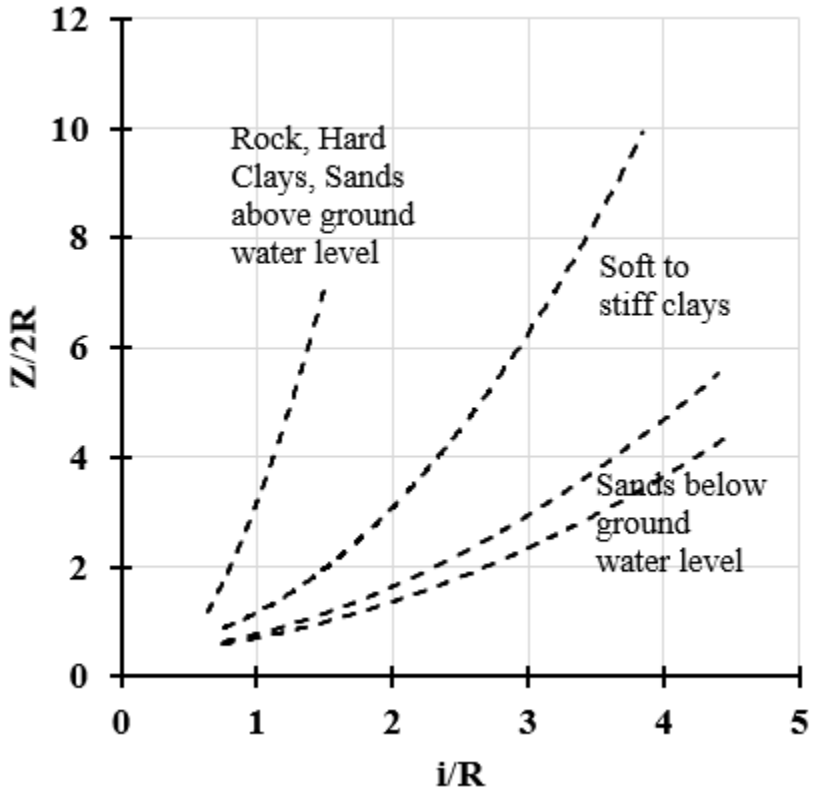

Figure 4- 7: Dimensionless relationship between width of settlement trough i/R and depth of tunnel Z/2R for various tunnels in different materials (Peck, 1969)

4.4.1.2 Evaluation of the settlement by Peck-Fujita method

From Table 4.3, the predicted maximum settlement can be obtained (i.e., 20 mm in this case). Also, by taking Z = 14 m and R = 2.75 m, the correspondence i value can be obtained 2.475 m (Fig. 4-7). By applying S_{max} = 20 mm with i = 2.475 m in equation (1), the surface settlement profile due to the tunnel excavation was determined. The resulted settlement troughs due to the effect of the tunnel excavation are shown in Figure 4-8.

It can be seen from Figure 4-8 that the settlement trough of the three methods were similar in shape, but the second 3D model trough was a little wider (flatter trough) and the empirical model trough was narrower as expected. It can be also seen that the maximum settlement of the 2D model

and the second 3D model, where the tunnel is constructed continuously, were underestimated compared to the predictions of the comprehensive 3D model, in which the tunnel excavation was simulated, by around 35% and 12%, respectively. Or one can say that the empirical model overestimated the maximum settlement by 35%.

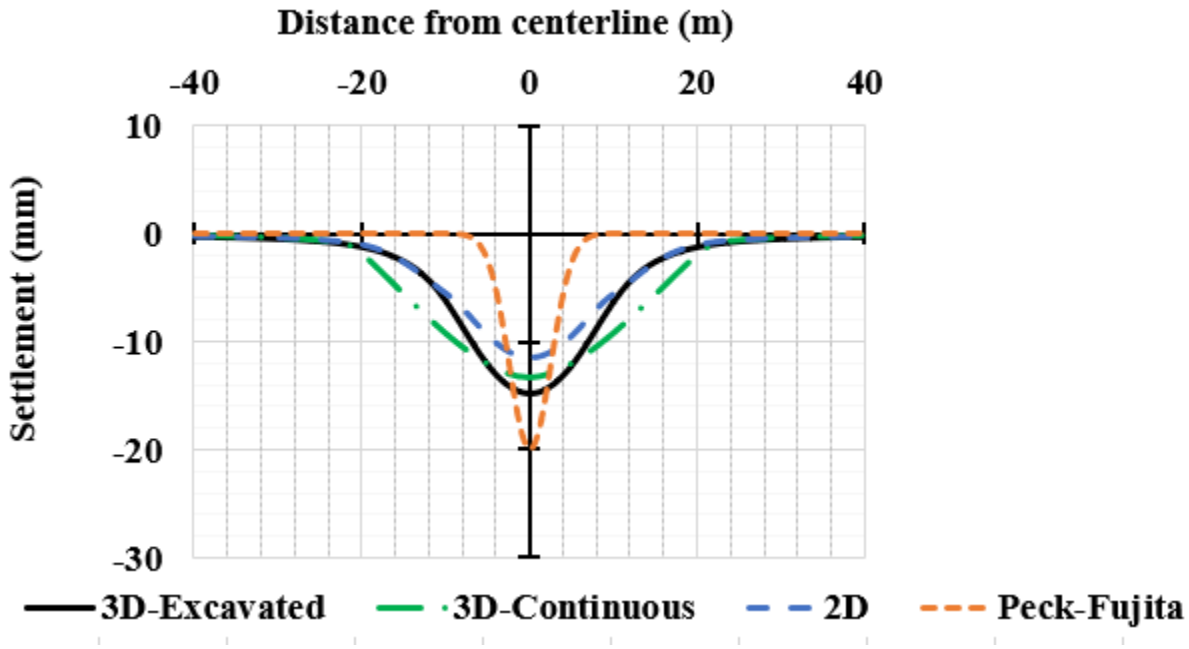

Figure 4- 8: Comparison of the settlement trough due to the tunnel excavation

4.4.2 Raft foundation settlement

Three different methods were considered to predict the settlement trough of the raft foundation. In the first method, the building laying on a raft foundation was modelled in three-dimensional as per the detailed method described in the previous section. In the second method, the study was conducted utilizing two-dimensional finite element analysis under plane strain conditions. The third method used the Winkler spring approach which is commonly used by structural engineers to investigate the settlement trough of the raft foundation.

4.4.2.1 The Winkler spring approach

A variety of methods are available for the structural analyses of mat (raft) foundations. The most common method in current design practice is the Winkler spring approach, in which the soil is presented in the analyses as linear vertical springs supporting the mat as shown in Figure 4-10 to equate the 2D continuum model shown in Figure 4-9. The stiffness coefficient of a Winkler spring K_s is expressed as the product of the area A_s of the portion of the slab influenced by the spring and the parameter is known as the modulus of subgrade reaction k_s, which is defined as:

$$k_s = \frac{q}{w} \qquad [2]$$

Where,

q is the foundation pressure exerted to the soil; and

w is the resulting settlement.

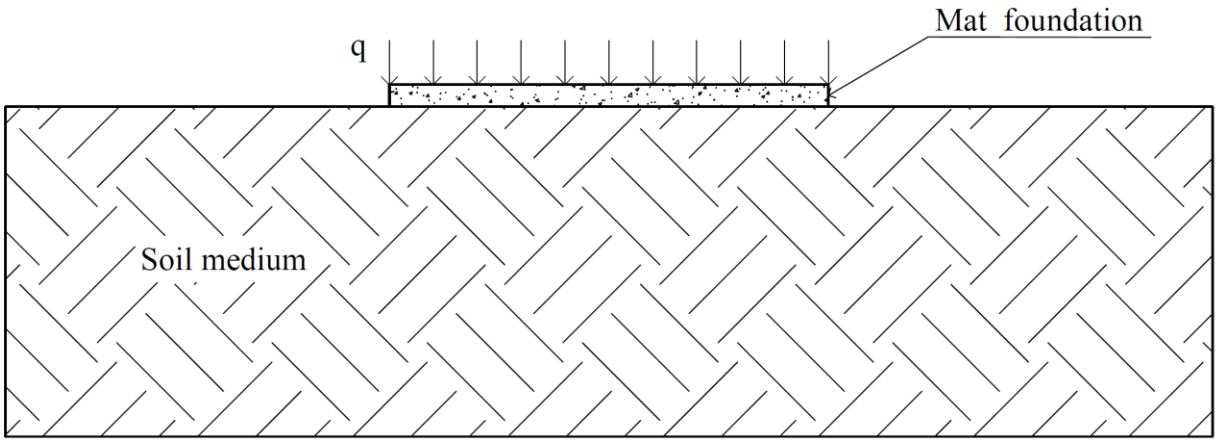

Figure 4- 9: Raft foundation resting on a semi-infinite, homogeneous, isotropic soil medium

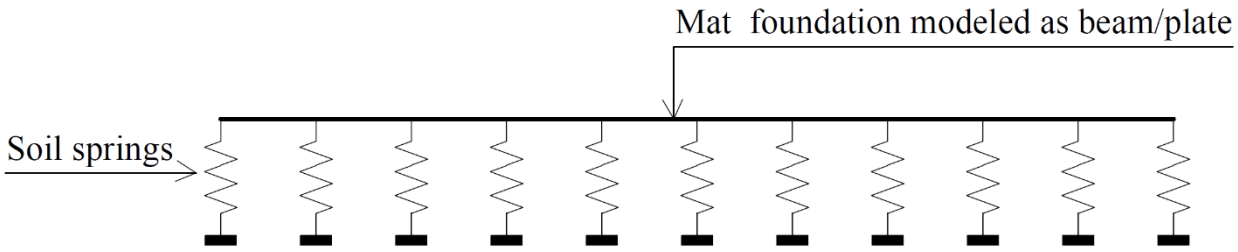

Figure 4- 10: Equivalent of mat foundation resting on a spring bed

It can be seen from Figure 4-11 that the trend of the settlement trough of the three methods are similar, but the 2D-numerical analysis and the empirical solution were offseted by 23% and 38% respectively.

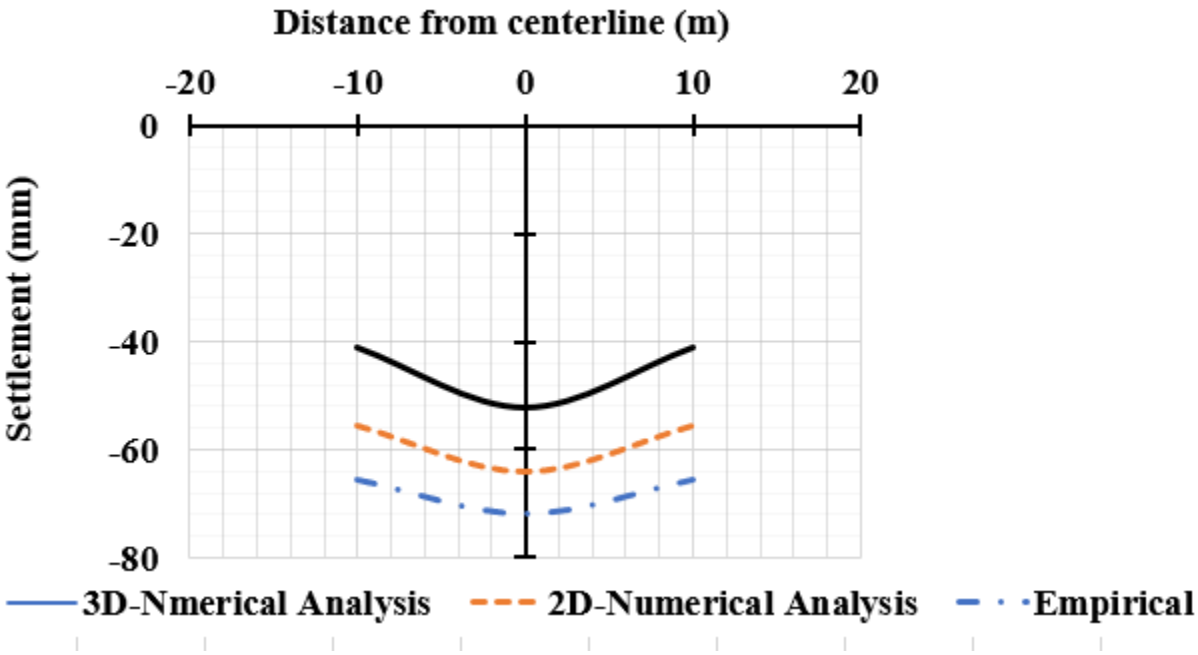

Figure 4- 11: Settlement trough of the raft foundation

4.5 Parametric Study Of The New Construction-Existing Tunnel Interaction

A parametric study was conducted to investigate the interaction between a new construction on a shallow foundation and an existing tunnel. The effect of the new structure was studied with regard

to moments and thrusts developed, increases in vertical and horizontal deformations of the tunnel lining, and maximum and differential settlements underneath the foundation.

In the parametric study, tunnel burial locations ranging from 1D to 6D in the vertical direction, and from 0D to 10D in the horizontal direction were considered as described previously.

To illustrate some of the characteristics of this tunnel-soil-structure interaction problem, the results of the analyses are presented in a normalized form. The normalized displacement, $u_{normalized}$; thrust, $T_{normalized}$; and moment, $M_{normalized}$ are normalized as per El Naggar et al., (2008):

$$\mathrm{u}_{normalized} = \frac{\mathrm{u}E_g}{\sigma_v R_{cl}\left(1 + \nu_g\right)} \quad [3]$$

$$\mathrm{T}_{\mathrm{normalized}} = \frac{\mathrm{T}}{\sigma_{\mathrm{v}}\,\mathrm{R}_{cl}} \quad [4]$$

$$\mathrm{M}_{\mathrm{normalized}} = \frac{\mathrm{M}}{\sigma_{\mathrm{v}}\,\mathrm{R}_{cl}^2} \quad [5]$$

where E_g is the elastic modulus of the ground, σ_v is the initial vertical stress in the ground, R_{cl} is the radius of the centerline of the liner, and ν_g is the Poisson's ratio for the ground.

4.5.1 Effect of the new structure on moments and thrusts developed in the existing tunnel lining

In the parametric study, the existing tunnel lining was considered to be loaded by the soil and the building. Only the combination of the dead load, DL, and the live load, LL, was taken into consideration (1.25 DL + 1.5 LL).

4.5.1.1 Effect of the new structure on thrusts developed in the existing tunnel lining

Figures 4-12a, b, c, d and e, respectively, show the relationship between the normalized thrust ($T_{normalized}$) at the crown, invert, right springline, left springline and right shoulder of the pre-existing tunnel lining, and the location of the tunnel center in relation to the centerline of the mat foundation of the newly constructed building. It should be noted that the influence of the newly constructed building is considered to be negligible when the tunnel center is located at least ten tunnel diameters away from the centerline of the mat foundation in the horizontal direction, i.e., two and half times the width of the raft foundation. This is similar to a greenfield case where there is no new construction. Accordingly, to define an exclusion zone to minimizes the effect of new construction on thrust forces developed in the tunnel lining, this study suggests setting the maximum allowed increase in thrust forces to 10% of the thrust forces existing in the Greenfield case.

In Figure 4-12a, it can be seen that at the crown level, the normalized thrust at a burial depth of one tunnel diameter is approximately doubled when the center position of the tunnel is shifted horizontally three tunnel diameters from the centerline of the shallow foundation. At an increasing distance from the centerline, the normalized thrust then decreases slightly and tends to stabilize and attain a greenfield value. At a burial depth of three tunnel diameters or more below the foundation (0.75 B), variation of the tunnel horizontal location did not affect the normalized thrust, which remained constant and similar to the greenfield value.

At the invert level (Figure 4-12b), the effect of the newly constructed building on the existing tunnel is found to be negligible when the burial depth of the tunnel center is three tunnel diameters or more below the foundation, and the horizontal location of the tunnel center is at least three tunnel diameters away from the foundation centerline.

At the level of the right and left springlines (see Figures 4-12c and d, respectively), at a burial depth of one tunnel diameter the normalized thrust is increased by 80% and 65%, respectively when the tunnel center is located directly below the centerline of the mat foundation. The normalized thrust tends to stabilize when the tunnel center is shifted horizontally three or four tunnel diameters, respectively, away from the centerline of the mat foundation (around one B from the centerline). The normalized thrust also declines and remains stable when the burial depth is at least three or four tunnel diameters, respectively, below the foundation.

At the right shoulder level (Figure 4-12e), the effect of the new structure is minimized when the tunnel center is shifted horizontally three tunnel diameters away from the centerline of the mat foundation and when the burial depth is at least two tunnel diameters below the foundation.

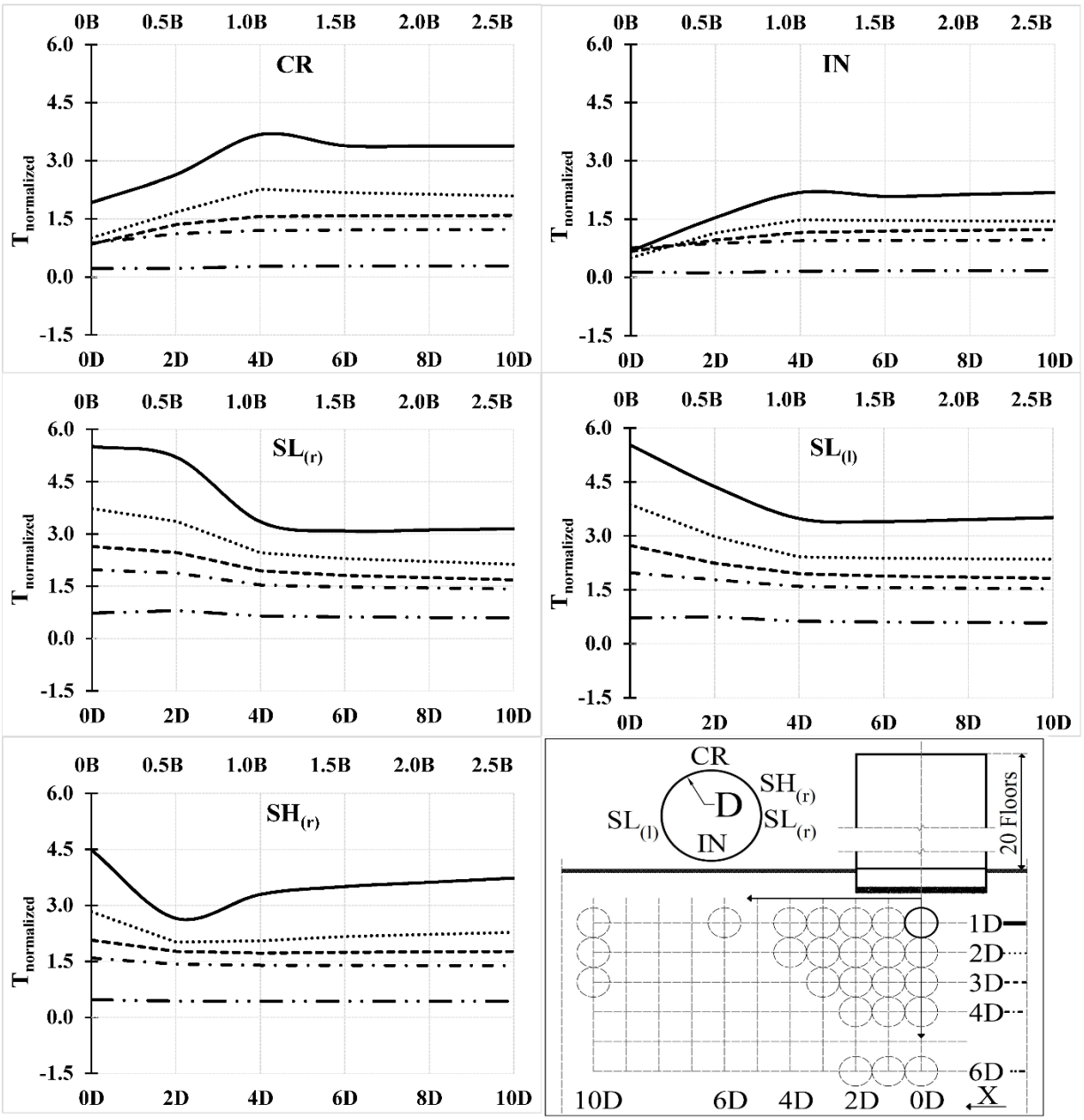

Figure 4- 11: Normalized thrust at the **(a)** crown, **(b)** invert, **(c)** right springline, **(d)** left springline, and **(e)** right shoulder of the tunnel lining

It can be concluded that the construction of a new building leads to an increase in the forces acting on the tunnel lining. However, this effect decreases with increasing burial depth of the tunnel. The load of new surface construction has a greater impact on shallow tunnels.

When the tunnel center is buried at a depth of one tunnel diameter directly below the centerline of the mat foundation, the maximum thrust is found to occur at the springline level, where it is 2.5 to 3 times greater than at the crown level. This non-uniformity of thrust force distribution is due to increased overburden pressure and the differences between vertical and horizontal pressures. However, when the tunnel center is shifted horizontally at least three tunnel diameters away from the centerline of the mat foundation, it can be seen that the thrust increases at the crown level and decreases at the springline and shoulder levels. This is because stress relief at the springline and shoulder is greater due to their proximity to the basement. The lining tends to elongate toward the basement. From Figure 4-13, it can be concluded that thrust effects of the newly constructed building on the existing tunnel lining can be minimized if the tunnel center is located at least four tunnel diameters away from the centerline of the mat foundation in the horizontal direction, and at least four tunnel diameters below the foundation in the vertical direction (i.e., be away one mat width, B, vertically and horizontally).

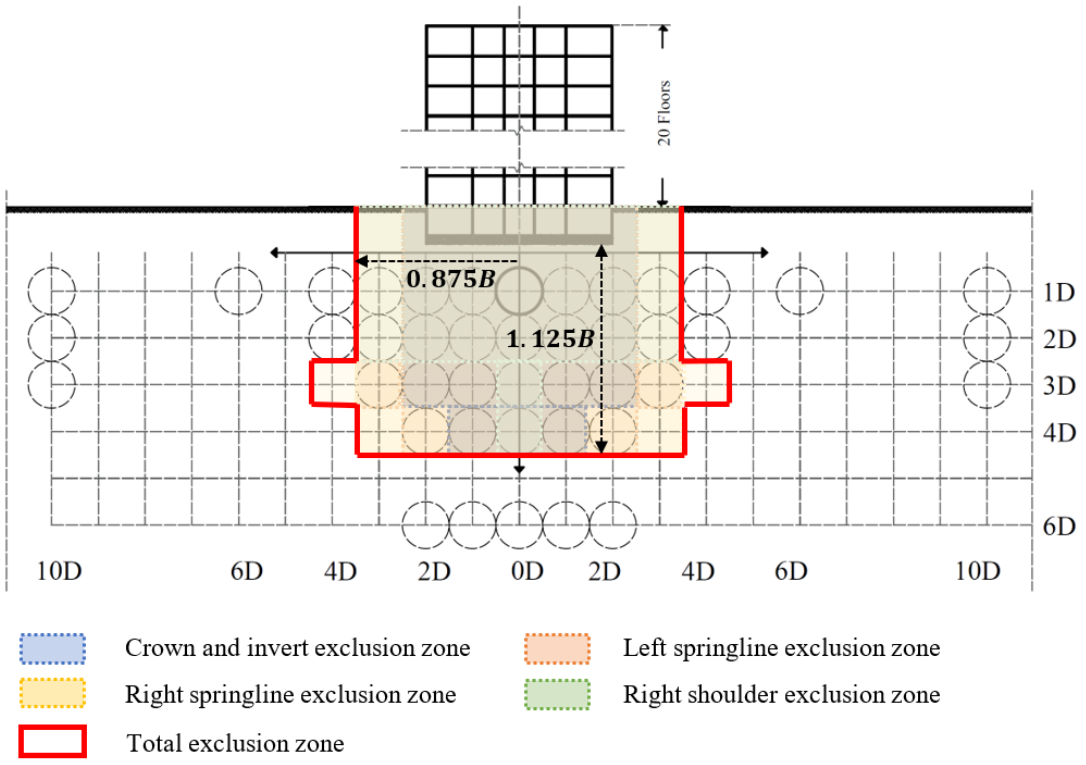

Figure 4- 12: Zone excluded due to the effect of the normalized thrust

4.5.1.2 Effect of the new structure on bending moments in the existing tunnel lining

Figures 4-14a, b, c, d and e show the relationship between the location of the tunnel center and the normalized bending moment ($M_{normalized}$) at the crown, invert, right springline, left springline and right shoulder of the tunnel lining. Bending moments arise because loads resulting from the soil and the surface structure vary around the tunnel lining rings. This is the main cause of ovalization, where the lining bends and becomes oval in shape. Accordingly, to define an exclusion zone to minimize the effect of new construction on bending moments developed in the tunnel lining, this study suggests setting the maximum allowed increase in the bending moments to 10% of those existing in the Greenfield case.

It can be seen from Figure 4-14a that for a burial depth of one tunnel diameter below the foundation, the bending moment at the crown decreases by around 95% when the tunnel center is

shifted horizontally from directly below the centerline of the shallow foundation to at least two tunnel diameters away (where the tunnel center is located beneath the edge of the building). At greater distances, the bending moment then tends to stabilize. The impact of new construction on the bending moment gradually decreases when the burial depth of the tunnel center is three tunnel diameters or more below the mat foundation.

At the invert location (see Figure 4-14b), the effect of a newly constructed building on the existing tunnel is reduced by around 23% when the tunnel center is buried at three tunnel diameters or more below the foundation, and by 64% when the tunnel center is shifted horizontally at least three tunnel diameters away from the mat foundation centerline.

Figures 4-14c and d show a similar trend for the normalized bending moments at the right and left springline locations, respectively. The effect is dramatically reduced when the tunnel center is shifted horizontally at least three or two tunnel diameters away from the mat foundation centerline, respectively; and decreases by 40% or 35%, respectively, when the burial depth is three or more tunnel diameters below the foundation.

At the right shoulder level (Figure 4-14e), the effect of new construction on the normalized bending moment is reduced by 74% when the tunnel center is buried three or more tunnel diameters below the foundation.

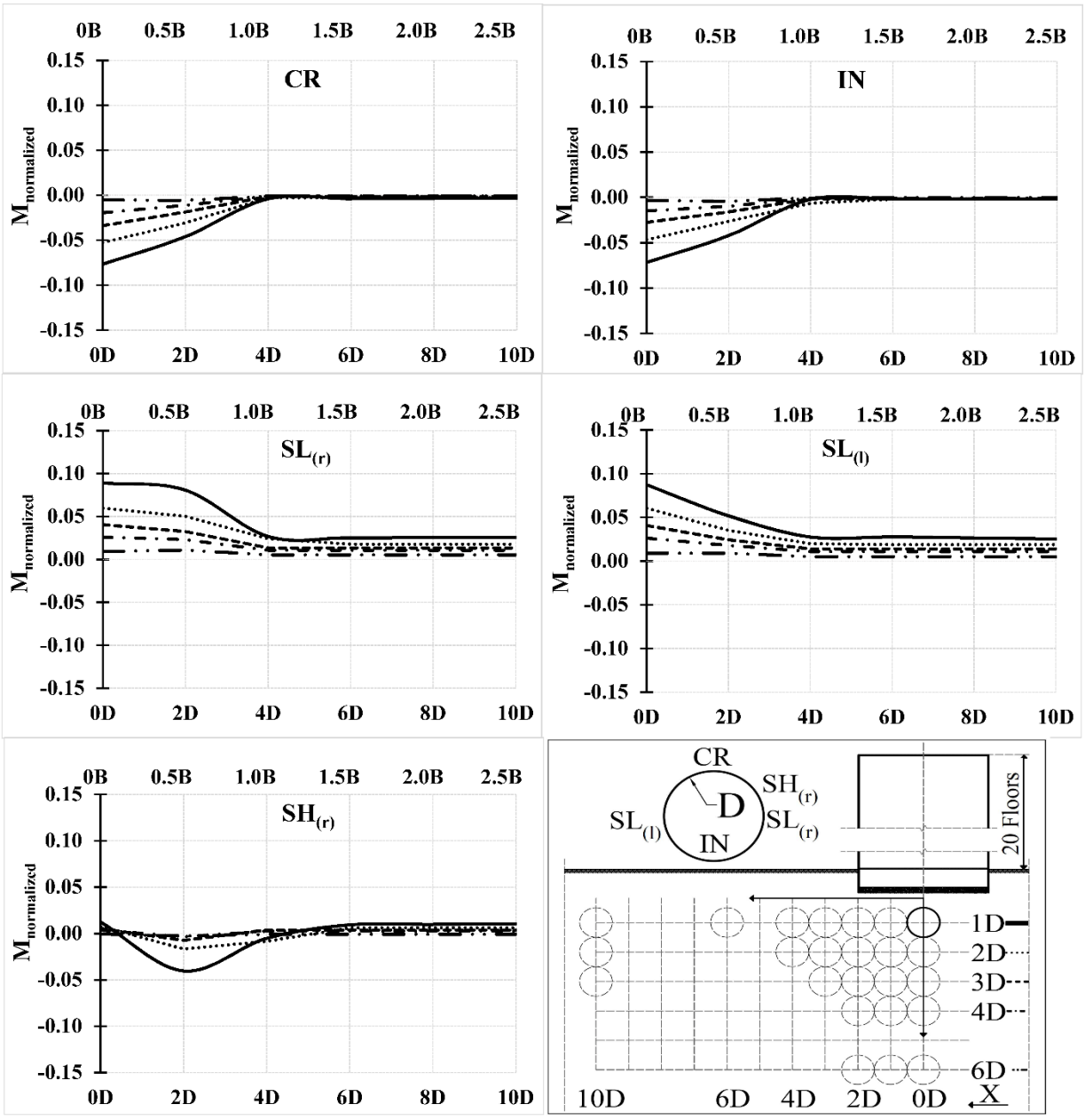

Figure 4- 14: Normalized bending moment at the **(a)** crown, **(b)** invert, **(c)** right springline, **(d)** left springline, and **(e)** right shoulder of the tunnel lining

Accordingly, increased tunnel burial depth and eccentricity from the centerline of the mat foundation of a newly constructed building reduces the effect of the new construction on the lining bending moment.

It can be concluded that the effect on the tunnel lining bending moment will be minimized if the tunnel center is located at least three tunnel diameters away from the centerline of the mat foundation of the newly constructed building in the horizontal direction, and at least three tunnel diameters below the foundation in the vertical direction (i.e., the tunnel be away 0.75 B, in the vertical and horizontal directions).

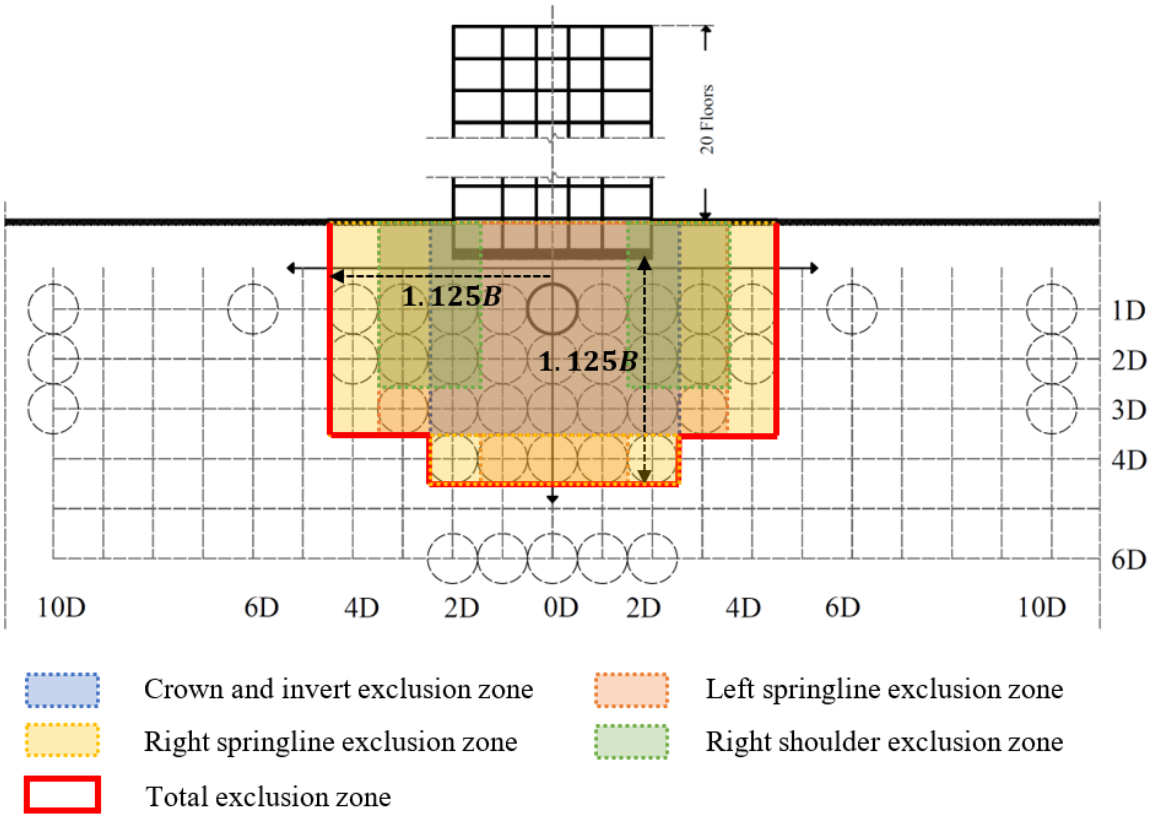

Figure 4- 15: Zone excluded due to the effect of the normalized bending moment

4.5.2 Effect of the new structure on deformations of the existing tunnel lining

4.5.2.1 Effect of the new structure on the vertical deformation of the existing tunnel lining

The normalized increase in vertical deformation at the crown, invert, and right shoulder locations of the tunnel lining can be seen in Figures 4-16a, b and c, respectively.

At the crown and right shoulder locations (Figures 4-16a and c), the increased vertical deformation is reduced by 65% and 50%, respectively, when the tunnel center is shifted horizontally at least three tunnel diameters away from the centerline of the mat foundation; and is reduced by 43% and 25%, respectively, when the burial depth is two tunnel diameters or more below the foundation.

At the invert level (Figure 4-16b), the effect of new construction is minimized when the tunnel center is located at a depth of one tunnel diameter or more below the foundation and is shifted horizontally more than two tunnel diameters away from the centerline of the mat foundation.

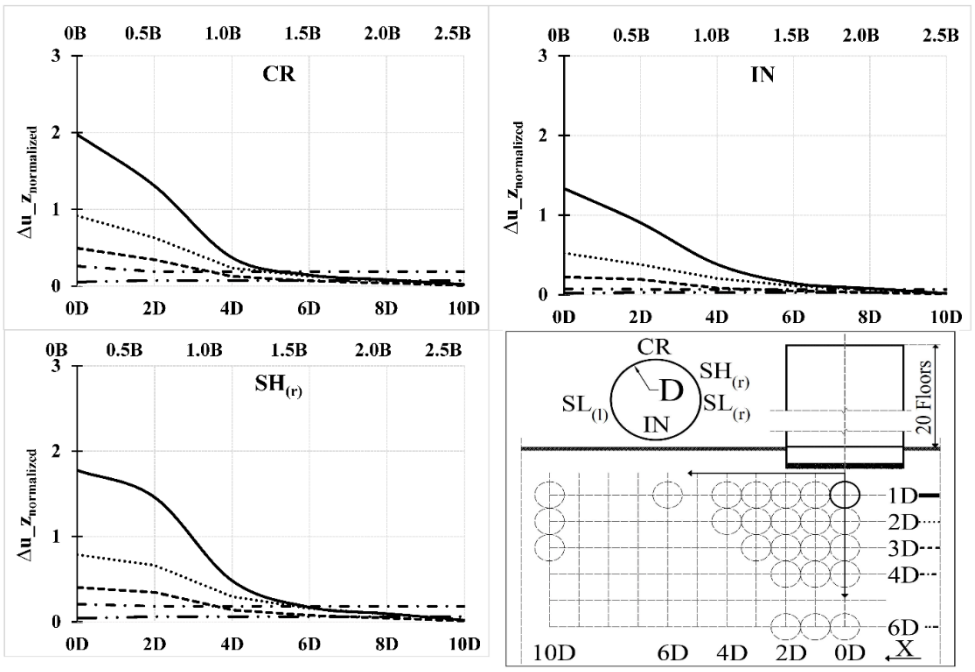

Figure 4- 16 Normalized increased vertical deformation at the (a) crown, (b) invert, and (c) right shoulder of the tunnel lining

It can be seen that the additional vertical deformation of the tunnel lining reaches a peak when the building is positioned directly above the tunnel, due to the increase in confining pressure (load) in the vertical direction. This impact gradually decreases as the position of the new building is shifted horizontally, and as the burial depth of the bored tunnel increases.

According to the Land Transport Authority of Singapore (LTA, 2000), the allowable limit for the total movement of a bored tunnel due to new construction is 15 mm in any direction. The present study accordingly suggests setting a value of 15 mm as the maximum displacement allowed for existing tunnels due to new construction, and when the displacement is greater than 10 mm, an

early warning is to be issued. Consequently, the zone excluded due to the effect of normalized increased vertical deformation is defined as shown in Figure 4-17.

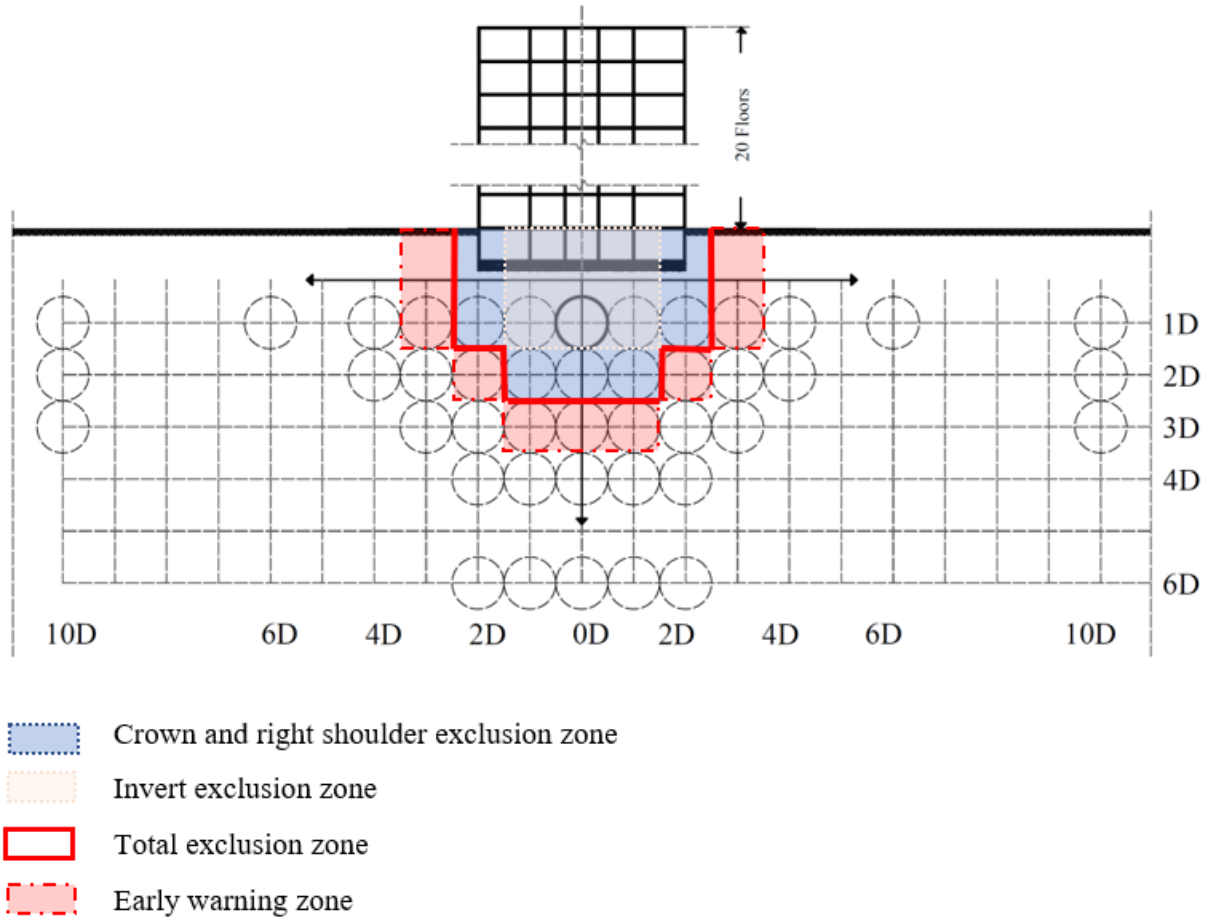

Figure 4- 17: Zone excluded due to the effect of normalized increased vertical deformation

4.5.2.2 Effect of the new structure on the horizontal deformation of the existing tunnel lining

The normalized increase in horizontal deformation at the right springline, left springline and right shoulder locations of the tunnel lining can be seen in Figures 4-18a, b and c, respectively. Figure 4-18 shows that the effect of the new structure leads to a small increase in the horizontal deformation. The peak horizontal deformation, which is less than 4 mm, occurs when the tunnel

center is shifted horizontally one tunnel diameter away from the centerline of the foundation of the new structure. The horizontal forces increase and reach their peak at this imbalanced location. At greater horizontal distances from the centerline, the horizontal deformation gradually decreases, and the stress returns to a balanced state. Therefore, the effect of new construction on increased horizontal deformation can be neglected.

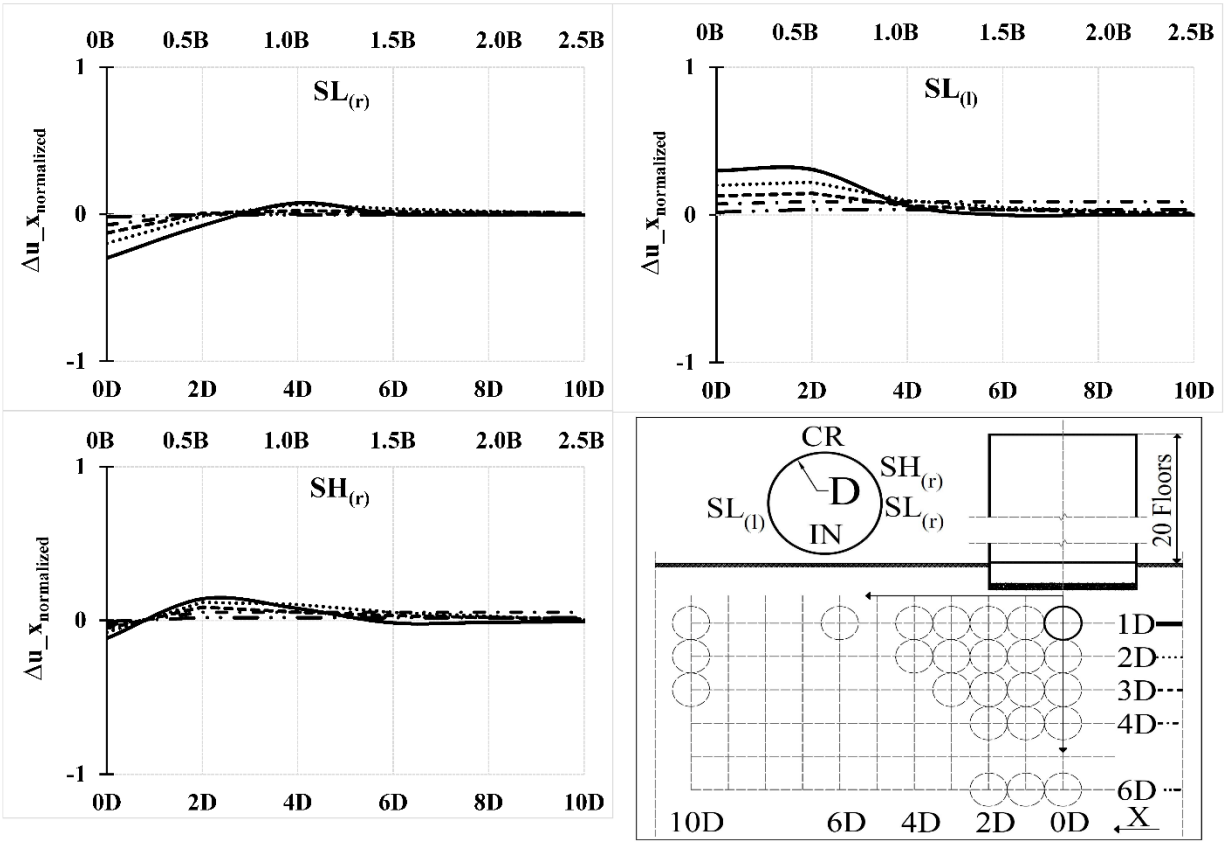

Figure 4- 18: Normalized increased horizontal deformation at the **(a)** right springline, **(b)** left springline, and **(c)** right shoulder of the tunnel lining

4.5.3 Effect of the new structure on the pre-existing tunnel lining

In light of these analyses concerning the effect of new construction on the thrust forces, bending moments, and vertical and horizontal deformation of an existing tunnel lining, an exclusion zone

for new construction in the vicinity of pre-existing tunnels can be defined, as shown in Figure 4-19.

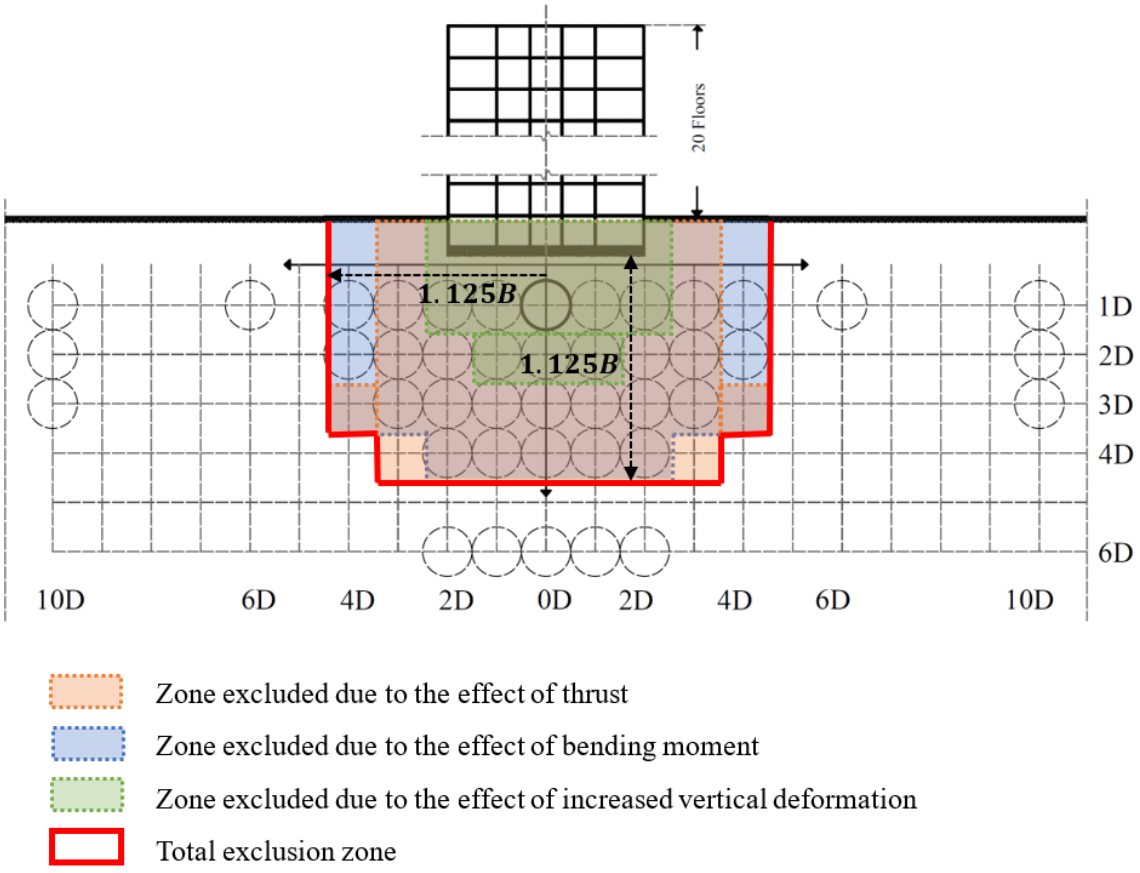

Figure 4- 19: Exclusion zone for new construction close to a pre-existing tunnel

4.5.4 Effect of the existing tunnel on the settlement of the new mat foundation

The normalized maximum settlement underneath the mat foundation is shown in Figure 4-20 (i.e., predicted settlements normalized by the mat settlement obtained from the green field case). Because the ground underneath the shallow mat foundation is defined as sandy soil, vertical deflection of the foundation is due to the drained settlement component, which is derived from compression of the foundation soil skeleton (i.e., a decrease in the void ratio and increase of

effective stresses). As loads are applied, the settlement of cohesionless soils generally occurs rapidly. It can be seen from Figure 4-20 that there is less settlement when the tunnel is located underneath the mat foundation, at a burial depth of one tunnel diameter. The maximum settlement is around 40 mm when the tunnel center is located directly below the centerline of the mat foundation and reaches 53 mm, an increase of 25% when the tunnel center is shifted ten tunnel diameters horizontally (i.e., 2.5 B). One of several factors influencing the settlement of shallow foundations is ground stiffness. Since the stiffness of the tunnel lining is greater than that of sand, the foundation soils become stiffer if a tunnel is present; thus, the settlement is reduced. For this reason, the presence of a tunnel underneath the mat foundation has a positive effect on the settlement trough of the mat as it can seen in Figure 4-20.

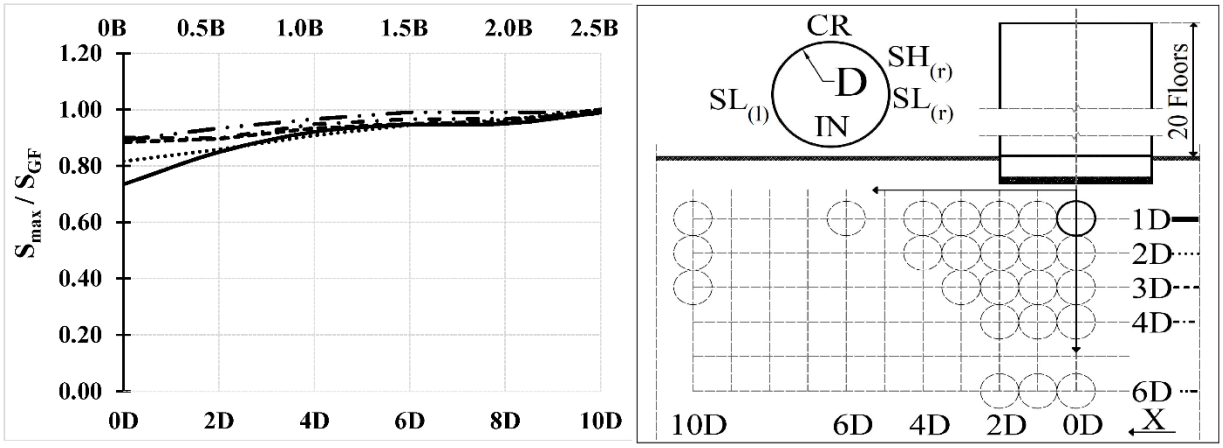

Figure 4- 20: Maximum settlement underneath the mat foundation

Figure 4-21 shows the differential settlement between the two edge points of the foundation (edges 1 and 2), for different tunnel locations normalized by the width of the mat foundation. In the case of differential settlement, edges 1 and 2 exhibit different total settlement magnitudes. It can be seen from Figure 4-21 that the differential settlement trends are similar for different tunnel burial depths. The differential settlement curves rose steadily and reached a peak when the tunnel center

is located two tunnel diameters away from the mat foundation centerline. At this location, the tunnel center is directly below the edge of the building. At greater distances the differential settlement then declines dramatically, becoming insignificant when the tunnel center is located far from the foundation. The differential settlement can lead to damage of the superstructure. Hence, several researchers define certain parameters that quantify differential settlement and develop limiting values for those parameters in order that the resulting structures be safe. ***Bjerrum*** *(Bjerrum 1963)* defined his criterion of damage the limiting ***angular distortion, β_{max}*** as the ratio of difference in total settlement between any two points, $\Delta S_{T(ij)}$ and the distance l_{ij} between points i an j. He found that danger of structural damage to most buildings occurred when $\beta_{max} > {}^{1}/_{150}$, the first cracking of panel walls started when $\beta_{max} > {}^{1}/_{300}$, and the safe limit for no cracking of building is $\beta_{max} = {}^{1}/_{500}$. Accordingly, in this study, for $\beta_{max} = {}^{1}/_{500}$ and the distance between the edges of the mat foundation is 20 m, the maximum differential settlement allowed is equal to 40 mm. This value is four times bigger than the maximum differential settlement detected (i.e., 10 mm). ***The European Committee for Standardization, 1994 b*** *(European Committee for Standardization 1994)*, recommend a magnitude of 20 mm as the maximum acceptable differential settlement for foundation. Or, this value is two times bigger than the value detected in this study. Therefore, it can be concluded that the differential settlement of the mat foundation is less impacted by the presence of tunnels. Based on the assumption that the stress from the foundation spreads out along lines with a vertical-to-horizontal slope of 2:1; the stress will increase with depth. It can be noticed from the figure 16, the increased differential settlement when the burial depth of the tunnel's center is six meters below referring to the 2:1 method.

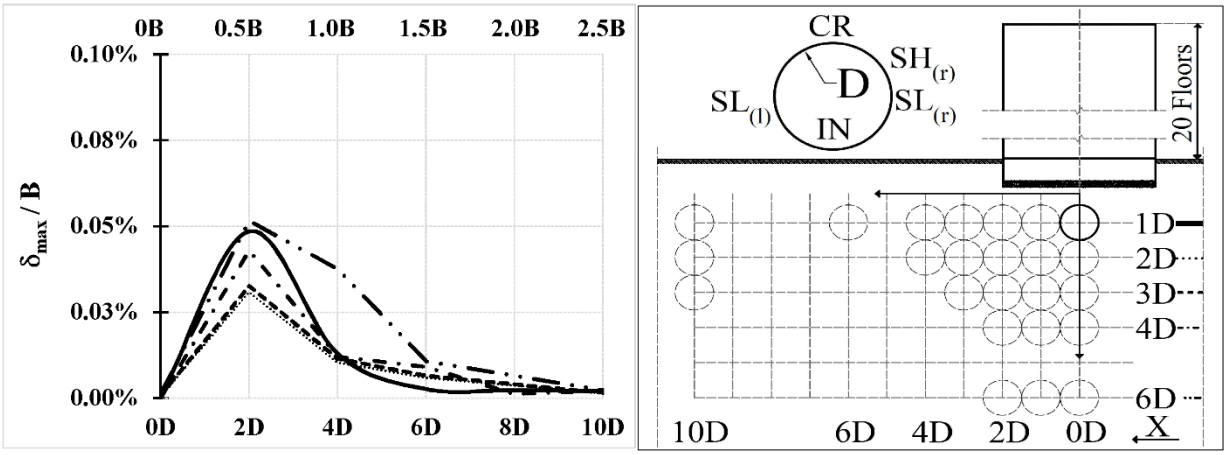

Figure 4- 21: Differential settlement underneath the mat foundation

4.6 SUMMARY AND CONCLUSIONS

A detailed investigation of the effect of constructing of a new high-rise building on a shallow foundation in a sandy layer near a pre-existing intact tunnel is presented. Predicted thrust forces, bending moments, vertical and horizontal deformations of structural elements in the tunnel lining, and maximum and differential settlements of the mat foundation are analyzed for different tunnel burial locations. In light of the evaluation of the building-tunnel interaction, a practical exclusion zone to minimize the effect of new construction on a pre-existing tunnel is defined. Accordingly, new design guidelines can be developed for shallow foundations adjacent to a pre-existing tunnel located in a sandy layer.

4.7 REFERENCES

Abdel-Meguid, M., Rowe, R. K., & Lo, K. Y. (2002). 3D effects of surface construction over existing subway tunnels. *International Journal of Geomechanics, 2*(4), 447-469.

Benz, T. (2006). Small-strain stiffness of soils and its numerical consequences. Ph.D. Thesis, Institut fur Geotechnik, Universitat Stuttgart, Germany.

Bjerrum, L. (1963). Allowable settlement of structures. *Proceedings, European Conference on Soil Mechanics and Foundation Engineering,* Wiesbaden, Germany, Vol. 3, pp. 135-137.

Burford, D. (1988). Heave of tunnels beneath the shell centre, London, 1959-1986, Oklahoma State University Interlibrary Loan.

Chang, C., Sun, C., Duann, S. W., & Hwang, R. N. (2001). Response of a 125aipei rapid transit system (TRTS) tunnel to adjacent excavation. *Tunnelling and Underground Space Technology Incorporating Trenchless Technology Research,* 16(3), 151-158. Doi:10.1016/S0886-7798(01)00049-9.

Code of practice for railway protection (2004). [LTA 2000]. Singapore: Development & Building Control Department, Land Transport Authority (LTA).

Devriendt, M., Doughty, L., Morrison, P., & Pillai, A. (2010). Displacement of tunnels from a basement excavation in London. *Proceedings of the Institution of Civil Engineers, 163*(3), 131-145. Retrieved from https://search.proquest.com/docview/906522924.

Doležalová, M. (2001). Tunnel complex unloaded by a deep excavation. *Computers and Geotechnics,* 28(6-7), 469-493. doi:10.1016/S0266-352X(01)00005-2.

Doran, S. R., Wood, T., Tham, S. K., Shirlaw, J. N., & Wen, D. (2000). The assessment of limits for the movement of subway tunnels and trackwork due to adjacent construction, Balkema, Rotterdam.

El Naggar, H., Hinchberger, S. D., & Lo, K. Y. (2008). A closed-form solution for composite tunnel linings in a homogeneous infinite isotropic elastic medium. *Canadian Geotechnical Journal, 45*(2), 266-287. doi:10.1139/T07-055.

European Committee for Standardization (1994b). *Geotechnical Design, General Rules-Part 1, Eurocode 7;* Brussels, Belgium.

Lo, K. Y., & Ramsay, J. A. (1991). The effect of construction on existing subway tunnels—a case study from Toronto. *Tunnelling and Underground Space Technology, 6*(3), 287-297.

National building code of Canada 2015 (2015). National Research Council.

Ng, C. W. W., Sun, H. S., Lei, G. H., Shi, J. W., & Masin, D. (2015). Ability of three different soil constitutive models to predict a tunnel's response to basement excavation. *Canadian Geotechnical Journal, 52*(11), 1685-1698. Doi:10.1139/cgj-2014-0361.

PLAXIS 3D manuals (2018).

Sharma, J. S., Hefny, A. M., Zhao, J., & Chan, C. W. (2001). Effect of large excavation on deformation of adjacent MRT tunnels. *Tunnelling and Underground Space Technology Incorporating Trenchless Technology Research, 16*(2), 93-98. doi:10.1016/S0886-7798(01)00033-5.

Shi, J., Ng, C. W. W., & Chen, Y. (2015). Three-dimensional numerical parametric study of the influence of basement excavation on existing tunnel. *Computers and Geotechnics, 63*, 146-158. doi: 10.1016/j.compgeo.2014.09.002.

United Nations World urbanization prospects: The 2018 revision. *International Journal of Psychology,* (S1), 443-447. Retrieved from https://onlinelibrary.wiley.com/doi/abs/10.1002/ijop.12312.

Wang, F. (2013). Impact of overhead excavation on an existing shield tunnel: Field monitoring and a full 3D finite element analysis. *Computers, Materials & Continua, 34*(1), 63-81.

Zheng, G., & Wei, S. (2008). Numerical analyses of influence of overlying pit excavation on existing tunnels. *Journal of Central South University of Technology, 15*(S2), 69-75. doi:10.1007/s11771-008-0438-4.

CHAPTER 5 EFFECT OF NEWLY CONSTRUCTED BUILDINGS WITH RAFT FOUNDATION SUPPORT ON PRE-EXISTING DEGRADED TUNNELS

5.1 ABSTRACT

This study uses a three-dimensional finite element method to examine the interaction between a newly constructed high-rise building on a shallow foundation and a nearby pre-existing tunnel with a degraded lining. The durability and sustainability of bored tunnels is primarily affected by chloride penetration through joints and cracks, especially in the case of exposure to ground water contaminated with chloride. Four different scenarios are considered in this study to illustrate tunnel lining degradation. Two scenarios represent degradation in the form of delamination of the intrados concrete lining, resulting in degraded material properties at the crown and shoulder zones. The other two scenarios represent a more extreme case, where the intrados lining is gradually and completely spalled. Stresses and deformations of the degraded tunnel lining under the influence of new construction are analyzed for different tunnel burial depths. A new design guideline for shallow foundations near pre-existing degraded tunnels will be developed accordingly.

Keywords: numerical modelling, tunnelling, high-rise building, lining degradation, radial stress, deformation, settlement, exclusion zone.

5.2 INTRODUCTION

Despite the high capital costs of maintaining and rehabilitating tunnel structures in comparison to costs for alternative highway structures such as bridges, viaducts and roadways, tunnels have environmental, social and economical advantages, such as reducing traffic congestion and pollution in urban areas, improving road safety, and creating more green space. Due to construction

booms, particularly in crowded world capitals, there is pressure for developers to construct high-rise buildings in challenging locations such as above or adjacent to pre-existing tunnels. In areas exposed to severe weather conditions, such as parts of North America, freezing and thawing are the most common problems leading to the degradation of concrete structures. During the freezing cycle, water migrates toward fine cracks, where it freezes and expands by about 9%. This causes the fine cracks to become enlarged by the pressure of the ice and to remain enlarged after the ice thaws. For example, thawed water seeping from some of the joints in the ceiling and upper wall areas of the Berlin Tegel Airport road tunnel in Germany led to the corrosion of steel reinforcement in the areas of the concrete cracks, the formation of icicles in the ceiling and wall areas, and the formation of ice on the road surface during the frost period (Howard 1991).

Another weather-related factor which significantly affects concrete tunnel liners is the use of salts as de-icing agents for snow and ice removal. The salts used are usually NaCl (sodium chloride) and $CaCl_2$ (calcium chloride). Chlorides enter the reinforced concrete through cracks, and the steel reinforcement becomes corroded in the presence of oxygen and moisture. Subsequently, the corrosion leads to cracking, spalling and delamination of the concrete. As the corrosion progresses, it reduces the load carrying capacity. For example, the inflow of saline ground water through joints and grout holes has led to the corrosion of reinforcing bars in areas of the interior face of precast reinforced concrete segments of the Ahmed Hamdi road tunnel in Egypt, the Hong Kong Mass Transit Railway metro tunnel in China, and the Tokyo underground road tunnel in Japan. This contributes to cracking and loosening of concrete from precast segments, which gradually reduces the strength of the concrete linings (Howard 1991).

Usually tunnel service life is around 100 years. Within the first 30 years of service most tunnels suffer from water leakage and exhibit deterioration in a variety of forms, such as cracks and

separation in the lining, and opening of the construction joints (Inokuma, Inano 1996). Results from previous studies on the evolution of material mechanical properties (Idris, Verdel et al. 2008a, Colback, Wiid 1965, Stead, Coggan et al. 2000) show that Young's modulus, compressive strength, tensile strength, cohesion, and friction angle parameters tend to decrease over time.

Several researchers have studied the degradation of tunnel linings by using a three-dimensional finite element (FE) method. ***Usman & Galler, 2013*** (Usman, Galler 2013) analyzed stresses in the shotcrete lining of a deep tunnel through simulation of the shotcrete degradation by reducing strength parameters such as Young's modulus (E), cohesion (C), and the friction angle ϕ, individually and in various combinations. ***El Naggar & Hinchberger, 2012*** (El Naggar, Hinchberger 2012) analyzed the static and seismic response of tunnels with intact and degraded tunnel linings by using non-linear numerical and analytical methods. Degradation of the lining intrados was simulated for three different scenarios. Two of them represented local delamination of the lining intrados and the third represented complete degradation of the intrados. **Idris et al., 2008** (Idris, Verdel et al. 2008b) studied the behaviour of masonry tunnel structures affected by aging phenomena. With the aid of numerical modelling, twenty-seven experiments were proposed by changing the value of three selected masonry mechanical properties: masonry block cohesion, tensile strength and friction angle.

In the present research, by varying the burial depth of the tunnel center, a comprehensive 3D finite element parametric study was conducted to investigate the complex interaction between a pre-existing degraded tunnel and a newly constructed high-rise building on a shallow foundation in a sandy layer. In the model developed, the simulation of the tunnel excavation process driven by a tunnel boring machine (TBM) involves repetitive excavation procedures with the installation of each ring. The simulation takes into consideration the main factors such as the support pressure at

the tunnel face, the conical shape and jacking forces of the TBM shield, and grouting of the gap between the soil and the newly installed lining. The lining of the tunnel is modelled by using the concrete material developed in the finite element software PLAXIS. Tunnel degradation is simulated according to four different scenarios. Two of them represent degradation in the form of delamination of the intrados concrete lining, by reducing the material strength properties at the crown and shoulder zones. The other two scenarios represent a more extreme case, where the intrados lining is gradually and completely spalled. The soil continuum is modelled by using an advanced non-linear constitutive model such as the hardening soil model with small strain stiffness, which can account for increased stiffness at small strains. Following analysis of the stresses and deformations in the degraded tunnel lining due to new construction, a workable exclusion zone to reduce the effect of new construction on the pre-existing degraded tunnel will be clearly outlined.

5.3 Methodology

The 3D finite element program PLAXIS was used to conduct a parametric study to investigate the new building-degraded tunnel interaction by varying the burial location of the tunnel center vertically from 1D to 6D (where D is the tunnel diameter), and horizontally from 0D (where the tunnel center is located directly beneath the centerline of the mat foundation) to 10D.

5.3.1 Problem geometry

As shown in Figure 5-1, a high-rise building with twenty above-ground stories and one basement was modelled as a flat slab (with a thickness of 200 mm) connected to columns with a shear wall structure (200 mm thick) lying on a shallow mat foundation in a sandy soil continuum. The inner diameter of the circular segmental concrete tunnel lining is 5 m and the outer diameter is 5.5 m.

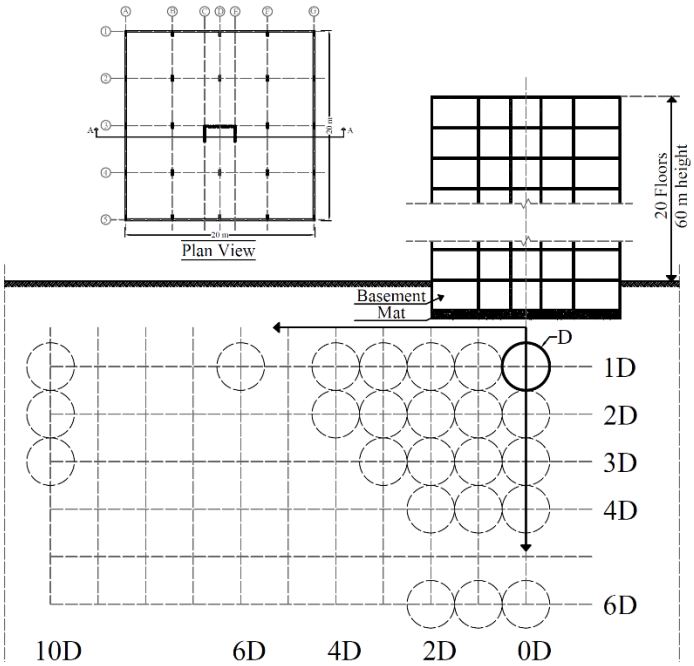

Figure 5- 1: Parametric study plan view and cross section

5.3.2 Material models

5.3.2.1 Soil continuum

In this study, the soil continuum was modelled by using the hardening soil model with small strain stiffness (HSSmall). The input parameters for the model are: secant stiffness in a standard drained triaxial test, E_{50}^{ref}; the tangent stiffness for primary oedometer loading, E_{oed}^{ref}; the unloading/reloading stiffness, E_{ur}^{ref}; the cohesion, c; the angle of internal friction, φ; the small-strain shear modulus, G_0^{ref}; and the strain level at which the shear modulus is reduced to about 70% of the small strain shear modulus, $\gamma_{0.7}$. The HSSmall advanced model can account for increased stiffness at small strains (Santos, Correia 2001, Hardin, Drnevich 1972). Table 5.1 summarizes the material properties of the sand adopted in the finite element analysis.

Table 5. 1: Summary of material properties adopted for the sand in the FE analysis.

Secant stiffness in standard drained triaxial test, E_{50}^{ref} (KN/m^2)	38,000
Tangent stiffness for primary oedometer loading, E_{oed}^{ref} (kN/m^2)	38,000
Unloading/reloading stiffness, E_{ur}^{ref} (kN/m^2)	114,000
Power for stress-level dependency of stiffness, m	0.5
Small-strain shear modulus, G_0^{ref} (kN/m^2)	103,000
Strain level at which the shear modulus is reduced to about 70% of the small strain shear modulus, $\gamma_{0.7}$	1.36x10^{-4}
Unit weight, γ (kN/m^3)	17.6
Cohesion, c (kN/m^2)	1
Angle of internal friction, φ (°)	36

5.3.2.2 Concrete tunnel lining

The tunnel lining was modelled as volume elements by using the nonlinear elastoplastic concrete model newly developed by Schadlich and Schweiger (Schadlich, Schweiger 2014) which takes into consideration strain hardening/softening in both compression and tension, as well as the time-dependent strength and stiffness of concrete. The model is also capable of simulating the creep and shrinkage behaviour of concrete. As shown in Figure 5- 2, the inner diameter of the tunnel is 5 m and the outer diameter is 5.5 m. The precast concrete lining is composed of six concrete segments. The length of each lining section is 2 m. Table 5.2 summarizes the material properties of the tunnel lining adopted in the finite element analysis.

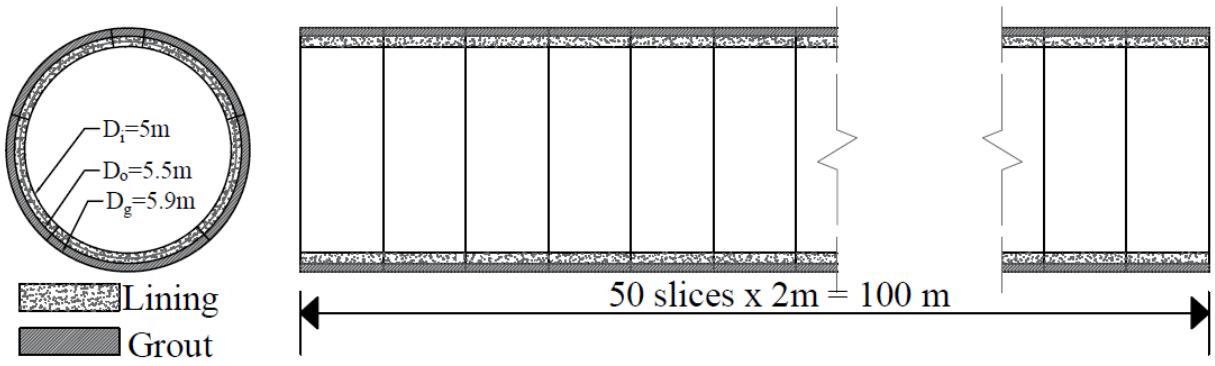

Figure 5- 2: Tunnel cross section and longitudinal section

Table 5. 2: Summary of tunnel lining material properties adopted for the finite element analysis.

Unit weight, γ (kN/m^3)	25
Young's modulus for cured shotcrete at t_{hydr}, E_{28} (kN/m^2)	31 x 10^6
Poisson's ratio, v	0.15
Uniaxial compressive strength of cured shotcrete at t_{hydr}, $f_{c,28}$ (kN/m^2)	45 x 10^3
Uniaxial tensile strength of cured shotcrete at t_{hydr}, $f_{t,28}$ (kN/m^2)	4,500
Time dependency of elastic stiffness, E_1/E_{28}	1
Time dependency of strength, $f_{c,1}/f_{c,28}$	1
Normalized initially mobilized strength, f_{c0n}	0.15
Uniaxial plastic failure strain at 1h, 8h, 24h, ϵ_{cp}^{p}	-1 x 10^{-3}
Compressive fracture energy of cured shotcrete at t_{hydr}, $G_{c,28}$ (kN/m)	100
Tensile fracture energy of cured shotcrete at t_{hydr}, $G_{t,28}$ (kN/m)	6.9
Increase of ε_{cp} with increase of p', a (m)	18
Maximum friction angle, φ_{max} (°)	37
Safety factor for compressive strength, γ_{fc}	1
Safety factor for tensile strength, γ_{ft}	1
Time for full hydration, t_{hydr} (days)	28

5.3.3 Finite element mesh

Figure 5-3 illustrates a typical finite element mesh used in the parametric study described above. The finite element mesh comprises around 350,000 10-node tetrahedral elements. The density of the mesh is very fine near the tunnel lining and new construction, and gradually becomes coarser

with increased distance from the lining. Plate elements were used to simulate the different parts of the building, with the exception of the columns which were simulated by using beam elements. The depth of the sandy soil continuum is 60 m, the model width is 160 m, and the model extends 100 m in the y-direction. These dimensions are appropriate to allow for the development of any possible collapse mechanism and to prevent any influence from the model boundaries. The bottom boundary of the model is fixed in all directions. Vertical model boundaries parallel to *yz*-plane are fixed in the *x*-direction and those parallel to *xz*-plane are fixed in the *y*-direction. To ensure proper modelling of the soil-structure interaction, interfaces were added for plate elements simulating the mat foundation, the basement walls and the tunnel lining.

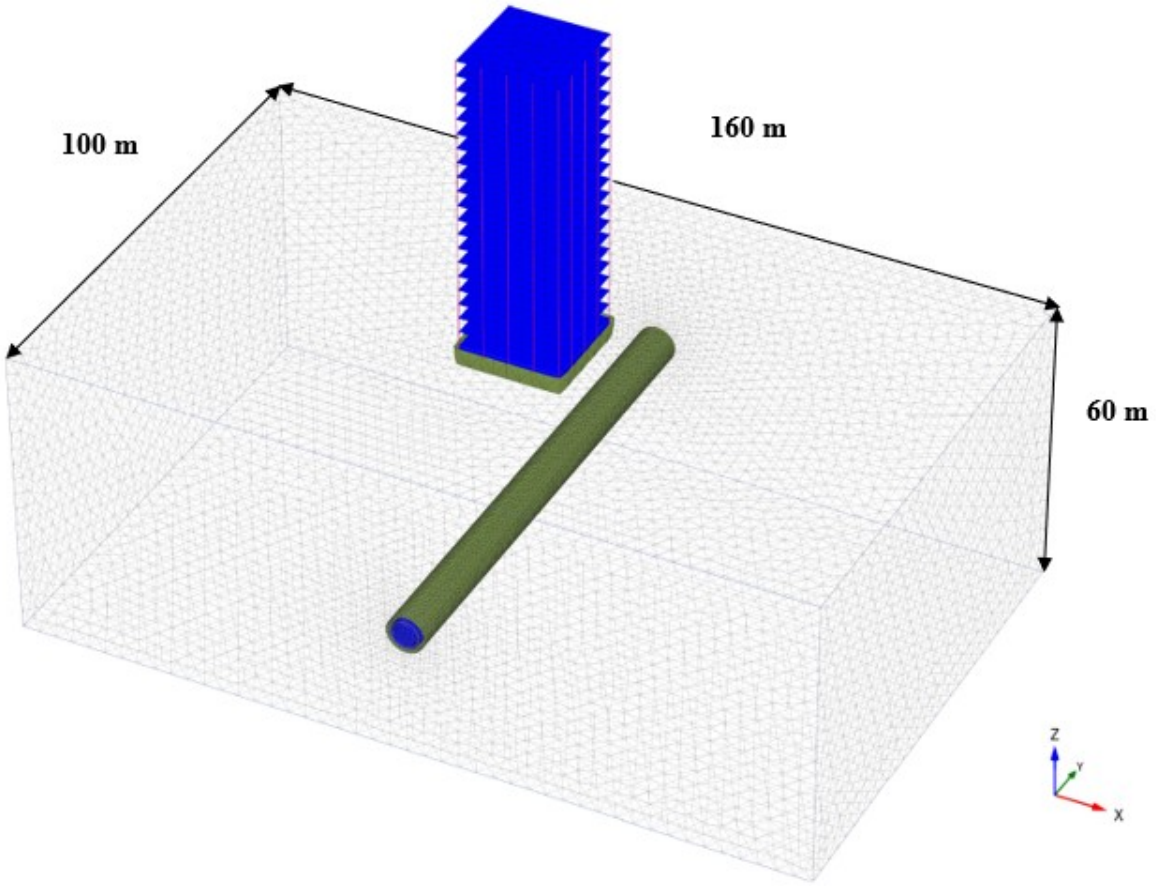

Figure 5- 3: Typical mesh generated for three-dimensional finite element model

5.3.4 Finite element solution sequence

5.3.4.1 Simulation of mechanised tunnelling processes

Tunnels with a circular cross section are excavated by using a tunnel boring machine (TBM) (Figure 5- 4). In the numerical simulation of the mechanised TBM tunnelling processes the face pressure, the conical shape of the shield, the jacking force, the grouting injection, the hardening of the grout and the installation of the new lining are taken into consideration (Figure 5- 5). The operation of a TBM shield can essentially be divided into two phases: the tunnelling phase, and the ring building phase. In the tunnelling phase, hydraulic thrust cylinders apply pressure to push the cutting wheel against the tunnel face to remove materials at the tunnel face. A screw conveyor

then moves the excavated soil to the conveyor belt behind the TBM shield. The soil excavated by the cutting wheel is used to support the tunnel face. The required support is generated when the pressure of the earth and water on the tunnel face and the pressure of the ground in the chamber are balanced. Once excavation at the tunnel face is complete, the cutting wheel and screw conveyor are stopped. For all excavation steps, the TBM face pressure is modelled as a perpendicular horizontal stress that increases linearly with depth. Due to the slightly conical shape of the shield, the soil-structure interaction must be modelled. The cross-sectional area at the tail of the TBM is smaller than that at the front of the TBM. The tail section thus has a constant diameter with a uniform contraction, while the remaining sections of the TBM have a reduced diameter realised via linear contraction, with a reference value equal to the tail section plus an increment. The ring building phase then commences. A complete tunnel ring consisting of several segments referred to as lining segments is set in place. After a complete ring is built, the machine can then push off from the newly installed tunnel ring and continue boring into the ground. A fast motion sequence illustrates the two operating phases of the TBM: The tunnelling phase and the ring building phase continuously alternate as the tunnel grows ring by ring. The gap left between the soil and the newly constructed lining is injected with grout. The grout pressure increases linearly with depth. With time, the elastic modulus and the strength of the fresh grout change as the grout hardens. Thus, the applied grout pressure decreases with distance. In the simulation, hardening of the injected grout is simulated by changing the material properties of the elements in the grouting annulus from fresh grout in the current step, to half-hardened grout, and then to fully hardened grout. This process is repeated for each tunnel advance.

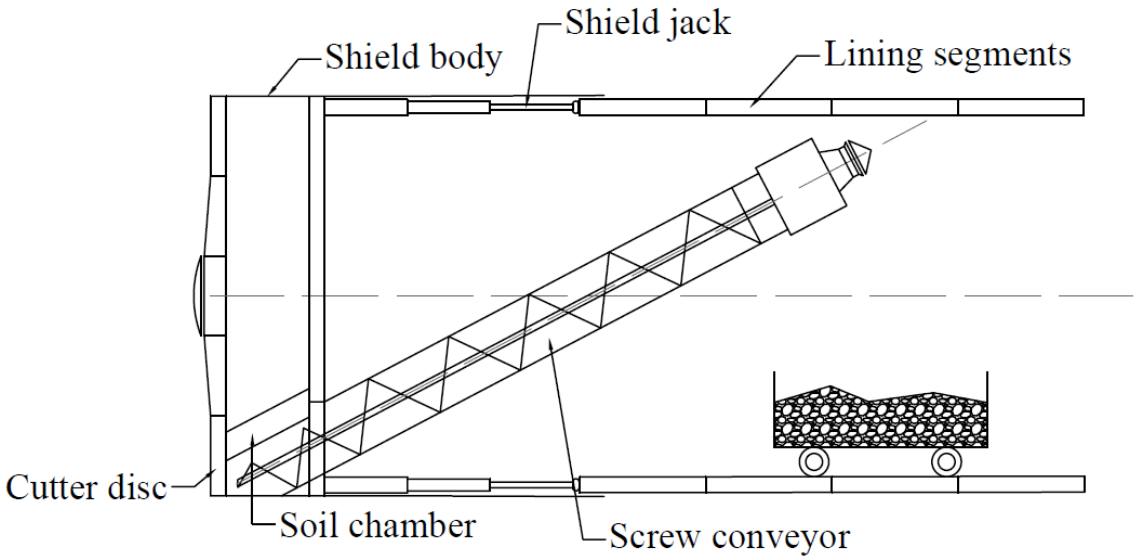

Figure 5- 4: Simplified sketch of the tunnel boring machine (TBM)

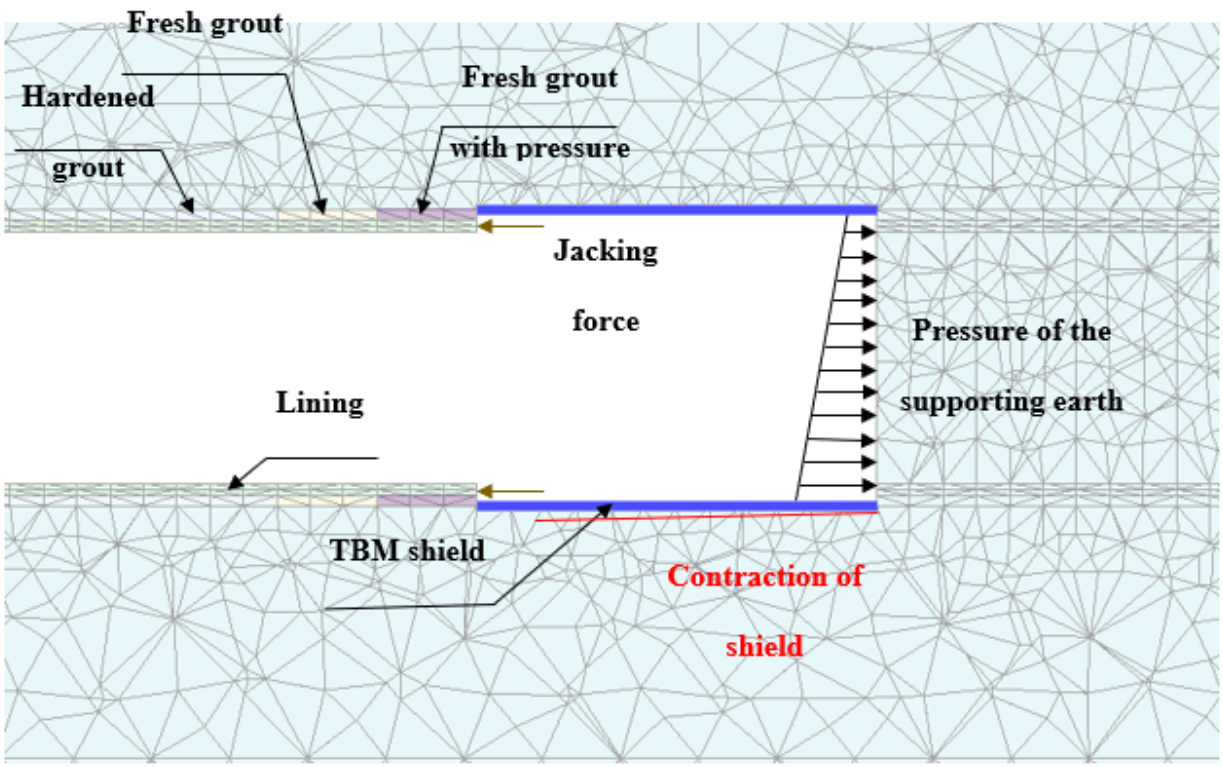

Figure 5- 5: Simulation of the mechanised tunnelling processes

5.3.4.2 Simulation of concrete degradation at the lining intrados

Four different scenarios are considered in this study to illustrate tunnel lining degradation. Two of the scenarios represent degradation in the form of delamination of the intrados concrete lining by reducing the material strength properties at the crown and shoulder zones. The other two scenarios represent a more extreme case, where the intrados lining is gradually and completely spalled. The four scenarios considered in this study are described below and illustrated in Figure 5-6.

Scenario 1: Local concrete degradation at the crown and shoulder zones is examined. At these zones, the material properties of the elements of the inner layer of the lining, to a depth of 12.5 mm, are reduced by 50% of their initial values to simulate the deterioration of the lining.

Scenario 2: Complete spalling of the concrete at the crown and shoulder zones is examined. At these zones, the elements of the inner layer of the lining, to a depth of 12.5 mm, are removed completely.

Scenario 3: Spalling degradation of all elements of the lining intrados (to a depth of 12.5 mm) is simulated. The material properties of the elements are reduced by 50% of their initial values to simulate the deterioration of the lining.

Scenario 4: Extensive spalling is simulated. All elements of the lining intrados (to a depth of 12.5 mm) are removed completely, to simulate an extreme case of complete intrados degradation.

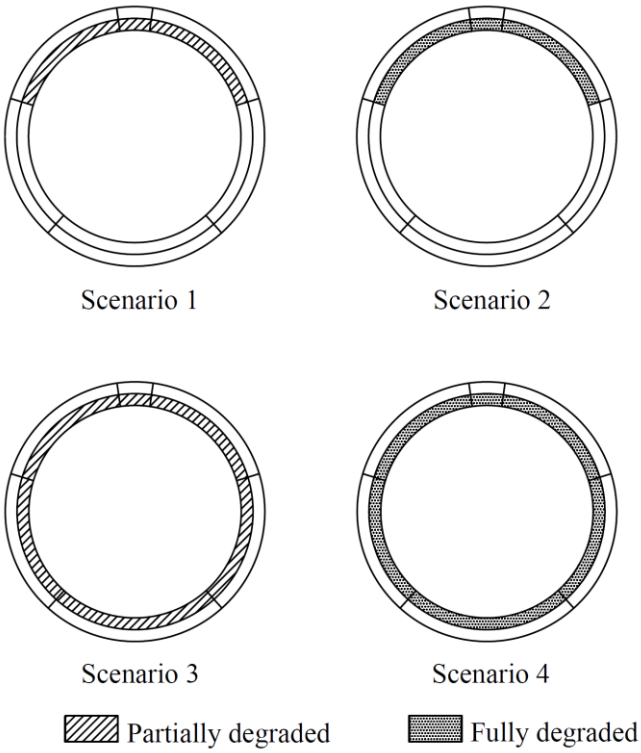

Figure 5- 6: The four degradation scenarios considered in this study

Figure 5- 7 shows the tunnel section capacity for an intact tunnel and for the four different degradation scenarios. For the intact tunnel section, the allowable compressive stress is 22.9 MPa and the allowable tension stress is 4.1 MPa. For scenarios 1 and 2, shown in Figure 7(a), the allowable compressive stresses for the degraded zone are 17.5 MPa and 12.5 MPa, respectively, and the allowable tensile stresses are 3.0 MPa and 2.1 MPa, respectively. For scenarios 3 and 4, shown in Figure7(b), the allowable compressive stresses for the degraded tunnel are 17.5 MPa and 11.9 MPa, respectively, and the allowable tensile stresses are 3.0 MPa and 2.0 MPa, respectively.

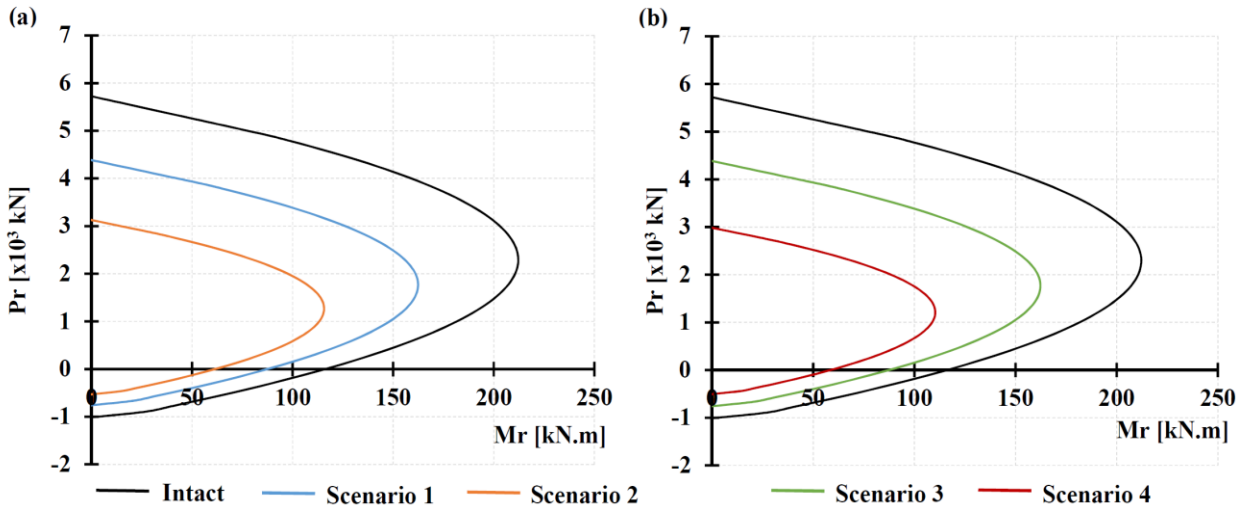

Figure 5- 7: Tunnel section capacity in **(a)** scenarios 1 and 2, and **(b)** scenarios 3 and 4

5.3.4.3 Calculations performed

The finite element solution commences with an initial phase where the initial stresses are generated, taking into consideration the loading history of the soil. The effective initial horizontal stresses are related to the effective initial vertical stresses via the coefficient of lateral earth pressure, K_0. The subsequent (approximately 55) phases simulate the advancement of the tunnel excavation by 2 m each time. After the entire tunnel is excavated, degradation of the tunnel lining is modelled according to one of the scenarios defined above. Then the construction of the nearby building is modelled.

5.4 RESULTS

Figure 5- 8 illustrates the design of the parametric study conducted to investigate the complex interaction between a pre-existing degraded tunnel lining and a newly constructed high-rise building on a mat foundation in a sandy continuum. It can be seen that the location of the tunnel center is varied vertically from 1D to 6D below the mat foundation (where D is the tunnel diameter) and horizontally from 0D (where the tunnel center is located directly beneath the centerline of the

new mat foundation) to 10D. For each of the four scenarios defined above, for each tunnel position an analysis is carried out of the stress distribution and the vertical and horizontal deformation at the crown, invert, right springline, left springline and right shoulder levels. In addition, the maximum settlement and the differential settlement of the newly constructed mat foundation are analyzed.

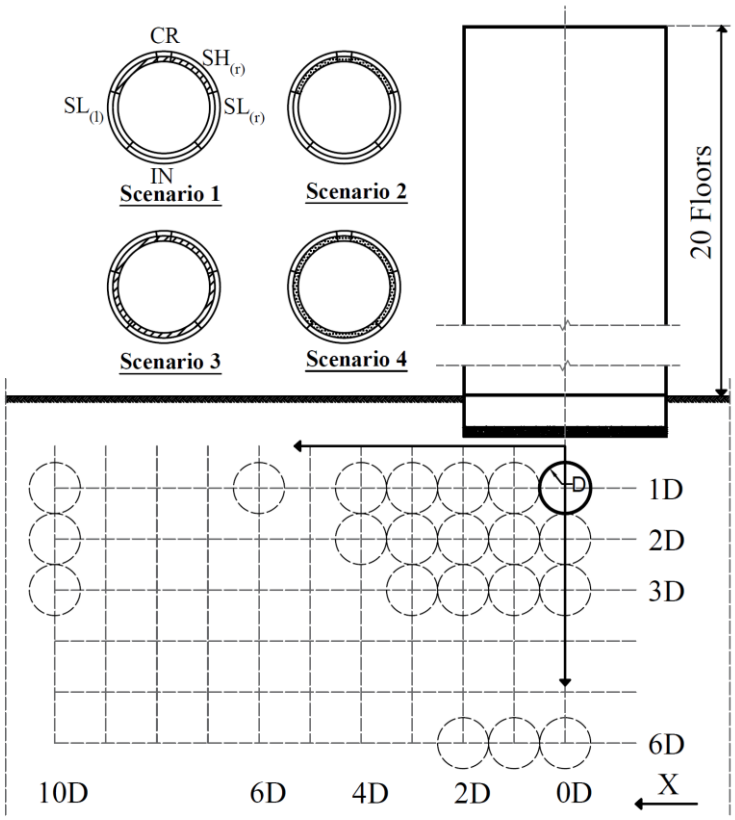

Figure 5- 8: Design of parametric study to investigate the interaction between pre-existing degraded tunnel linings and new construction

5.4.1 Effect of new construction on the distribution of radial stresses in pre-existing degraded tunnel linings

In the parametric study, to define an exclusion zone to minimize the effect of new construction on radial stresses developed in the degraded tunnel lining intrados and extrados for degradation scenarios 1, 2, 3 and 4, this study suggests that the maximum allowable increase in radial stresses

be set to 15% of the radial stresses existing in the case of an intact tunnel lining (i.e., where the tunnel lining is not degraded).

5.4.1.1 At the crown

Figure 5- 9 shows the distribution of extrados and intrados radial stresses at the crown level in an intact tunnel lining and in degradation scenarios 1 and 2 for tunnel burial depths of 1D, 2D, 3D, and 6D (where D is the tunnel diameter). Figure 5- 9 indicates a similar trend for extrados and intrados radial stresses in the intact lining and in scenarios 1 and 2. The radial stresses remain almost unchanged when the tunnel center is shifted horizontally from 0D (directly beneath the mat foundation centerline) to 1D. The radial stresses then decrease significantly to 3D, and subsequently continue to decline gradually as the horizontal distance from the new construction increases.

It can be seen from Figure 5- 9(a) that at a burial depth of one tunnel diameter, when the tunnel center is located directly beneath the centerline of the mat foundation, the extrados compressive stress in scenario 1 exhibits a 10% decrease in comparison to the extrados compressive stress of the intact lining. When the tunnel center is shifted horizontally two and six tunnel diameters from the mat foundation centerline, the extrados compressive stress decreases by 9% and 3%, respectively. For scenario 2, the extrados compressive stress decreases by 28%, 18%, and 1% when the tunnel center is shifted horizontally one, two, and six tunnel diameters from the foundation centerline, respectively. As shown in Figure 5- 9(b), at a tunnel burial depth of two tunnel diameters, directly beneath the mat foundation centerline, decreases of 12% and 36% in the extrados compressive stress are observed for scenarios 1 and 2, respectively, as compared to the situation in the intact lining. At a tunnel burial depth of six tunnel diameters, as shown in Figure 5- 9(d), declines of 4% and 13% in the extrados compressive stress are found for scenarios 1 and

2, respectively, as compared to the extrados compressive stress in the intact lining. As illustrated in Figure 5- 9, the extrados compressive stresses of scenarios 1 and 2 are lower than 8 MPa and are thus less than the limit compressive stress of concrete, which is 17.5 MPa and 12.5 MPa for scenarios 1 and 2 respectively. Thus, this will not result in failure of the concrete in compression. From Figure 5- 9, it is clear that the intrados radial stresses of scenarios 1 and 2 transition from tensile (T) to compressive (C) when the tunnel center is shifted horizontally more than one tunnel diameter from the mat foundation centerline. For scenario 1, at locations directly beneath the mat foundation centerline, the intrados tension stress decreases by 36%, 45%, and 41% in comparison to the intrados tension stress in the intact lining, at tunnel burial depths of one, two, and three tunnel diameters, respectively. For scenario 2, in comparison to the intrados stresses in the intact lining, the intrados stresses increase by 12%, 9%, and 23% at tunnel burial depths of one, two, and three tunnel diameters beneath the foundation centerline, respectively. For scenario 1, the tension stresses are less than the allowable tension stress of concrete, which is 3.0 MPa. However, for scenario 2, the tension stresses are larger than the allowable tension stress of concrete, which is 2.1 MPa for tunnel burial depths of one, two, and three tunnel diameters at horizontal locations less than 1D from the foundation centerline. Thus, a failure of concrete in tension may be observed at these locations, and tiny cracks can be expected to appear and propagate in the concrete.

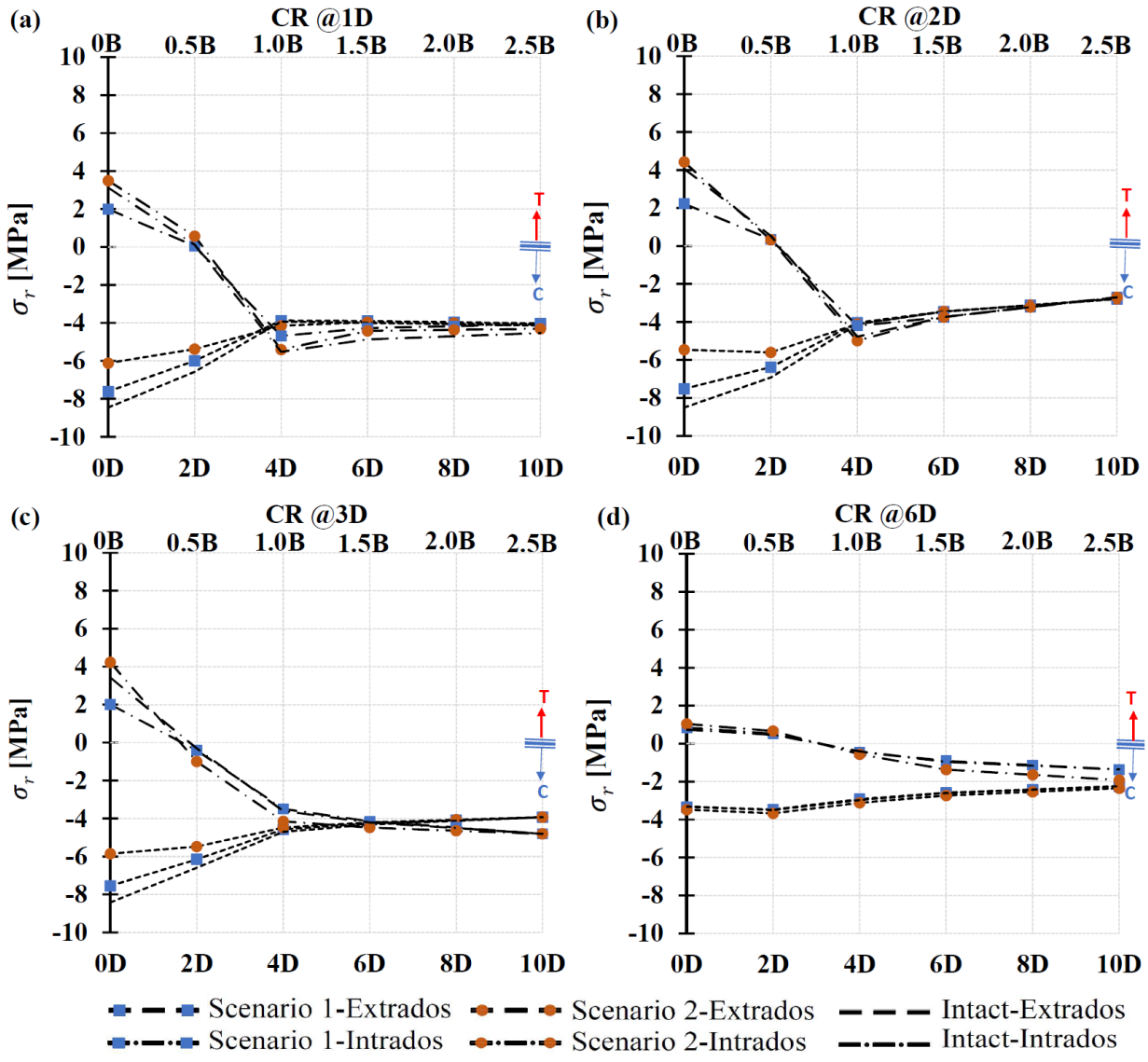

Figure 5- 9: Distribution of radial stresses in the lining extrados and intrados at the crown level in degradation scenarios 1 and 2, for tunnel burial depths of (a) 1D, (b) 2D, (c) 3D, and (d) 6D

Figure 5- 10 represents the distribution of extrados and intrados radial stresses at the crown level in an intact tunnel lining and in degradation scenarios 3 and 4 for tunnel burial depths of 1D, 2D, 3D, and 6D (where D is the tunnel diameter). A similar trend for extrados and intrados radial stresses is shown for the intact lining and scenarios 3 and 4. The radial stress remains almost unchanged when the tunnel center is shifted horizontally from 0D (where the tunnel center is

located directly beneath the mat foundation centerline) to one tunnel diameter away from the centerline. The radial stress then decreases sharply to 3D, and subsequently continues to decline gradually as the distance from new construction increases.

As seen in Figure 5- 10(a), at a tunnel burial depth of one tunnel diameter, when the tunnel center is located directly beneath the mat foundation centerline, there is a 10% decrease in the extrados compressive stress in scenario 3 and a 30% decrease in scenario 4. At a tunnel burial depth of two tunnel diameters, as shown in Figure 5- 10(b), decreases in the extrados compressive stress of 11% and 38% are seen in scenarios 3 and 4, respectively. At a tunnel burial depth of six tunnel diameters, as shown in Figure 5- 10(d), declines of 4% and 11% are found in scenarios 3 and 4, respectively. The compressive stresses are lower than 8 MPa and thus less than the limit compressive stress of concrete, which is 17.5 MPa and 11.9 MPa for scenarios 3 and 4, respectively. Thus, this will not result in failure of the concrete in compression. In scenario 3 the intrados tension stress decreases by 35%, 45%, and 41% at tunnel burial depths of one, two, and three tunnel diameters, respectively; while in scenario 4 it increases by 24%, 16%, and 22% at tunnel burial depths of one, two, and three tunnel diameters, respectively. In scenario 3, the tension stresses are less than the limit tension stress of concrete, which is 3.0 MPa. However, in scenario 4, the tension stresses are larger than the limit tension stress of concrete, which is 2.0 MPa at tunnel burial depths of one, two, and three tunnel diameters at horizontal locations less than 1D from the foundation centerline. Thus, a failure of concrete in tension may be observed at these locations.

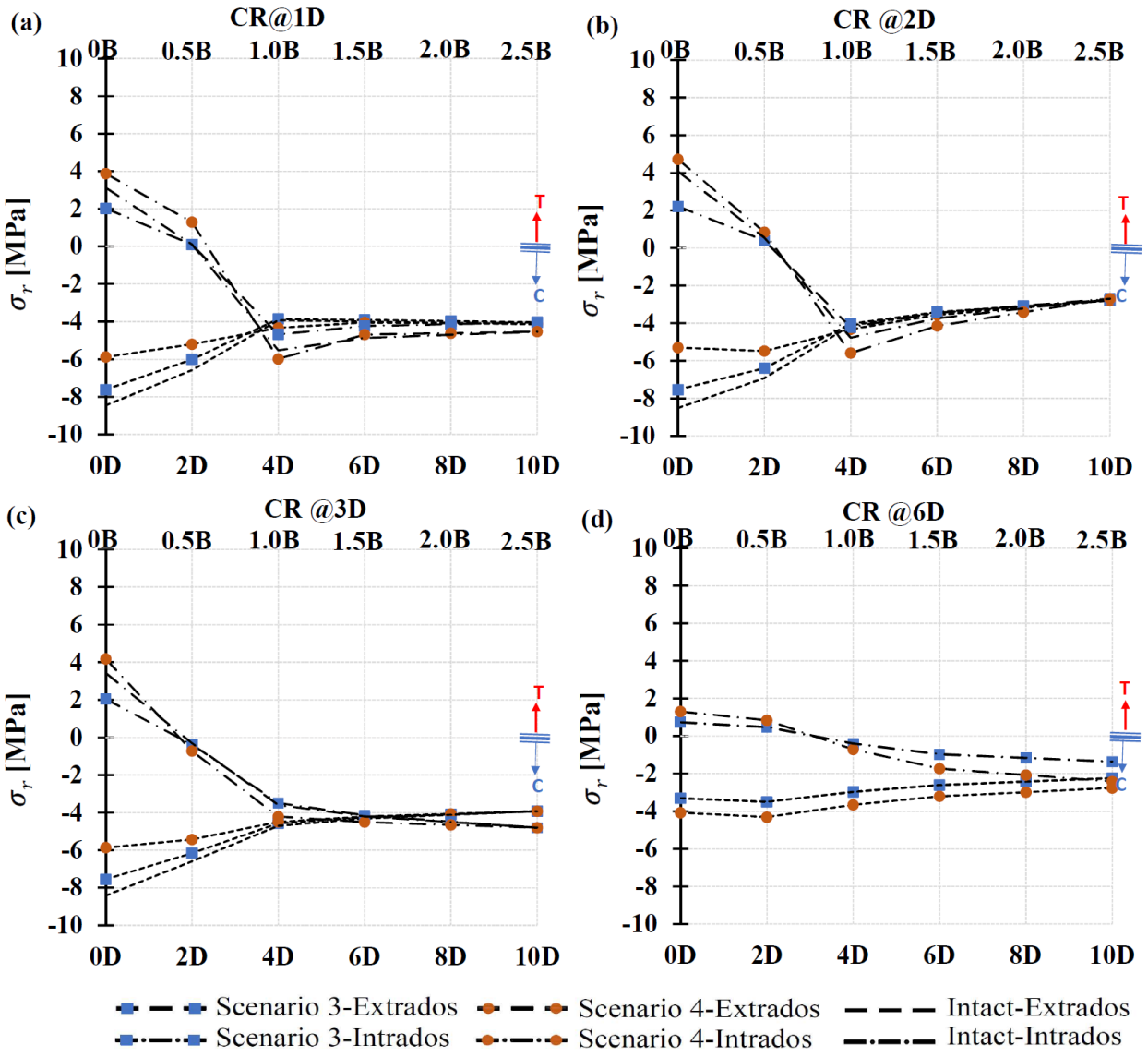

Figure 5- 10: *Distribution of radial stresses in the lining extrados and intrados at the crown level in degradation scenarios 3 and 4*

It can be concluded from Figures 5- 9 and 5- 10 that the extrados crown stresses are compressive. As the lining stiffness decreases, they can be observed to decrease. In accordance with Terzaghi's arching theory (Therzaghi, 1943) most of the load added by the new structure arches away from the degraded tunnel lining sections to stiffer ground. Intrados tensile stresses are observed to increase as the lining stiffness decreases. These stresses exceed the ultimate tensile strength of concrete at tunnel burial depths of one, two, and three tunnel diameters at horizontal locations less

than one tunnel diameter from the foundation centerline in scenarios 2 and 4. Thus, a failure of concrete in tension may be observed at these locations, and tiny cracks can be expected to appear and propagate in the concrete at the crown. In general, increased burial depth and increased horizontal distance from the mat foundation centreline reduce radial stresses at the crown.

5.4.1.2 At the invert

Figures 5- 11 and 5- 12 represent the distribution of extrados and intrados radial stresses at the invert level in an intact lining and in degradation scenarios 1, 2, 3, and 4 for tunnel burial depths of 1D, 2D, 3D, and 6D (where D is the tunnel diameter). Similar trends for extrados and intrados radial stresses in the intact lining and in the different scenarios are indicated in Figures 5- 11 and 5- 12.

Figure 5- 11 shows that the radial stress remains almost unchanged when the tunnel center is shifted horizontally from 0D (where the tunnel center is located directly beneath the mat foundation centerline) to one tunnel diameter away from the centerline. The radial stresses decrease sharply between one and four tunnel diameters away from the centerline, and then decline steadily with increasing distance from the new construction, up to ten tunnel diameters away from the foundation centerline. The compressive extrados stresses are lower than 8 MPa and thus are less than the limit compressive stress of concrete, which is 22.9 MPa for scenarios 1 and 2 at the invert level. However, in scenarios 1 and 2, the tension stresses are larger than the limit tension stress of concrete, which is 4.1 MPa at the invert level, for tunnel burial depths of one and two tunnel diameters at horizontal locations less than one tunnel diameter from the foundation centerline. Thus, a failure of concrete in tension may be observed at these locations.

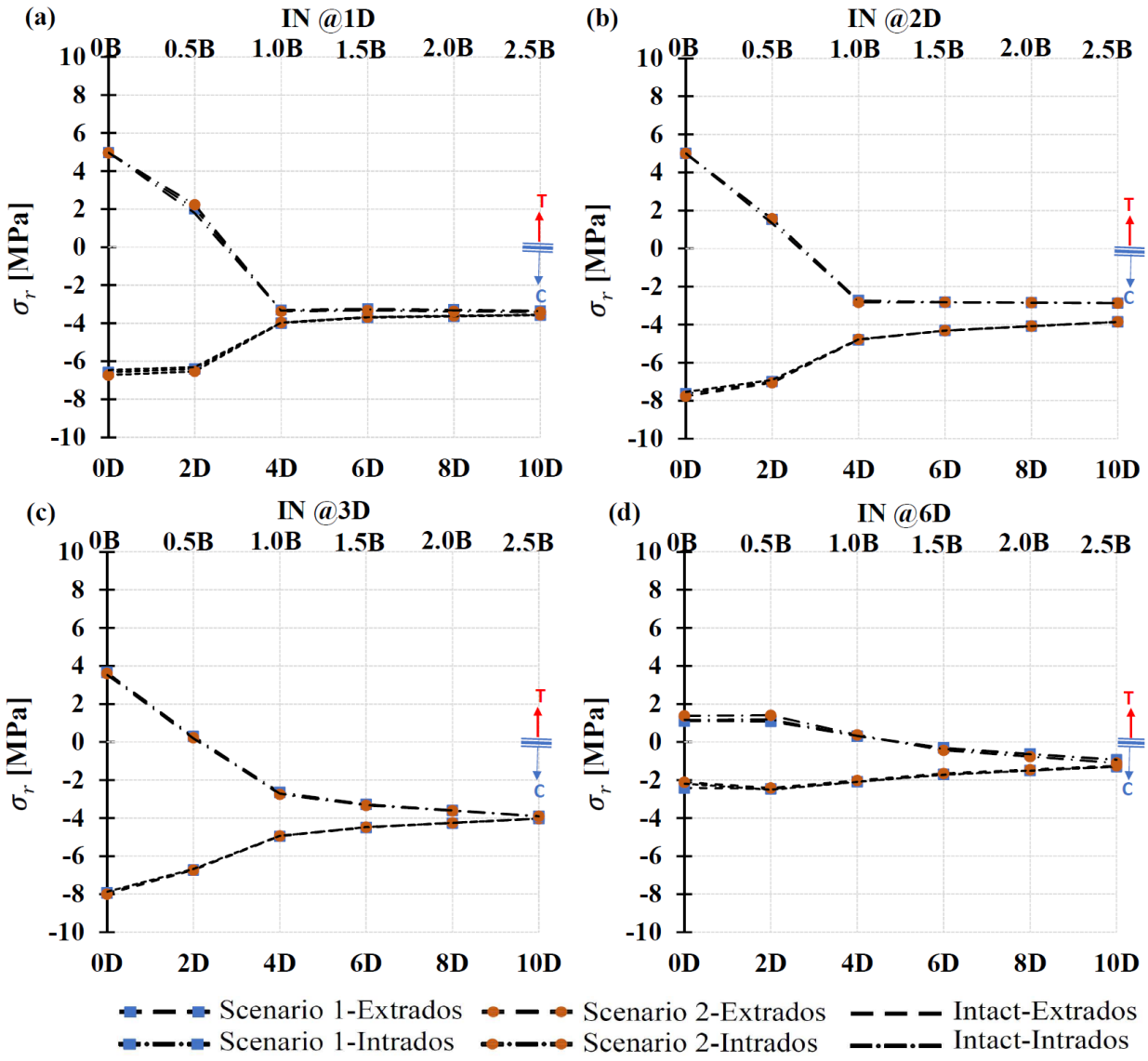

Figure 5- 11: Distribution of radial stresses in the lining extrados and intrados at the invert level in degradation scenarios 1 and 2

As shown in Figure 5- 12, for tunnel burial depths of one, two, and six tunnel diameters, at a location directly beneath the mat foundation centerline, the extrados radial stresses decrease 14%, 11%, and 6%, respectively, in scenario 3; and 33%, 26%, and 11%, respectively, in scenario 4. The maximum compressive stress for both scenarios is lower than 8 MPa and thus less than the limit stress, which is 17.5 MPa and 11.9 MPa for scenarios 3 and 4, respectively. However, the intrados stresses for tunnel burial depths of one and two tunnel diameters, at a horizontal location

one tunnel diameter or less from the mat foundation centerline, are larger than the limit tensile stress for concrete. Thus, failure in tension may be observed at these locations.

It can be concluded from Figures 5- 11 and 5- 12 that radial stresses at the invert level decrease with increased tunnel burial depth and increased horizontal distance from the mat foundation centerline. The intrados and extrados radial stresses in scenarios 1 and 2 are similar to those in the intact lining. As expected, in these scenarios no degradation occurs at the invert level in the tunnel lining. However, in scenarios 3 and 4, the radial stresses are observed to decrease as the stiffness decreases. Failure in tension may occur and cracks may propagate at the invert when the tunnel center has a burial depth of one or two tunnel diameters, and a horizontal location less than one tunnel diameter from the centerline of the mat foundation.

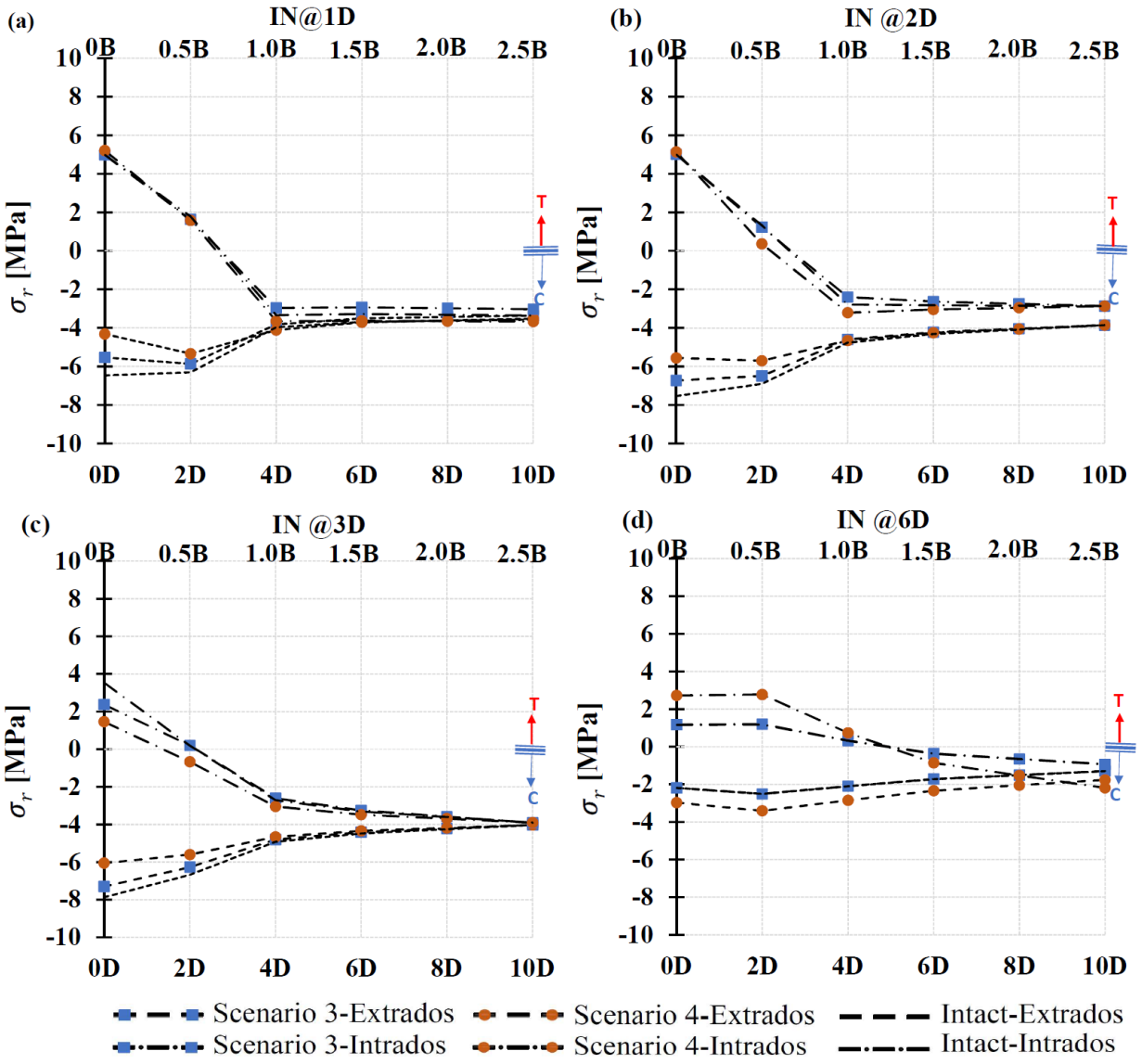

Figure 5- 12: Distribution of radial stresses in the lining extrados and intrados at the invert level in degradation scenarios 3 and 4

5.4.1.3 At the right springline

The variation of radial stresses in the tunnel lining extrados and intrados at the right springline level is shown in Figure 5- 13 for scenarios 1 and 2, and in Figure 5- 14 for scenarios 3 and 4, at tunnel burial depths of 1D, 2D, 3D, and 6D (where D is the tunnel diameter). These figures indicate

a similar trend for radial stresses in the intact lining and the different scenarios. The extrados stresses are in the compression (C) state for all degradation scenarios and are found to decrease as the lining stiffness increases. Large compressive stresses occur in the lining intrados. As illustrated in Figure 5- 13, in comparison to intrados compressive stresses in the intact lining, the intrados compressive stresses in scenarios 1 and 2 exhibit a slight decrease of approximately 1% and 10%, respectively, for burial depths varying from one tunnel diameter to six tunnel diameters, at a horizontal location directly beneath the mat foundation centerline. In Figure 5- 14, it can be seen that there is an 18% decrease in scenario 3 and a 14% increase in scenario 4. The axial stresses due to thrust forces at the lining springline level are larger than the bending stresses due to the bending moment. The compressive strength of concrete is generally much greater than its tensile strength, which is a favorable situation at the springline level. For scenarios 1, 2, and 3, the compressive stresses are less than the limit compressive stress. For scenario 4, the intrados compressive stresses for tunnel burial depths of one, two, and three tunnel diameters, at horizontal locations two tunnel diameters or less from the centerline of the mat foundation are larger than 11.9 MPa, the limit compressive stress. Thus, failure in compression may be seen. However, the compressive stresses decrease with increasing horizontal distance of the tunnel center from the mat foundation centerline.

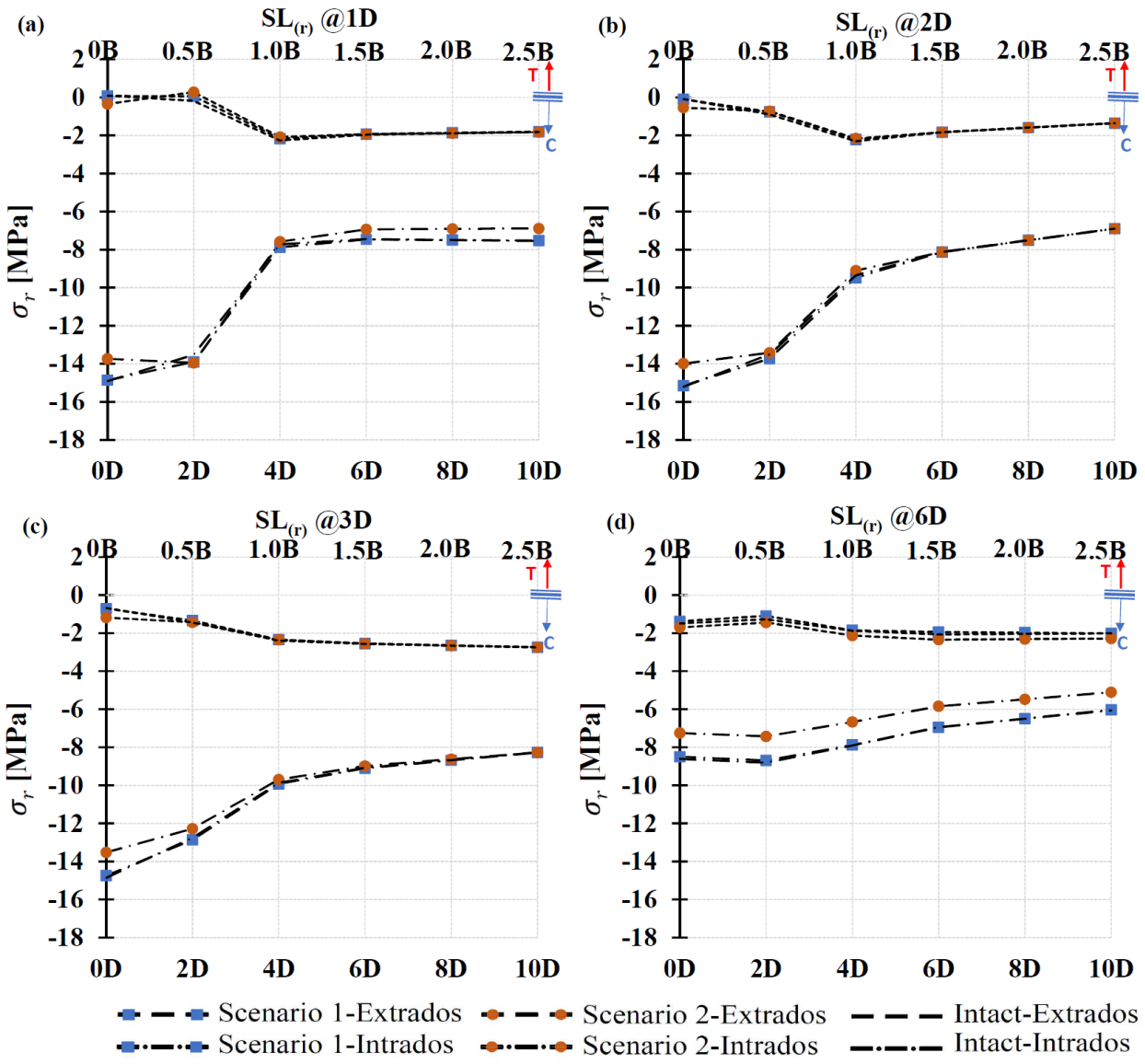

Figure 5- 13: Distribution of radial stresses in the lining extrados and intrados at the right springline level in degradation scenarios 1 and 2

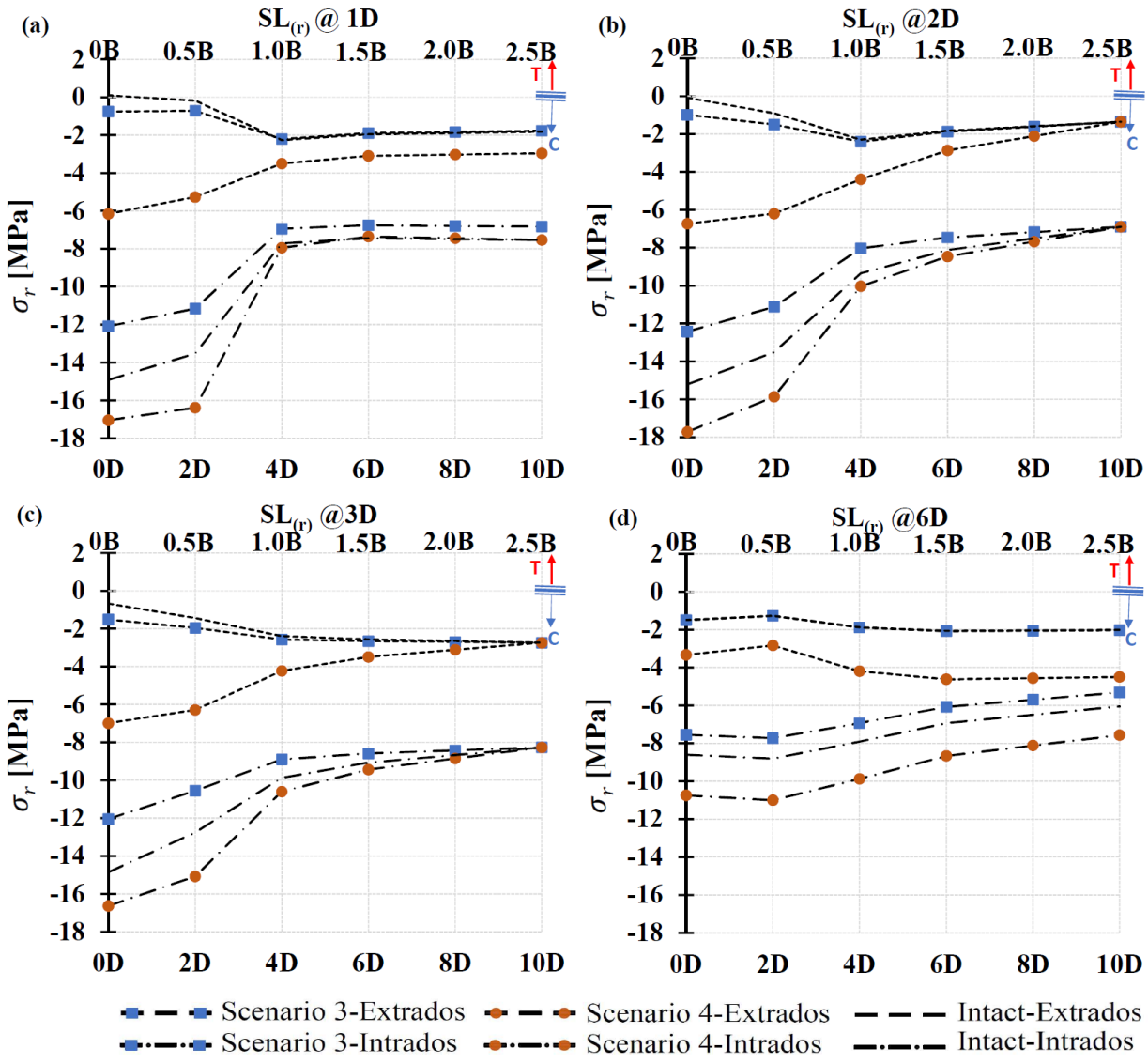

Figure 5- 14: Distribution of radial stresses in the lining extrados and intrados at the right springline level in degradation scenarios 3 and 4

5.4.1.4 At the left springline

Figures 5- 15 and 5- 16 represent the distribution of extrados and intrados radial stresses at the left springline level in an intact lining and in degradation scenarios 1, 2, 3, and 4 for tunnel burial depths of 1D, 2D, 3D, and 6D (where D is the tunnel diameter). Figure 5- 16 shows a similar trend for extrados and intrados radial stresses in the intact lining and in scenario 4. The radial stress remains relatively unchanged when the tunnel center is shifted horizontally from 0D (where the

tunnel center is located directly beneath the mat foundation centerline) to one tunnel diameter from the centerline. The radial stress then decreases sharply to 3D, and from there continues to decline gradually as the horizontal distance from the new construction increases. As at the right springline level, large compressive stresses occur in the lining intrados. Figure 5- 15 shows that in comparison to the situation with an intact tunnel lining, in scenarios 1 and 2, the intrados compressive stress decreases slightly by approximately 1% and 10%, respectively, at tunnel burial depths of one tunnel diameter and six tunnel diameters, located directly beneath the mat foundation centerline. In both scenarios, the compressive stresses are less than the limit compressive stress. Figure 5- 16 shows a decline of 19% in scenario 3 and an increase of 12% in scenario 4. Otherwise, the compressive stresses are less than the limit compressive stress in scenario 3. In scenario 4, the intrados stresses for tunnel burial depths of one, two, and three tunnel diameters, at horizontal locations two tunnel diameters or less from the mat foundation centerline are larger than the limit compressive stress. Thus, failure in compression may be seen. However, the compressive stresses decrease with increasing horizontal distance of the tunnel center from the mat foundation centerline.

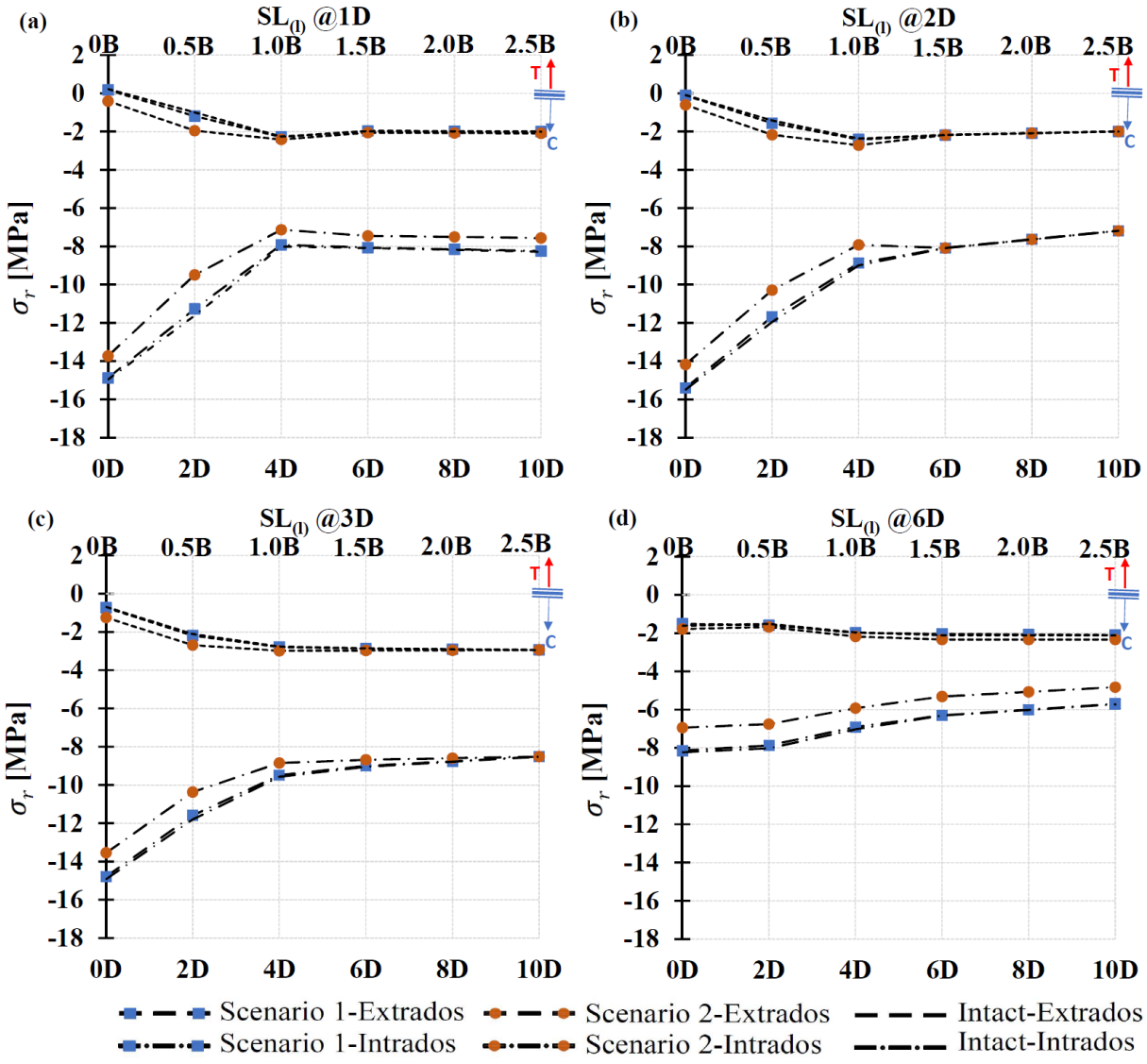

Figure 5- 15: Distribution of radial stresses in the lining extrados and intrados at the left springline level in degradation scenarios 1 and 2

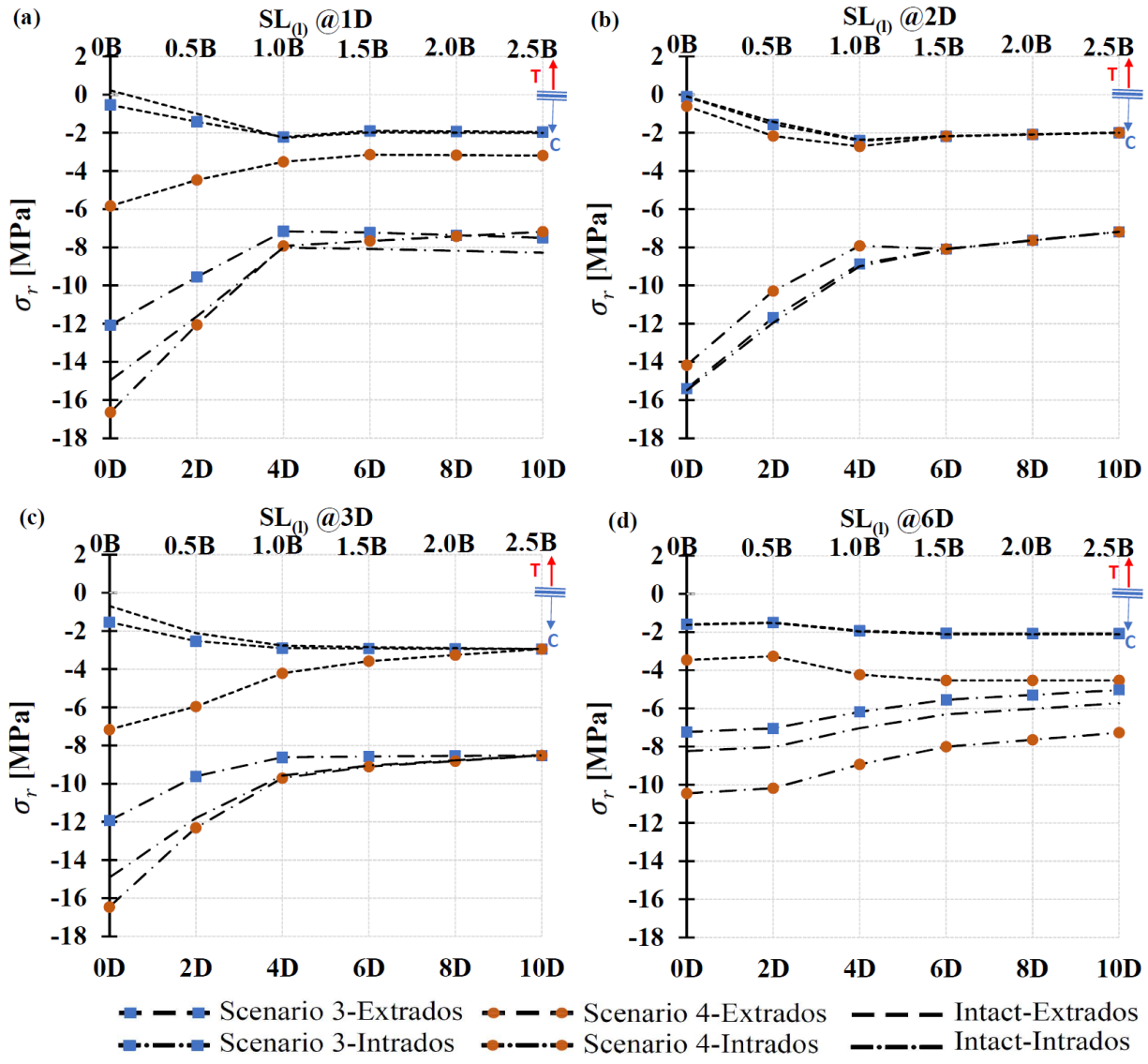

Figure 5- 16: Distribution of radial stresses in the lining extrados and intrados at the left springline level in degradation scenarios 3 and 4

5.4.1.5 At the right shoulder level

Figures 5- 17 and 5- 18 represent the distribution of extrados and intrados radial stresses at the right shoulder level in an intact lining and in degradation scenarios 1, 2, 3, and 4 for tunnel burial

depths of 1D, 2D, 3D, and 6D (where D is the tunnel diameter). These figures show a similar trend for extrados and intrados radial stresses in the intact lining and the different scenarios. From the figures, it can be seen that the intrados and extrados radial stresses are in a compressive (C) state and fluctuate with the horizontal distance from the mat foundation centerline. However, because the radial compressive stresses are less than the compressive stress limit for scenarios 1, 2, 3, and 4, this will not result in failure of the concrete in compression.

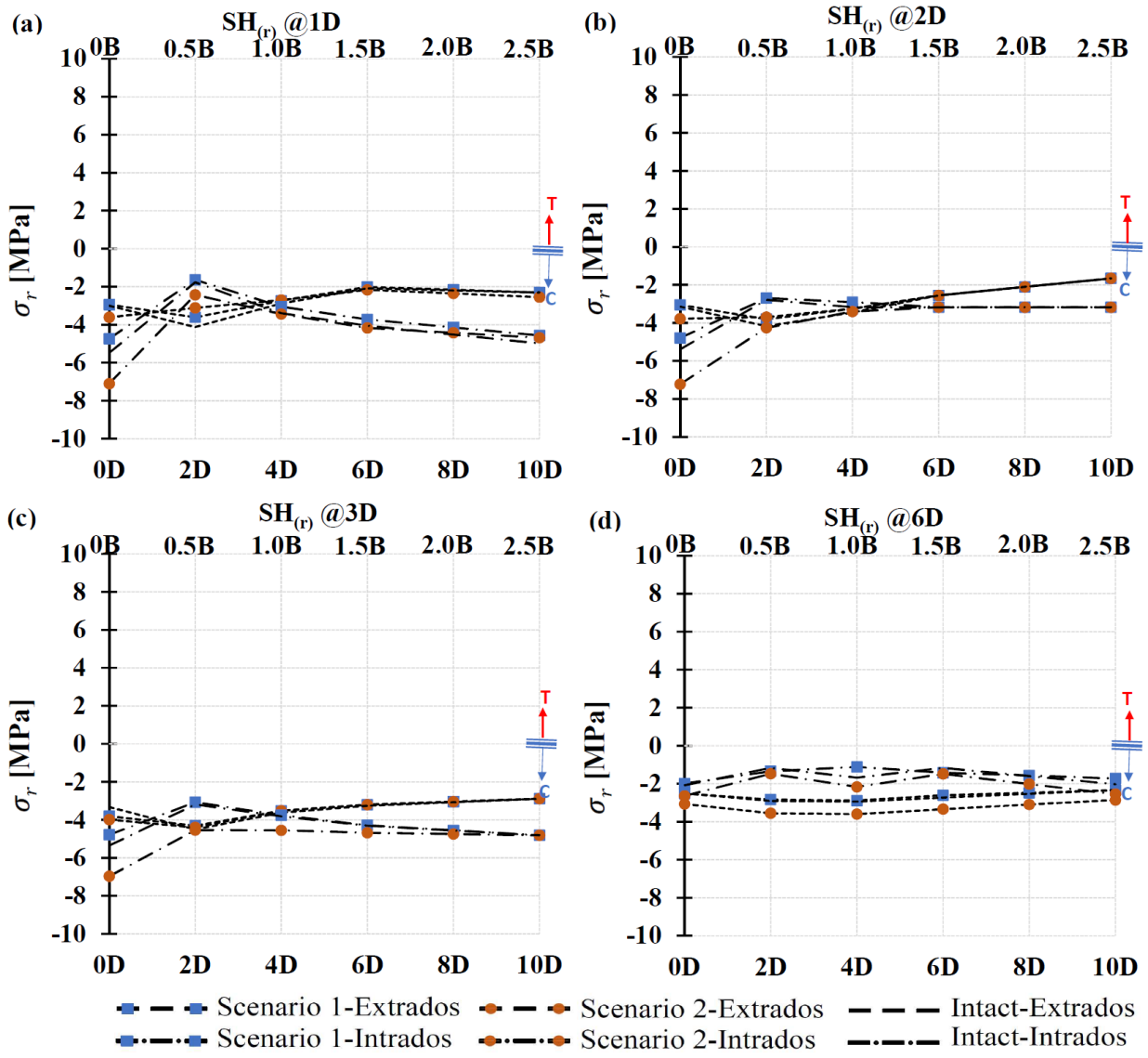

Figure 5- 17: Distribution of radial stresses in the lining extrados and intrados at the right shoulder level in degradation scenarios 1 and 2

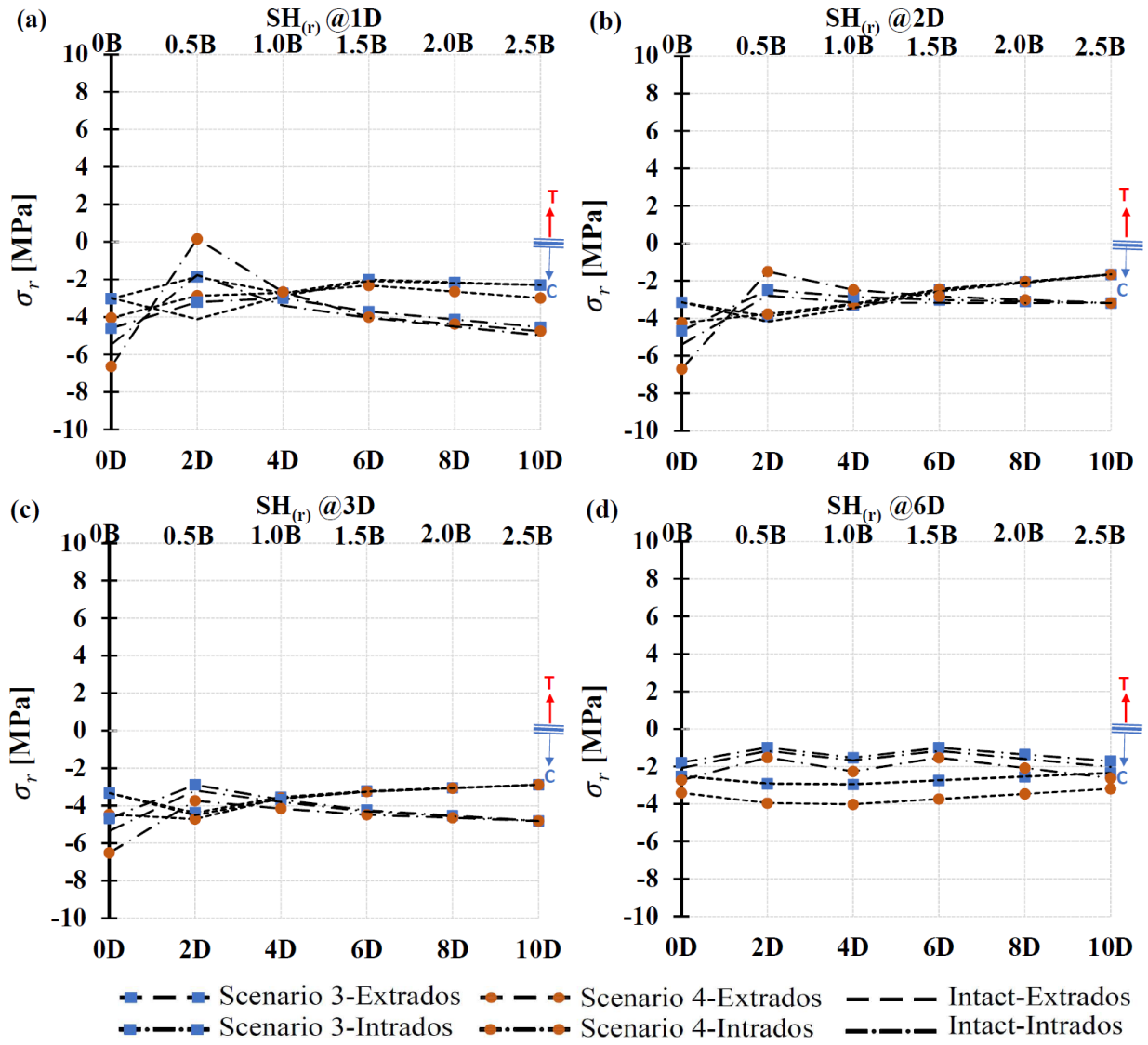

Figure 5- 18: Distribution of radial stresses in the lining extrados and intrados at the right shoulder level in degradation scenarios 3 and 4

5.4.1.6 Zone excluded due to the effect of radial stresses

In light of the findings described above regarding the redistribution of radial stresses in degradation scenarios 1, 2, 3, and 4, an exclusion zone based on the effect of radial stresses can be defined, as illustrated in Figure 5- 19.

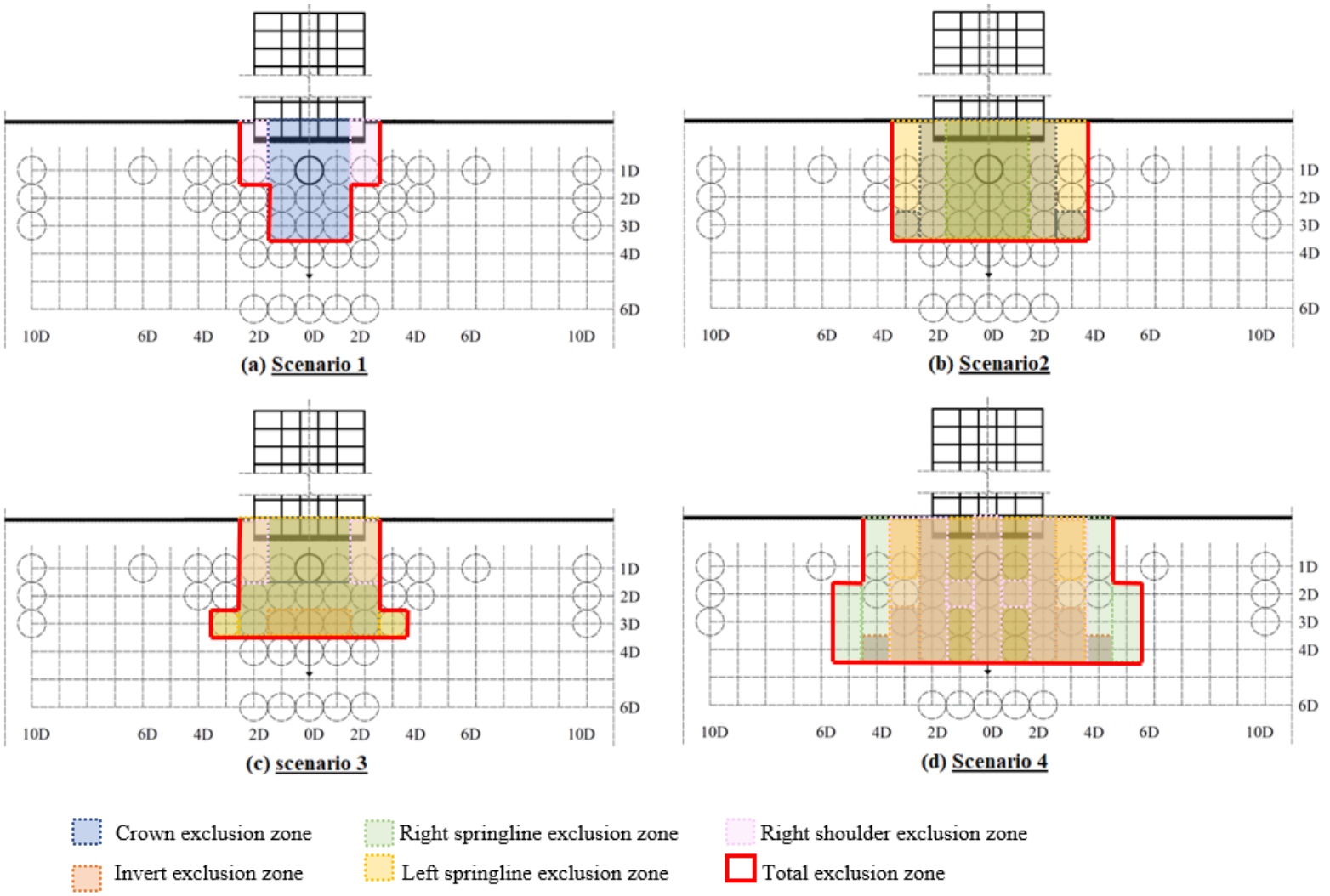

Figure 5- 19: Zone excluded due to the effect of radial stresses

5.4.2 Effect of new structure on vertical deformation of the pre-existing degraded tunnel lining

5.4.2.1 At the crown

Figures 5- 20 and 5- 21 represent the distribution of additional vertical deformation at the crown level in an intact tunnel lining and in degradation scenarios 1, 2, 3, and 4, for tunnel burial depths of 1D, 2D, 3D, and 6D (where D is the tunnel diameter). These figures show that similar trends of additional vertical deformation at the crown level occur in the intact lining and in the four different degradation scenarios. The additional vertical deformation decreases as the tunnel lining stiffness increases; as the position of the new construction is shifted horizontally away from tunnel; and as the burial depth of the bored tunnel increases. The maximum additional vertical deformation in the four scenarios is compared with that of an intact tunnel lining when the tunnel center is directly beneath the mat foundation centerline. The increase in vertical deformation at the crown is 2.5% in scenario 1 for a tunnel burial depth of one tunnel diameter; 9.6% in scenario 2; 4.4% in scenario 3; and 18.0% in scenario 4. These variations show the impact of tunnel lining stiffness on the additional vertical deformation. The stiffer the tunnel, the less additional vertical variation is found at the crown.

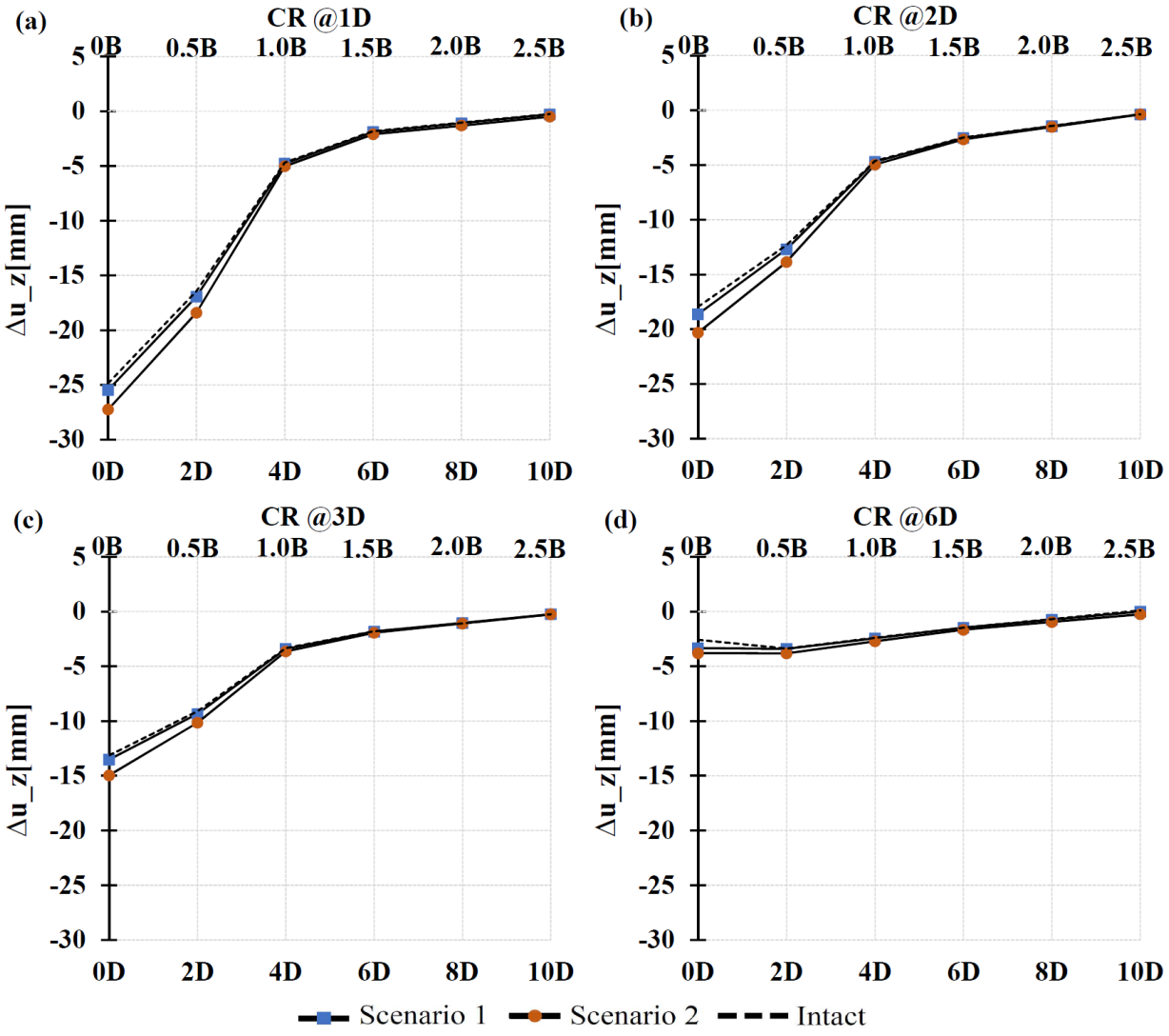

Figure 5- 20: Vertical deformation degradation at the crown level in scenarios 1 and 2

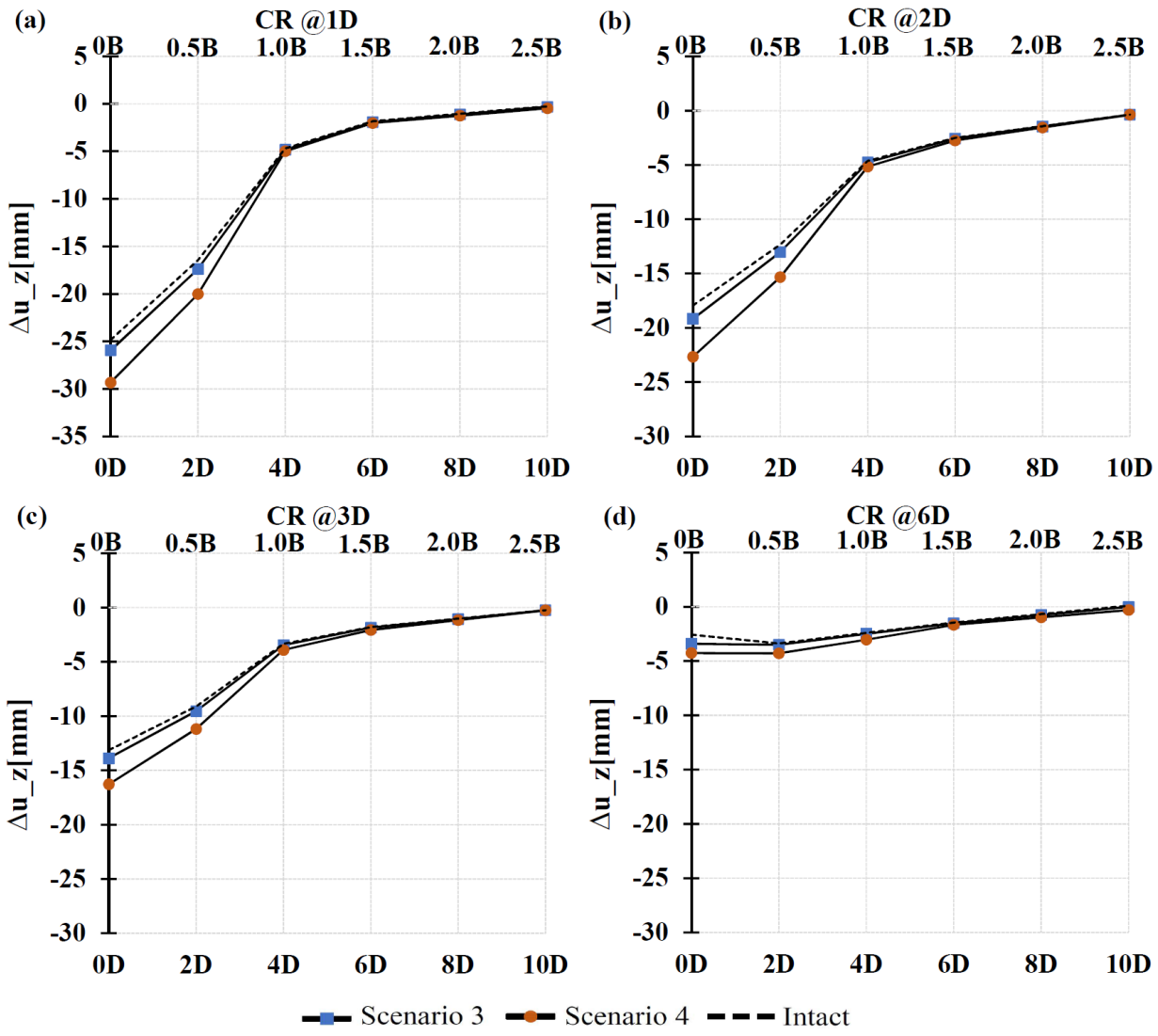

Figure 5- 21: Vertical deformation degradation at the crown level in scenarios 3 and 4

5.4.2.2 At the invert

The additional vertical deformation at the invert level as a function of the position of the tunnel center in relation to the mat foundation centerline is shown in Figure 5- 22 for degradation scenarios 1 and 2 and in Figure 5- 23 for degradation scenarios 3 and 4, for tunnel burial depths of 1D, 2D, 3D, and 6D (where D is the tunnel diameter). These different scenarios are compared with the situation for an intact tunnel lining. As illustrated in Figure 5- 22, in scenarios 1 and 2 the vertical deformation is unchanged in comparison

to the situation with an intact lining, since the lining at the invert level in scenarios 1 and 2 is not degraded. In scenario 3 (see Figure 5- 23), the additional vertical deformation remains fairly stable at approximately 5%. In scenario 4 (see Figure 5- 23), the vertical deformation decreases by 11.9%, 23.4%, and 31.9% when the tunnel center beneath the mat foundation centerline is located at burial depths of one, two, or three tunnel diameters, respectively. It can be concluded that additional vertical deformation at the invert increases as the lining stiffness decreases.

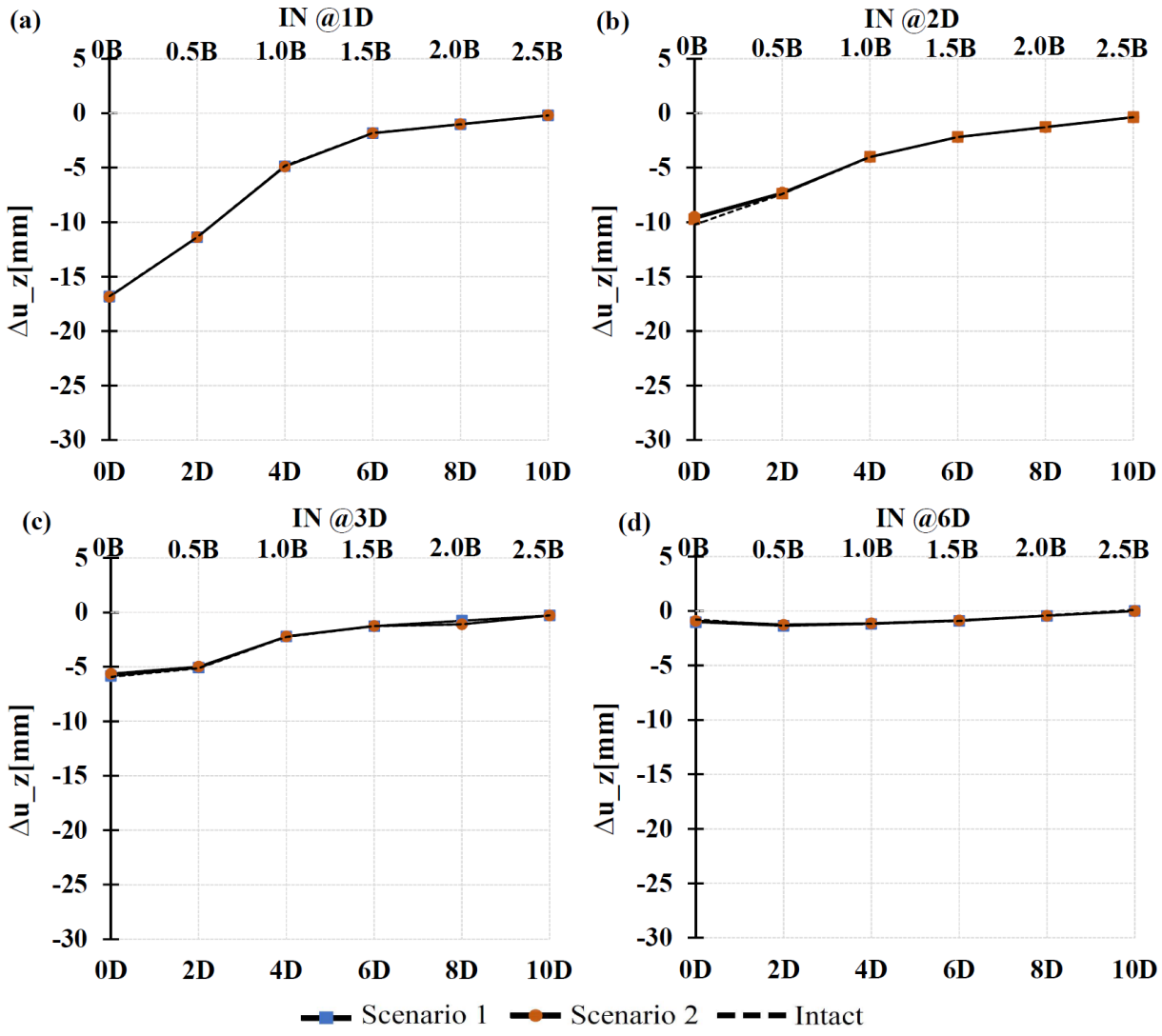

Figure 5- 22: Vertical deformation degradation at the invert level in scenarios 1 and 2

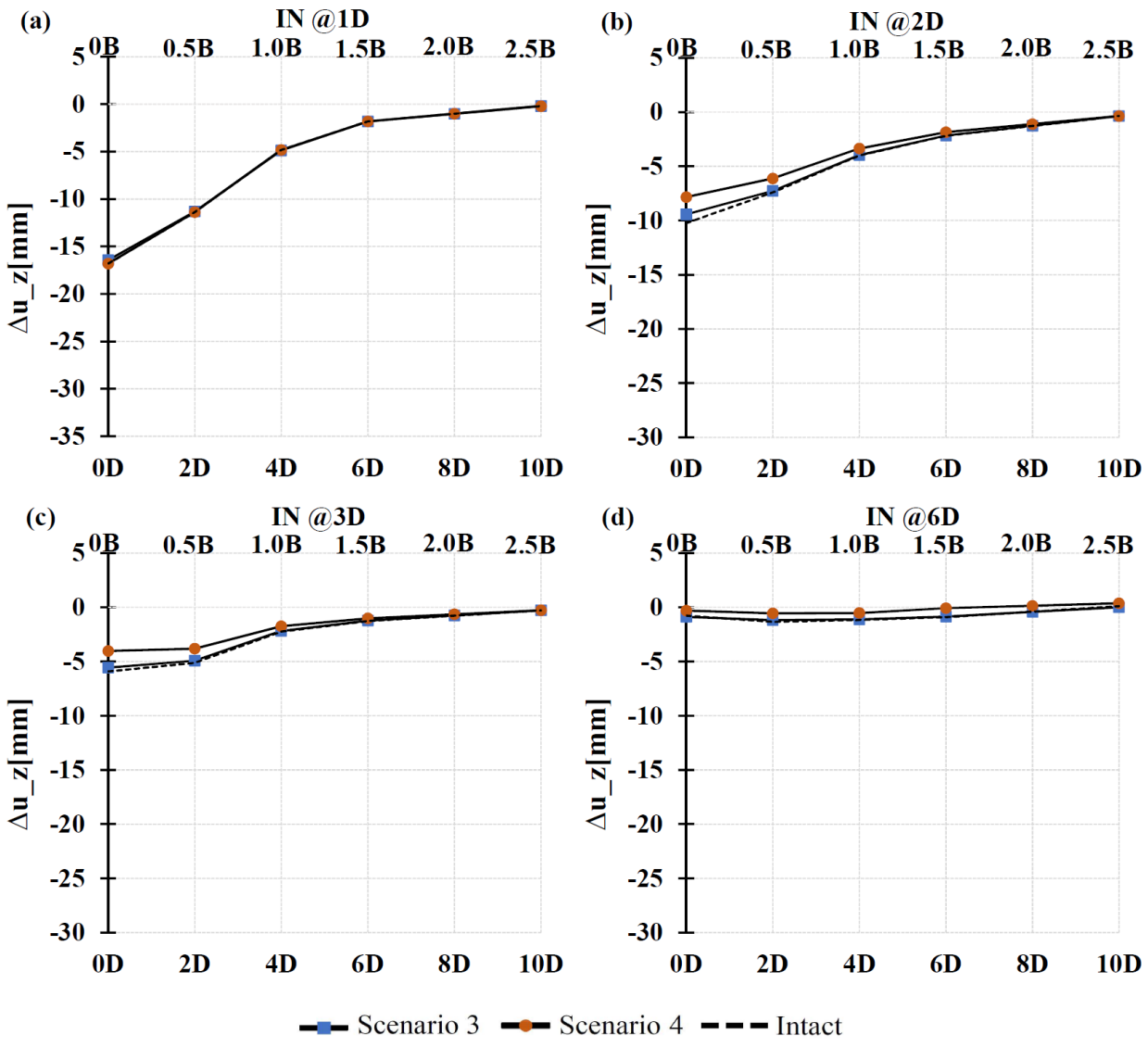

Figure 5- 23: Vertical deformation degradation at the invert level in scenarios 3 and 4

5.4.2.3 At the right shoulder

Figures 5- 24 and 5- 25 represent the distribution of additional vertical deformation at the right shoulder level in an intact tunnel lining and in degradation scenarios 1, 2, 3, and 4, for tunnel burial depths of 1D, 2D, 3D, and 6D (where D is the tunnel diameter). There is an increase in the additional vertical deformation at the right shoulder of around 1% in scenario 1, 4% in scenario 2, 3.5% in scenario 3, and around 14% in scenario 4 when the tunnel center is located directly beneath the mat foundation at a burial depth of one, two, or three tunnel diameters. The variation of additional vertical deformation remains almost unchanged when the tunnel center is shifted horizontally three or more tunnel diameters; in these tunnel locations, the influence of the new structure is negligible. These variations show the impact of tunnel lining stiffness on the additional vertical deformation. The stiffer the tunnel lining, the less additional vertical variation is found at the right shoulder.

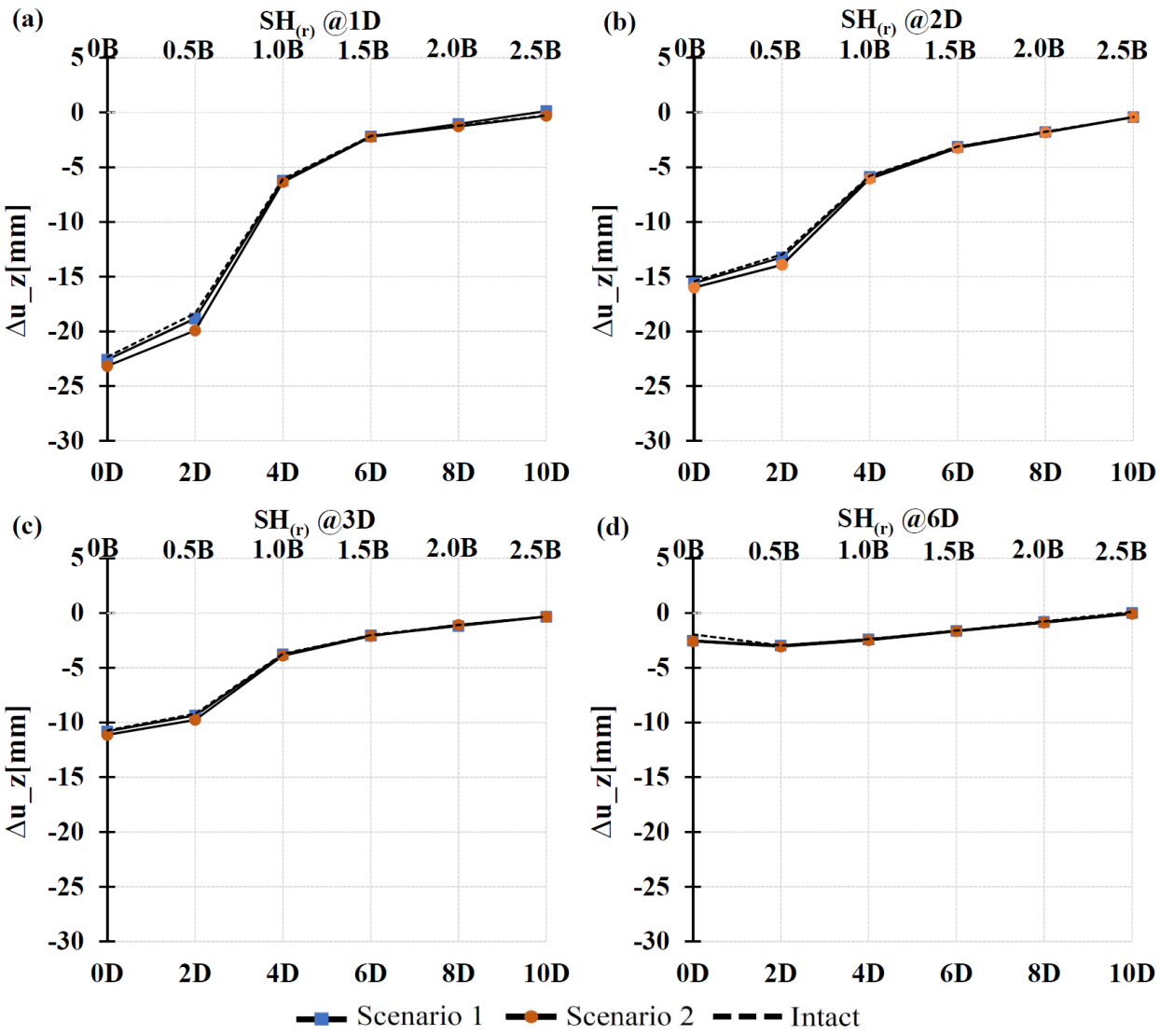

Figure 5- 24: Vertical deformation degradation at the right shoulder level in scenarios 1 and 2

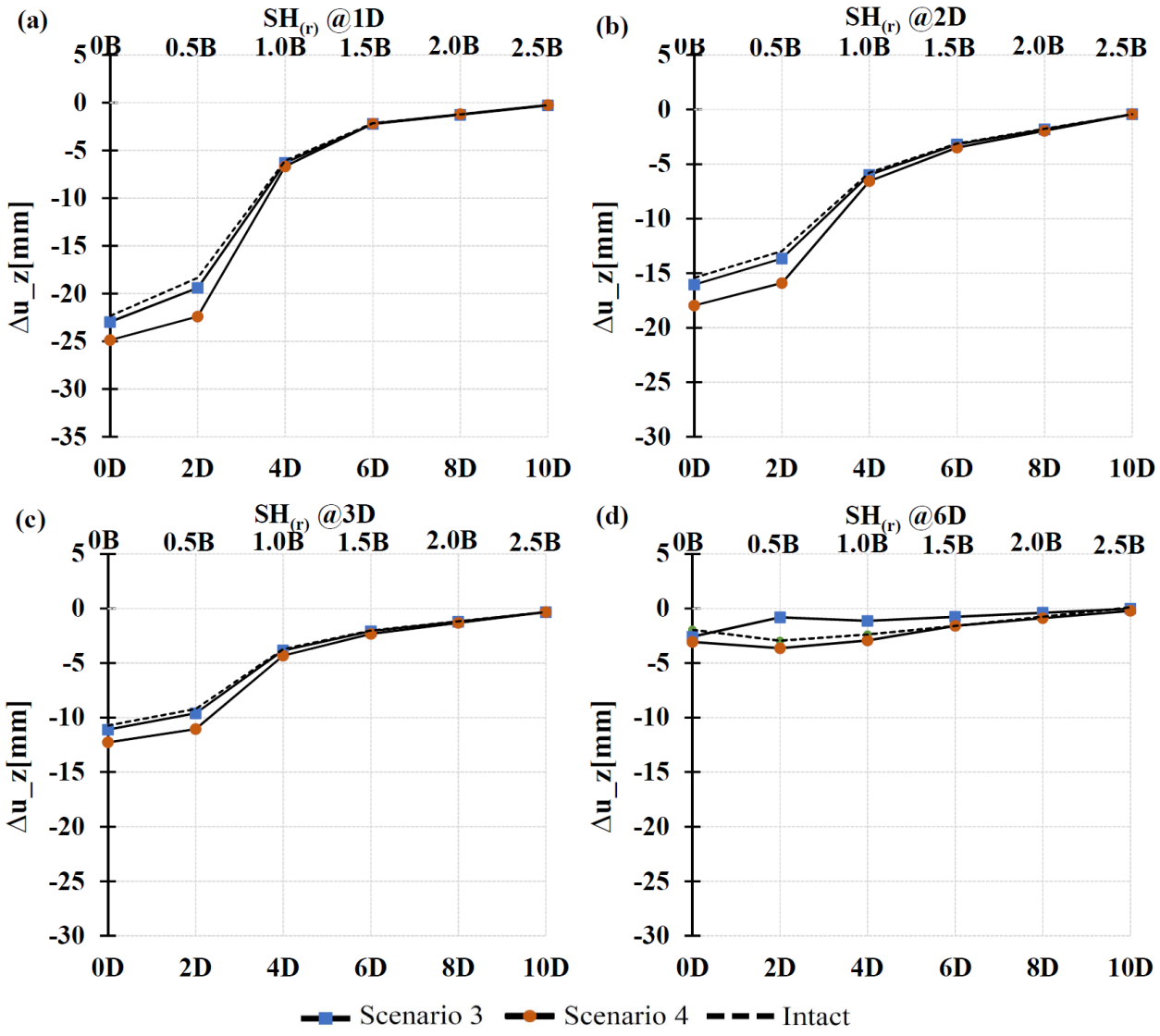

Figure 5- 25: Vertical deformation degradation at the right shoulder level in scenarios 3 and 4

5.4.2.4 Zone excluded due to the effect of vertical deformation

According to the Land Transport Authority of Singapore (*Code of Practice for Railway Protection.* 2004)(LTA, 2000), the allowable limit for the total movement of a bored tunnel due to new construction is 15 mm in any direction. The present study accordingly suggests setting a value of 15 mm as the maximum displacement allowed for existing tunnels due to new construction; and when the displacement is greater than 10 mm, an early warning is to be issued. Figure 5- 26 shows the zone excluded due to the effect of increased vertical deformation.

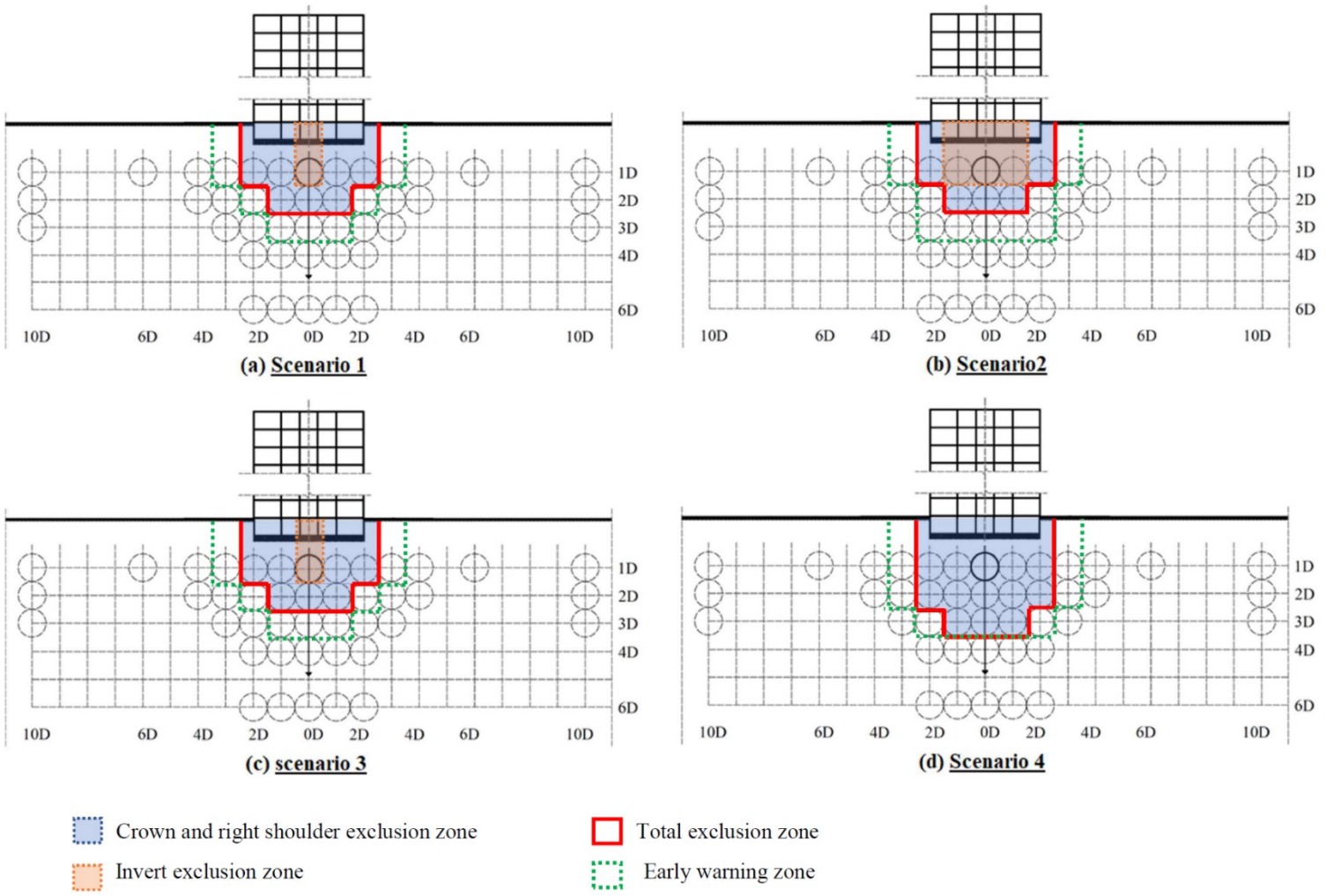

Figure 5- 26: Zone excluded due to the effect of increased vertical deformation

5.4.3 Effect of new structure on horizontal deformation of the pre-existing degraded tunnel lining

5.4.3.1 At the right springline

The additional horizontal deformation at the right springline of the tunnel lining is shown in Figure 5- 27 for scenarios 1 and 2, and in Figure 5- 28 for scenarios 3 and 4. Similar trends can be observed for the intact lining and the different scenarios. The horizontal deformation decreases considerably when the tunnel center is shifted three tunnel diameters horizontally from the mat foundation centerline. At a greater distance of the tunnel from the foundation centerline, the horizontal deformation increases slightly. When the tunnel is located directly beneath the mat foundation centerline at burial depths of one, two, and three tunnel diameters, in comparison to the situation with an intact tunnel lining, the decrease in additional horizontal deformation is around 5% in scenario 1, 15% in scenario 2, 17% in scenario 3, and 73% in scenario 4. These variations illustrate the relationship between tunnel stiffness and horizontal deformation. The horizontal deformation and tunnel lining stiffness are inversely proportional. In all four degradation scenarios, the additional horizontal deformation is similar to that for an intact lining when the tunnel is shifted horizontally more than four tunnel diameters from the mat foundation centerline at the different burial depths. The building loading has less effect on the tunnel lining at these tunnel locations.

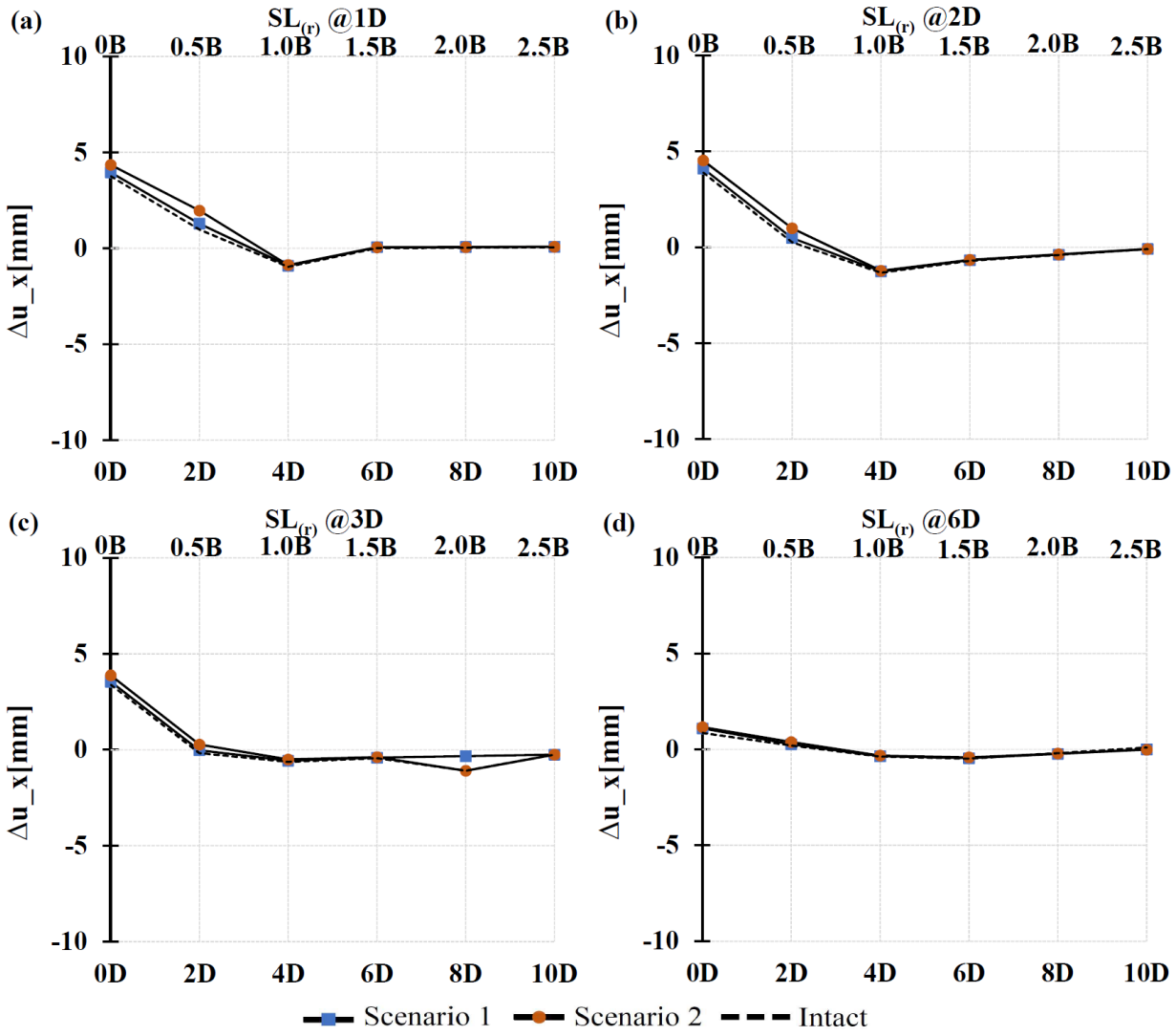

Figure 5- 27: Horizontal deformation degradation at the right springline level in scenarios 1 and 2

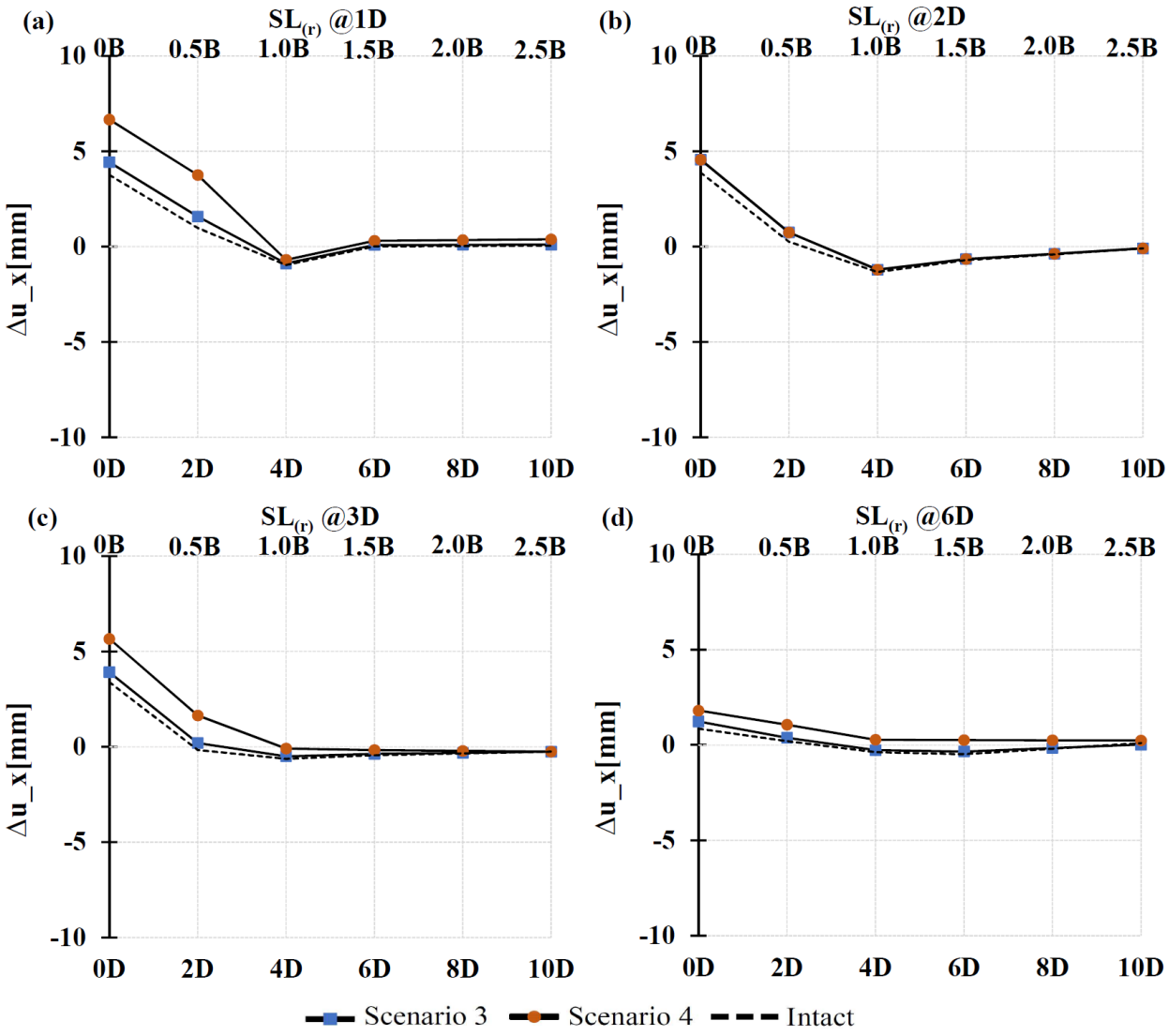

Figure 5- 28: Horizontal deformation degradation at the right springline level in scenarios 3 and 4

5.4.3.2 At the left springline

Figures 5- 29 and 5- 30 show the additional horizontal deformation at the left springline of the tunnel lining for scenarios 1, 2, 3, and 4. Horizontal deformations at the right springline are similar to those at the left springline. It should be noted that negative values in Figures 5- 29 and 5- 30 indicate movements to the left at the left springline level of the tunnel and positive values in Figures 5- 27 and 5- 28 indicate movements to the right at the right springline level.

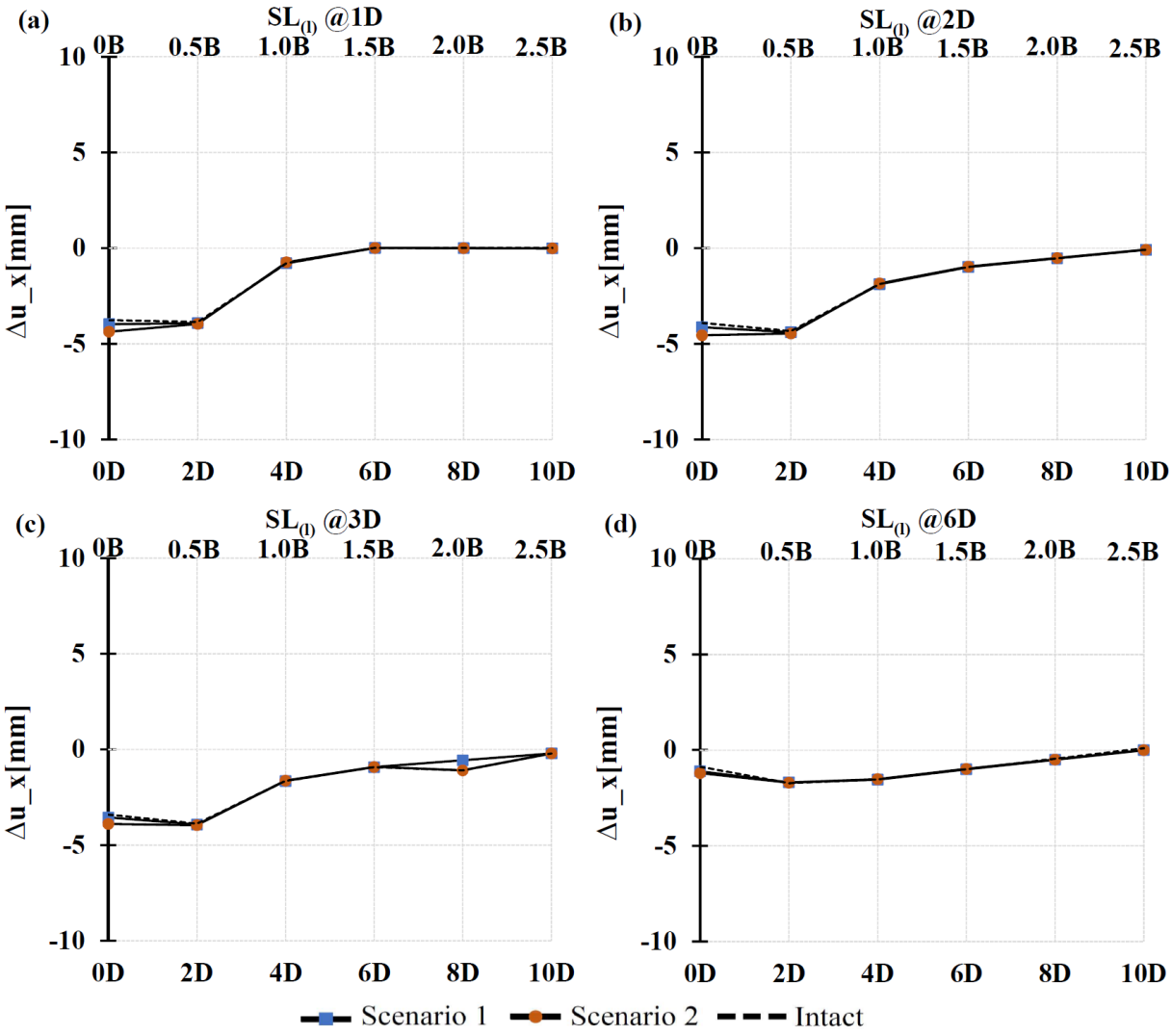

Figure 5- 29: Horizontal deformation degradation at the left springline level in scenarios 1 and 2

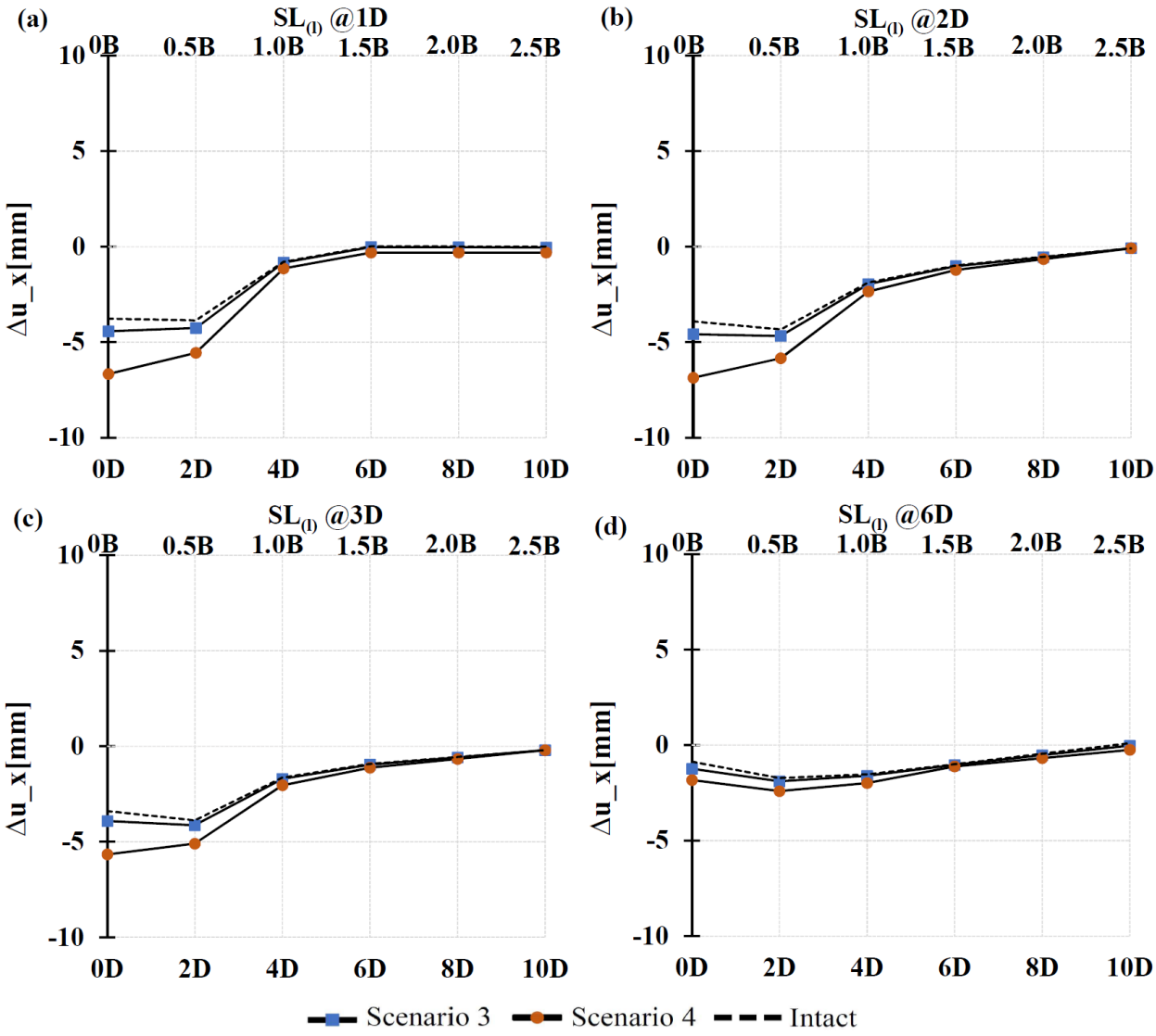

Figure 5- 30: Horizontal deformation degradation at the left springline level in scenarios 3 and 4

5.4.3.3 At the right shoulder

The variation of horizontal deformation at the right shoulder can be seen in Figure 5- 31 for scenarios 1 and 2, and in Figure 5- 32 for scenarios 3 and 4, for tunnel burial depths of 1D, 2D, 3D, and 6D (where D is the tunnel diameter). Similar trends can be seen. The horizontal deformation decreases and reaches its lowest point when the tunnel center is shifted horizontally three tunnel diameters from the mat foundation centerline. At greater

tunnel distances from the foundation centerline the horizontal deformation then increases more gradually.

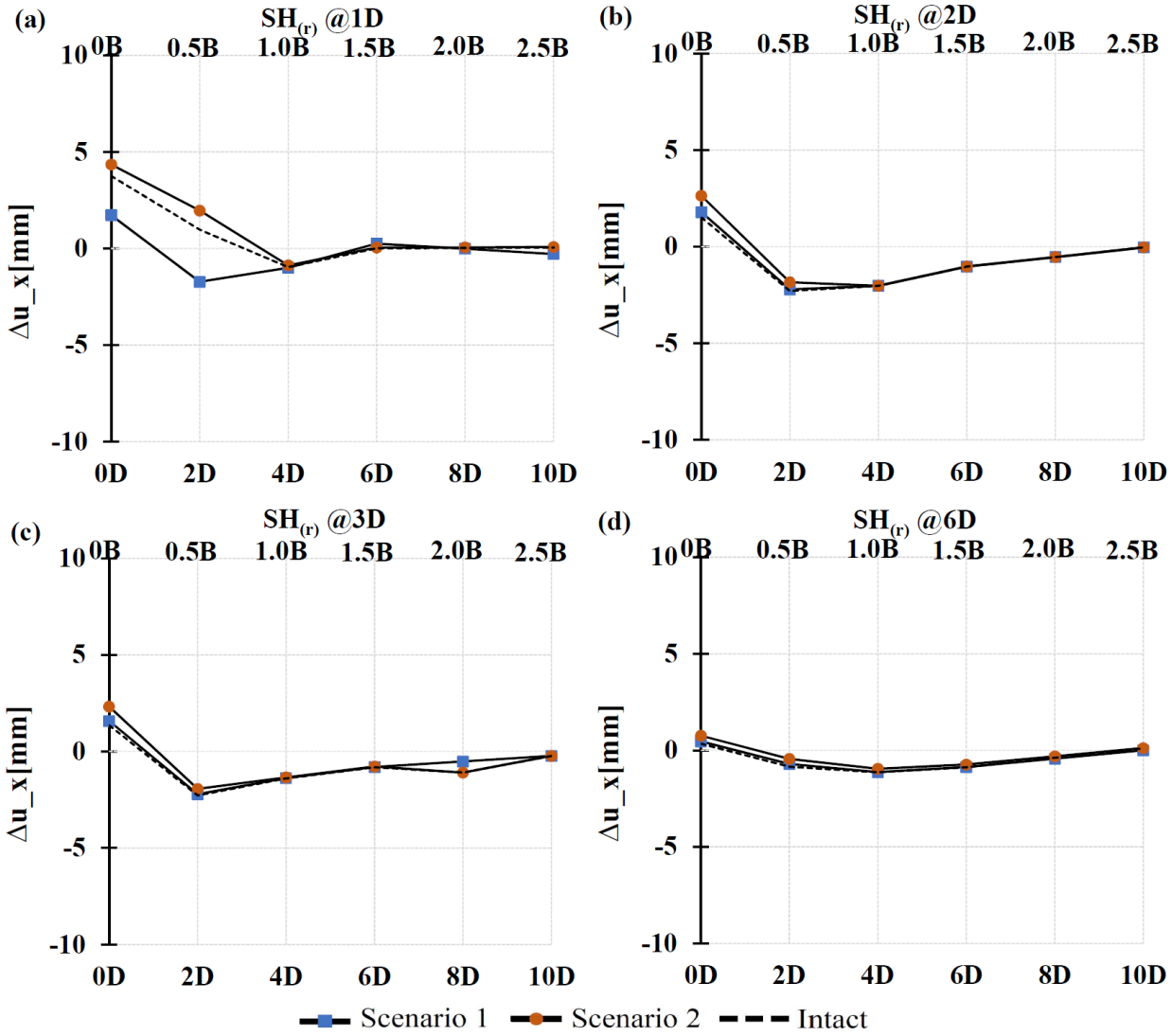

Figure 5- 31: Horizontal deformation degradation at the right shoulder level in scenarios 1 and 2

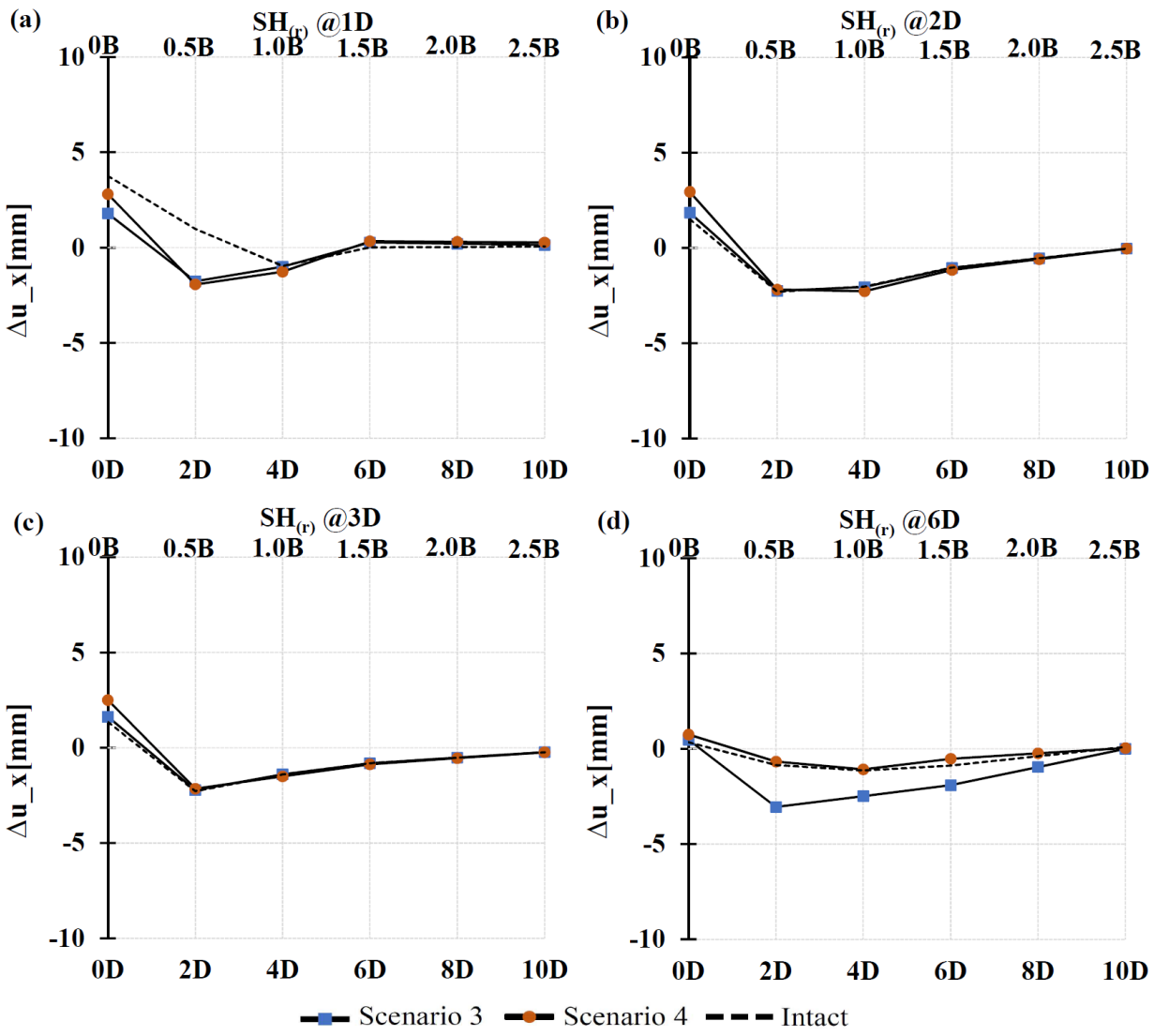

Figure 5- 32: Horizontal deformation degradation at the right shoulder level in scenarios 3 and 4

5.4.3.4 Zone excluded due the effect of horizontal deformation

As described above, the effect of the new structure on the degraded tunnel lining leads to a small variation in the horizontal deformation. The peak increase in horizontal deformation, which is less than 8 mm, occurs at the left springline level in scenario 4, when the tunnel center is shifted horizontally one tunnel diameter away from the centerline of the mat foundation of the new structure (see Figure 5- 30). The horizontal forces increase

and reach their peak at this imbalanced tunnel location. At greater horizontal distances of the tunnel from the foundation centerline, the horizontal deformation gradually decreases, and the stress returns to a balanced state. Therefore, the effect of new construction on increased horizontal deformation of the degraded lining, as compared with an intact lining, can be considered to be negligible.

5.4.4 Effect of new structure on the pre-existing degraded tunnel lining

In light of these analyses concerning the effect of new construction on radial stresses and on the vertical and horizontal deformation of a pre-existing degraded tunnel lining, an exclusion zone for new construction in the vicinity of pre-existing degraded tunnels can be defined, as shown in Figure 5- 33.

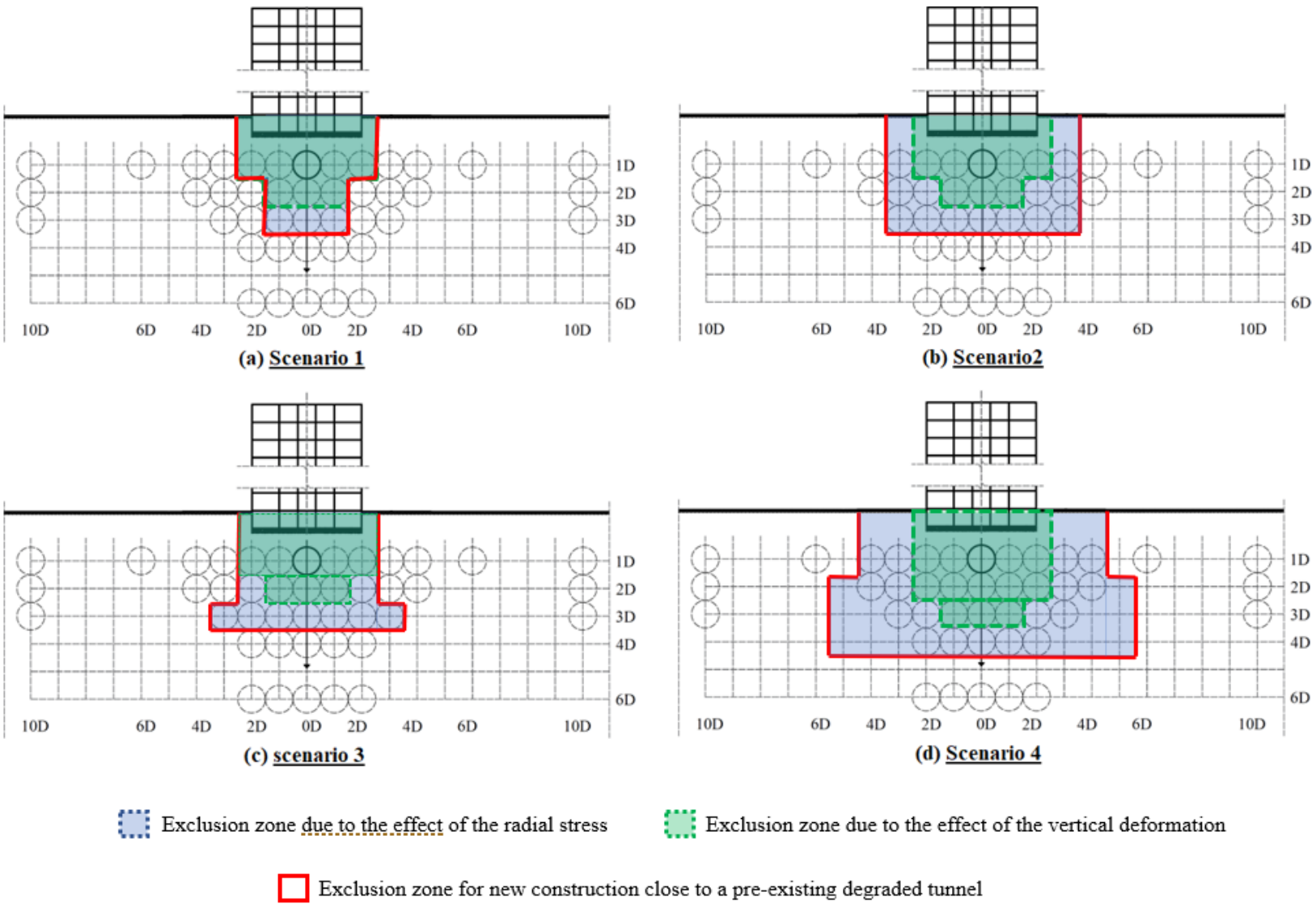

Figure 5- 33: Exclusion zone for new construction in the vicinity of a pre-existing degraded tunnel

5.4.5 Effect of a pre-existing tunnel on the settlement of a new mat foundation

5.4.5.1 Maximum settlement

Figures 5- 34 and 5- 35 show the distribution of maximum settlement beneath a new mat foundation for an intact tunnel lining and for degradation scenarios 1, 2, 3, and 4, at tunnel burial depths of 1D, 2D, 3D, and 6D (where D is the tunnel diameter). The settlement of a shallow mat foundation constructed over granular soil (i.e., sand) deposits occurs rapidly as loads are applied. Due to the interaction between the soil and the tunnel lining, it can be concluded that the stiffer the tunnel lining, the less deformation, volume loss and settlement occurs. For example, as shown in Figure 5- 34(a), in scenario 1 the maximum settlement when the tunnel center is located directly beneath the mat centerline at a burial depth of one tunnel diameter is around 40 mm. As shown in Figure 5- 35(a), in scenario 4 this value is 43 mm. Moreover, because ground stiffness plays an important role in the settlement of shallow foundations, it can be clearly seen that settlement is reduced in the presence of tunnels, since tunnel stiffness is greater than that of sand, and hence the foundation soil becomes stiffer. For instance, as shown in Figure 5- 34(a), in scenario 1 for a tunnel burial depth of one tunnel diameter the maximum settlement is around 40 mm when the tunnel center is located directly below the centerline of the mat foundation; whereas the maximum settlement reaches 53 mm when the tunnel center is shifted ten tunnel diameters horizontally. This amounts to a 25% increase in settlement.

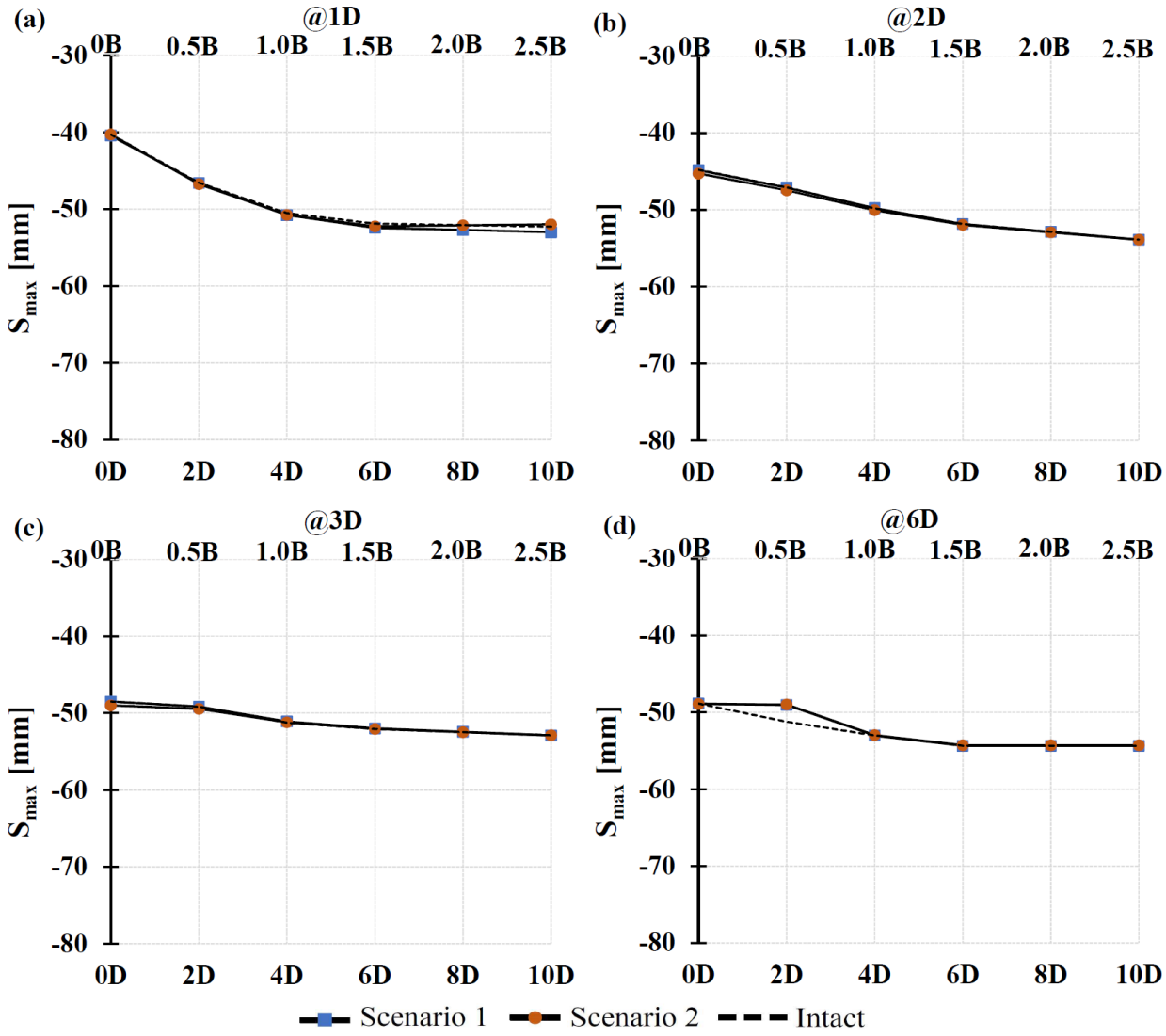

Figure 5- 34: Settlement degradation in scenarios 1 and 2

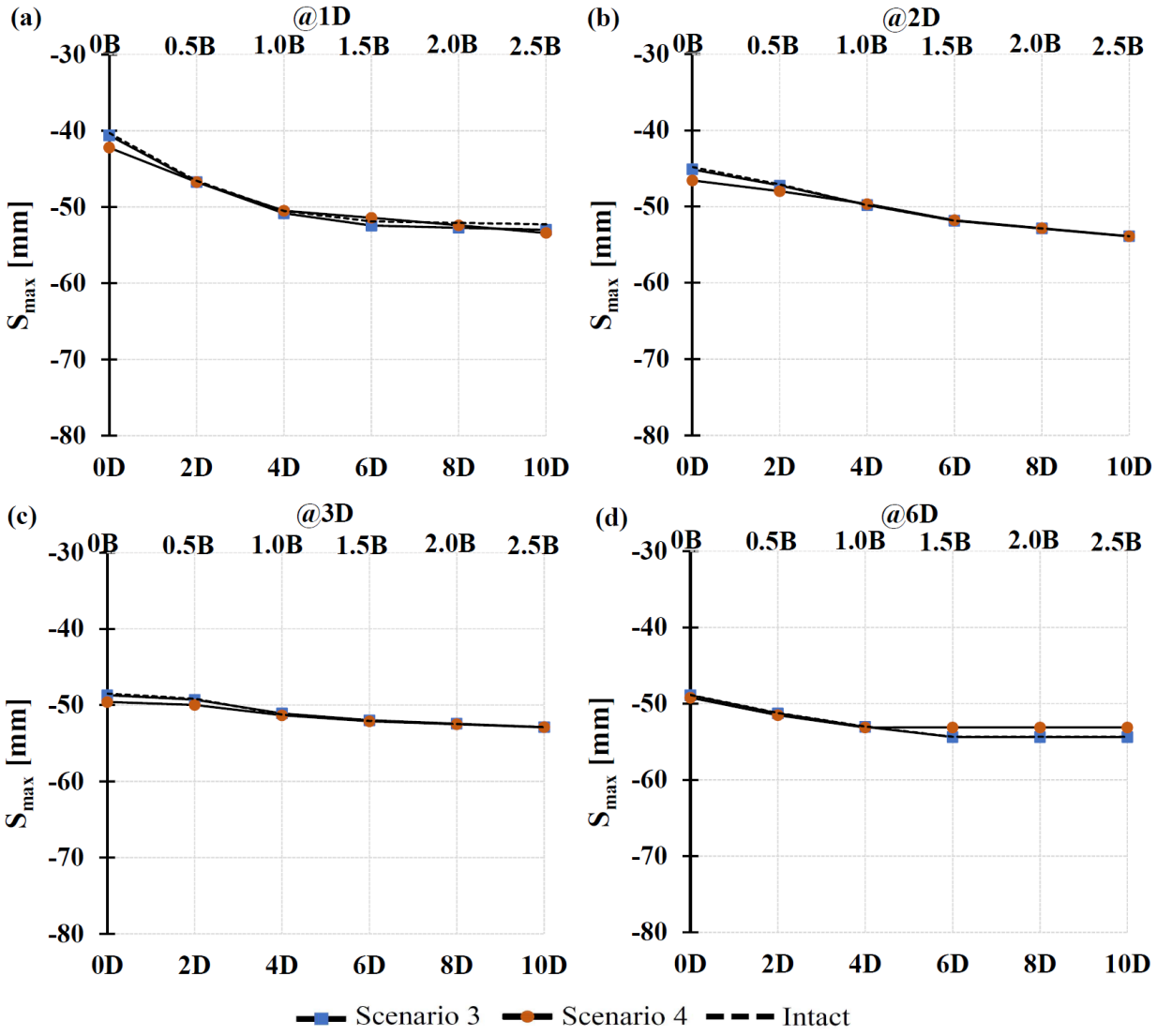

Figure 5- 35: Settlement degradation in scenarios 3 and 4

5.4.5.2 Differential settlement

Figures 5- 36 and 5- 37 show the differential settlement of the mat foundation for different tunnel locations. The differential settlement trends are similar for the different degradation scenarios. The differential settlement curves rise steadily and reach a peak when the tunnel center is located two tunnel diameters away from the mat foundation centerline. At this location, the tunnel center is directly below the edge of the building. When the tunnel is located further from the mat foundation, the differential settlement declines sharply, becoming insignificant as the distance from the

foundation increases. Differential settlement can lead to damage to the superstructure. For this reason, several researchers have defined parameters to quantify differential settlement, in order to develop limiting values for these parameters to ensure safety of the structures. As a damage criterion, *Bjerrum (Bjerrum 1963)* defined the limiting angular distortion, β_{max}, as the ratio of the difference in total settlement between any two points, $\Delta S_{T(ij)}$, to the distance l_{ij} between the points, i and j. He found that danger of structural damage to most buildings occurs when $\beta_{max} > {}^{1}/_{150}$; the first cracking of panel walls begins when $\beta_{max} > {}^{1}/_{300}$; and the safe limit to avoid cracking of the building is $\beta_{max} = {}^{1}/_{500}$. Accordingly, in the present study, for $\beta_{max} = {}^{1}/_{500}$ and a distance between the edges of the mat foundation of 20 m, the maximum allowable differential settlement is 40 mm. This value is four times larger than the maximum differential settlement observed, which is 10 mm. The European Committee for Standardization, 1994 b *(European Committee for Standardization 1994)* recommends 20 mm as the maximum acceptable differential settlement for a foundation. This value is twice as large as the value observed in this study. Hence the influence of the tunnel on differential settlement falls within acceptable limits.

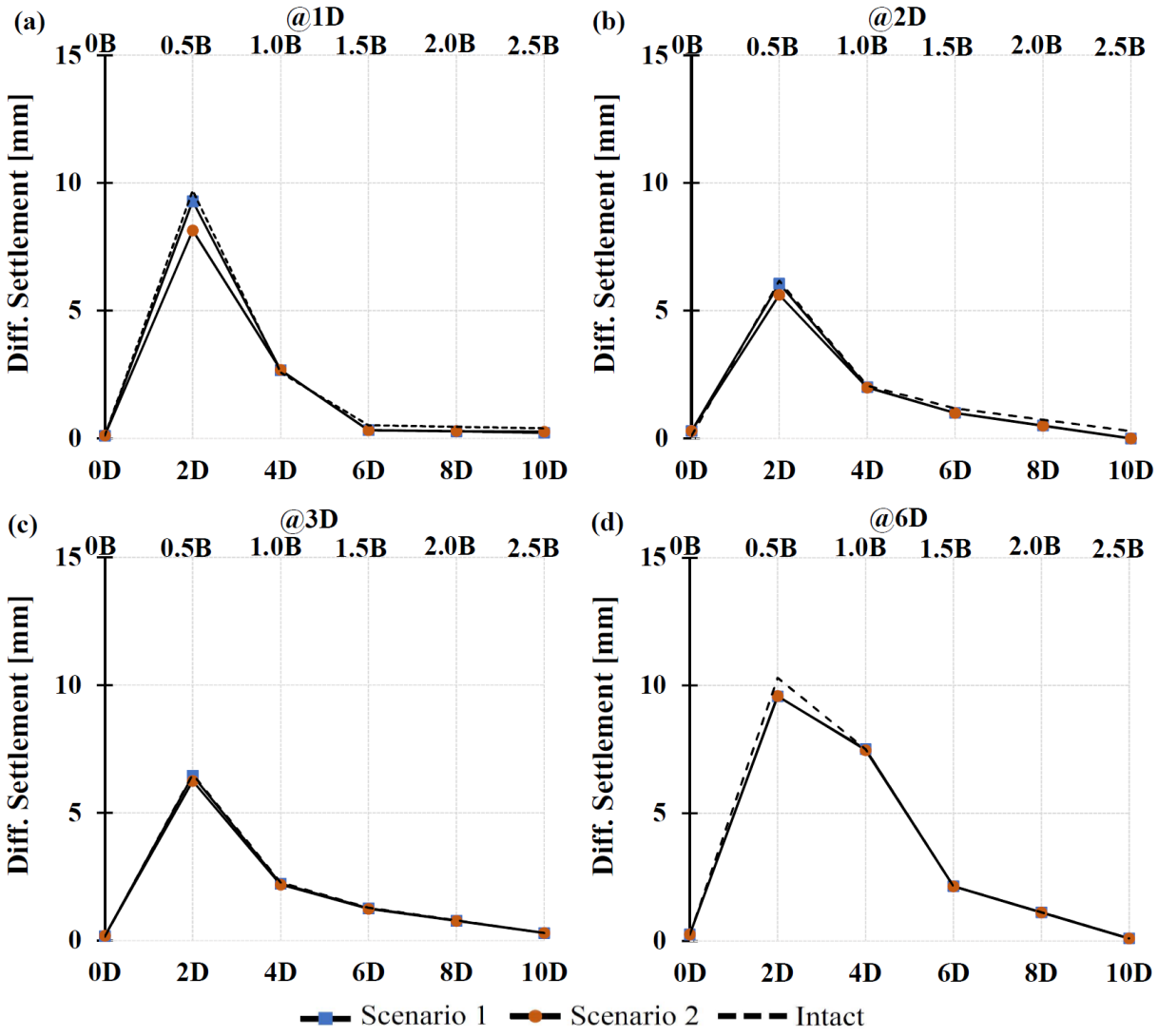

Figure 5- 36: Differential settlement in scenarios 1 and 2

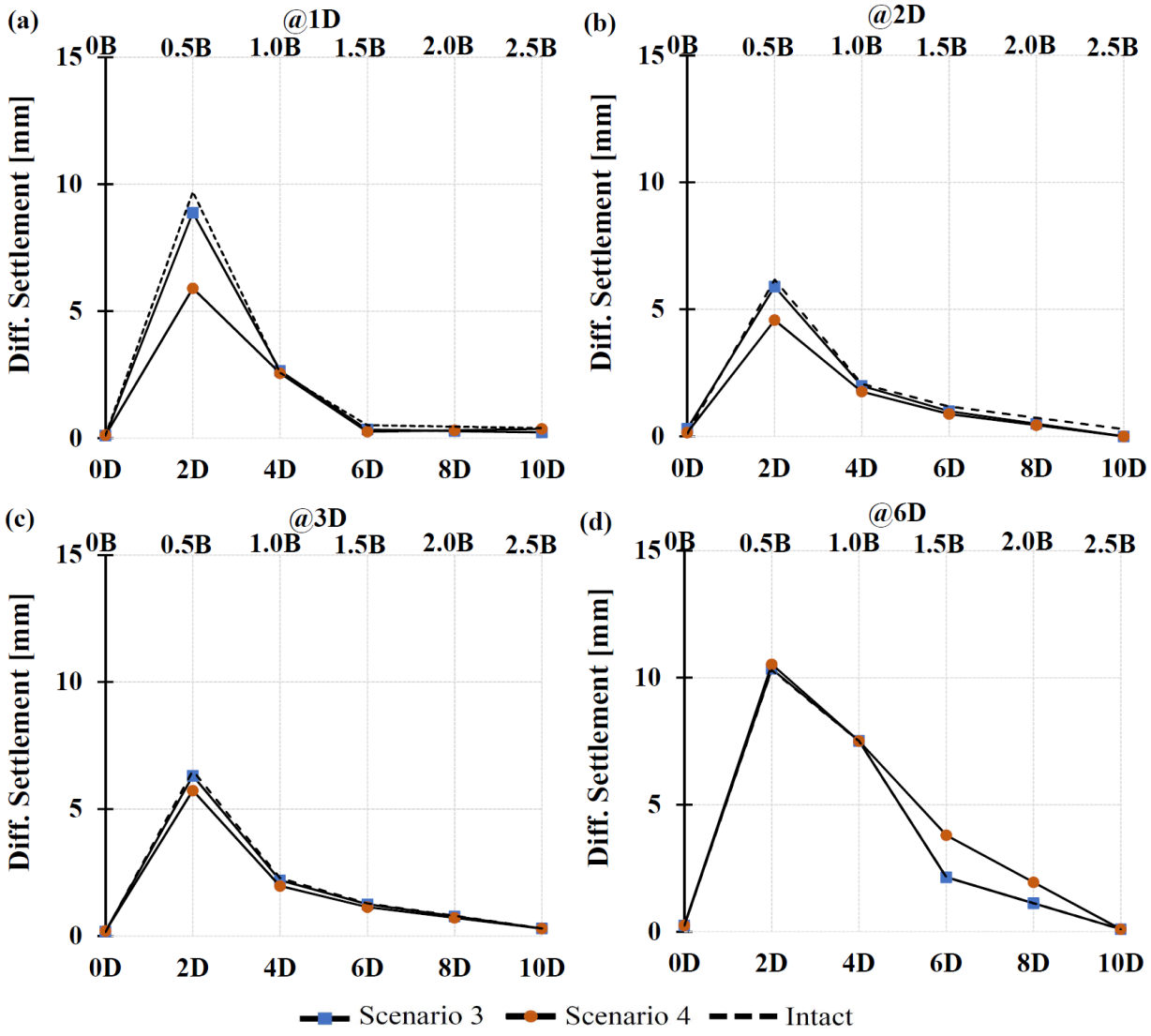

Figure 5- 37: Differential settlement in scenarios 3 and 4

5.5 CONCLUSIONS

A detailed investigation of the effect of constructing a new high-rise building on a shallow foundation in a sandy layer near a pre-existing degraded tunnel is presented. Predicted radial extrados and intrados stresses, vertical and horizontal deformations of structural elements in the tunnel lining, and maximum and differential settlements of the mat foundation are analyzed for different tunnel burial locations and different degradation scenarios. In light of the evaluation of

the building-tunnel interaction, a practical exclusion zone to minimize the effect of new construction on a pre-existing degraded tunnel is defined. Accordingly, new design guidelines can be developed for shallow foundations adjacent to a pre-existing degraded tunnel located in a sandy layer.

5.6 REFERENCES

Abbas, S., Soliman, A., & Nehdi, M. (2014). *Chloride ion penetration in reinforced concrete and steel fiber-reinforced concrete precast tunnel lining segments*. Farmington Hills: doi:10.14359/51686991

Ai, Q., Yuan, Y., Mahadevan, S., & Jiang, X. (2016). Probabilistic degradation modelling of circular tunnels assembled from segmental linings. *Structural Concrete, 17*(2), 257-273. doi:10.1002/suco.201400122

Amleh, L., & Ghosh, A. (2006). Modeling the effect of corrosion on bond strength at the steelconcrete interface with finite-element analysis. *Canadian Journal of Civil Engineering, 33*(6), 673-682. doi:10.1139/l06-052

Bian, K., Liu, J., Xiao, M., & Liu, Z. (2016). *Cause investigation and verification of lining cracking of bifurcation tunnel at huizhou pumped storage power station*doi://doi.org/10.1016/j.tust.2015.10.030

Bjerrum, L. (1963), "Allowable Settlement of Structures," Proc., European Conf. on Soil Mech. and Found. Engr., Weisbaden, Germany, Vol. 3, pp. 135-137

Chen, J., Song, X., Zhao, T., & Tian, L. (2010). Service life prediction of lining concrete of subsea tunnel under combined compressive load and carbonation. *Journal of Wuhan University of Technology-Mater.Sci.Ed., 25*(6), 1061-1064. doi:10.1007/s11595-010-0150-8

Colback, P. S. B., & Wiid, B. L. (1965). The influence of moisture content on the compressive strength of rocks Paper presented at the 65-83.

El Naggar, H., & Hinchberger, S. D. (2012). *Approximate evaluation of stresses in degraded tunnel linings* doi://doi.org/10.1016/j.soildyn.2012.07.016

European Committee for Standardization. (1994). *Geotechnical design, general rules-part 1, eurocode 7 * (). Brussels, Belgium:

Fathi Salmi, E., Soltani Asadi, Z., Bayati, M., & Sharifzadeh, M. (2019). Assessing the hydrogeological conditions leading to the Corrosion and deterioration of pre-cast segmental concrete linings (Case of Zagros tunnel). *Geotechnical and Geological Engineering,* doi:10.1007/s10706-019-00886-1

Gulikers, J. (2003). Problems encountered in the detection of reinforcement corrosion in concrete tunnel linings – theoretical considerations. *Materials and Corrosion, 54*(6), 454-459. doi:10.1002/maco.200390097

Hardin, B. O., & Drnevich, V. (1972). Shear modulus and damping in soils: Design equations and curves. *Geotechnical Special Publication, 98*(118)

Howard, A. J. (1991). Report on the damaging effects of water on tunnels during their working life. *Tunnelling and Underground Space Technology, 6*(1), 11-76. Retrieved from http://www.sciencedirect.com/science/book/9781555582890

Idris, J., Verdel, T., & Al-Heib, M. (2008a). *Numerical modelling and mechanical behaviour analysis of ancient tunnel masonry structures* doi://doi.org/10.1016/j.tust.2007.04.006

Idris, J., Verdel, T., & Al-Heib, M. (2008b). *Numerical modelling and mechanical behaviour analysis of ancient tunnel masonry structures* doi://doi.org/10.1016/j.tust.2007.04.006

Inokuma, A., & Inano, S. (1996). *Road tunnels in japan: Deterioration and countermeasures* doi://doi.org/10.1016/0886-7798(96)00026-0

Jiang, M., & Yin, Z. (2012). *Analysis of stress redistribution in soil and earth pressure on tunnel lining using the discrete element method* doi://doi.org/10.1016/j.tust.2012.06.001

Santos, J., & Correia, A. (2001). Reference threshold shear strain of soil, its application to obtain a unique strain-dependent shear modulus curve for soil. Paper presented at the 267-270.

Schadlich, B., & Schweiger, H. (2014). A new constitutive model for shotcrete. In M. A. Hicks, R. B. J. Brinkgreve & A. Rohe (Eds.), *Numerical methods in geotechnical engineering* (pp. 103-108). London: Taylor & Francis Group. doi:10.1201/b17017-20

Skripkiūnas, G., Nagrockienė, D., Girskas, G., Vaičienė, M., & Baranauskaitė, E. (2013). *The cement type effect on freeze – thaw and deicing salt resistance of concrete*doi://doi.org/10.1016/j.proeng.2013.04.132

Stead, D., Coggan, J. S., & Howe, J. H. (2000). Engineering geology and hazard assessment of excavated china clay slopes. Paper presented at the 72-76.

Sun, J. (2011). Durability problems of lining structures for xiamen xiang'an subsea tunnel in china. *Journal of Rock Mechanics and Geotechnical Engineering, 3*(4), 289-301. doi:10.3724/SP.J.1235.2011.00289

Tian, L., Chen, J., & Zhao, T. (2012). Durability of lining concrete of subsea tunnel under combined action of freeze-thaw cycle and carbonation. *Journal of Wuhan University of Technology-Mater.Sci.Ed., 27*(4), 779-782. doi:10.1007/s11595-012-0547-7

Usman, M., & Galler, R. (2013). Long-term deterioration of lining in tunnels. *International Journal of Rock Mechanics and Mining Sciences, 64*, 84-89. doi://doi.org/10.1016/j.ijrmms.2013.08.028

Yuan, Y., Bai, Y., & Liu, J. (2012). *Assessment service state of tunnel structure* doi://doi.org/10.1016/j.tust.2011.07.002

Zhiqiang, Z., & Mansoor, Y. A. (2013). Evaluating the strength of corroded tunnel lining under limiting corrosion conditions. *Tunnelling and Underground Space Technology Incorporating Trenchless Technology Research, 38*, 464-475. doi:10.1016/j.tust.2013.08.003

CHAPTER 6 SIMPLIFIED PROCEDURE TO INCORPORATE THE EFFECT OF PRE-EXISTING TUNNELS IN THE ANALYSIS OF NEW BUILDINGS

6.1 ABSTRACT

The analysis of the interactive process of stresses and strains involving the mat foundation of a high-rise building and the soil is complex and challenging. Current structural analysis and design software often does not consider soil medium elements or the effect of pre-existing tunnels. This paper aims to develop a simplified procedure to incorporate the effect of pre-existing tunnels in the analysis of new buildings. The objective is to produce mat deflection diagrams similar to those of a finite element analysis that treats the soil as a continuum, so that the results can be easily applied in most automated structural analysis programs. Correction factors have also been obtained to accompany the proposed procedure. For this purpose, analytical and finite element parametric analyses using three- and two-dimensional elements were performed to investigate the settlement trough of a mat foundation of a newly constructed high-rise building, for different tunnel burial locations. The finite element analysis results were used to obtain the correction factor expressions for the proposed simplified procedures.

Keywords: Mat foundations, tunnel, soil-structure interaction, Winkler spring, modulus of subgrade, simplified approach, correction factors, two and three-dimensional finite element analysis

6.2 INTRODUCTION

Since the late nineteenth century, the demand for thousands of new residential units due to unprecedented population growth, especially in megacities, has led to a worldwide boom in the

construction of new buildings. According to Mckinsy and the U.N. Habitat report, building the additional units needed by 2025 would require $9 trillion to $11 trillion in construction spending alone (McKinsey Global Institute 2014). High-rise buildings have practical and economic benefits in urban areas, particularly those with high population density, and have become a typical housing feature in all megacities worldwide. Hence, large numbers of high-rise buildings are expected to be constructed worldwide over the next few decades. In high-rise buildings containing a one-level or multiple-level basement, the base of the building may be close to, or even embedded in, competent ground. In this case, a raft (mat) foundation to support the entire building may be feasible for buildings of moderate height. However, for very tall buildings more than 100 m high, such a shallow foundation system may not be able to provide adequate resistance for the structure. The interaction between the foundations of high-rise buildings and the supporting ground is a complex problem that presents several challenges for engineers, especially in relation to structural and geotechnical design. Many traditional design methods cannot be applied with confidence if they exceed the realm of prior experience, for example in the case of new buildings over pre-existing infrastructure such as sewer and/or transportation tunnels. Accordingly, structural and geotechnical designers need to utilize new analysis and design methods to achieve resilient designs.

To simplify the analysis of buildings supported on shallow foundations, it is customary for structural engineers to use a system called a “subgrade model” to represent the stiffness of the ground when analyzing the superstructure. In designing a building foundation, the structural engineer typically asks a geotechnical engineer to provide the stiffness values for spring elements to model the ground-foundation interaction via elastic supports. The use of an inappropriate spring stiffness value for the design can lead, for example, to excessive settlement of the raft, if not

undesired differential settlement that may lead to serious structural consequences. In the design of the raft foundation for a Mass Rapid Transit railway station, in order to reduce the overestimated settlement, the center of the raft was strengthened unnecessarily with an excess of more than twenty bored piles (GOUW Tjie-Liong, PT Limara).

The concept of using springs to represent the ground was first introduced in 1867 by ***Winkler***, who modelled a flexible raft foundation standing on independent discreet spring elements or supports idealizing the soil continuum. The coefficient of subgrade reaction, k_s, is defined as the ratio of the distribution of the soil reaction to the settlement of the underlying soil. By considering a flexible beam of infinite length on a semi-infinite homogeneous, elastic, isotropic solid under a concentrated load, ***Biot*** (Biot 1937) found that the value of the modulus k_s is equal to:

$$k_s = \frac{0.95E_s}{B(1-\nu_s^2)}\left[\frac{B^4E_s}{(1-\nu_s^2)EI}\right]^{0.108} \quad [1]$$

where E_s is the modulus of elasticity, ν_s is Poisson's ratio, B is the footing width, and EI is the flexural rigidity of the footing. ***Terzaghi*** *(Terzaghi 1955)* demonstrated that k_s is not only influenced by the elastic characteristics of the subgrade, but is also related to the footing geometry and the loading distribution:

$$k_s = k_{s1}\left(\frac{B+1}{2B}\right)^2 \qquad (for\ sands) \quad [2]$$

$$k_s = k_{s1}\frac{1}{B} \qquad (for\ clays) \quad [3]$$

where k_{s1} is the coefficient of subgrade reaction for a plate one foot wide.

Due to the fact that the Winkler model does not consider the distribution of soil stresses in the deeper soil layer forming the so-called "bulb pressure", this factor was considered by ***Vesic*** (Vesic 1961). He assumed that the soils inside the bulb pressure zone are homogeneous, and considered that k_s depends upon the foundation width, B; the elastic parameters of the soil, E_s and ν_s; and the shape factor for the foundation, I_p:

$$k_s = \frac{E_s}{BI_p(1-\nu_s^2)} \qquad [4]$$

In the above-mentioned methods, a unique value of k_s is applied. However, if the distribution of the soil beneath the mat foundation is non-linear, k_s should not be a single value. ***Bowels*** suggested providing different values for k_s: a higher value at the edge of the mat foundation and smaller values at the center position.

Today the availability of sophisticated finite element (FE) software, such as PLAXIS, that is specialized for geotechnical applications, makes it possible to solve various soil-structure interaction problems efficiently with a high level of accuracy. In a comparison of the result of contact pressure diagrams obtained by using the PLAXIS finite element software with results obtained by using the Biot (1937) and Vesic (1961) relations for a rectangular raft foundation of a 22-story building southeast of the city of Tabriz, Iran, it was found that the Biot and Vesic relations lead to approximately equal contact pressure values, but these are 35% greater than the results generated by the PLAXIS soft soil model (Sadrekarimi, Akbarzad 2009). The lateral pressure of soil elements on the soil-foundation interface reduces the vertical pressure. This feature is considered in the soft soil model (PLAXIS MANUAL) (*PLAXIS 3D user's manual, version 2018. Material model manual.* 2018), but is ignored in the Biot and Vesic models, which is one reason for the difference in the results.

The above-mentioned methods for computing the coefficient of subgrade reaction, k_s, are often used in the structural design of raft foundations for high-rise buildings. However, for buildings with foundations close to pre-existing tunnels, there are currently no provisions to account for the effect of the tunnels on the new foundations. Hence, a versatile procedure is needed to account for the stiffness of pre-existing tunnels, so that this factor can be included in the analysis of the superstructure.

Accordingly, the main objective of this paper is to develop a simplified procedure to incorporate the effect of pre-existing tunnels in the analysis of new buildings. The proposed procedure is designed so that it can be applied easily in most automated structural analysis programs without the need for any other specialized software. The proposed procedure relies on applying a system similar to the Winkler model and then utilizing a number of correction factors to account for the various variations. It should be noted that the present analysis assumes that the soil behaves in a linear elastic fashion. This is an assumption commonly used in current raft design practice, as it is assumed that the magnitude of applied pressures is within the linear range of the ground (with the use of a factor of safety ranging from 2 to 3). To develop the proposed procedure, analytical and finite element parametric analyses using three- and two-dimensional finite element models were performed to investigate the settlement trough of a raft foundation of a newly constructed high-rise building for different tunnel burial locations with respect to the raft. The finite element analysis results were then used to obtain two correction factor equations to accompany the proposed simplified procedure.

6.3 DEVELOPMENT OF THE SIMPLIFIED PROCEDURE

This section presents the proposed simplified procedure, which begins with the current practice commonly used by structural engineers for analyzing a superstructure (i.e., by utilizing the concept

of elastic springs and obtaining their stiffness). Then, by assuming that the loads applied by the superstructure to the supporting ground are distributed in a fashion similar to that assumed by Boussinesq for a surface loaded area on an elastic half-space, an approximate distribution of the load is obtained at the location of the tunnel. The load obtained is then back distributed (as a reaction) to each of the springs utilized, according to the relative proximity of each spring to the tunnel. The stiffness of each spring is thus adjusted according to the location of the tunnel. The closer the spring is to the tunnel, the greater its share in the increased stiffness. Then, by utilizing the results of the 2D and 3D finite element models, two correction factors are obtained: One to correct the results obtained by the proposed procedure to match the 2D finite element results; and the other to match the proposed procedure results to those obtained from the 3D models. The aim of the proposed procedure is to help attain the best possible accuracy in terms of the ground stiffness to be used in analyzing the superstructure, while incorporating the effect of pre-existing tunnels.

6.3.1 Settlement of the mat foundation

The first step in the proposed procedure is to compute the settlement of the raft (mat) foundation situated on the surface of an elastic half-space and subjected to a uniform pressure (see Figure 6-1). When soils are subjected to loads, they deform primarily due to a change in void volume rather than through deformation of the soil solids. During loading, air is expelled from the voids and the soil undergoes a relatively immediate decrease in void volume. The vertical settlement, Δs, under an area carrying a uniform pressure, q, on the surface of a semi-infinite, homogeneous, isotropic medium can expressed as:

$$\Delta s_{Greenfield} = \frac{qB}{E}(1-\nu^2)I_s \qquad [5]$$

where

I_s is an influence factor depending upon the shape of the loaded area,

B is the width of the loaded area,

E is the elastic modulus and ν is Poisson's ratio.

Table 6. 1: Influence factors for vertical displacement under a flexible area carrying uniform pressure

Shape of area	Influence factor, I_s		
	Center	Corner	Average
Square	1.12	0.56	0.95
Rectangle, L/B=2	1.52	0.76	1.30
Rectangle, L/B=5	2.10	1.05	1.83
Circle	1.00	0.64	0.85

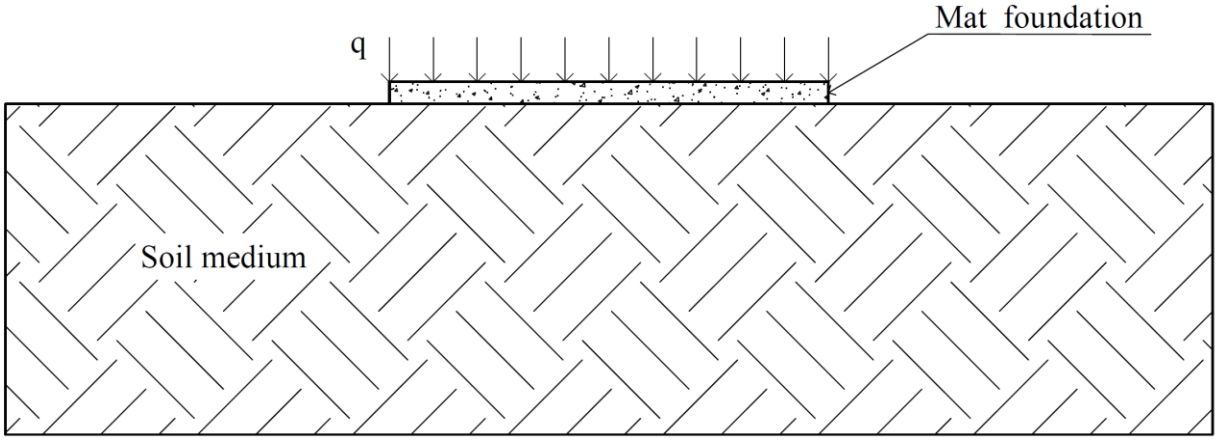

Figure 6- 1: Raft (mat) foundation resting on a semi-infinite, homogeneous, isotropic soil medium

6.3.2 Coefficient of subgrade reaction, ks

As illustrated in Figure 6- 2, the soil medium is represented as a system of equally spaced elastic springs. At any point, the modulus of subgrade reaction, k_s, can be calculated as:

$$k_s = \frac{q}{\Delta s_{Greenfield}} \quad (\mathrm{kN/m}) \qquad [6]$$

where

q is the magnitude of the uniform pressure, and

$\Delta s_{Greenfield}$ is the deflection, calculated from Equation 5.

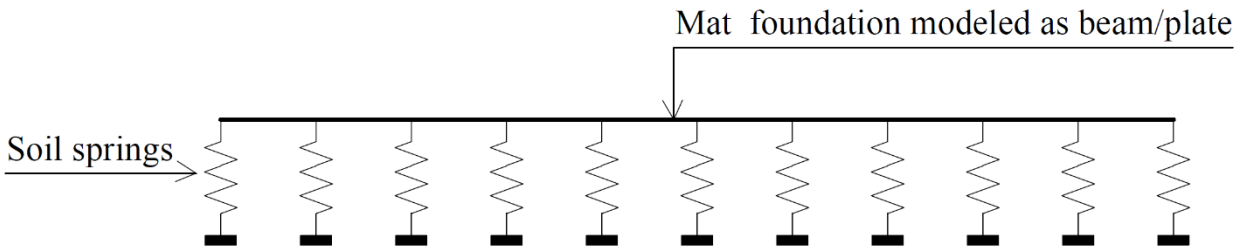

Figure 6- 2: Equivalent of mat foundation resting on a spring bed

6.3.3 Effect of pre-existing tunnel

To incorporate the effect of a pre-existing tunnel in the analysis of a new building, a force, P_i, is added at each spring, as discussed above, to represent the reaction developed because of the stiffening due to the presence of the tunnel (see Figure 6- 3). The magnitude of this force is derived by using the Boussinesq theory (see Figure 6- 4) to obtain an approximate estimate of the share of stresses from the superstructure received near the tunnel location. The vertical and horizontal stresses at any point, x, in the ground medium due to a uniform pressure, q, acting on a strip area having a width, B, and an infinite length is given by the following relations:

$$\sigma_z = \frac{q}{\pi}\{\alpha + \sin\alpha\cos(\alpha + 2\beta)\} \quad [7]$$

$$\sigma_x = \frac{q}{\pi}\{\alpha - \sin\alpha\cos(\alpha + 2\beta)\} \quad [8]$$

Then, the vertical component, P_{iv}, and the horizontal component, P_{ih}, of the load at each spring can expressed as follows:

$$P_{iv} = \Delta w_y \times D\left(\frac{1/l_i}{\sum_{i=1}^{N} 1/l_i}\right) (kN) \quad [9]$$

$$P_{ih} = \Delta w_x \times D\left(\frac{1/l_i}{\sum_{i=1}^{N} 1/l_i}\right) (kN) \quad [10]$$

where

$$\Delta w_y = \sigma_{z(at\ the\ center\ of\ the\ tunnel)}\ calculated\ by\ Boussinesq's\ equation\ [7], \quad [11]$$

$$\Delta w_x = \sigma_{x(at\ the\ center\ of\ the\ tunnel)}\ calculated\ by\ Boussinesq's\ equation\ [8], \quad [12]$$

D is the tunnel diameter,

L_i is the distance from the tunnel center to the location of the i^{th} spring, and

N is the total number of springs.

Accordingly, the upward deflection at each spring due to the tunnel effect, Δiv, can expressed as:

$$\Delta iv = \frac{P_{iv}}{K_s} (kN/m) \quad [13]$$

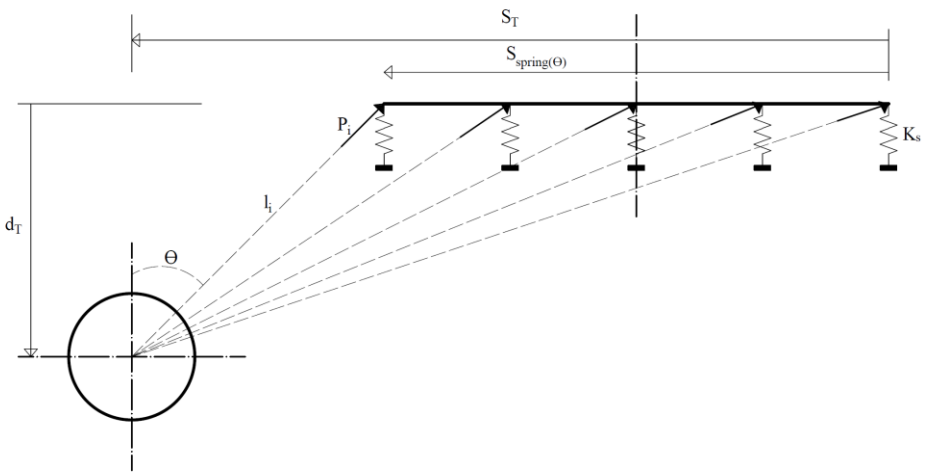

Figure 6- 3: Effect of pre-existing tunnel

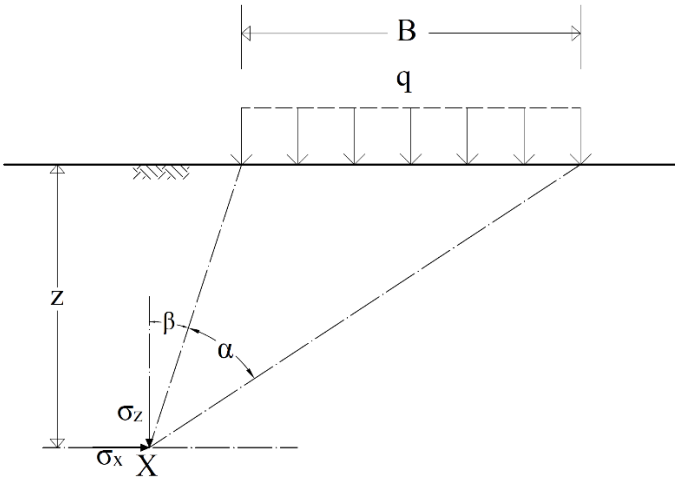

Figure 6- 4: Strip area carrying uniform pressure (Boussinesq theory)

6.3.4 Correction factors

A tunnel boring machine (TBM, see Figure 6- 5) is a large-diameter conically shaped horizontal drill that continuously excavates primarily circular tunnel sections. Different machines are designed for different ground conditions. A type of TBM called an earth-pressure-balance boring

machine (EPBM) is designed particularly for drilling through soils that are not self-supporting. A TBM consists of a cutterhead, followed by a unit that powers the cutterhead. The excavated soil is conveyed to the back end of the TBM, and the TBM is advanced forward by means of hydraulic jacks. As the TBM advances, pressure is maintained at the cutterhead to support the ground and to control ground subsidence. A typical earth-pressure-balance (EPB) shield is constructed so that cement grout is injected at the back end of the shield to fill the annular gap between the extrados of the lining and the surrounding ground. Thus, tunnelling problems are by nature three dimensional, due to the sequence of the tunnel construction process. The presence of a surface structure (e.g., a nearby high-rise building) likewise adds another layer of geometric and load complexity that requires 3D modelling for an adequate description of the problem. Three-dimensional modelling is therefore essential to capture fully all the mechanisms of ground deformation and stress redistribution induced by tunnelling (Attewell et al., 1986; Burd et al., 1994; Augarde, 1997; Vermeer, 2001; and Zakhem and El Naggar, 2019).

Figure 6- 5: Tunnel boring machine (Brox, 2013)

Nevertheless, two-dimensional plane strain analyses are commonly used, because they require fewer computer resources and less time than 3D analyses (Augarde, 1997). However, 2D representations are unable to model tunnel effects in the longitudinal direction, complex three-dimensional geometries such as surface structures, the soil-structure interaction (SSI) between the

foundations of new buildings and pre-existing tunnels, or other inherently 3D effects, as noted by Augarde (1997), Mahranha and Maranha das Neeves (2000), and Zakhem and El Naggar, 2019.

Accordingly, in this paper two correction factors are introduced to accompany the proposed simplified procedure. The first correction factor is to be used to correct the proposed elastic spring procedure to match 2D models; whereas, the second correction factor can be used to correct the 2D results to match those obtained from the 3D analysis.

6.3.4.1 Two-dimensional finite element parametric analysis

6.3.4.1.1. Numerical analysis program

A comprehensive 2D parametric study was conducted to establish the relationship between 2D and 3D results regarding the effect of a pre-existing tunnel on a newly constructed high-rise building supported on a raft foundation. The problem considered modelled only a raft foundation resting on a thick sandy layer. The 2D model also considered the basement walls and used a uniform pressure to simulate the load imposed by a typical 20-storey building with one basement. Many 2D FE models were developed. Each model considered a different burial location of the pre-existing tunnel. Tunnel burial depths ranging from 1D to 6D (where D is the tunnel diameter) and horizontal locations ranging from 0D (with the tunnel center located directly beneath the centerline of the shallow foundation) to 10D from the centerline were examined (see Figure 6- 6). The FE models had a depth of 60 m and extended 160 m in the *x*-direction. These dimensions are sufficient to allow for the development of any possible collapse mechanism and to avoid influence from the model boundaries.

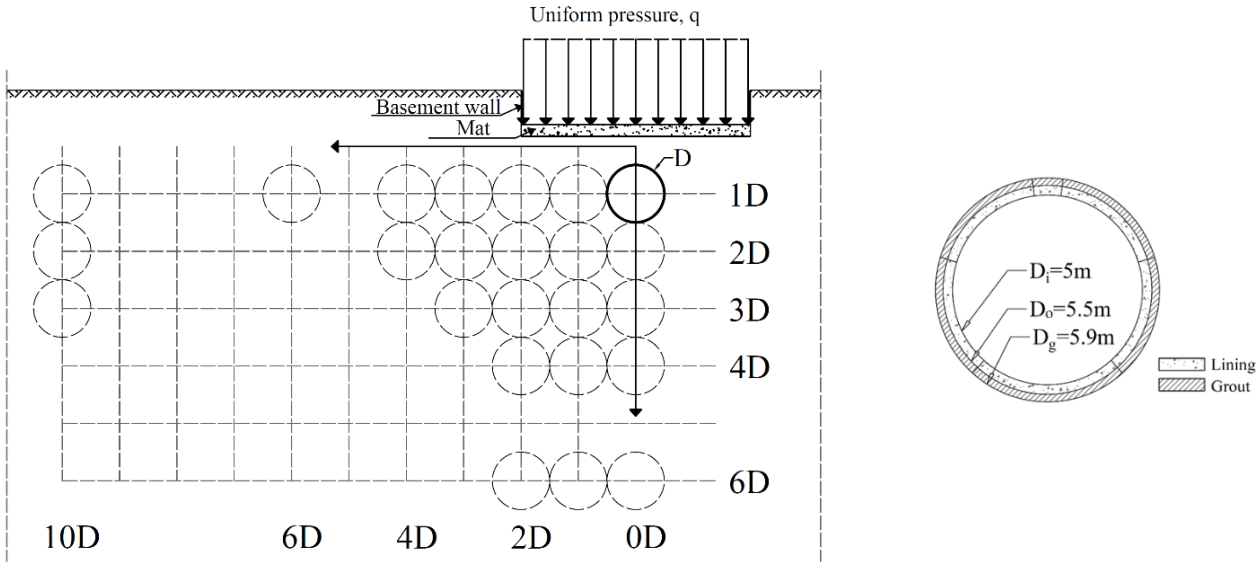

Figure 6- 6: Design of the parametric study

6.3.4.1.2. Typical finite element mesh

Figure 6- 7 shows a typical mesh generated for the model. To ensure high-quality results, the FE mesh was refined close to the tunnel and near locations where non-linear behavior could be expected. The model was constructed by using approximately 7,500 elements and 60,000 nodes. The sand stratum, the new raft foundation and the pre-existing tunnel clusters were modelled by using 15-noded plane strain elements from the PLAXIS library. The bottom boundary of the model was fixed in all directions.

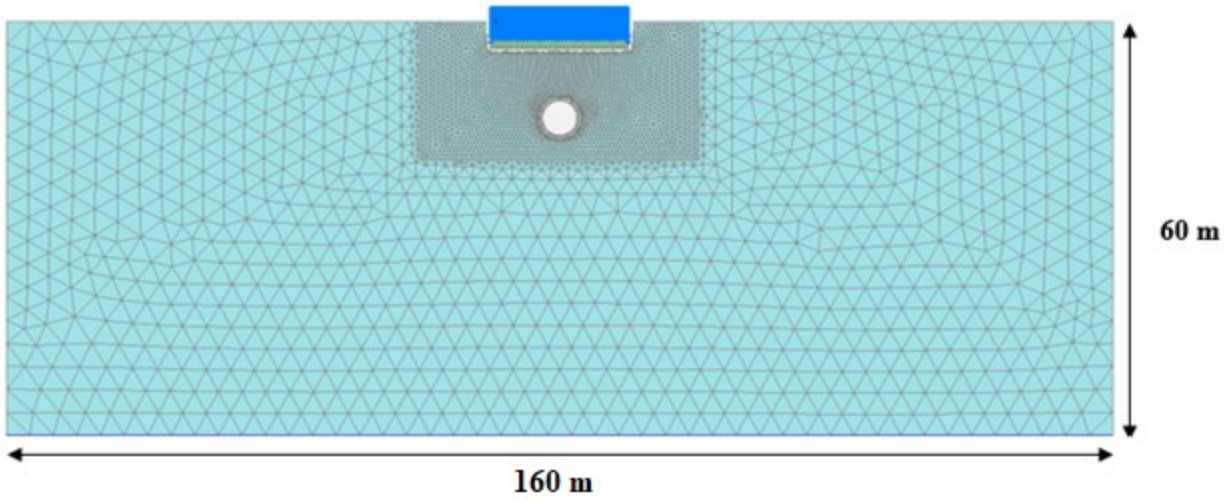

Figure 6- 7: Typical two-dimensional finite element mesh

6.3.4.1.3. Simulation of the tunnel construction process

A cross-section of the tunnel lining is shown in Figure 6- 6. The outer diameter is 5.5 m and the inner diameter is 5 m. In the analysis, the tunnel lining is assumed to obey the concrete model, a new constitutive model in the PLAXIS software. Table 6.2 summarizes the tunnel lining material parameters used. Interface elements permitting the occurrence of either slippage or gapping are used to model the interface between the soil and the tunnel lining.

The tunnel is assumed to have been driven by a tunnel boring machine (TBM), with grouting material injected into the gap left between the tunnel lining and the TBM tail skin. The behavior of fresh and hardened grouting materials is simulated by a linear elastic model, with a modulus of elasticity of 10 GPa, a Poisson's ratio (v) of 0.2, and a unit weight of 18 kN/m^3.

Table 6. 2: Summary of the tunnel lining material parameters adopted in the finite element analysis

Unit weight, γ (kN/m^3)	25
Young's modulus of cured shotcrete at t_{hydr}, E_{28} (kN/m^2)	31 x 10^6
Poisson's ratio, v	0.15
Uniaxial compressive strength of cured shotcrete at t_{hydr}, $f_{c,28}$ (kN/m^2)	45 x 10^3
Uniaxial tensile strength of cured shotcrete at t_{hydr}, $f_{t,28}$ (kN/m^2)	4,500
Time dependency of elastic stiffness, E_1/E_{28}	1
Time dependency of strength, $f_{c,1}/f_{c,28}$	1
Normalized initially mobilized strength, f_{c0n}	0.15
Uniaxial plastic failure strain at 1h, 8h, 24h, ϵ_{cp}^{p}	-1 x 10^{-3}
Compressive fracture energy of cured shotcrete at t_{hydr}, $G_{c,28}$ (kN/m)	100
Tensile fracture energy of cured shotcrete at t_{hydr}, $G_{t,28}$ (kN/m)	6.9
Increase of ε_{cp} with increase of p', a (m)	18
Maximum friction angle, φ_{max} (°)	37
Safety factor for compressive strength, γ_{fc}	1
Safety factor for tensile strength, γ_{ft}	1
Time for full hydration, t_{hydr} (days)	28

Figure 6- 8 illustrates the sequencing of the tunnel construction. The sequencing simulation procedures can be summarized in detail as follows.

Step_1, Tunnel: The clusters inside the tunnel are excavated, and the water condition is set to dry. At the outer surface, the TBM shield, the negative interface, and construction are activated. Volume loss is simulated by applying contraction.

Step_2, Grouting: At the outer surface, the TBM shield and contraction are deactivated. For the outer clusters, the lining is activated, and fresh grout is activated with defined pore water conditions, simulating the pressure due to backfill grouting.

Step_3, Pre-final lining: The water condition of the fresh grout material is set to dry.

Step_4, Final lining: The fresh grout material is reset to hardened grout.

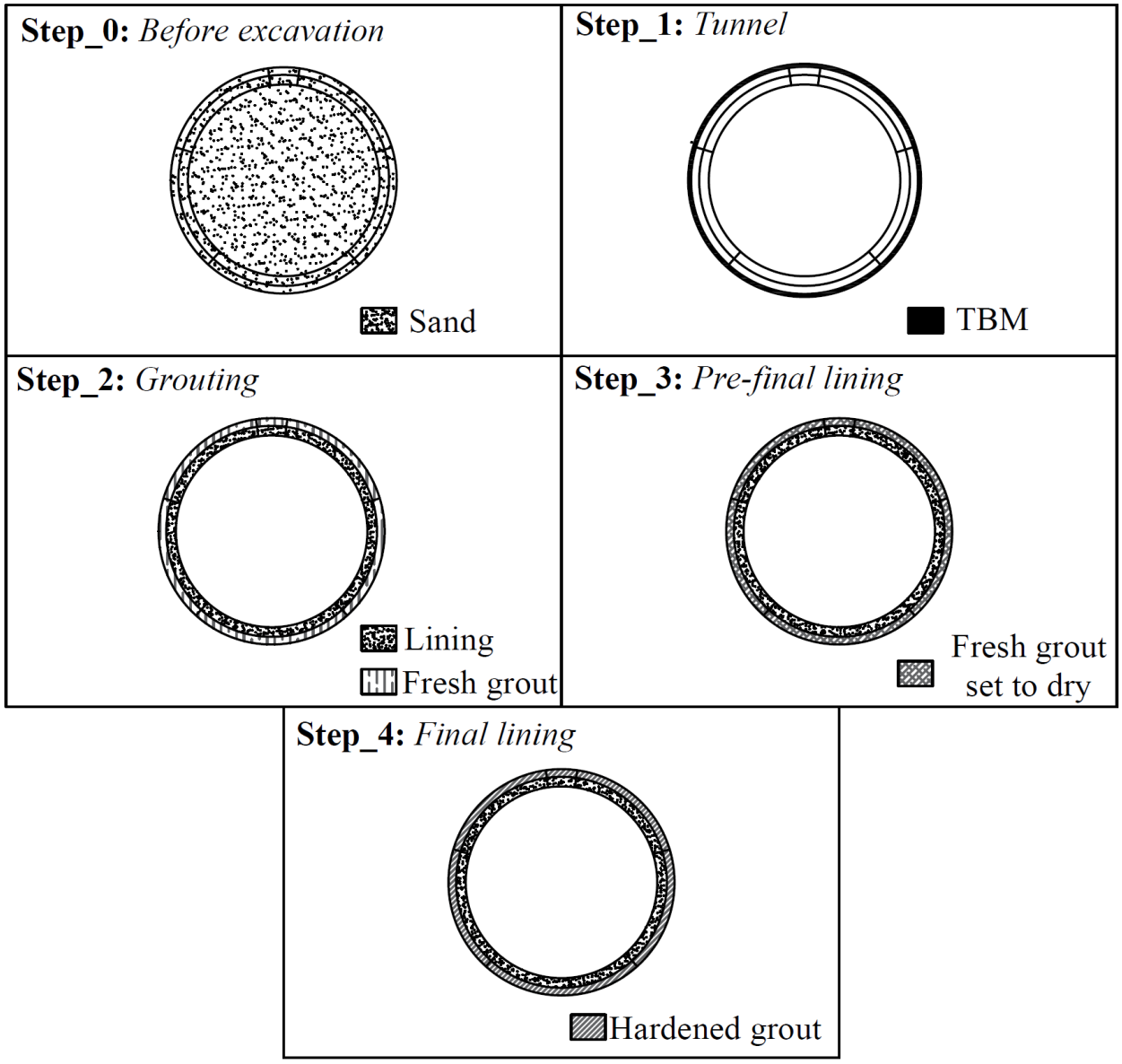

Figure 6- 8: Numerical simulation steps for tunnel excavation sequencing

6.3.4.1.4. Constitutive models and parameters

Sand behaviors are described by using the hardening soil model with small-strain stiffness (HSSmall) that is included in the PLAXIS software package. This material model accounts for increased stiffness at small strains. More details concerning HSSmall can be found in Benz (2006). Table 6.3 summarizes the material parameters of the sand that are adopted in the finite element analysis.

Table 6. 3: Summary of material parameters of the sand adopted in the finite element analysis

Secant stiffness in standard drained triaxial test, E_{50}^{ref} (KN/m^2)	38,000
Tangent stiffness for primary oedometer loading, E_{oed}^{ref} (kN/m^2)	38,000
Unloading/reloading stiffness, E_{ur}^{ref} (kN/m^2)	114,000
Power for stress-level dependency of stiffness, m	0.5
Small-strain shear modulus, G_0^{ref} (kN/m^2)	103,000
Strain level where shear modulus is 70% of small strain shear modulus, $\gamma_{0.7}$	1.36x10^{-4}
Unit weight, γ (kN/m^3)	17.6
Cohesion, c (kN/m^2)	1
Angle of internal friction, φ (°)	36

The raft foundation considered in this analysis consists of concrete 1 m thick, with a unit weight, γ = 25 kN/m^3. The foundation is positioned so that its centerline coincides with the centerline of the sand deposit. The foundation is modelled by using continuum elements with linear isotropic behavior, with Young's modulus, E = 30 GPa; and Poisson's ratio, v = 0.15. The basement walls are simulated as plate elements. Uniform loads are assigned to simulate the total loads of a high-rise building. Interface elements are used to model the interface between the soil and the raft foundation and basement walls.

6.3.4.1.5. Numerical modelling calculations

The simulation procedures can be summarized in detail as follows.

Step 1: Initial in-situ stresses for the model are generated.

Step 2: Tunnel construction is simulated by using the numerical method described in Section 2.4.1.3.

Step 3: Construction of the building is simulated in terms of excavating the basement, laying the mat foundation, building the basement enclosure, and then applying the uniform load sequentially.

6.3.4.2 Three-dimensional finite element parametric analysis

The problem considered in the 2D modelling was adopted in the 3D analysis. However, in the 3D analysis, the entire building is considered, with the main structural system of the high-rise building consisting of flat slabs of uniform thickness connected to columns (without the use of beams). The gravity and lateral loads are withstood by lift shear walls. To establish the relationship between the 2D and 3D results regarding the effect of a pre-existing tunnel on a newly constructed high-rise building supported on a raft foundation, another parametric study utilizing 3D models was conducted, considering the same variables as used in the 2D study. In both the 2D and 3D studies, the tunnel burial depth ranges from 1D to 6D (where D is the tunnel diameter) and the horizontal location of the tunnel ranges from 0D to 10D. The 3D FE model considered has a depth of 60 m and extends 160 m in the *x*-direction and 100 m in the *y*-direction (see Figure 6- 9). These dimensions are sufficient to allow for the development of any possible collapse mechanism and to avoid influence from the model boundaries. Additional details concerning the three-dimensional finite element parametric analysis can be found in the paper entitled: "*Three-dimensional*

investigation of how newly constructed buildings supported on raft foundations affect pre-existing tunnels".

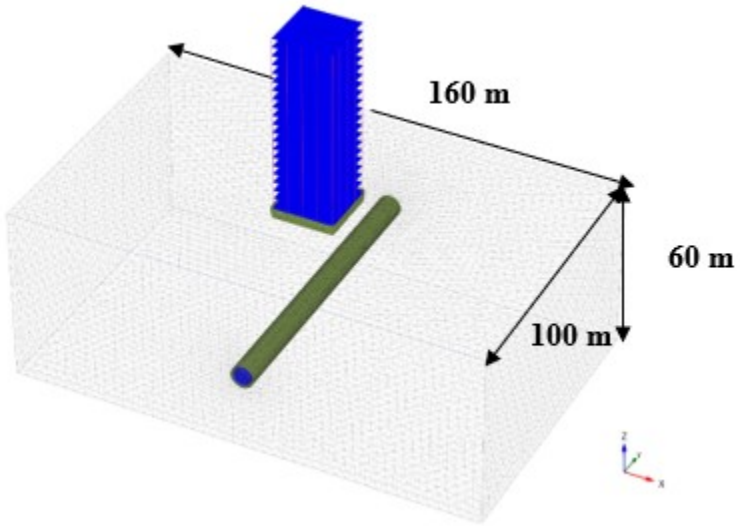

Figure 6- 9: Model for the 3D finite element parametric analysis

6.3.4.3 Spring model finite element parametric analysis

Structural analysis and design software often do not include the capability of simulating the soil continuum. Hence, the only way for such software to consider the soil response or the effect of a pre-existing tunnel is through spring schemes. Consequently, in order to develop such a scheme, the performance of a raft foundation on springs is simulated by using the PLAXIS 2D software. The parametric study conducted in the two-dimensional finite element analysis (described in Section 2.4.1) is utilized. However, the soil is replaced by equally spaced springs (as described in Section 2.2) and the tunnel is represented by equivalent horizontal and vertical forces added at each spring (as described in Section 2.3) (See Figure 6- 10). The raft foundation and the basement walls are modelled as plate elements with a linear isotropic behavior, with Young's modulus, E = 30 GPa; and Poisson's ratio, v = 0.15.

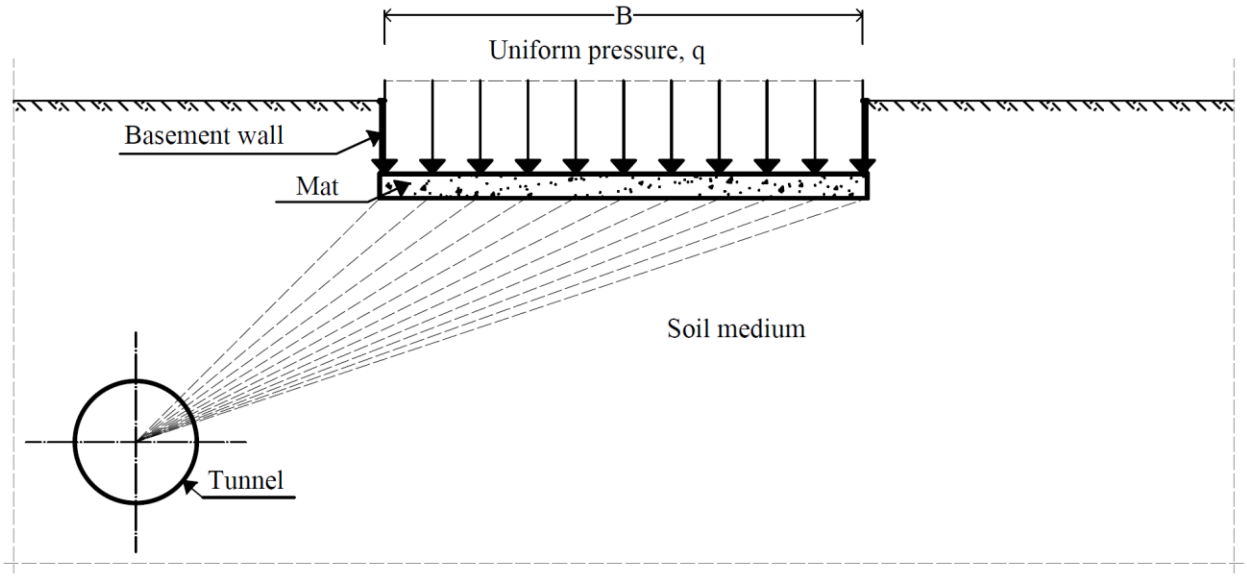

(a) 2D-Model

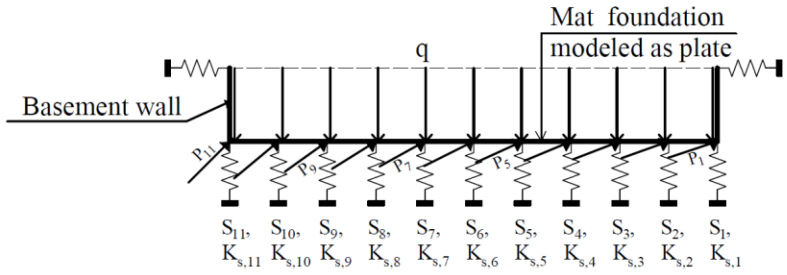

(b) Spring-Model

Figure 6- 10: (a) 2D model, and **(b)** equivalent spring model

6.3.4.4 Influence on the settlement trough of the raft foundation

Figure 6- 11 shows mat foundation settlement troughs for a tunnel center burial depth of 0.25B (where B is the width of the mat foundation), and tunnel center horizontal locations of 0B (directly beneath the centerline of the mat foundation), 0.25B, 0.50B, 0.75B, 1.00B and 1.50B. It can be seen that the settlement troughs calculated by the two-dimensional, three-dimensional and spring model analyses have similar trends, but with values offset by around 15% to 20%. Similar results can be found in Figures 6- 12, 6- 13, 6- 14 and 6- 15, which illustrate mat foundation settlement

troughs for tunnel center burial depths of 0.50B, 0.75B, 1.00B and 1.50B, respectively. One of several factors influencing the settlement of shallow foundations is ground stiffness. Since the stiffness of the tunnel lining is greater than that of sand, foundation soils become stiffer if a tunnel is present; thus, settlement is reduced. For example, it can be seen from Figure 6- 16 that the figures obtained for the maximum settlement of the mat foundation in the greenfield case (where there is no pre-existing tunnel) are 58 mm for the 3D analyses, 65 mm for the 2D analysis, and 70 mm for the spring analysis. In contrast, as shown in Figure 6- 12(a), when a tunnel is present at a burial depth of 0.50B and a horizontal location directly beneath the mat foundation (H=0B), the figures obtained for the maximum settlement of the mat foundation are 45 mm for the 3D analyses, 55 mm for the 2D analysis, and 58 mm for the spring analyses. Thus, decreases in maximum settlement of 22%, 15%, and 17% are found for the 3D, 2D, and spring model analyses, respectively, when a tunnel is present. For this reason, the presence of a tunnel beneath the mat foundation has a positive effect on the settlement trough of the mat.

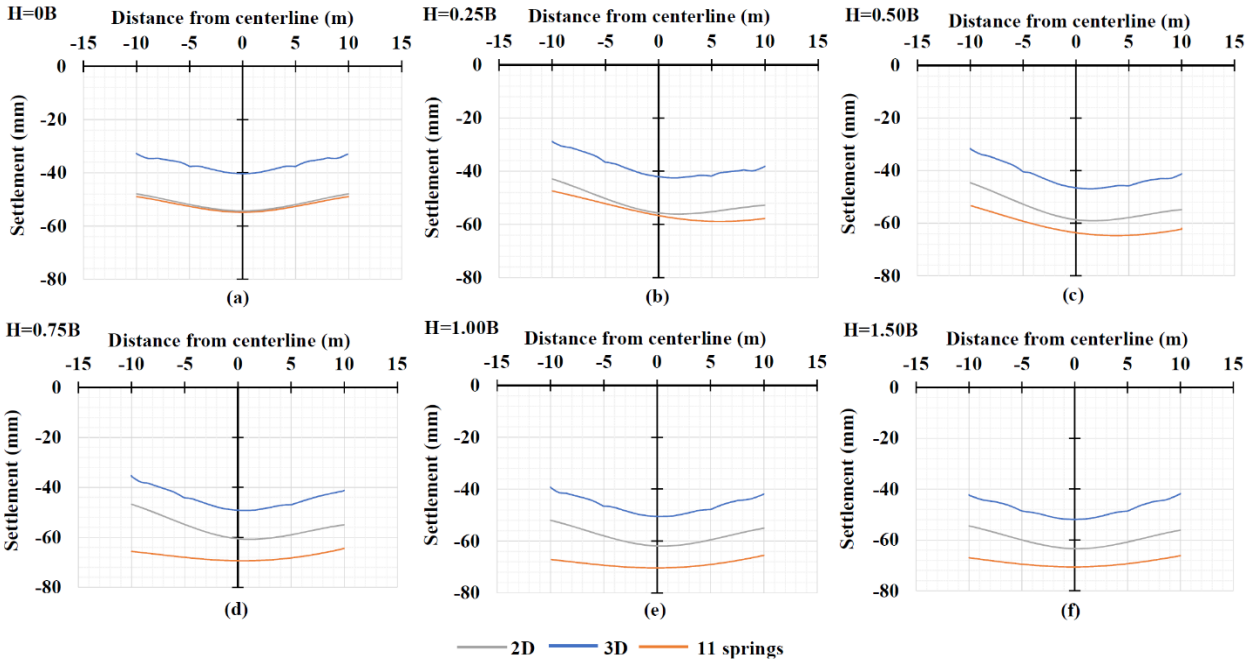

Figure 6- 11: Mat foundation settlement troughs for a tunnel center burial depth of 0.25B

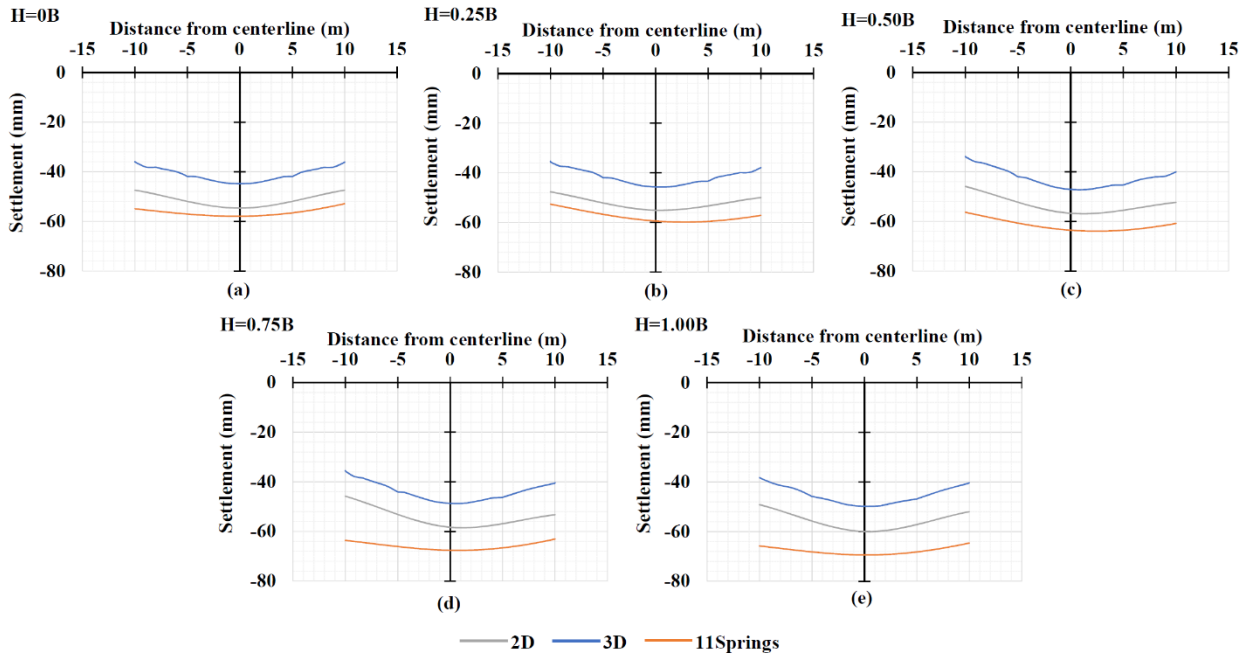

Figure 6- 12: Mat foundation settlement troughs for a tunnel center burial depth of 0.5B

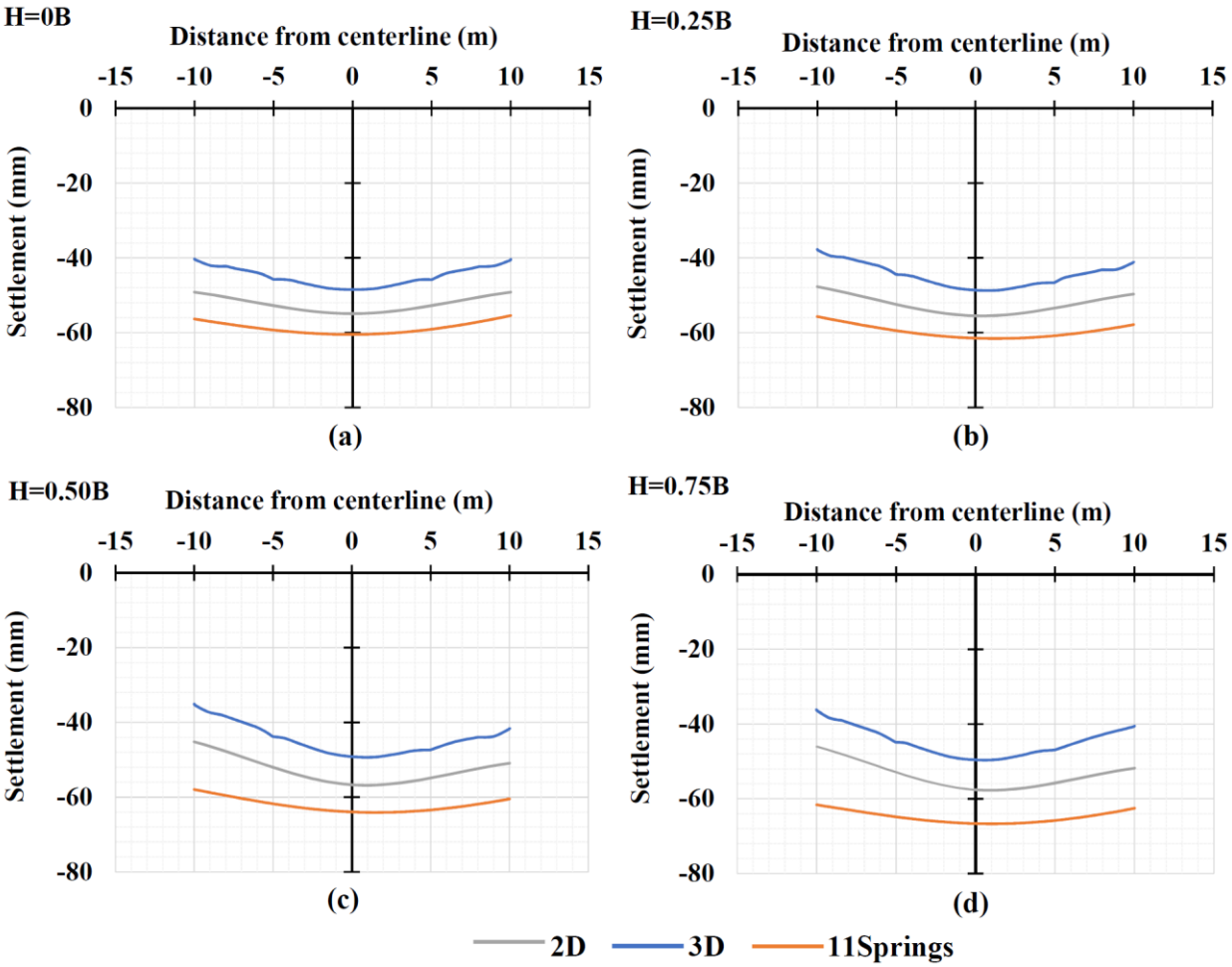

Figure 6- 13: Mat foundation settlement troughs for a tunnel center burial depth of 0.75B

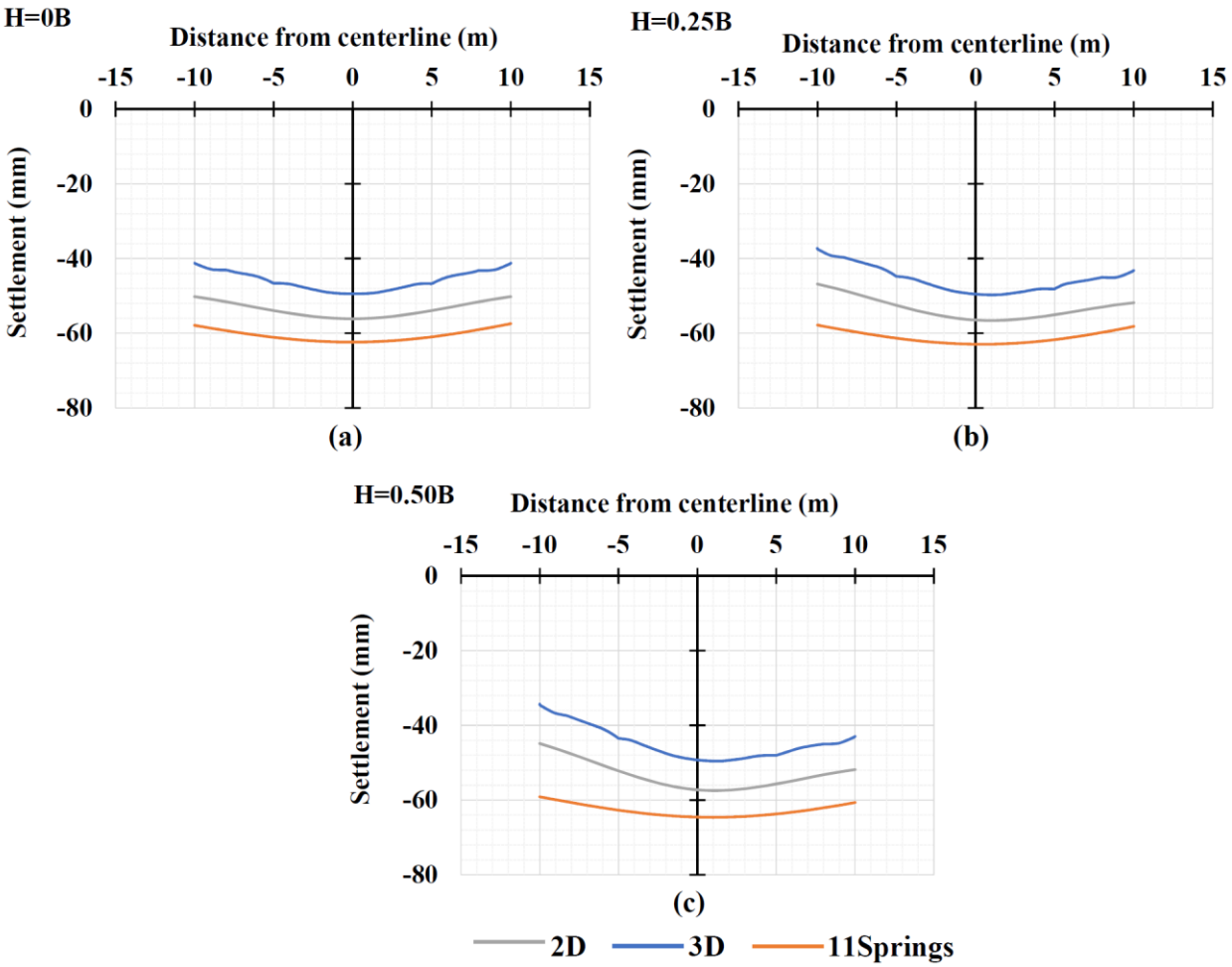

Figure 6- 14: Mat foundation settlement troughs for a tunnel center burial depth of 1.00B

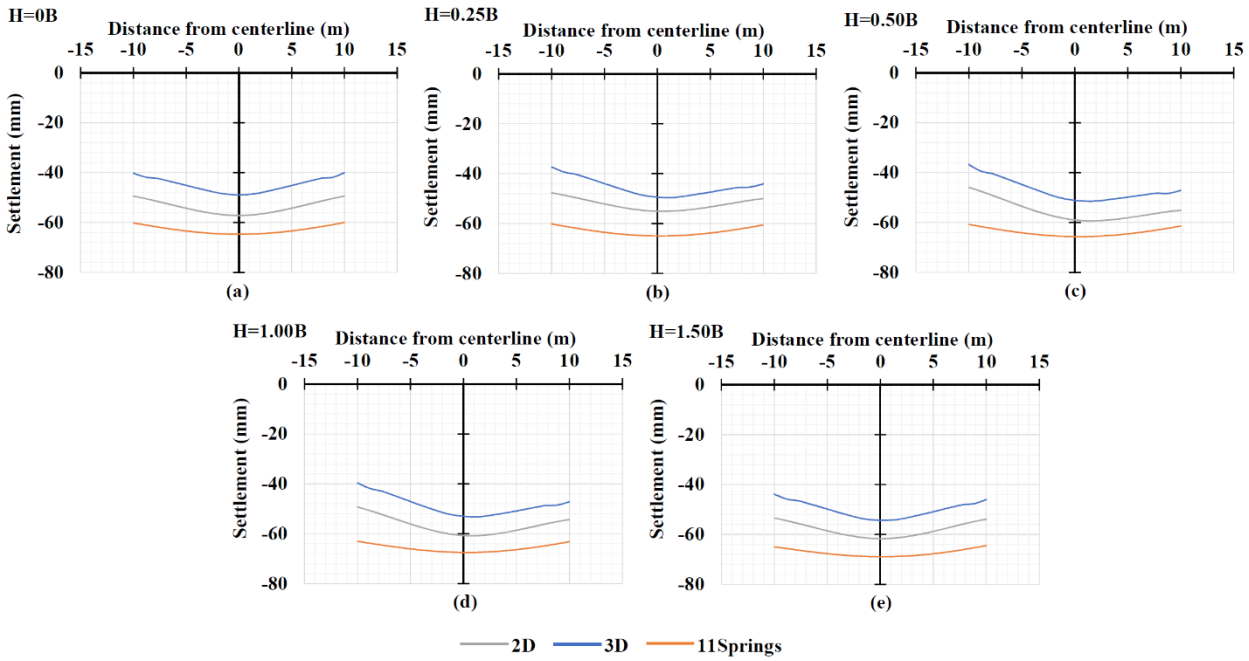

Figure 6- 15: Mat foundation settlement troughs for a tunnel center burial depth of 1.50B

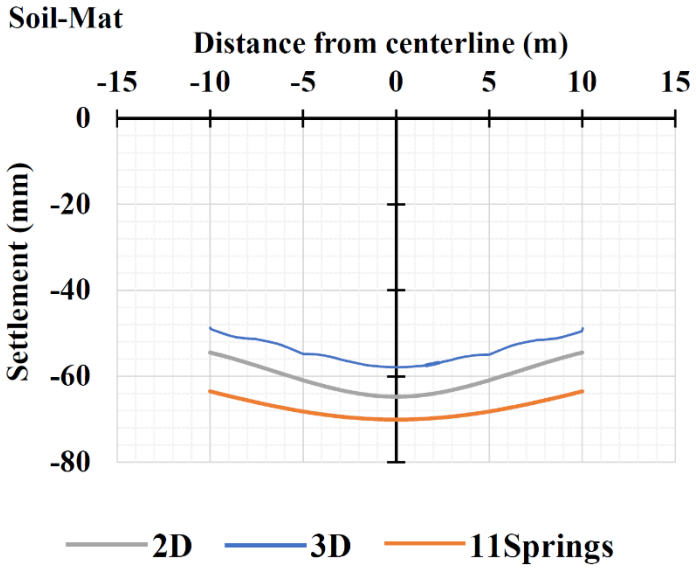

Figure 6- 16: Mat foundation settlement troughs for the greenfield case

Because the three-dimensional finite element analysis establishes more accurate estimates of the mat foundation settlement than is the case with the two-dimensional and spring model analyses, two coefficient correction factors are introduced: Coefficient correction factor α_1 accounts for the 3D effect, and coefficient correction factor α_2 accounts for the 2D effect, in the spring model.

6.3.4.5 Correction factor α_1 for the three-dimensional effect

A linear regression analysis was performed by using the maximum settlement results of the 3D and 2D finite element analyses to determine the best fit and the coefficients for the power equation for the correction factor α_1, which is dependent on the independent variable *Z/B*. The following expression was obtained for the correction factor:

$$\alpha_1 = \frac{Z}{B}\left\{0.8587\left(\frac{Z}{B}\right)^{-0.958}\right\} \quad [14]$$

where

$\frac{Z}{B}$ is the ratio of the depth of the tunnel center to the width of the mat foundation.

6.3.4.6 Correction factor α_2 for the two-dimensional effect

A linear regression analysis was performed by using the maximum settlement results of the 2D and spring model finite element analyses to determine the best fit and the coefficients for the power equation for the correction factor α_2, which is dependent on the independent variable *Z/B*. The following expression was obtained for the correction factor:

$$\alpha_2 = \frac{Z}{B}\left\{0.8867\left(\frac{Z}{B}\right)^{-0.997}\right\} \quad [15]$$

where

$\frac{Z}{B}$ is the ratio of the depth of the tunnel center to the width of the mat foundation.

6.3.5 Corrected settlement

To obtain the corrected settlement value, after the mat foundation settlement has been calculated, and the effect of a pre-existing tunnel has been incorporated as described in Section 2.3, the result is then multiplied by the two correction factors α_1 (see Section 2.4.5) and α_2 (see Section 2.4.6):

$$\Delta s_{corrected} = \left(\Delta s_{greenfield} - \Delta iv\right) \times \alpha_1 \times \alpha_2 \quad [16]$$

6.3.6 Limitations of the work

It must be emphasized that the conclusions of this simplified procedure are dependent upon the validity of the assumption that the soil can be considered as a linear elastic material, an assumption commonly used in current mat foundation design practice. It should be noted that if a 3D finite element program has been employed to compute the greenfield settlement, $\Delta s_{Greenfield}$, (see Section 2.1), the correction factors α_1 and α_2 should not be used. Similarly, if a 2D finite element program has been employed, only the correction factor α_1 should be used.

6.4 Procedure For Calculating The Settlement Beneath The Mat Foundation

The following procedure is hereby proposed to correct mat foundation settlement predictions by taking into account the effect of a pre-existing tunnel:

1. Calculate the greenfield settlement, $\Delta s_{Greenfield,}$ given by Eq. 5, which corresponds to the settlement of a mat foundation under uniform pressure on the surface of a semi-infinite, homogeneous, isotropic medium.
2. Calculate the coefficient of subgrade reaction, k_s, given by Eq. 6.

3. Calculate the predicted settlement, given by Eqs. 7 to 13.
4. Calculate the corrected settlement by using Eqs. 14 to 16.

6.5 VERIFICATION OF THE PROPOSED SIMPLIFIED PROCEDURE

The aim of this section is to verify the applicability of the correction factor obtained. A sample is presented to demonstrate the applicability of the proposed correction factor. In the case considered, the burial depth of the tunnel center is 0.50B and its horizontal location is shifted from 0.25B to 1.00B (where B is width of the mat foundation). Figure 6- 17 presents the mat foundation settlement troughs calculated by the 3D, 2D and spring finite element analyses (as described in previous sections), together with the corrected settlement trough as proposed by the simplified procedure. As shown in Figure 6- 17, the predictions of the corrected solution are within 9% of the results of the 3D finite element analysis when the horizontal location of the tunnel center is 0.25B from the mat foundation centerline (see Figure 6- 17(a)), and within 5% and 2% when the tunnel center is shifted horizontally 0.50B and more than 0.75B, respectively. These verification process results indicate that when the correction factor is employed, the settlement trough predictions of the proposed simplified procedure are within 10% of the 3D finite element calculations.

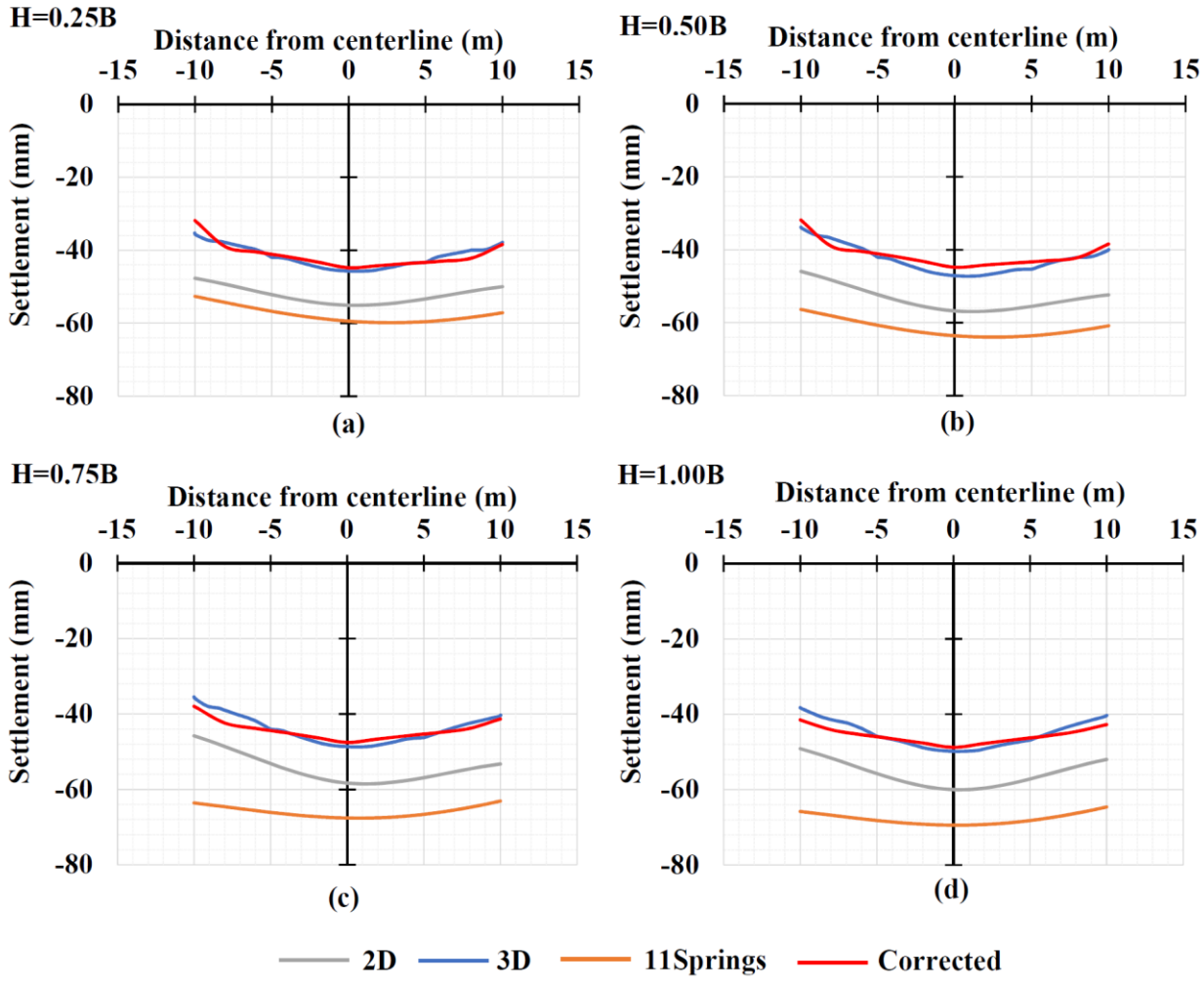

Figure 6- 17: Corrected settlement trough for a tunnel center burial depth of 0.5B

6.6 CONCLUSIONS

To make an appropriate mat foundation settlement trough prediction for a building constructed near a pre-existing tunnel, a simplified procedure is established to incorporate the effect of a pre-existing tunnel in the analysis of a new building. An analytical and finite element parametric analysis using three- and two-dimensional elements was performed to investigate the settlement trough of a mat foundation of a newly constructed high-rise building, with different tunnel burial

locations. The finite element analysis results were then used to obtain an expression for the correction factors for the proposed simplified procedures. The results obtained by using the proposed method to estimate the deflection of the mat foundation are within 10% of the values obtained by using the 3D finite element calculations. Finally, it must be emphasized that the simplified procedure proposed in this study depends upon the assumption that the soil behaves as a linear elastic material.

6.7 REFERENCES

Attewell, P., Yeates, J., & Selby, A. (1986). Soil movements induced by tunnelling and their effects on pipelines and structures. Glasgow, U.K.: Blackie and Son Ltd.

Augarde, C. (1997). Numerical modelling of tunnelling processes for assessment of damage to buildings. Oxford University Research Archive.

Benz, T. (2006). Small-strain stiffness of soils and its numerical consequences. Ph.D. Thesis, Institut fur Geotechnik, Universitat Stuttgart, Germany

Biot, M. A. (1937). Bending of an infinite beam on an elastic foundation   Journal of Applied Mechanics, 59, A7.

Boussinesq J. (1885). Applications des potentiels à l'étude de l'équilibre et mouvement des solides elastiques, Gauthier–Villard, Paris.

Bowles, J. E. (1997). Foundation analysis and design (5th ed.). Singapore: McGraw Hill Int. Ed., Singapore.

Burd, H., Houlsby, G., Augarde, C., & Liu, G. (1994). Prediction of tunnel-induced settlement damage to masonry structures. Parks Road, Oxford: University of Oxford, Departement of Engineering Science.

McKinsey Global Institute. (2014). A blueprint for addressing the global affordable housing challenge.

PLAXIS 3D user's manual, version 2018. material model manual. (2018).

Sadrekarimi, J., & Akbarzad, M. (2009). Comparative study of methods of determination of coefficient of subgrade reaction. Electronic Journal of Geotechnical Engineering, 1-14.

Terzaghi, K. (1955). Evaluation of coefficients of subgrade reaction. Geotechnique, 4, 297-326.

Tjie-Liong, GOUW & Limara PT. Notes on the application of the spring. Indonesia. PLAXIS Practice.

Vermeer, P. (2001). On a smart use of 3D-FEM in tunnelling Plaxis Bulletin (11), 2-7. 11, 2-7. Plaxis Bulletin.

Vesic, A.B. (1961). Beam on Elastic Subgrade and The Winckler's Hypothesis, Proc. 5th Int. Conf. On Soil Mechanics and Foundation Engineering, Vol.1, p. 845-850.

Vesic, A. B. (1961). Bending of beams resting on isotropic elastic solid. Journal of the Engineering Mechanics Division, 87(2), 35-53.

Winkler, E. (1867). Die Lehre Von Elasticitaet Und Festigkeit. 1st Edn., H. Dominicus, Prague.

Zakhem, AM., El Naggar, H. (2019). Effect of the newly constitutive material model employed on predictions of the behaviour of earth pressure balance (EPB) shield driven tunnels. Transportation Geotechnics, Elsevier.

CHAPTER 7 CONCLUSION

This chapter summarizes the results of this thesis and the contributions made. Suggestions for future work are also discussed.

7.1 CONCLUSION

Nowadays, construction of new buildings with basements very close to the pre-existing tunnels is a big challenge for practicing engineers. The nature of the interaction between tunnels and foundations is complex and complicated. The construction of new structure changes the stress path in the soil and can affect the safety and the durability of the existing tunnel. An increase or decrease in the tunnel diameter imply cracking at various locations around the tunnel lining resulting in the entry of saline water that could lead to significant deterioration of the concrete.

To investigate the considered problem, this thesis involved a comprehensive numerical modelling of all of its geometric and material aspects using the finite element (FE) code PLAXIS 3D. In this thesis, the excavation process of the tunnel driven by a tunnel boring machine (TBM) was simulated in detail and divided into several phases. The face pressure, the conical shape of the shield, the jacking force, the grouting injection, the hardening of the grout and the installation of the new lining were taken into consideration. Also, different scenarios were considered in this thesis to illustrate tunnel lining degradation due to chloride penetration through joints and cracks, especially in the case of exposure to ground water contaminated with chloride. The intact and degraded concrete lining were modelled using the new concrete constitutive model included in the PLAXIS library taken into consideration the non-linearity of the material behaviour. The soil and the interface which allowed for both slippage and gapping to occur were simulated using soil

hardening and elasto-plastic constitutive models from the PLAXIS library. New design guidelines for shallow foundation in close vicinity of existing tunnel were developed.

A general overview of soft ground tunnelling and its interaction with the surrounding soil was presented in Chapter 2 and a two-dimensional numerical analysis of the effect of tunneling on existing building was investigated in detail.

By utilizing a well-documented case study of twin tunnels in Shanghai, in Chapter three, the complex soil-structure interaction problem involved by the earth pressure balance (EPB) shield tunneling was investigated. Therefore, a 3D finite element numerical model focused on selecting appropriate constitutive models for soils and structures, simulating construction procedures and sequences, and modelling the soil/structure interface was developed. Predictions of four different advanced soil constitutive models were compared with measured field results to assess the model effectiveness and suitability. The undrained behaviour of the saturated soft silty clay soil at the tunnelling site was studied during and after advancement of the shield tunnelling machine. The comparison matrix included surface settlement troughs along transverse sections, and changes developing in earth and pore water pressures around the tunnel. The HSSmall soil model, which accounts for increased soil stiffness at small strains, was found to be the most suitable for addressing these problems. Reliable numerical models to predict expected settlements, lining pressures and other design parameters are essential for safe tunnel design.

In the Chapters four and five of this thesis, a detailed investigation of the effect of constructing of a new high-rise building on a shallow foundation in a sandy layer near a pre-existing tunnel was presented. A comprehensive 3D finite element model capable of capturing, to a great extent, the complex soil-structure interaction associated with the tunnel excavation process was established.

The model developed accounts for a staged construction sequence, including the interaction between the TBM machine and the surrounding soil, the applied face pressure and jacking forces, the interaction between the segmental tunnel lining and the surrounding soil, and the injection pressure of the tail void grout and its hardening with time. A concrete material model newly developed in PLAXIS is utilized to model the reinforced concrete elements of the tunnel lining. Tunnel degradation is simulated according to four different scenarios. Two of them represent degradation in the form of delamination of the intrados concrete lining, by reducing the material strength properties at the crown and shoulder zones. The other two scenarios represent a more extreme case, where the intrados lining is gradually and completely spalled. In addition, the conducted numerical analyses utilized an advanced, non-linear constitutive soil model to model the soil behaviour. Predicted thrust forces, bending moments, radial stresses, vertical and horizontal deformations of structural elements in the tunnel lining, and maximum and differential settlements of the mat foundation are analyzed for different tunnel burial locations. In light of the evaluation of the building-tunnel interaction, a practical exclusion zone to minimize the effect of new construction on a pre-existing tunnel is defined. Accordingly, new design guidelines can be developed for shallow foundations adjacent to a pre-existing tunnel located in a sandy layer.

Finally, in chapter 6, a simplified procedure to incorporate the effect of pre-existing tunnels in the analysis of new buildings was developed. The objective is to produce mat deflection diagrams similar to those of a finite element analysis that treats the soil as a continuum, so that the results can be easily applied in most automated structural analysis programs. Correction factors have also been obtained to accompany the proposed procedure.

7.2 FUTURE WORK

Due to the potential value of the findings and results of this study, further investigations are recommended which can be summarized as follows:

- 3D effect of a newly constructed structure supported on a raft foundation on the intact and degraded existing tunnel under seismic load;
- 3D effect of a newly constructed structure supported on a deep foundation on the intact and degraded existing tunnel under static load;
- 3D effect of a newly constructed structure supported on a deep foundation on the intact and degraded existing tunnel under seismic load.

REFERENCES

Abbas, S., Soliman, A., & Nehdi, M. (2014). Chloride ion penetration in reinforced concrete and steel fiber-reinforced concrete precast tunnel lining segments. Farmington Hills: doi:10.14359/51686991.

Abdel-Meguid, M., Rowe, R. K., & Lo, K. Y. (2002). 3D effects of surface construction over existing subway tunnels. International Journal of Geomechanics, 2(4), 447-469.

Addenbrooke , T., Potts , D., & Puzrin , A. (1997). The influence of prefailure soil stiffness on the numerical analysis of tunnel construction. Geotechnique 47 (3), 693–712, 47(3), 693-712.

Addenbrooke, T., & Potts D.M. , D. (1996). Twin tunnels construction-ground movements and lining behaviour. Proceedings of geotechnical aspects of underground construction in soft ground, (pp. 15-7). City University, London.

Ai, Q., Yuan, Y., Mahadevan, S., & Jiang, X. (2016). Probabilistic degradation modelling of circular tunnels assembled from segmental linings. Structural Concrete, 17(2), 257-273. doi:10.1002/suco.201400122.

Amleh L. & Ghosh A. (2006). “Modeling the effect of corrosion on bond strength at the steel concrete interface with finite element analysis”. Can. J. Civ. Eng., 33, pp. 673–682.

Atkinson, J., & Sallfors, G. (1991). Experimental determination of soil properties. Proceedings of the 10th ECSMFE, 3, pp. 915-956. Florence.

Attewell, P. B. (1978). “Ground movements caused by tunnelling in soil.” Proc., Int. Conf. on Large Movements and Structures, J. D. Geddes, ed., Pentech, London, 812–948.

Attewell, P. B., Yeates, J., and Selby, A. R. (1986). Soil movements induced by tunnelling and their effects on pipelines and structures, Blackie and Son Ltd., London.

Attewell P.B. (1988). “An overview of site investigation and long-term tunnelling induced settlement in soil”. Engineering Geology of Underground Movements, Bell et al. (eds.), Geological Society Engineering Geology Special Publication No. 5, 55-61.

Augarde, C. (1997). Numerical modelling of tunnelling processes for assessment of damage to buildings. Oxford University Research Archive.

Benton L. J. & Phillips A., (1991). “The behaviour of two tunnels beneath a building on piled foundations’’. Proc. 10th European Conf. on Soil Mechanics and Foundation Engineering: 665-668.

Benz, T. (2006). Small-strain stiffness of soils and its numerical consequences. Ph.D. Thesis, Institut fur Geotechnik, Universitat Stuttgart, Germany.

Bian, K., Liu, J., Xiao, M., & Liu, Z. (2016). Cause investigation and verification of lining cracking of bifurcation tunnel at huizhou pumped storage power stationdoi://doi.org/10.1016/j.tust.2015.10.030

Biot, M. A. (1937). Bending of an infinite beam on an elastic foundation   Journal of Applied Mechanics, 59, A7.

Bjerrum, L. (1963), "Allowable Settlement of Structures," Proc., European Conf. on Soil Mech. and Found. Engr., Weisbaden, Germany, Vol. 3, pp. 135-137

Boonpichetvong M. & Rots J.G. (2004). “Settlement damage of masonry buildings in soft ground”. The Structural Engineer, 4 January, 32-37.

Boscardin M. D. & Cording, E. J. (1989). “Building response to excavation-induced settlement.” J. Geotech. Eng., 115(1), 1–21.

Boussinesq J. (1885). Applications des potentiels à l’étude de l’équilibre et mouvement des solides elastiques, Gauthier–Villard, Paris.

Bowles, J. E. (1997). Foundation analysis and design (5th ed.). Singapore: McGraw Hill Int. Ed., Singapore.

Burd, H., Houlsby, G., Augarde, C., & Liu, G. (1994). Prediction of tunnel-induced settlement damage to masonry structures. Parks Road, Oxford: University of Oxford, Departement of Engineering Science.

Burford, D. (1988). Heave of tunnels beneath the shell centre, London, 1959-1986, Oklahoma State University Interlibrary Loan.

Burland J. B. (1995). “Assessment of risk of damage to buildings due to tunnelling and excavation.” Proc., 1st Int. Conf. on Earthquake Geotechnical Engineering, K. Ishihara, ed., Vol. 3, Balkema, Rotterdam, Netherlands, 1189–1201.

Burland, J.B., Broms, B. and De Mello, V.F.B. (1977) Behaviour of foundations and structures. State of Art. Report. Session 2. Proc. 9th Int. Conf. on Soil Mech. and Found. Eng., 2, pp. 495.

Burland J. B. & Wroth C. P. (1974). “Settlement of buildings and associated damage.” Proc., Conf. on Settlement of Structures, Pentech Press, London, 611–654.

Calabresi, G., Rampello, S., & Callisto, L. (1999). Prediction of tunnel-induced displacements in historic buildings: the case of Castel S. Angelo. Twelfth European Conference on Soil Mechanics and Geotechnical Engineering . Amsterdam, Netherlands.

Chang, C., Sun, C., Duann, S. W., & Hwang, R. N. (2001). Response of a 231aipei rapid transit system (TRTS) tunnel to adjacent excavation. Tunnelling and Underground Space Technology Incorporating Trenchless Technology Research, 16(3), 151-158. Doi:10.1016/S0886-7798(01)00049-9.

Chapman, D., Metje, N., & Stärk, A. (2010). Introduction to tunnel construction (Applied geotechnics). Milton Park, Abingdon, Oxon; New York, NY: Spon Press.

Chen, W., & Baldauf, S. (1994). Prediction of ground deformation due to excavation-Application to tunnel lining design in weak rock. Computer Methods and advane in Geomechanics, 2565-2570.

Chen, Jingru, Song Xiaocui, Tiejun, Zhao, Li & Tian. (2010). “Service Life Prediction of Lining Concrete of Subsea Tunnel under Combined Compressive Load and Carbonation”. Journal of Wuhan University of Technology-Mater. Sci. Ed.

Chow, L. (1994). Prediction of surface settlement due to tunneling in soft ground. M.Sc. thesis, University of Oxford.

Code of practice for railway protection (2004). [LTA 2000]. Singapore: Development & Building Control Department, Land Transport Authority (LTA).

Colback, P. S. B., & Wiid, B. L. (1965). The influence of moisture content on the compressive strength of rocks Paper presented at the 65-83.

De Melo, G. P., & Pereira, S. C. (2002). Three-dimensional numerical modelling of the construction of an EPBS tunnel for Shanghai Metro - Line 2. Geotechnical Aspects of Underground Construction in Soft Ground, 323-328.

Devriendt, M., Doughty, L., Morrison, P., & Pillai, A. (2010). Displacement of tunnels from a basement excavation in London. Proceedings of the Institution of Civil Engineers, 163(3), 131-145. Retrieved from https://search.proquest.com/docview/906522924.

Doležalová, M. (2001). Tunnel complex unloaded by a deep excavation. Computers and Geotechnics, 28(6-7), 469-493. doi:10.1016/S0266-352X(01)00005-2.

Doran, S. R., Wood, T., Tham, S. K., Shirlaw, J. N., & Wen, D. (2000). The assessment of limits for the movement of subway tunnels and trackwork due to adjacent construction, Balkema, Rotterdam.

Dowding C. H. & Rozen A. (1978) "Damage to Rock Tunnels from Earthquake Shaking". Journal of the Geotechnical Engineering Division, ASCE, Vol. 104, No. GT2.

Duncan, J. M. (1970). Non-linear analysis of stress and strain in soils. Journal of the Soil Mechanics and Foundations Division, 96(5), 1629-1653.

El Naggar, H., & Hinchberger, S. (2008). An analytical solution for jointed tunnel linings in elastic soil or rock. Canadian Geotechnical Journal, 45(11), 1572-1593.

El Naggar, H., Hinchberger, S., & Lo, K. (2008). A closed-form solution for composite tunnel linings in a homogeneous infinite isotropic elastic medium. Canadian Geotechnical Journal, 45(2), 266-287.

El Naggar, H., & Hinchberger, S. D. (2012). Approximate evaluation of stresses in degraded tunnel linings doi://doi.org/10.1016/j.soildyn.2012.07.016

European Committee for Standardization (1994b). Geotechnical Design, General Rules-Part 1, Eurocode 7; Brussels, Belgium.

Fathi Salmi, E., Soltani Asadi, Z., Bayati, M., & Sharifzadeh, M. (2019). Assessing the hydrogeological conditions leading to the Corrosion and deterioration of pre-cast segmental concrete linings (Case of Zagros tunnel). Geotechnical and Geological Engineering, doi:10.1007/s10706-019-00886-1.

Finno, R., & Clough, G. (1985). Evaluation of soil response to EPB shield tunneling. Journal of Geotechnical Engineering, 111(2), 155-173.

Frischmann W.W., Hellings J.E., Gittoes G. & Snowden C. (1994). "Protection of the Mansion House against damage caused by ground movements due to the Docklands Light Railway extension". Proc. Instn. Civ. Engrs. Geotech. Engng., April 107, 65-67.

Gulikers J. (2003). "Problems encountered in the detection of reinforcement corrosion in concrete tunnel linings – theoretical considerations". Mater. Corros., 54, pp. 454–459.

Hardin, B. O., & Drnevich, V. (1972). Shear Modulus and Damping in Soils: Design Equations and Curves. Geotechnical Special Publication, 98(118).

Hejazi , Y., Dias, D., & Kastner, R. (2008). Impact of constitutive models on the numerical analysis of underground constructions. Acta Geotech. , 3(4), 251-258.

Higgins K. G., Chudleigh I., St John H. D. & Potts D. M. (1999). “An example of pile tunnel interaction problems”. Proc. Int. Symp. Geotech. Aspects of Underground Construction in Soft Ground, IS-Tokyo, pp. 99–103.

Howard, A. J. (1991). ‘’Report on the damaging effects of water on tunnels during their working life.’’ Tunnelling and underground space technology, 6(1), pp. 11-76.

Idris, J., Verdel, T., & Al-Heib, M. (2008a). Numerical modelling and mechanical behaviour analysis of ancient tunnel masonry structures doi://doi.org/10.1016/j.tust.2007.04.006

Idris, J., Verdel, T., & Al-Heib, M. (2008b). Numerical modelling and mechanical behaviour analysis of ancient tunnel masonry structures doi://doi.org/10.1016/j.tust.2007.04.006

ITA Working Group (2012). Urban Problems – Underground Solutions. ITA Report Nº011/APR 2012. International Tunneling and Underground Space Association, Chatelaine, Switzerland.

Inokuma, A., & Inano, S. (1996). Road tunnels in japan: Deterioration and countermeasures doi://doi.org/10.1016/0886-7798(96)00026-0.

Jiang, M., & Yin, Z. (2012). Analysis of stress redistribution in soil and earth pressure on tunnel lining using the discrete element method doi://doi.org/10.1016/j.tust.2012.06.001

Kolmybas D. (2005). Tunnelling and Tunnel Mechanics, Springer, Berlin.

Leca, E., & Clough, W. (1992). Preliminary design for NATM tunnel support in soil. Journal of Geotechnical Engineering, 118(4), 558-575.

Lee, K., & Rowe, R. (1990a). Finite element modelling of the three-dimensional ground deformations due to tunnelling in soft cohesive soils. Part I. Methods of analysis. Computers and Geotechnics, 10(2), 87-110.

Lee, K., & Rowe, R. (1990b). Finite element modelling of the three-dimensional ground deformations due to tunnelling in soft cohesive soils. Part II. Results. Computers and Geotechnics, 10(2), 111-138.

Lee, K., Ji , H., Shen , C., Liu , J., & Bai , T. (1999). Ground response to the construction of Shanghai metro tunnel-line 2. Soils and foundations, 39(3), 113-134.

Li, Q. (2013). Long-term settlement mechanisms of shield tunnels in Shanghai soft clay. Hong kong: Hong Kong University of Science and Technology.

Li, Tian, Jingru, Chen, Tiejun & Zhao. (2012). “Durability of Lining Concrete of Subsea Tunnel under Combined Action of Freeze-thaw Cycle and Carbonation”. Journal of Wuhan University of Technology-Mater. Sci. Ed.

Lo, K. Y., & Ramsay, J. A. (1991). The effect of construction on existing subway tunnels—a case study from Toronto. Tunnelling and Underground Space Technology, 6(3), 287-297.

Loganathan , N., & Poulos, H. (1998). Analytical prediction for tunneling-induced ground movements in clays. J. Geotech. Geoenviron. Eng. ASCE, 124(9), 846-586.

Mair, R., Gunn, M., & O'Reilly, M. (1981). Ground movements around shallow tunnels in soft clay. Proc. Xth Int. Conf. SMFE, 2. Stockholm.

Mair, R., Gunn, M., & O'Reilly, M. (1982, June). Ground movements around shallow tunnels in soft clay. Tunnels &Tunnelling.

Mair, R. J., and Taylor, R. N. (1997). "Theme lecture: Bored tunnelling in the urban environment." Proc., 14th Int. Conf. on Soil Mechanics and Foundation Engineering, Hamburg, Balkema, Rotterdam, The Netherlands, 2353–2385.

Mair, R. J., Taylor, R. N., and Bracegirdle, A. (1993). "Subsurface settlement profiles above tunnels in clays." Geotechnique, 43(2), 315–320.

Mansur , M., Chin, M., & Wee , T. (1999). Stress-strain relationship of high-strength fiber concrete in compression. ASCE Journal of Materials in Civil Engineering, 11(1), 21-29.

McKinsey Global Institute. (2014). A blueprint for addressing the global affordable housing challenge.

Miliziano F.M., Soccodato F.M. & Burghignoli, A. (2002). "Evaluation of damage in masonry buildings due to tunnelling in clayey soils". Geotechnical Aspects of Underground Construction in Soft Ground, Kastner, Emeriault, Dias, Guilloux (eds.), Balkema, Rotterdam, 335-340.

Moeinossadat, S. R., & Ahangari, K. (2019). Estimating maximum surface settlement due to EPBM tunneling by Numerical-Intelligent approach – A case study: Tehran subway line 7. Transportation Geotechnics, 18, 92-102.

Moller , S., & Vermeer , P. (2008). On numerical simulation of tunnel installation. Tunn. Undergr. Sp. Technol. , 23(4), 461-475.

Namazi E. & Mohamad, H. (2012). “Potential damage assessment in buildings undergoing tilt.” Proc., Inst. Civil Eng. Geotech. Eng., in press.

Namazi E. & Mohamad H. (2013) “Assessment of Building Damage Induced by Three-Dimensional Ground Movements”. Journal of Geotechnical and GeoEnvironmental Engineering, ASCE Vol. 139 (4): 608-618.

National building code of Canada 2015 (2015). National Research Council.

Ng, C. W. W., Sun, H. S., Lei, G. H., Shi, J. W., & Masin, D. (2015). Ability of three different soil constitutive models to predict a tunnel’s response to basement excavation. Canadian Geotechnical Journal, 52(11), 1685-1698. Doi:10.1139/cgj-2014-0361.

Oteo, C., & Moya, J. (1979). Estimation of the soil parameters of Madrid in relation to the tunnel construction. Proc 7th Euro conf. on soil mechanics and foundation engineering, 3, pp. 239-47. Brighton.

Peck, R. (1969). Deep excavation and tunneling in soft ground. State-of-the-art report. Proc 7th int. conf. soil mechanics and found engineering, (pp. 225-90). Mexico.

PLAXIS 3D user's manual, version 2018. material model manual. (2018).

Polshin D. E. & Tokar, R. A. (1957). “Maximum allowable non-uniform settlement of structures.” Proc., 4th Int. Conf. on Soil Mechanics and Foundation Engineering, Vol. 1, Butterworths, London, 402–405.

Potts D.M. & Addenbrooke T.I. (1997). “A structure’s influence on tunnelling-induced ground movements”. Proc. Inst. Civ. Engrs., Geotech. Engng., 125, 2, 109-125.

Robotic hydro demolition speeds repairs – TunnelTalk, February 2015

Roscoe, K., & Burland, J. (1968). On the Generalized Stress-Strain Behavior of Wet Clays. J. Heyman, F. Leckie (Eds.), Engineering plasticity, Cambridge University Press, (pp. 535-609). Cambridge.

Rowe, R., & Kack, G. (1983). A theoretical examination of the settlements induced by tunnelling: four case histories. Canadian Geotechnical Journal, 20, 299-314.

Rowe, R., & Lee, K. (1989). Parameters for predicting deformations due to tunnelling. Proceedings, 12th International Conference on Soil Mechanics and Foundation Engineering, (pp. 793-796). Rio de Janeiro.

Sadrekarimi, J., & Akbarzad, M. (2009). Comparative study of methods of determination of coefficient of subgrade reaction. Electronic Journal of Geotechnical Engineering, 1-14.

Sagaseta , C., Moya, J., & Oteo, C. (1980). Estimation of ground subsidence over urban tunnels. Proc 2nd conference on ground movement and structure, (pp. 331-44). Cardiff.

Sagaseta, C. (1988). Discussion on: Sagaseta C.: “Analysis of undrained soil deformation due to ground loss”. Author’s replay to B. Smhmidt. Géotechnique, 38(4), 647-649.

Santos, J., & Correia, A. (2001). Reference threshold shear strain of soil, its application to obtain a unique strain-dependent shear modulus curve for soil. Proceedings of the 15th International Conference on Soil Mechanics and Geotechnical Engineering, 1, pp. 267-270. Balkema, Istanbul.

Schadlich, B., & Schweiger , H. (2014). Shotcrete model. Internal report: Implementation, validation and application of the shotcrete model. Computational Geotechnics Group, Institute for Soil Mechanics and Foundation Engineering, Graz University of technology.

Schanz, T. (1999). Formulation and verification of the Hardening-Soil Model. RBJ Brinkgreve, Beyond 2000 in Computational Geotechnics, 281-290.

Schmidt, B. (1969). Prediction of settlements due to tunneling in soil: three case histories. Proc 2nd rapid excavation tunneling conference, (pp. 801-12). San Francisco, CA.

Schroeder F. C. (2002). "The influence of bored piles on existing tunnels: a case study". Ground Engng. Vol. 35 (7), pp. 32–34.

Schütz, R., Potts, D., & Zdravkovic, L. (2011). Advanced constitutive modelling of shotcrete: Model formulation and calibration. Computers and Geotechnics, 38(6), 834-845.

Sharma, J. S., Hefny, A. M., Zhao, J., & Chan, C. W. (2001). Effect of large excavation on deformation of adjacent MRT tunnels. Tunnelling and Underground Space Technology Incorporating Trenchless Technology Research, 16(2), 93-98. doi:10.1016/S0886-7798(01)00033-5.

Shi, J., Ng, C. W. W., & Chen, Y. (2015). Three-dimensional numerical parametric study of the influence of basement excavation on existing tunnel. Computers and Geotechnics, 63, 146-158. doi: 10.1016/j.compgeo.2014.09.002.

Skempton A. W. & MacDonald D. H. (1956). "The allowable settlement of buildings." Proc. Inst. Civil Eng., 5(3), 727–768.

Skripkiūnas, G., Nagrockienė, D., Girskas, G., Vaičienė, M., & Baranauskaitė, E. (2013). The cement type effect on freeze – thaw and deicing salt resistance of concretedoi://doi.org/10.1016/j.proeng.2013.04.132

Son M. & Cording E. J. (2005). "Estimation of building damage due to excavation-induced ground movements." J. Geotech. Geoenviron. Eng., 131(2), 162–177.

Stead, D., Coggan, J. S., & Howe, J. H. (2000). Engineering geology and hazard assessment of excavated china clay slopes. Paper presented at the 72-76.

Sun Fu. (2007). "Life Prediction of Tunnel Lining Theoretical and Experimental Study", PhD thesis, Tongji University. China.

Sun, J. (2011). Durability problems of lining structures for xiamen xiang'an subsea tunnel in china. Journal of Rock Mechanics and Geotechnical Engineering, 3(4), 289-301. doi:10.3724/SP.J.1235.2011.00289

Swoboda, G., Mertz, W., & Schmid, A. (1989). Three dimensional numerical models to simulate tunnel excavation.

Terzaghi, K. (1955). Evaluation of coefficients of subgrade reaction. Geotechnique, 4, 297-326.

Tian, L., Chen, J., & Zhao, T. (2012). Durability of lining concrete of subsea tunnel under combined action of freeze-thaw cycle and carbonation. Journal of Wuhan University of Technology-Mater.Sci.Ed., 27(4), 779-782. doi:10.1007/s11595-012-0547-7.

Tjie-Liong, GOUW & Limara PT. Notes on the application of the spring. Indonesia. PLAXIS Practice.

The hardening soil model (isotropic hardening). (2018). In Material models manual (pp. 69-83). PLAXIS.

UN-HABITAT, Urbanization and Development: Emerging Futures, World Cities Report 2017.

United Nations World urbanization prospects: The 2018 revision. International Journal of Psychology, (S1), 443-447. Retrieved from https://onlinelibrary.wiley.com/doi/abs/10.1002/ijop.12312.

URBANIZATION AND THE MEGACITY https://worldpopulationhistory.org/urbanization-and-the-megacity.

Uriel , A., & Sagaseta, C. (1989). Selection on design parameters for underground construction. Proc. of the 12th international congress on soil mechanics, Rio de Janeiro, 9, pp. 2521-2551. Balkema, Rotterdam.

Usman, M., & Galler, R. (2013). Long-term deterioration of lining in tunnels. International Journal of Rock Mechanics and Mining Sciences, 64, 84-89. doi://doi.org/10.1016/j.ijrmms.2013.08.028

Van Jaarsveld, E., Plekkenpol, J., & Messemaeckers van ed Graa, C. (1999). Ground deformations due to the boring of the second Heinenoord tunnel. Twelfth European Conference on Soil Mechanics and Geotechnical Engineering . Amsterdam, Netherlands.

Vermeer , P. (2001). On a smart use of 3D-FEM in tunnelling Plaxis Bulletin (11), 2-7. 11, 2-7. Plaxis Bulletin .

Verrujit, A., & Booker, J. (1996). Surface settlements due to deformation of a tunnel in an elastic half plane. Géotechnique, 46(4), 753-756.

Vesic, A.B. (1961). Beam on Elastic Subgrade and The Winckler's Hypothesis, Proc. 5th Int. Conf. On Soil Mechanics and Foundation Engineering, Vol.1, p. 845-850.

Vesic, A. B. (1961). Bending of beams resting on isotropic elastic solid. Journal of the Engineering Mechanics Division, 87(2), 35-53.

Wang, F. (2013). Impact of overhead excavation on an existing shield tunnel: Field monitoring and a full 3D finite element analysis. Computers, Materials & Continua, 34(1), 63-81.

Wee , T., Chin , M., & Mansur , M. (1996). Stress-strain relationship of high-strength concrete in compression. ASCE Journal of Materials in Civil Engineering, 8(2), 70-6.

Winkler, E. (1867). Die Lehre Von Elasticitaet Und Festigkeit. 1st Edn., H. Dominicus, Prague.

Xia, B., Hong, Z.-S., & Ding, J.-W. (2016). Evaluating the effect of soil structure on the ground response during shield tunnelling in Shanghai soft clay. Tunnelling and Underground Space Technology, 58, 120-132.

Yongdong & Wang (2008). "Chloride Induced Corrosion of Steel Corrosion Durability of Underground Structures". Master thesis, Tongji University, China.

Yuan, Y., Bai, Y., & Liu, J. (2012). Assessment service state of tunnel structure doi://doi.org/10.1016/j.tust.2011.07.002

Zakhem A.M., EL-Naggar H. (2016). "Damage to Nearby Surface Structures Caused by Tunneling Induced Ground Displacements". Conference: CSCE 2016 Annual Conference, London, Canada.

Zakhem, AM., El Naggar, H. (2019). Effect of the newly constitutive material model employed on predictions of the behaviour of earth pressure balance (EPB) shield driven tunnels. Transportation Geotechnics, Elsevier.

Zheng, G., & Wei, S. (2008). Numerical analyses of influence of overlying pit excavation on existing tunnels. Journal of Central South University of Technology, 15(S2), 69-75. doi:10.1007/s11771-008-0438-4.

Zhiqiang, Z., & Mansoor, Y. A. (2013). Evaluating the strength of corroded tunnel lining under limiting corrosion conditions. Tunnelling and Underground Space Technology Incorporating Trenchless Technology Research, 38, 464-475. doi:10.1016/j.tust.2013.08.003.

Appendix A: Co-Authorship Statement

This thesis is prepared in accordance with the regulation for Integrated-Article format thesis stipulated by the school of graduate studies at Dalhousie University, Halifax, Nova Scotia, Canada. All the numerical modeling, interpretation of results and writing of the draft and the final thesis were carried out by the candidate herself, under the supervision of Dr. Hany El Naggar. The supervisor contribution consisted of providing advice throughout the research program and reviewing the draft and the final thesis and publications results from this research. The results of the numerical modeling presented will be used in journals and conferences publications, which will be coauthored with Dr. Hany El Naggar.

Appendix B: Copyright Permission

Appendix C: Anna Maria Zakhem, Engineer

3227 Joseph Howe Drive

Halifax, NS

B3L 4H3

Mobile: (902) 210-0776

Home: (902) 800-8399

Email: anna-maria-z@hotmail.com

a.zakhem@dal.ca

EDUCATION

Ph.D. degree, Civil Engineering ▪ 2014/2019 Dalhousie University – Halifax, NS, Canada.

Master's degree, Civil Engineering / Structures and soil mechanic ▪ 2009/2010 Saint Joseph University – Mar Roukos, Mkalles, Beirut, Lebanon

(Two years of education)

Master's degree, Civil Engineering / Public Works ▪ 2002/2007

Lebanese University – Tripoli, Lebanon

(Five years of education)

Baccalaureate degree / General Science ▪ 1987/2002

Collège Notre Dame Du Balamand – Kelhat, Lebanon

PROFESSIONAL EMPLOYMENT

Dalhousie University, Department of Civil and Resource Engineering, Halifax, NS, Canada.

Teaching assistant and marker, September/2018-December/2018

Course: CIVL 4515: Reinforced Concrete Design.

Dalhousie University, Department of Civil and Resource Engineering, Halifax, NS, Canada.

Teaching assistant and marker, January/2018-April/2018

Course: CIVL 3515: Structural Systems II: Loads and Behavior.

Dalhousie University, Department of Civil and Resource Engineering, Halifax, NS, Canada.

Teaching assistant and marker, September/2017-December/2017

Course: CIVL 4515: Reinforced Concrete Design.

Dalhousie University, Department of Civil and Resource Engineering, Halifax, NS, Canada.

Teaching assistant and marker, September/2016-December/2016

Course: CIVL 4111: Geotechnical Engineering.

Dalhousie University, Department of Civil and Resource Engineering, Halifax, NS, Canada.

Teaching assistant and marker, September/2015-December/2015

Courses: 1. CIVL 4111: Geotechnical Engineering.

2. CIVL 4515: Reinforced Concrete Design.

Dalhousie University, Department of Civil and Resource Engineering, Halifax, NS, Canada.

Teaching assistant and marker, January/2015-April/2015

Course: CIVL 3515: Structural Systems II: Loads and Behavior.

Dalhousie University, Department of Civil and Resource Engineering, Halifax, NS, Canada.

Teaching assistant and marker, September/2014-December/2014

Courses: 1. CIVL 4111: Geotechnical Engineering;

2. CIVL 3505: Structural Systems I: Form and Analysis.

Bureau D'études et Travaux Hydrauliques Electriques (Elie Selwan), Beirut, Lebanon

Site and Office Engineer, June/2010-June/2012

Project: UTDP/Grade Separation at Bechara El-Khoury Street and Independence Avenue Intersection

Budget: US $ 5.50 million.

Owner: Council of Development and Reconstruction (CDR).

Consultant*:* Dar Al Handasah Nazih Taleb & Partners.

The project consisted of a grade separation at Bechara El-Khoury Street and Independence Avenue Intersection by constructing an underpass with two cells carrying both Bechara El-Khoury and BCD (Beirut Central District) south bound and north bound traffic respectively under the independence street (Basta – Sodeco and vice versa). The overall length of the project is 360 Lm

approximately, comprising 127 Lm underpass section and 233 Lm ramps at both ends of the underpass.

Main Responsibilities

- Supervision of the quality of work and follow up of site activities.
- Offering assistance in planning, scheduling and progress reports.
- Quantity surveying including bar bending schedule.
- Adjustment of prices.
- Materials and drawings submittals to the consultant.
- Preparation and submitted of shop and as-built drawings.
- Internal correspondence (Internal daily, weekly and monthly reports).

Bureau D'études et Travaux Hydrauliques Electriques (Elie Selwan), *Beirut,Lebanon*

Site and Office Engineer, November/2009-June/2010

Project: Sin El Fil Municipality Lot 160

Budget: US $ 2 million.

Owner: Sin El Fil Municipality

Consultant: Builders design consultants

Main Responsibilities

- Quantity surveying including bar bending schedule.
- Preparation and submitted of shop drawings.

Bureau D'études et Travaux Hydrauliques Electriques (Elie Selwan), *Beirut,Lebanon*

Office Engineer, June/2009-November/2009

Project: UTDP/Grade Separation at Bechara El-Khoury Street and Independence Avenue Intersection.

Owner: Council of Development and Reconstruction (CDR) – Bidding Stage.

The project consisted of a grade separation at Bechara El-Khoury Street and Independence Avenue Intersection by constructing an underpass with two cells carrying both Bechara El-Khoury and BCD (Beirut Central District) south bound and north bound traffic respectively under the independence street (Basta – Sodeco and vice versa). The overall length of the project is 360 Lm approximately, comprising 127 Lm underpass section and 233 Lm ramps at both ends of the underpass.

Main Responsibilities

- Pricing of the bid and studying of the project drawings to determine the method of execution.

Bureau D'études et Travaux Hydrauliques Electriques (Elie Selwan), *Beirut, Lebanon*

Site and Office Engineer, August/2007-June/2009

Project: UTDP/Grade Separation at Adlieh Junction and at Abdullah Yafi Avenue and Damascus Road Intersection

Budget: US$14 million

Owner: Council of Development and Reconstruction (CDR)

Consultant*:* Dar Al Handasah Nazih Taleb & Partners / Mott Macdonald (Adlieh) and Team International / SaudConsult (Museum)

The two projects consisted of executing two underpasses at Adlieh and Museum junctions with adjoining service roads, in addition to introducing new utilities and upgrading and relocating existing ones. The utilities included potable water ductile iron pipes, telephone network, electric network, storm water network including Ø2000, 1800 and 1200 mm GRP pipes, waste water network, monocell and double cell concrete culverts for storm water and waste water disposal. The underpasses shoring system required of a total length of 766 m and 350 piles with struts, whaler beams and shotcrete.

Main Responsibilities

- Supervision of the quality of work and follow up of site activities.
- Offering assistance in planning, scheduling and progress reports.
- Quantity surveying including bar bending schedule.
- Adjustment of prices.
- Materials and drawings submittals to the consultant.
- Preparation and submitted of shop and as-built drawings.
- Internal correspondence (Internal daily, weekly and monthly reports).

Site and Office Engineer, July/2006-September/2006

Trainee with a civil engineering contractor (building construction)

Site and Office Engineer, July/2005-September/2005

Trainee with a civil engineering contractor (building construction)

SUPERVISION OF UNDERGRADUATE ENGINEER

- Wael Helou, master's degree student, June/2010-September 2010
- Basma Abou Antoun & Roland Rizk, master's degree student, June/2008-September 2008
- Marie A. Geagea & Hanaa Haddad, master's degree student, August/2007-September 2007

COMPUTER SKILLS

▪AutoCAD	▪Safe	▪Primavera	▪ Turbo Pascal
▪PLAXIS 3D	▪PCACOL	▪MS Project	▪ C
▪S-FRAME	▪Robot Millennium	▪MS Word	▪ C#
▪STAAD	▪Minitab 17	▪MS Excel	
▪Etabs	▪MatLab	▪MS Access	
▪ALLPILE	▪Visual Basic	▪MS PowerPoint	

LANGUAGES

English, French, and Arabic

PROFESSIONAL MEMBERSHIPS

The Association of Professional Engineers of Nova Scotia (EIT 28106);

Order of Engineers and Architects of Lebanon (No. 6119).

SCHOLARSHIPS

Faculty of Graduate Studies Scholarship for the 2014/2015 academic year;

Faculty of Graduate Studies Scholarship for the 2015/2016 academic year;

Bruce and Dorothy Rosetti Engineering Research Scholarship for the 2015/2016 academic year;

Faculty of Graduate Studies Scholarship for the 2016/2017 academic year.

Faculty of Graduate Studies Scholarship for the 2017/2018 academic year.

Faculty of Graduate Studies Scholarship for the 2018/2019 academic year.